THE UNIVERSITY OF ADELAIDE
Department of Mechanical Engineering

Advanced Modelling of the Fatigue of Butt-Welded Structures

A Thesis

by

Ninh T. Nguyen

B.E.(Hons.)(Slovakia), M.E. (AIT, Bangkok)

Submitted to the Research and Graduate Studies Branch

for the Degree of **Doctor of Philosophy**

March, 1996

AUSTRALIA

ABSTRACT

The effects of various influential weld geometry parameters, residual stresses and the combined axial and bending loadings on the fatigue behaviour of butt-welded steel joints are studied by developing a mathematical model to predict the fatigue S-N curves and fatigue notch factor. This model is broadly based on the principles of Dimensional Analysis, Linear Elastic Fracture Mechanics (LEFM) and Finite Element Analysis (FEA) approaches, Weight Function Technique and Superposition Principles. A dimensional analysis for the prediction of fatigue behaviour of butt joints is carried out by considering the effects of all the important parameters including: weld geometry, welding process, residual stresses and cyclic loading condition. In the present model, only the most influential parameters of weld geometry (tip radius at the undercut, weld toe radius, flank angle and plate thickness), residual stresses at the weld toe and the combined loading ratio (the ratio between the bending and axial loads) are considered.

The fatigue strength and the fatigue life of butt welded joints are found to be strongly influenced by the weld geometry parameters i.e the tip radius at the undercut, weld toe radius, flank angle, plate thickness as well as the misalignments but less strongly influenced by the edge preparation angle. The effect of the flank angle and the weld toe radius is more pronounced than that of the plate thickness. Furthermore, the fatigue test data of welded specimens of different thicknesses are influenced by the combined effect of all the weld geometry parameters, not solely by the effect of the

plate thickness as suggested by the data available in the literature. It has also been found that the fatigue strength of butt welded joints can be improved by reducing the flank angle, increasing the weld toe radius, eliminating the effect of undercut at the weld toe by post-weld grinding or using specific welding techniques which improve weld geometry profile. The flank angle needs to be reduced to less than 20° for a noticeable improvement.

The effect of the induced surface compressive residual stresses on the welded joints for the improvement of the fatigue life is successfully simulated. The study suggests that these processes are effective only in the early stage of crack propagation and up to a crack length corresponding to the depth of the compressive residual stress field. Once the crack has propagated beyond that length, the induced compressive residual stresses have an insignificant effect on the fatigue life. Furthermore, using a relatively low levels of the induced compressive residual stresses would result in an improvement of the same order as those obtained by thermal stress-relieving treatments (e.g. annealing).

Good agreements are found among the predicted fatigue S-N curves, predicted fatigue notch factors, the author's fatigue test results and the experimental data from the literature. Furthermore, the present study provides the basic understanding of the combined effect of weld geometry, residual stresses and the combined loadings on the fatigue behaviour of butt-joints. It also explains the phenomenon of large scatter band associated with fatigue test results and suggests a new procedure for performing and evaluating the fatigue tests which can ensure a reduced scatter band.

ORIGINALITY STATEMENT

This work contains no material which has been accepted for the award of any other degree or diploma in any university or other tertiary institution and, to the best of my knowledge and belief, contains no material previously published or written by another person, except where due reference has been made in the text.

I consent to this copy of my thesis, when deposited in the University Library, being available for loan and photocopying.

NINH T. NGUYEN

February, 1996

ACKNOWLEDGMENTS

The author wishes to thank his supervisor Dr. M. A. Wahab for his valuable assistance, advice and encouragement throughout the project. Without his guidance this work would have not been possible. His suggestions and editorial corrections during preparation of this thesis are gratefully acknowledged.

The author whishes to thank Mr. Ron Jager, Mr. Ian Brown, Mr. Herwig Bode, Mr. George Osborne and Ms. Corina M. Stamatoiu for their help during the fabrication of specimens, experimentation and photography. A special thanks is owed to Dr John Yellup for his help and valuable suggestions during fatigue tests carried out at the Division of Manufacturing Technology, CSIRO, Woodville North, South Australia.

The author also wishes to express his sincere appreciation for the enthusiastic support and suggestions of Prof. R.E. Luxton, Professor of Mechanical Engineering, during his Ph.D research project. The author is indebted to all the other academic members and fellow postgraduate students of the Department of Mechanical Engineering for their valuable assistance and support.

The author wishes to acknowledge the assistance of the Australian Commonwealth Government for providing an Overseas Postgraduate Research Scholarship (OPRS) without which this study would never have been possible. The financial support of the University of Adelaide Major Research Grant # 2840-4066, the University of Adelaide

Scholarship (UAS) and Frank Perry Scholarship from the Faculty of Engineering are also acknowledged with great gratitude.

The author is deeply indebted to his family, his wife Lan Anh and daughter Anna Minh Trang for their love, understanding, patience and encouragement during his course of study.

TABLE OF CONTENTS

GLOSSARY OF SYMBOLS

VARIABLES AND PARAMETERS

α	- distortion angle in radians (Fig. 2.2); also coefficient of thermal expansion of the base material
a	- crack length (edge crack; semi-elliptical surface crack); also half-length of central through-thickness crack
a^*	- Peterson's material constant (Eq. 3.40)
B, ρ_o	- material constants in Buch's and Switek's model (Eq. 3.41).
a_f	- final crack length
a_i	- crack initiation length
A_i, A_i^*	- proportional constants (Eqs. 3.26 & 3.27)
a_k	- regression coefficients for stress distribution function for k=1 to 8 (Eq. 3.39)
b	- half-width of cracked plate
c	- half-length of major elliptical surface crack
C, m	- material constants in Paris' equation (Eq. 2.9)
C_A, C_B	- material constants in Paris' equation at points A and B of crack front respectively
d_{eff}	- effective depth of surface treatments
ΔK	- range of stress intensity factor ($\Delta K = K_{max} - K_{min}$)

ΔK^{A}_{eff} - range of effective stress intensity factor at point A (Fig. 3.2)

ΔK^{B}_{eff} - range of effective stress intensity factor at point B (Fig. 3.2)

ΔK_{eff} - range of effective stress intensity factor

ΔK_{th} - fatigue crack growth threshold

ΔS, S - the range of remotely applied nominal stress

e - axial misalignment (Fig. 2.2)

E - Modulus of elasticity of the material

ϕ - plate-edge preparation angle for transverse butt welded joint

F - stress intensity boundary correction factor

$f(\pi_i)$ - transformation functions

ϕ_o - parametric angle of the ellipse

$G(c,y)$ - Kanazawa's weight function for through-thickness central crack in a finite plate (Appendix C)

h - weld bead height (reinforcement height); half-length of cracked plate; material constant (Eq. 3.41)

k - proportional constant (Eq. 3.23)

$k^{*}_{m,RL}$, $k^{*}_{A,RL}$ - proportional constants due to the combined effect of residual stress and loading conditions (Eqs. 5.6 & 5.7).

k^{*}_{mG}, k^{*}_{AG} - proportional constants due to the combined effect of (r) and (θ) (Eqs. 5.4 & 5.5).

K_A - stress intensity factor due to axial loading

K_{app} - applied stress intensity factor

K_B - stress intensity factor due to bending load

K_{cen} - stress intensity factor for central through-thickness crack in a finite plate

K_{ed} - stress intensity factor for edge crack in a finite plate

K_{eff} - effective stress intensity factor ($K_{eff} = K_{app} + K_{res}$)

K_f - fatigue notch factor

k_i - exponential constants in Eq. (3.24) (for i=1 to n)

K_I - stress intensity factor (mode-I)

k_m, k_A - proportional constants in mathematical model equations for the prediction of fatigue behaviour of butt-welded joints (Eqs. 3.35 & 3.36).

K_{max} - maximum stress intensity factor

k_{mG}, k_{AG} - proportional constants representing the effects of weld geometries (Eqs. 3.37 & 3.38).

K_{min} - minimum stress intensity factor

K_{res} - residual stress intensity factor

K_{sc} - stress intensity factor for surface crack in finite plate

$K_{sc,A}$ - stress intensity factor at point A for semi-elliptical surface crack in flat plate (Fig. 3.2)

$K_{sc,B}$ - stress intensity factor at front surface point B for semi-elliptical surface crack in flat plate (Fig. 3.2)

K_t - theoretical elastic stress concentration factor

$K_{t,a}(x)$, $K_{t,b}(x)$ - local stress concentration at distance (x) from the weld toe due to axial and bending load respectively ($K_{t,a}(x) = S_{w,a}(x) / S_A$ & $K_{t,b}(x) = S_{w,b}(x) / S_B$)

$K_{t,eff}$ - the effective stress concentration factor (Eq. 5.3)

K^{w}_{cen} - stress intensity factor of welded plate for a central through-thickness crack

K^{w}_{ed} - stress intensity factor of welded plate for an edge crack

$K^{w}_{sc,A}$ - stress intensity factor at point A for a semi-elliptical surface crack in welded plate (Fig. 3.2)

$K^{w}_{sc,B}$ - stress intensity factor at front surface point B for a semi-elliptical surface crack in welded plate (Fig. 3.2)

l - weld length (Fig. 2.1); also half length dimensions of the specimens (Fig. 2.2)

L - length dimension of the specimens (Fig. 2.2)

λ - a constant subject to the end boundary condition (λ= 3 for fixed ends and λ=6 for pinned ends)

m , A - regression constants due to traditional S-N equation (Eq. 3.30)

m(a,x) - Bueckner's weight function for an edge crack in a finite strip (Appendix C)

m_1, m_2 - coefficients due to Bueckner's weight function (Appendix C)

$M^{A}_{k,eff}$ - the effective stress intensity magnification factor induced by weld geometry, residual stress and loading conditions in (x)-direction at the deepest point A (Fig. 3.2)

$M^{A}_{k,r}$ - stress intensity magnification factor produced by weld profile geometry and residual stress in (x) direction at the deepest point A (Fig. 3.2)

$M^B_{k,eff}$ - the effective stress intensity magnification factor induced by weld geometry, residual stress and loading conditions in (y)-direction at the surface crack front point B (Fig. 3.2)

$M^B_{k,r}$ - stress intensity magnification factor produced by weld profile geometry and residual stress in through plate width direction at the surface crack front point B (Fig. 3.2)

M_k - stress intensity magnification factor produced by weld profile geometry ($M_k = Y/Y_o$)

$M_{k,a}$ - stress intensity magnification factor induced by weld profile geometry in axial loading

$M_{k,b}$ - stress intensity magnification factor induced by weld profile geometry in bending load

$M_{k,eff}$ - effective stress intensity magnification factor induced by weld profile geometry, residual stresses in combined loadings (axial and bending)

$M_{k,r}$ - stress intensity magnification factor induced by weld profile geometry and residual stress

m_o, A_o - the values of regression constants (Eq. (3.30)) corresponding to fatigue curves of flush-ground butt-joints in residual stress-free axially loaded condition ($m_o=3$, $A_o=f(t/b)$).

n - size exponent in modified Gurney's equation expressing the effect of plate thickness (Eq. 2.3)

N_i - fatigue crack initiation life

N_p - fatigue crack propagation life

N_{pred}, N_{exp} - Predicted and experimental values of fatigue life of butt-welded joints respectively

N_T - total number of cycles to failure

$p(x)$ - local stress at the distance (x) from the weld toe surface along the potential crack line ($p(x) = K_{t,a}(x)$ in case of pure axial loading and $p(x) = K_{t,b}(x)$ for pure bending load)

π_d - dependent dimensionless product in dimensional analysis

π_i - independent dimensionless products (for i=1 to n)

Q - heat input level per unit of weld length

θ - weld bead flank angle

Q_{sec} - shape factor due to elliptical surface crack (Eq. 3.15)

ρ - the radius of the notch root (Eq. 3.40)

r - weld toe radius of butt-welded joint

r' - tip radius of undercut

R - cyclic stress ratio R ($R=S_{min}/S_{max}$)

R_{ba} - ratio between the ranges of bending and axial nominal stress ($R_{ba} = S_B / S_A$)

S_{logN} - standard deviation of the fatigue test results in terms of log N

S_{logS} - standard deviation of the fatigue test results in terms of log S

S - remotely applied stress ($S = P / 2tb$) for pure axial load and $S = 3M / (bt^2)$ for bending load, where P is applied tensile load and M is applied bending moment

$S(x)$ - stress distribution along potential crack line in x-direction

$S(y)$ - stress distribution along potential crack line in y-direction

S_A - the range of axial nominal stress

S_B - the range of bending nominal stress

S_e - fatigue limit (fatigue strength at 2×10^6 cycles)

S_{eo} - fatigue strength of parent material (or fatigue strength of flush-ground welded plate)

S_m - mean applied stress

S_{max} - maximum nominal applied cyclic stress

$S_{max,\ pred}$ - upper boundary of the predicted scatter band of S-N curves

S_{min} - minimum nominal applied cyclic stress

$S_{min,\ pred}$ - lower boundary of the predicted scatter band of S-N curves

S_o - fatigue strength of welded joint for a reference plate thickness; fatigue strength of welded joint due to repeated loading (R=0). S - fatigue strength of butt-welded joint in term of stress range

S_r - maximum residual stress at weld toe surface

S_{rc}^* - peak of self-balanced compressive residual stress at the opposite side of the treated surface

S_{rc}^{max} - peak compressive residual stress along through-thickness direction

S_{rt}^{max} - peak tensile residual stress along through-thickness direction

S_u - ultimate tensile stress

$S_w(x)$, $S_w(y)$ - the range of the local stress along the potential crack line of a butt-joint in directions (x) and (y) respectively

$S_{w,a}(x)$,$S_{w,a}(y)$ - the local stress components subjected to the axial load in (x) and (y) direction respectively (Fig. 3.2)

$S_{w,b}(x)$, $S_{w,b}(y)$ - the local stress components subjected to the bending load in (x) and (y) direction respectively (Fig. 3.2)

$S_{w,r}(x)$, $S_{w,r}(y)$ - residual stresses in (x) and (y) direction respectively (Fig. 3.2)

S_y - yield stress

t, t_o - plate thickness and reference plate thickness respectively

U, I - welding voltage and welding current respectively

v - welding travel speed

w - weld bead width

W - width of the cracked body

x - through thickness distance from weld toe

Y - stress intensity geometry-configuration correction factor

y - through plate width distance from centre of plate; also a roof-topping distance due to angular distortion (Fig. 2.2)

Y_o - stress intensity geometry-correction factor subjected to crack geometry and loading configuration in flat plate

$Y_{o,a}$ - stress intensity geometry-configuration correction factor in axial loading for flat plate

$Y_{o,b}$ - stress intensity geometry-configuration correction factor in bending for flat plate

Chapter 1

INTRODUCTION

1.1 Introduction

Most of the steel structures in engineering practice today are fabricated by welding. These welded steel structures are often subjected to dynamic loads ranging from cyclic fluctuation to completely random loads due to service conditions such as pressure changes, temperature fluctuations, vibrations, waves and wind forces etc. Welded structures such as bridges, cranes, ships, ground vehicles, aircraft, pipelines, offshore structures and pressure vessels are mostly affected by fatigue loading. In general, fatigue behaviour of these welded structures is complicated by many factors intrinsic to the nature of welded joints. Normally crack-like defects such as slag inclusions, gas pores, lack of penetration at weld root or undercut at weld toes may be introduced in welded joints. Stress concentrations usually arise at locations of crack-like defects and at weld toes due to unpredictable variation in the profile of weld geometry. The practical factors such as the type and geometry of welded joints, the welding process used and the way in which filler metal is deposited at the welded joints may also affect the fatigue behaviour of the welded structures. Residual stresses which arise in the welded joints, as a consequence of incompatible thermal strains caused by heating and cooling cycles during the welding process, also affect the fatigue behaviour of welded

structures. Tensile residual stresses of yield magnitude may exist in welded structures and could detrimentally affect their fatigue behaviour (Maddox, 1991). All these factors have a negative effect on the fatigue behaviour of welded structures. Therefore, fatigue information of welded structures under dynamic loading is desirable to reduce the probability of premature progressive fatigue cracking. This problem has attracted a considerable number of research studies during the past two decades and as a result, several national standards for fatigue design of welded structures have been developed.

The predicted fatigue life of welded structures is dependent on the quality of the fatigue information incorporated into the fatigue design codes which represents the nature of the fatigue problem. Despite vigorous adherence to governing the rules of fatigue design, welded structures continue to fail as the present codes have many inadequacies due to a lack of knowledge in the specific areas. In some situations the present fatigue design rules are too conservative (Gurney, 1991) resulting in enormous cost increases for some welded structures. Therefore, more research studies are needed on the fatigue behaviour of welded structures in order to improve the present codes for fatigue design, testing and evaluation. In addition, increased use of welded steel structures in dynamic loading conditions will furthermore accentuate the need for a thorough investigation of the problem related to fatigue of welded structures.

Considerable research has been conducted on various aspects of the fatigue of welded joints and structures e.g. the crack initiation in welded joints (Mattos and Lawrence

1977; Bellow, Wahab and Faulkner 1986; Solberg 1990) and the fatigue crack propagation in various types of welded joints (Maddox 1970; Lawrence et al. 1973; Kim and Tsai et al. 1989; Tsai and Kim et al. 1991); the influence of weld shape geometry relating to fatigue properties (Martins Ferreira and Moura Branco 1989); weld defects assessment and notch severity (Harrison 1972; Maddox 1974; Haagensen 1988); the effect of residual stresses and post-weld thermal or mechanical surface treatments (Ohta et al. 1981; Mateffy et al. 1984; Bellow, Wahab and Faulkner 1984, 1986; Miki and Mori et al. 1986); the sensitivity of parent materials and welding processes to fatigue cracking (Coopers et al. 1986; Gurney 1969; Maddox 1981)); the effect of plate thickness or size effect (Stig Berge 1985; Yee and Burns et al. 1988; Haagensen 1990; Ohta and Toshio Mawari et al. 1990) and the effect of environment (Vosikovsky et al. 1980).

The fatigue assessment of welded structures must take into account the combined effect of all the influencing parameters wherever possible. The combined effect of these parameters on the fatigue behaviour of welded joints and welded structure can be so complex that the fatigue problem appears to be insoluble. The solution of this problem is one of the most challenging in engineering practice, if improvements are to be made in the fatigue performance of welded joints and welded structures.

The initiation period of a fatigue crack is generally considered to be negligible in the case of welded joints in the as-welded condition containing high tensile residual stresses, and inevitably welding defects (Lieurade, 1993). Given the low significance of the steel microstructure on the crack growth rate (Maddox 1972; Braid et al 1981),

the fatigue behaviour of such welded joints and structures are subject to crack propagation only. It suggests that studies to improve fatigue performance of welded joints and structures should focus on those parameters that allow for significant increases in the crack initiation life or which retard the first stages of crack growth. Published research studies have shown the following two methods offer promising results:

- Diminishing the stress concentrations in the areas subject to the greatest applied forces, such as geometry of weld toes and weld defects.
- Changing the residual stress field either by thermal stress relieving or by compressive residual stresses induced by mechanical surface treatments. This reduces residual tensile stresses in the crack initiation areas during early stages of crack propagation.

Todate, there is no complete study which has considered the combined and interacting effects of all the relevant important parameters. The present research is an attempt to find a reasonable answer to this fundamental problem.

1.2 Specific Objectives

This study aims to provide fatigue information on the combined effect of various influential parameters on the fatigue behaviour of butt welded joints. A mathematical model is developed to predict the combined effect of the most influential parameters on the fatigue life and strength of butt welded joints in structural steel under the combined cyclic pulsating tensile loading (i.e. zero stress ratio, R=0) and bending.

These paprameters are considered to be the weld geometry (i.e. tip radius of undercut, weld toe radius, flank angle and plate thickness), residual stresses and the combined loading ratio (the ratio between the bending and axial loads R_{bs}). The model is developed based on the concepts of Dimensional Analysis, Linear Elastic Fracture Mechanics, Finite Element Analysis and Superposition Principles. A single-V transverse butt welded joint was selected in this study for the fatigue modelling.

Specific objectives of the present study are outlined as follows:

1. To investigate the effect of various weld geometry parameters on the stress intensity factor and subsequently its influence on the fatigue life, fatigue strength and fatigue notch factor of butt welded joints in the combined axial and bending load condition.
2. To study the effect of residual stresses in butt welded joints in terms of fatigue strength and fatigue life improvement by post-weld mechanical and thermal treatments.
3. To develop a mathematical model which includes the most important parameters of weld geometry, residual stresses and the combined loading ratios to predict the fatigue life, fatigue strength and fatigue notch factor of butt welded joints in structural steels under the combined constant amplitude pulsating tensile loading and bending.
4. To verify the model developed in this study by comparing the predicted results with those obtained from the fatigue tests and with the data available from the literature.

5. To propose a new procedure to evaluate the fatigue behaviour of welded joints with a reduced scatter band and to provide some useful recommendations.

1.3 Scope of the Thesis

In Chapter 2, a thorough review of the classical papers and recently published research works on the fatigue aspect of welded joints was reported. The effects of various important parameters on fatigue behaviour of welded joints and the application of the Linear Elastic Fracture Mechanics (LEFM) on the fatigue evaluation of welded joints are discussed.

A theoretical analysis of the fatigue of butt welded joints including the dimensional analysis of the transverse single-V butt welded joint, the concepts of mathematical modelling and detailed numerical procedures are discussed in Chapter 3. The design and fabrication of test specimens and the fatigue testing procedure are reported in Chapter 4.

The numerical and experimental results obtained from this study are discussed in Chapter 5. In this chapter, the numerical results predicted by the model are also compared with the fatigue test results and the experimental data available in the literature.

Important conclusions inferred from numerical findings and fatigue test results are included in Chapter 6. A new procedure for fatigue testing and evaluation of welded

joints is proposed in Chapter 7 together with the recommendations for methods of improving fatigue performance and further research study.

Refereed journal and conference publications originated from this work are listed in Appendix A. The investigated ranges of weld geometry parameters, residual stresses and the combined loading ratios used for the numerical modelling are given in Appendix B. The coefficients of the curve-fitted function for the local stress distributions through the thickness of the welded joint due to the variation of weld geometry parameters are also given in Appendix B. The Kanazawa's and Bueckner's weight functions and the equations for the residual stress distribution in as-welded and surface treated conditions are discussed in Appendix B. The computer programs for the calculation of fatigue life of butt joints and for monitoring the fatigue tests with the MTS-testing system are listed in the Appendix C. Fatigue test results in terms of S-N curves and fatigue notch factors are shown in Appendix D. The values of the butt weld geometry profiles for various sets of fatigue test specimens are also indicated in Appendix D. A derivation of the equation for the fatigue notch factor from the basic S-N model equation is discussed in Appendix E. The strain-gauge method used to measure the effective residual stresses at the weld toes of fatigue test specimens are described in Appendix F. Finally, the tensile test stress-strain diagrams for various sets of test specimens are shown in Appendix G.

Chapter 2

LITERATURE REVIEW

2.1 Introduction

Fatigue performance of welded structures is a more complicated phenomenon than that of the parent material due to the existence of non-homogenous metallurgical zones created during the welding process. These are considered to be the main sources affecting the fatigue behaviour of welded joints. In order to review important published works on the fatigue of welded joints, it is necessary to consider the effects of various factors on the fatigue behaviour of welded joints separately. In the following sections, the effects of plate thickness, weld geometry, stress concentrations, parameters relevant to welding technique, post-weld residual stresses in the as-welded condition, mechanically induced surface residual stresses and the effect of mean applied stresses are discussed. The concepts of fracture mechanics applied to the fatigue life assessment of welded joints are also discussed. Finally, some important conclusions from the literature review are drawn and reported. All these factors will be considered in this study to determine the most important variables which should be included in the proposed model.

2.2 Effect of Weld Geometry Parameters

It is reported by many researchers (Mattos and Lawrence 1977, Gurney 1979, and others) that weld geometry such as plate thickness (t), weld toe radius (r), flank angle (θ), weld bead reinforcement height (h), plate edge preparation angle (ϕ) of butt welded joints as shown in Fig. 2.1 play an important role in the fatigue behaviour of welded joints.

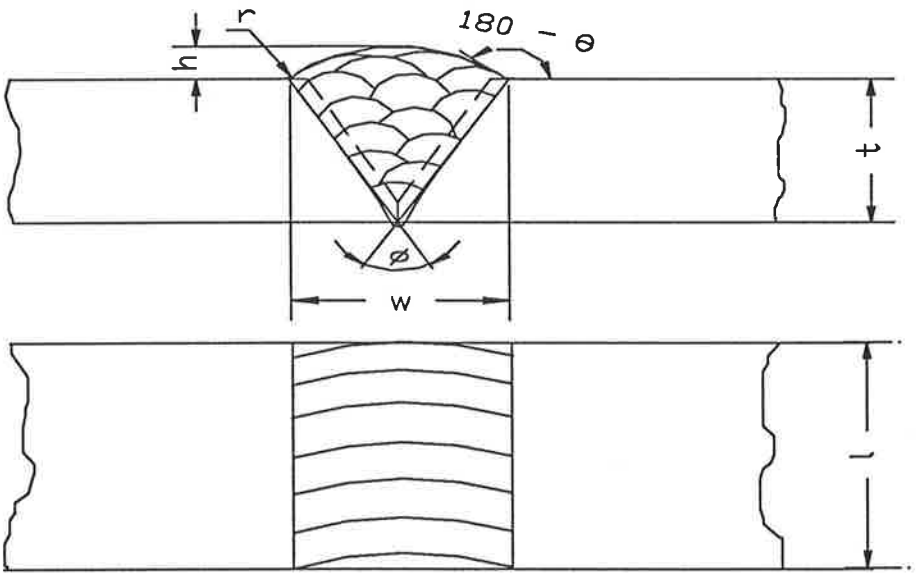

Figure 2.1 Geometry parameters of butt welded joints

Gurney (1981) analysed the data obtained from the United Kingdom Offshore Steel Research Project (UK OSRP) and the European Coal and Steel Community (ECSC) test programs in terms of the effect of various parameters on the fatigue strength of welded joints. These included plate thickness, weld shape parameters, cumulative damage, the effect of residual stresses and the effect of the environment. Based on the available experimental data and by using regression analysis Gurney suggested an

empirical formula representing the effect of plate thickness on the fatigue strength of welded joints as follows:

$$S.t^{1/4} = \text{constant} \tag{2.1}$$

where S - fatigue strength of welded joint

t - plate thickness of the welded plate.

This proved to be a satisfactory relationship when applied to tubular welded joints of offshore structures (Gurney, 1981). If t_o and S_o are the reference plate thickness and the reference fatigue strength, respectively, then this formula can be rewritten (Gurney, 1981) in a more convenient form as:

$$S = S_o.(t_o/t)^{1/4} \tag{2.2}$$

This relationship was confirmed and later extended by Haagensen (1988) in terms of the effect of thickness of T-welded joints and the effect of notch caused by weld toe radii. Fatigue crack initiation was estimated by using a localised stress-strain method while the crack growth rate was evaluated by using fracture mechanics. From his results, Gurney's formula was proposed as:

$$S = S_o.(t_o/t)^n \tag{2.3}$$

where n - the size exponent related to stress concentration factor

Haagensen's prediction model and experimental results showed that the size exponent (n) decreased with a decreased value of the stress concentration factor (SCF). The improvement obtained by reducing the SCF resulted in a reduced effect of thickness when compared with as-welded joints. It was concluded that the size effect on the fatigue life of T-welded joints was significantly affected by SCF.

Another study describing the effect of plate thickness on the fatigue strength of transverse fillet welds in axial loading condition was conducted by Berge (1985). The study was based on a fracture mechanics model which assumed a geometric similarity of weldments regardless of their plate thickness for plates in the range of 12.5 to 80 mm thick. He stated that for proportional scale load-carrying welded joints the effect of thickness was found to follow a power law with a decrease in fatigue strength of 40 % when the plate thickness was increased from 12.5 mm to 80 mm. Although the result of Berge's study is consistent with the study reported by Gurney (1981), both assumed that the geometry of the weldments was similar regardless of the plate thickness. The conclusions drawn from both Gurney's and Berge's studies are only valid if the assumption about similarity of specimen geometry is correct. In fact, this assumption is acceptable only for a highly automatic welding process which produces welded joints with a uniform weld profile geometry. For manual arc welding or submerged arc welding, geometry parameters vary significantly even for the same thickness of parent material. It suggests that Gurney's and Berge's studies are conservative by ignoring the effect of weld profile geometry. Furthermore, no satisfactory explanations of the nature of the effect of plate thickness were attempted.

Ohta (1990) endeavoured to explain the effect of plate thickness by introducing a new method of fatigue testing. Transverse butt welded specimens made from 9 mm and 40 mm thick plates were tested by maintaining a maximum cyclic loading stress equivalent to the yield stress of the base material under repeated tensile loading (R = 0). He found that fatigue strength of 40 mm thick specimens was lower than that of 9 mm thick specimens if standard fatigue testing procedures were followed. However, the effect of thickness disappeared when the maximum load was maintained at the yield stress during the test and the fatigue strength of 9 mm and 40 mm thick plate were found to be equivalent. He explained that the effect of thickness appeared in the zero stress ratio condition (R=0) was due to the result of residual stresses at the weld toes. This effect disappeared when the maximum loading stress reached the yield stress level since at this level of applied stress, a saturated state of the fatigue notch factor was reached in the region of high stress concentration at the weld toes. As a result, despite the difference of stress concentration factors at the weld toes for different thicknesses, fatigue strength of the welded joints remained the same.

Aside from the effect of plate thickness, the effect of other weld geometry parameters such as weld toe radius (radius of curvature at weld toe) on the fatigue strength of a welded joint has been studied by Ferreira and Branco (1989). Their experimental and theoretical study was carried out on transverse non-load-carrying fillet welded joints for various plate thicknesses in tensile and bending loading. They reported that the fatigue strength increased with increased weld toe radius. They noted that the effect was insignificant for small thicknesses (4 and 6 mm) and tended to increase for a larger thickness (12 and 20 mm) and there was a reduction in fatigue strength of 50 % when the plate thickness was increased from 6 to 100 mm. However, they suggested

that a fillet radius with a sufficiently high ratio of radius to thickness should not produce a reduction in fatigue strength with an increase in thickness. Although not offering a clear theoretical explanation, they concluded that the radius of curvature at the weld toe was a very important parameter for fatigue life and it should be taken into account in any fatigue life assessment.

Hentchel et al (1990) investigated the effect of weld toe geometry on the fatigue behaviour of butt joints in structural steels. Their results showed that the fatigue behaviour of butt welds in small samples of construction steel St 38, H52 and H75 was influenced by the weld and toe groove geometries. Fatigue behaviour of these joints was improved as the stress concentration factor decreased. They also found that the geometry of the weld toes can be controlled by the welding parameters, the type of welds, the choice of filler materials and the post-weld groove-reducing treatments.

Castiglioni and Gianola (1992) carried out a parametric FEA study of the weld toe joint geometry in full penetration longitudinal attachments. They proposed a mathematical model for the stress intensity factor for this type of joint which included geometrical parameters such as stiffener length and thickness, base plate thickness and weld toe flank contact angle. They found that the fatigue strength of longitudinal attachments was influenced considerably by the length of the stiffeners, the thickness of base plate and the weld toe flank angle. They also found that the thickness of the stiffener and the width of the main plate had an insignificant effect on fatigue behaviour of the joints.

Cole et al. (1992) investigated the effect of thickness on the fatigue life of welded joints in air and in sea water with cathodic protection. They carried out both theoretical and experimental investigations of the effect of plate thickness, whilst varying toe radius, flank angle and welding process parameters. They found that the effect of thickness was more significant than that suggested by Gurney's Formula (Eq. 2.2). The values of the size exponent (n) obtained by curve-fitting the experimental data to Eq. (2.3) for the in-air and in-sea water conditions were 0.39 and 0.38, respectively. The 50 mm thick joints showed a reduction in the fatigue life of 40 % compared with that of thinner joints made from 32 mm plates. It was concluded that the effect of thickness appeared to be the resulting effect of geometrical/mechanical properties rather than material properties.

A recent experimental study by Huther et al (1995) emphasised the importance of the weld quality including weld geometry such as toe radius, flank angle, weld width and height in the assessment of fatigue behaviour of welded joints. These parameters were investigated with respect to welding process, filler materials and welding position. Fatigue tests were carried out on T-joints made from 10 mm thick E460 TM steel plates. Two welding positions (flat and vertical upwards) and several types of electrodes were used. They found that for a particular cross section, there was no apparent correlation between the measured values of flank angle and toe radius. However, for a large number of cross sections from the same welded plate, a correlation was found between the mean values of these two geometric parameters. The endurance limit increased as the flank angle decreased or toe radius increased. This behaviour reflected the effect of stress concentration factor (K_t) on the endurance limit i.e as K_t increased the endurance limit decreased. However, an attempt to use

local stress range (K_t.S) instead of nominal stress range (S) to determine the S-N curve did not reduce the scatter of the fatigue test results. They concluded that the endurance limit of welded joints can be increased by 50 % by controlling the weld quality which includes local geometry parameters.

2.3 Effect of Weld Imperfections

Deviations from the ideal weld bead shape often occurs in welded joints. These imperfections can considerably reduce the fatigue performance of welded joints and structures. A large amount of research dealing with the subject of crack-like imperfections has been published. The International Institute of Welding (IIW) has developed a classification of weld imperfections in the following categories:

(a) Three-dimensional internal imperfections (e.g. pores, slag inclusions),

(b) Two- dimensional flat internal imperfections (e.g. cracks, fusion defects),

(c) Imperfections of the structural part geometry (e.g. angular contraction, axial misalignment),

(d) Imperfections of weld geometry (e.g. weld bead reinforcement, weld toe undercut).

The present study is concerned with sound welded joints and hence internal weld imperfections were not considered. Therefore, only the effect of the above categories (c) and (d) i.e weld imperfections in the form of misalignment and angular distortion and weld toe undercut are reviewed and discussed below.

2.3.1 Misalignment and angular distortion

The effect of misalignment is to increase the stress experienced by the joint under loading as a result of the introduction of local secondary bending stresses. This reduces the fatigue strength of the joint (Gurney 1979, Maddox 1991). Therefore, misalignment does not introduce an alternative site for fatigue crack initiation but rather enhances the severity of existing stress concentrations, notably at the weld toe surface; i.e., angular distortion and axial misalignment produce additional bending in tensile-stressed or compression-stressed plates. The effect of misalignment on fatigue strength is detrimental only if it represents a discontinuity to the applied loading path, i.e., if bending is the only type of loading then misalignment does not have any effect on fatigue strength of the joint (Maddox 1985, Petershagen 1990).

A study of the effect of misalignment on butt welded joint in a residual stress-free condition has been carried out by Maddox (1985). In this study, he pointed out that the misalignment of a butt joint can be classified into two types: eccentricity and angular distortion, as illustrated for the butt joint in Figure 2.2. The forces transmitted by the misaligned butt joints in axial loading can be divided into axial and bending stress component, as follows:

$$S = S_A + S_B = S_A (1 + R_{ba}) \tag{2.4}$$

where S_A and S_B are the nominal axial and bending stress range, respectively

This equation can be rewritten in the form of stress concentration factor (K_t) for axial misalignment and for angular misalignment respectively as follows (Berge and Myhre, 1977):

$$K_t = 1 + \lambda\,(e/t)\,(l/L) \tag{2.5}$$

$$K_t = 1 + 0.25\,\lambda\,\alpha\,(L/t) \tag{2.6}$$

where
- λ - a constant subject to the end boundary condition (λ= 3 for fixed ends and λ=6 for pinned ends).
- e - axial misalignment (Fig. 2.2)
- α - distortion angle in radians (Fig. 2.2)
- L, l - length and half-length dimensions of the specimens, respectively (Fig. 2.2)

The formula of K_t for angular misaligned joints can also be expressed in terms of roof-topping distance (y) (Fig. 2.2.) as follows (Petershagen and Zwick, 1982) :

$$K_t = 1 + \lambda\,(y/t) \tag{2.7}$$

Using Eqs. (2.4) to (2.7) the effects of various types and levels of misalignment can be related to the induced bending stress and nominal axial stress which are used for fatigue analysis.

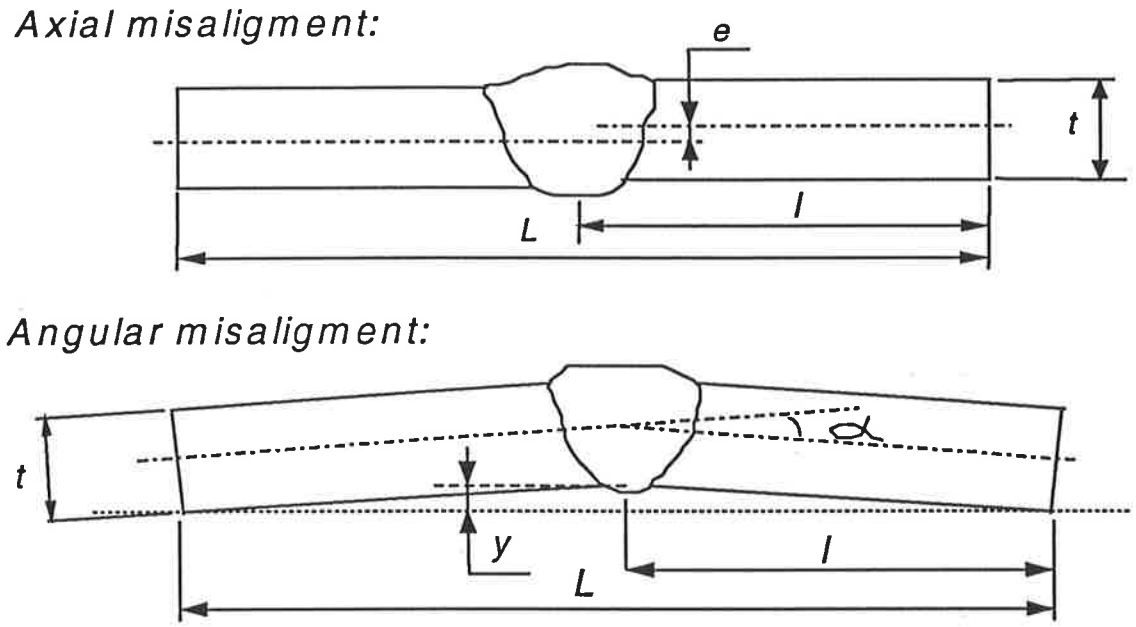

Figure 2.2. Typical misalignments in butt welded joint

2.3.2 Weld toe undercut

An undercut at the weld toe is a defect which affects the fatigue behaviour of welded joints. It is described by Jubb (1981) as an irregular groove caused by the welding process, situated along the toe of a weld in the parent metal or in the weld metal already deposited during a previous run. According to Jubb, the undercut may be divided into three types: (1) wide and curved, (2) narrow and very narrow (crack-like) and (3) shallow and narrow (micro-flaw with depth up to about 0.25 mm) (Fig. 2.3).

Type 1 undercut is the most common form of undercut, occurring during automatic welding of long single run fillet welds in the horizontal / vertical position with high level of heat input. This type of undercut often found in Manual Metal Arc Welding

(MMAW) due to a lack of sufficient weld metal being deposited at the weld toes. When the groove at weld toe is almost filled by the solidifying weld metal, the type 2 undercut occurs. Type 3 undercut is considered to be present at the toe of majority of welds irrespective of the presence of type 1 undercut. This type of undercut is thought to be caused by metallurgical inclusions at the weld toes and by the lack of ductility in the heat-affected-zone (HAZ) adjacent to the toes (Petershagen, 1990). Type 1 undercut has been chosen for modelling since it is the most common form of undercut in welded joints. Types 2 and 3 are less common and have not been included in the present study.

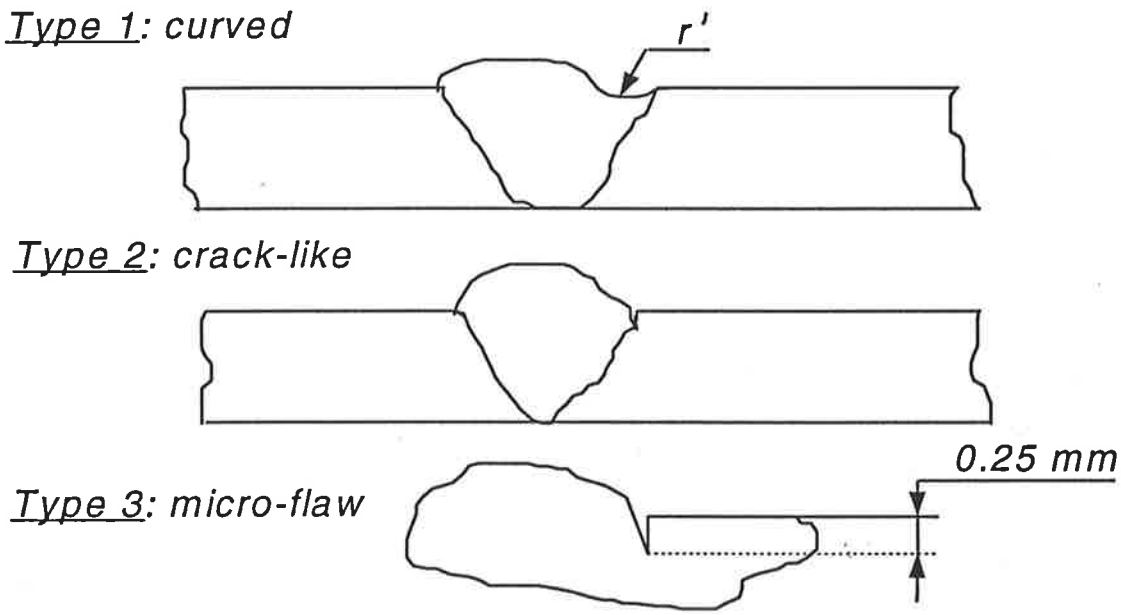

Figure 2.3 A classification of undercuts at the weld toe of butt-welded joints

An earlier study of the effect of the undercut on the fatigue strength of fillet welds was carried out by Petershagen (1980). His fatigue test results showed that the

number of fatigue cycles for a given probability of survival decreases as the depth of undercut increases. Good correlation was found between the experimental and the prediction by established fracture mechanics techniques. Further, he reported that the fatigue limit of welded joints containing an undercut of 0.8-1.1 mm was approximately 10 % lower than joints with no undercut.

2.3.3 **Stress concentrations**

Stress concentration factor is defined as the ratio of the local stress to the nominal stress. Any discontinuity in a stressed member introduces a stress concentration where localised stress is higher than the remotely applied nominal stress. Under a cyclic loading condition the material in this region is repeatedly stressed and as a result the fatigue damage occurs in the form of fatigue cracks. For a welded joint a stress concentration is unavoidable due to the geometry of the joint and its specific features such as weld metal inclusions, fusion line, HAZ, lack of penetration etc. Normally high local stress concentration occurs in welded joints at the weld toes and undercuts which causes an abrupt convex profile of the welded joint. Small crack-like flaws being introduced into the weld metal at the weld toe regions during the welding process may also act as stress concentrators. All these factors will reduce the crack initiation life as well as accelerate the fatigue crack growth and hence reduce the total fatigue life (sum of crack initiation and propagation cycles) of the welded joints.

A lack of penetration at the weld root may cause more severe local stress concentration than the defects at the weld toe. Under these conditions, the zone at the weld root may be a potential site for fatigue crack initiation and propagation.

Itoh (1987) investigated the initiation and propagation of butt welded joints with the assumption that fatigue cracks are normally initiated at weld toes. He claimed that weld toe configuration with high stress concentrations significantly affects the crack initiation life of welded joints. In the early stages of fatigue crack growth, a shallow crack of 0.5 -1 mm grows rapidly in the high stress concentration field at the weld toe. Beyond that the rate of crack propagation was not affected by the weld toe geometry. He suggested that the fatigue life of butt welded joints can be satisfactorily estimated assuming that a small fatigue crack of 0.5 mm to 1 mm already exists at the weld toes and the total fatigue life is virtually the same as crack propagation life which can be calculated by using an appropriate crack propagation law.

A study of the effect of stress concentration on fatigue behaviour of notched members was carried out by Peterson (1959). He suggested that the fatigue notch factor (K_f) of any notched member (defined as the ratio of fatigue strength of un-notched member to that of a notched member) is strongly influenced by theoretical stress concentration factor (K_t) and can be expressed in terms of (K_t) and notch root radius (ρ) as:

$$K_f = 1 + (K_t - 1) / (1 + a^* / \rho) \qquad (2.8)$$

where a^* - material constant ($a^* = (1.087 \times 10^5 . S_u^{-2})$ mm for steel; S_u is the ultimate strength in MPa

This formula can be used to investigate the fatigue notch factor of a welded joint in terms of stress concentration factor at the weld toes and the weld toe notch root radius.

2.4 Effect of Residual Stresses and Stress Ratio

Residual stress is defined as the remaining stress in the welded joints when the external load is withdrawn. The existence of residual stresses in welded structures results from an uneven strain distribution of various regions of the joints during welding process. As a result, the pattern of the applied stress during the loading cycles can be significantly influenced, particularly, when the tensile residual stresses are of the order of the yield stress of the base metal exists at the toes (Maddox, 1991). Under these circumstances there is a high risk of damage of welded structures during dynamic loading. In order to improve the fatigue life of the welded structures various thermal/mechanical treatments are commonly used to change the tensile residual stress field. However, these treatments impose time delay and cost increases and may alter the mechanical and metallurgical properties of the joints. Therefore, many of the welded joints and structures are often left untreated and they referred them in the as-welded condition.

Residual stresses in welded joints are divided into several types depending on the dimensions of the joints. First order residual stresses cause macroscopic strains in the joints. Second and third order residual stresses are those that cause micro-strains in the grains and crystals respectively. Residual stress of the first order play a major role in fatigue behaviour of the welded joints whilst the second and the third order stresses play a part in the stability of residual stresses under cyclic loading (Lieurade, 1988). A typical welding residual stress distribution in longitudinal and transverse directions of butt welded joints is shown in Fig. 2.4 (Maddox, 1991).

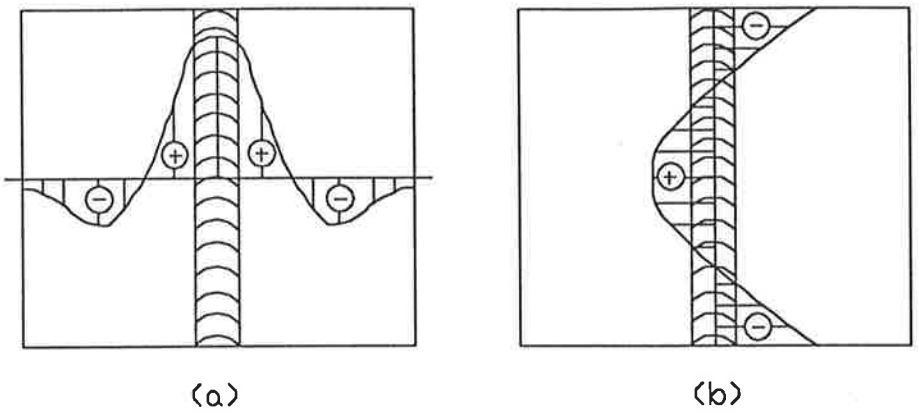

Figure 2.4 Typical distributions of welding residual stresses in butt-welded joints (Maddox, 1991).

The majority of the previous studies have concentrated on the effect of the first order residual stresses. Some of these are reviewed here together with the effect of the stress ratio.

Gurney et al. (1973) have compared a number of fatigue test results carried out at three levels of stress ratio, i.e. alternating stress (R = - 1), repeated stress (R = 0) or pulsating tensile stresses (R = 0.5). He reported that when compared with tests conducted at a repeated stress level (S_o), the fatigue limit under conditions of alternating stress S_{-1} (S_{-1} = $1.235S_o$) and a pulsating tensile stress $S_{0.5}$ ($S_{0.5}$ = 0.815 S_o) were altered by factors of 1.2 and 0.8 respectively.

A study by Elber (1974) has noted the effect of compressive residual stresses introduced by shot peening on the crack-growth properties of the material. He assumed a simple pattern of compressive residual stresses to simulate the effect of

shot-peening and used the principle of superposition to calculate the range of the effective stress intensity factor (SIF). He suggested that the range of effective SIF could be used in Paris' equation (Paris and Erdogan, 1963) rather than range of stress intensity factors. He reported that the results of the effect of shot-peening also revealed the effect of applied stress level. He concluded that the compressive residual stress near the surface caused shallow cracks to grow more slowly than observed for cases without residual stresses. He also found that tensile residual stresses below the shot-peened layer caused deeper cracks to grow more rapidly then observed for cases without residual stress.

Miki, Nishino and Hirabayashi (1982) used fracture mechanics concepts to investigate fatigue crack propagation in single bevel-groove welded joints. They observed that effect of residual stress on the rate of fatigue crack growth was significant in the region of low stress intensity range. They reported that in longitudinal welds with inadequate penetration there was a reduction in the fatigue strength due to residual tensile stress.

Maddox (1982) tested non-load-carrying fillet welded joints in as-welded and stress-relieved state at various stress ratios ($R = -\infty, -1, 0, 0.5, 0.67$). Four different types of steels: mild steel, carbon-manganese steel and two high strength low-alloyed quenched and tempered steels with yield strengths varying from 332 to 727 MPa were used in the tests. The experimental results obtained from as-welded joints showed that the effect of stress ratio was inconsistent except under zero-compression loading ($R = -\infty$), which usually lie near the upper limits of scatter. The test results obtained for stress-relieved joints also showed no consistent influence of positive stress ratio ($R>0$). However, his results for $R = -1$ were generally higher than those obtained in

tension. He suggested that the fatigue life under alternating loading (R=-1) may be expected to be up to 10 times greater than that under pulsating tensile loading condition (R = 0.67). Further for as-welded joints containing high tensile residual stresses, the applied stress ratio (R) had little influence on the fatigue strength. In spite of the scatter of the test results, the yield point of the base metal had no influence on the fatigue behaviour of welded joints.

Mateffy, Mikan and Abel (1984) studied the effect of stress relieving on fatigue life of fillet welded cruciform joints and they stated that the benefits of the effect of stress relieving on fatigue life were dependent on the applied stress range. This effect was not found to be beneficial at high levels of applied stress. At very high applied stress levels the stress relieving may even be detrimental to the fatigue performance of welded joints. This may be associated with strain ageing effect which reduces the total ductility of these joints. They also reported that the effect of residual stress on the fatigue behaviour of welded joints is less significant than that of stress concentration factors which are always of a high magnitude at the weld toes.

Toyooka et al. (1985) carried out fatigue tests under pulsating tensile loading on stress induced specimens manufactured from carbon steel weldments. Their experimental results showed that the level of tensile residual stress had no pronounced effect on the fatigue strength of as-welded and post-weld heat treated specimens. This may be explained by the reduction in tensile residual stress during first few loading cycles. The reduction in fatigue strength in the as-welded specimens was due to embrittlement resulting from thermo-plastic straining during welding. Post-weld heat treatments improved the ductility and hence the fatigue strength of the welded

specimens. The effect of residual stress on the fatigue behaviour of welded joints claimed by Toyooka et al. (1985) seems to conflict with other authors. However, the effect of embrittlement in the (HAZ) to cause a reduction in the mechanical properties of welded joints is widely accepted (Gurney, 1979; Maddox, 1991).

Reynold (1985) in his review of papers from "Corrosive Fatigue Program 1983-1985" mentioned that the reduction of the level of residual stresses by post-weld heat treatment (PWHT) resulted in an improvement in fatigue life of up to 30 %. The increase in fatigue life was observed during early stage of crack growth. In some cases the post-weld heat treatment reduced the residual stresses from a level close to the yield stress of the base material to a level of half of the yield stress.

Reynold reported that the effect of PWHT could be more significant on larger joints where tensile residual stress may reach the level of yield stress over a large volume. He noted that an increased effect of compressive residual stress at the weld toe can be expected from shot-peening. Furthermore, an improvement in fatigue strength of welded joints can be expected from other treatments such as grinding or hammer peening in the early stages of the crack growth.

Bellow, Wahab and Faulkner (1986) developed a model to predict fatigue life of welded steel structures. Their model simulated the effect of residual stresses on crack initiation and crack propagation life. Residual stress field in as-welded butt joints and in the joints treated by various surface treatments such as glass and steel shot peening, hammer peening, tensile pre-loading and stress peening were measured and used for numerical modelling. It was concluded that surface treatments which induced

compressive residual stresses could improve the fatigue strength of welded joints by as much as 83 %.

Ohta et al. (1986) developed a new procedure using small-scale test specimens to carry out the fatigue test which simulate high tensile residual stress of the yield stress in real welded structures whilst maintaining the maximum applied stress equal to the yield stress of the base metal. It was reported that this high level of tensile residual stresses can be simulated by using this new procedure proposed by the above authors. They noted that the test results with $S_{max} = S_y$ are comparable with those of the specimens with high tensile residual stresses and with the S-N curve proposed by Gurney et al. (1973).

Wohlfart (1986) investigated the effect of welding residual stresses on the fatigue strength of butt welded joints in high strength structural steels. Tungsten Inert Gas (TIG) and TIG dressed joints were used. He reported that after approximately $1x10^3$ cycles the magnitude of the residual stresses were reduced considerably. The effect of the welding tensile residual stresses with a reduced magnitude was less significant than that of notches at the weld toes. He also claimed that TIG dressing, TIG welding and pulsed arc TIG welding followed by shot peening proved to be an effective measure to improve the fatigue strength of butt welded joints. These welding techniques produced extremely flat weld seam profiles whilst the shot peening produced beneficial compressive residual stresses at the weld toe surfaces.

Maddox and Webber (1987) welded transverse stiffeners to plates to create test specimens with high stress concentrations; to some of these specimens "hot spots"

heating was applied to the ends of the stiffeners which on cooling resulted in high tensile residual stresses. They noted that the fatigue strength of the specimens with high tensile residual stresses when tested at stress ratio of R=0 was comparable with that of the other specimens with lower residual stress tested at a high stress ratio (R>0). From this study, they concluded that the stress range of the loading cycle must be considered even if the loading cycle has a compressive component. However, when the level of residual stress reached the yield stress of base metal, stress range was limited only by the yield stress and was independent of the stress ratio.

Lieurade (1988) carried out a comprehensive literature survey on the effect of residual stresses and stress ratios from a number of research work available in the literature. He noted that the effects of stress ratio and residual stresses on fatigue of welded joints as reported in the literature were often contradictory. After analysing the effect of various interacting parameters he concluded the following:

(i) The stress ratio had a significant effect on the fatigue behaviour of small size welded joints ($t < 20$ mm). However, the fatigue test results showed no such effect on large size or thicker welded joints.

(ii) The propagation of cracks was highly influenced by the stress ratio and the levels of residual stresses.

(iii) The improvement in the fatigue behaviour of welded joints may result from thermal stress-relieving in the case of $R = -1$. However, this effect was not certain in the case of large welded structures.

(iv) The effect of a number of influential parameters on fatigue cracking, particularly the effect of stress ratio and residual stress could be eliminated by

taking into account the "crack closure phenomenon" and expressing the test results in terms of the range of effective stress intensity.

(v) The fatigue behaviour of welded joints could be improved by either lengthening the crack initiation stage or delaying the first stages of crack propagation.

Nakamura, Nishijma and Ohta (1988) carried out fatigue tests using the new procedure to simulate high levels of residual stresses in welded joints as proposed earlier by Ohta et al. (1986). It was found that the actual cyclic stress range experienced at the weldment varied downwards from the yield stress regardless of the actual applied cyclic stress. They reported that the high tensile residual stress present in slit-welded specimens was a key factor in reducing the fatigue strength of welded joints. Their test results of slit-welded specimens coincided with those specimens tested by the new procedure. They claimed that the fatigue strength of the large welded structures carrying high tensile residual stresses was dependent on the stress range and independent of the stress ratio.

Matsuoka et. al. (1993) studied the effect of residual stress on the fatigue strength of non-load carrying fillet welds. They found that the plate width of a specimen had a significant effect on the longitudinal residual stresses but an insignificant effect on the transverse residual stresses. They also reported that the transverse residual stresses decreased as the welding heat input increased during fabrication. As a results, for the same level of the heat input, the plate width had no effect on the fatigue strength. However, for the same plate thickness the fatigue strength significantly increased as the heat input increased.

In the following section, the effect of various post-weld treatments on the fatigue behaviour of welded joints are reviewed for improving the fatigue performance of the joints which are based on the modification of the weld geometries or residual stresses.

2.5 Fatigue Improvement by Post-weld Treatments

The fatigue strength of welded joints is mainly affected by the notch effect of the weld toe geometry where the stress concentration reaches the highest level. This means that the fatigue strength of welded joints can be significantly improved by reducing the effect of stress raisers at the weld toes. Several commonly used methods of surface treatments are briefly listed as follows:

- Reducing the weld reinforcement by machining it to the level of the parent plate
- Grinding or peening the surface of the weld toe to increase the weld toe radius
- Increasing the weld reinforcement by adding an additional weld bead at the weld toes using a coated electrode or by TIG-dressing. With these methods the weld toe radius and flank angle can also be improved.
- Introducing compressive residual stresses at the surface of the weld toes by work hardening the surface layers (stress peening, shot peening etc.)
- Optimising the welding parameters and filler metal to simultaneously increase the weld toe radius and decrease the flank angle.

Some of the important research studies concerning the above aspects are reviewed here.

2.5.1 Effect of post-weld heat treatments (PWHT)

Post-weld heat-treatment (PWHT) is a commonly used techniques to change the residual stress field and improve the fatigue performance of welded joints. For structural steels, stress-relieving heat-treatment consists of holding the weldment at a temperature between 500° C to 600° C for approximately one hour for every 25 mm of the plate thickness followed by cooling at 10° C / hr (IIW/IIS Doc. 1090-90). Maddox (1982) found that after such a treatment at 580° C to 620° C magnitude of the tensile residual stresses in mild steel was of the order of 60 MPa.

A study by Haibach (1978) on the fatigue behaviour of the V-joints prepared from 10 mm and 50 mm thick plates showed that PWHT had an insignificant effect on the fatigue behaviour of the joints under cyclic tensile bending loads (R = 0). However, its effect became more noticeable when the joints were subjected to alternating bending loads (R = - 1). In the latter case, the fatigue limit was increased by 50 % due to PWHT of specimens with tensile residual stresses. However, he noted that if the residual stresses were compressive, the PWHT decreased the fatigue strength of the joints.

A study by Berge and Eide (1982) revealed that the magnitude of residual stresses after PWHT at 580° C did not exceed one tenth of the yield stress of the parent material. In their study, they also considered the combined effect of residual stress and stress ratio on the welds in structural steel with longitudinal stiffeners. They reported that as a result of high tensile residual stress in the weld joints, results from specimens in as-welded condition were comparable for the two levels of stress ratios (R = 0 and

R = -1). However, the fatigue test results for these joints in both the stress-relieved and as-welded condition were the same. This suggests that the effect of heat treatment was not significant. However, they noted that in the stress-relieved condition the fatigue strength obtained for R = -1 was greater than that for R = 0.

Lieurade et al. (1993) studied the effect of several techniques which improved the fatigue strength of fillet welded joints (cruciform and T-joint) made from an HSLA steel (AFNOR E690 steel). Five types of fillet welded joints were subjected to various loading conditions. Each type of joint was tested under the following four conditions: as-welded, PWHT, TIG-dressing and shot peening. Results of their study showed that under pulsating tensile loading condition (R = 0.1) a PWHT did not have any significant effect on the fatigue performance of the joints. They suggested that the application of these techniques was effective only when there was no risk of a crack being initiated at the root of the welded joints. Further they reported that shot peening lead to 95 % improvement in the fatigue limit whilst the application of TIG-dressing at the weld toes resulted in 65 % improvement. They claimed that the scatter of the fatigue limits was of the order of 50 % and was dependent on the welding procedures, types of loading (tensile or bending) and the site of the initiation of the crack (at the weld toes or at the root of the joint). They suggested that in order to assess the effect of shot peening on the fatigue strength, the residual stresses induced by shot peening could be algebraically added to the mean stress of the loading cycle.

An explanation for the behaviour of PWHT in the improvement of the fatigue strength of the welded joints was given by Bignonnet (1983). He suggested that only the tensile portion of the loading cycle can cause damage to welded joints and structures.

He postulated that when a welded joint with residual stresses is subjected to a zero-to-tensile loading (R = 0), then the effective stress range ($\Delta\sigma_{eff}$) remains unchanged but the mean stress moves to a higher position i.e the effective stress ratio (R_{eff}) changed. On the other hand, if R = -1, the effective stress range ($\Delta\sigma_{eff}$) depends on the level of residual stresses. In the as-welded condition, the tensile residual stresses are sufficiently high to move the stress cycles into the pulsating tensile condition ($R_{eff} > 0$), the effective stress range ($\Delta\sigma_{eff}$) will be equivalent to the nominal stress range ($\Delta\sigma_{eff} = \Delta\sigma_{nom}$). However, in the PWHT condition, residual stress is relatively small or zero, the effective stress range will vary between half of the nominal stress range and the nominal stress range i.e $0.5\ \Delta\sigma_{nom} \leq \Delta\sigma_{eff} \leq \Delta\sigma_{nom}$. As a result, fatigue life of the welded joints increased correspondingly. In the surface treated condition, the effective stress range became smaller as a result of the induced compressive residual stresses for both the loading cases (R = 0 and R = -1). The mean stress moved towards a lower position and only the tensile part of the loading cycles were expected to cause damage to the joints.

2.5.2 Initial overloading and mechanical surface treatments

Techniques to improve fatigue lives such as initial overloading, hammering and shot peening are based on the change of the portion of tensile residual stresses by inducing compressive stresses. The compressive residual stresses in the vicinity of the notch is produced by initial overloading of the specimens so that the localised stress is raised beyond the yield stress of the material and followed by the removal of the load. This mechanism can also be applied for a welded joint if the weld toes are considered as a severe notch. Hammering or shot peening applied to the weld toes introduces the

compressive residual stresses beyond the surface to a depth of 0.6 mm (Bignonnet, 1987). During shot peening, the surface of the joint is peened with projected balls. This process depends on a number of factors including the size and type of the shot. Bignonnet also reported that the force of the impact should be at least 0.75 times the yield stress of the material surface to be treated to achieve cold-working depth of a few tenths of a millimetre.

Masumoto et al (1984) investigated the effect of prestrain and hammer peening on the fatigue of mild steel welded joints. They reported that the fatigue limits of prestrained butt welded joints increased by 13 % to 25 % as the prestrain volume increased by 0.15 % to 4 %. It was found that the increase in tensile prestrain volume was accompanied by an increase in the hardness at the weld toes. They noted that the distribution of residual stress at the weld surface was influenced by tensile prestraining and the residual stress changed from tensile to compressive when the welded joints were prestrained in tension by more than 1 %. They further claimed that the fatigue strength improvement resulting from tensile prestraining was also due to an increase in the hardness of the weld toes. It was concluded that optimum hammer peening condition for improving the fatigue strength of the welded joints was found to be using a hammer tip with a 5 mm radius, hammering at an angle of 40°, 392 kPa percussion air pressure, 400 mm/min travelling speed with a 50 % rising rate. They also attributed the fatigue strength improvement to the change in the shape of the weld profile as a result of the deformation produced by peening.

Maddox (1985) reviewed the results of several other investigators to examine the effect of peening on fatigue strength of welded joints. He reported that a more

significant improvement could be achieved by peening than by either grinding or remelting of the weld toes. Furthermore, the peening techniques were cheaper and often easier to apply. The limitations of both methods i.e shot peening and hammer peening were that they only significantly improved the fatigue strength in the high-cycle fatigue regime (> 10^5 cycles), and when the loadings corresponded to low positive or negative value of the stress ratio. He noted that high-strength materials were more suitable for peening since higher compressive residual stresses could be introduced in these materials. He reported that the optimum conditions for hammer peening mild steel fillet welds were those which resulted in a depth of penetration of 0.6 mm. He recommended that for effective shot peening the depth of deformation had to be controlled and the treated area must be visually inspected. He also suggested that the Almen strip intensity presently used for quality control of shot peening, may not be adequate and additional work would be required to establish a new quality criterion to determine the peening conditions which will give rise to the optimum benefits.

Bellow, Wahab and Faulkner (1986) studied the effect of various surface treatments on fatigue strength of butt welded joints. The surface compressive residual stress field induced by various surface treatments such as single and multiple hammer peening, glass and steel shot peening and stress peening were measured by the "Thomas Method-B" X-ray diffraction technique and used for calculation of fatigue strength of butt welded joints. Their experimental results showed the following levels of compressive surface residual stress were induced by various surface treatments i.e. -62 MPa by glass shot peening, -110 MPa by steel shot peening, -152 MPa by single point hammer peening, -172 MPa by multiple point hammer peening or by stress

peening. From fatigue test results for different surface treatments they found that the fatigue strength of butt welded joints could be improved by up to 50 % after tensile pre-loading, 59 % after glass shot peening, 73 % after steel shot peening, 74 % after single point hammer peening, 83 % after multiple point hammer peening or stress peening.

Robakowski and Czuchryj (1990) studied the effect of overloading in the "St3W" steel welded joints. They found that the fatigue strength of the joints could be increased by overloading from 5 to 12 % depending on the type of the joints and the associated stress concentration factor and overloading levels. They explained that the plastic deformation which occurred at the bottom of the notch was due to overloading. This resulted in a change in the internal residual stress field which produced a substantial increase in fatigue strength of overloaded joints.

Thieuleux (1994) compared the effect of various post-weld finishing treatments techniques with shot peening of welded joints. He reported that when compared with the stress-relieving and static overloading, shot peening was the most cost effective method for increasing the service life of welded joints. He found that a combination of stress-relieving and shot peening could produce an even better improvement in fatigue performance of welded joints.

2.5.3 Modifying the weld toe geometry by TIG dressing or grinding

Zaczek (1984) used the TIG dressing process to improve the fatigue strength of butt welded joints in low alloy high strength steel with a yield stress of 385 MPa. He

designed a welding torch which remelted both weld toes simultaneously during a single welding pass. It was found that by using this technique the weld profile was improved and the weld toe radii were increased by 46 %. As a result, the fatigue strength of the joints was increased when compared with joints prepared using standard industrial procedures.

Gregor (1989) studied the fatigue behaviour of TIG remelted butt and fillet welded joints. He reported that a large transition toe radius of more than 5 mm could be achieved by using TIG remelting. As a result, the stress concentration factor of these joints was reduced by as much as 50 % with the corresponding increase in the fatigue strength. However, he claimed that the degree of fatigue strength improvement that could be achieved by TIG remelting was dependent on the geometry of the original welds. He also noted that the TIG remelting method was only effective for sound joints and it was proven to be ineffective for joints which showed a lack of penetration. In the latter case, the crack initiation site shifted from the regions of the weld toes to the regions of showing the lack of penetration.

Dattoma (1990) surveyed the literature to investigate the effect of several post-weld improvement techniques i.e TIG remelting, plasma remelting, hammering, stress-relieving, weld toe machining, local grinding and the use of special electrodes on the scatter band of fatigue data. He reported that the techniques based on remelting were more effective and could produce improvements in the fatigue limit of approximately 90 %, whilst the use of a special electrode was less effective and produced improvements of approximately 24 %. He concluded that hammering, stress-relieving

and weld toe machining can produce the improvements of 52 %, 34 % and 32.5 % respectively.

Pyle & Pitrun (1990) suggested methods to improve fatigue life of welded joints in which fatigue cracks have been initiated. They noted that if the fatigue crack had not grown too far and it was associated with a stress raiser, then it is possible to remove the initial fatigue damage by remelting or alternatively by grinding.

2. 6 Effect of other Relevant Parameters on Fatigue of Welded Joints

The fatigue of welded joints is complicated by many factors dependent on the welding technique used. The welding process parameters i.e current (I), voltage (U) and welding speed (v) play important roles in determining the quality of the welded joints. Surface or internal defects may be introduced due to a lack of operator skill and by the use of unsuitable electrodes or by an inappropriate edge-cutting preparation. All of these factors affect the weld quality and hence the fatigue strength of welded joints. Research relating to the influence of some of these variables on the fatigue of welded joints is reviewed below.

2.6.1 Influence of the yield stress of the parent metal and the type of electrode

Solumsmoen (1969) investigated the relationship between the properties of the base metal and the type of electrodes on the fatigue strength of welded joints. Fatigue tests were carried out on butt-joints welded with low hydrogen iron powder electrodes and basic electrodes. The specimens were fabricated from two types of structural steel

plate, NV-27 and NV-40, with yield stresses of 272 MPa and 400 MPa respectively. He found that the fatigue behaviour of butt welded joints was unaffected by the yield stress of the parent material or the type of electrode.

Based on a statistical analysis of published data Gurney and Maddox (1972) proposed a revision to the fatigue design rules contained in the British Standard (BS 153). They suggested that for structural steels with the yield stress in the range of 232 MPa to 850 MPa, the fatigue strength under high cycle fatigue was independent of the static strength of the parent material.

On the basis of these two studies the effects of the yield stress of the parent material and electrode type were not considered in the present work.

2.6.2 **Influence of welding processes**

Elliot (1984) compared the fatigue strength of transverse butt welded joints fabricated by Electron Beam Welding (EBW) and by the other welding methods. His experimental results showed that the fatigue strength of EBW joints was superior to Submerged Arc Welded (SAW) joints but comparable with Gas Shielded Arc Welded (GSAW) joints. He explained that this behaviour was due to the variations in the geometry of welded joints fabricated by different welding methods. It suggested that a parametric study of the effect of weld geometry resulted from different welding processes can alternatively represent the effect of the welding process considered.

Guda, Pathak et al. (1988) studied the effect of several welding techniques i.e Manual Metal Arc (MMA) welding and Metal Inert Gas (MIG) welding on the fatigue strength of welded joints subjected to cyclic tensile bending. It was reported that the fatigue strength of MMA welds was higher than that of MIG welds in un-notched specimens, however, this trend was quite reversed if a notch was present. They attributed this behaviour to the higher surface hardness of the MIG weld metal.

2.7 Fracture Mechanics Application in the Fatigue Assessment of Welded Joints

Fatigue failures occur in service components, despite the vast increase in knowledge of the failure mechanism which has taken place during the past several decades. The fatigue behaviour of welded joints and structures is related to the presence of defects such as undercuts at the weld toes, porosity in the weld metal, non-metallic inclusions in the weld metal and a lack of penetration at the weld root etc. A considerable number of research studies have shown that the fatigue crack initiation phase can be reduced by the presence of these defects and the fatigue life of welded joints is determined by the rate of crack propagation. Therefore, the fatigue life of these welded components and structures can be calculated using a suitable fracture mechanics based crack propagation law to predict the number of fatigue cycles necessary to propagate an initial crack to failure (Maddox, 1991). The fracture mechanics based calculations require a knowledge of the stress spectrum applied and the crack propagation properties of the material. The most widely accepted crack growth law is Paris' equation (Paris and Erdogan, 1963) in which the crack growth rate is expressed in terms of the range of the stress intensity factor as:

$$da / dN_p = C. (\Delta K)^m \quad (2.9)$$

where
- a - half the crack length
- N_p - number of cycles needed to propagate the fatigue crack
- C, m - material constants
- ΔK - range of the stress intensity factor ($\Delta K = K_{max} - K_{min}$ where K_{max} , K_{min} are the maximum and minimum values of the stress intensity factor respectively.)

Although Paris' equation adequately describes the fatigue crack growth in the mid-range rate from 10^{-6} mm/cycle to 10^{-3} mm/cycle, it underestimates and overestimates crack growth at higher and lower rate respectively. Subsequently, a number of limitations of this simplistic approach have been recognised. These include:

- A threshold condition, corresponding to stress intensity threshold range (ΔK_{th}) is observed, below which a fatigue crack will not grow.
- Cracks may become non-propagating after growing for some time.
- Overloads may cause retardation of the subsequent crack growth rate.
- High local stress concentrations may lead to local plasticity and the LEFM approach may no longer be valid.
- Environmental effects (e.g. humidity, temperature, corrosive conditions etc.) can markedly affect the conditions for crack initiation and the rate of crack growth.
- The cyclic stress ratio or mean stress can significantly affect the rate of crack growth.

- Short cracks less than a few grains diameter in length or longer cracks containing a more extensive plastic zone do not follow LEFM.
- Crack closure phenomenon, firstly reported by Elber (1970), leads to a reduction in the effective range of the stress intensity factor and hence fatigue crack growth deviates significantly from Eq. (2.9).
- Microstructural effects which are considered to be relatively unimportant in fatigue crack growth predictions can become very significant for short cracks under threshold conditions.

Fracture mechanics have been used to investigate the fatigue behaviour of welded joints in numerous studies. Only some of the most important investigations relevant to the present study are reviewed here.

2.7.1 Effect of various factors on fatigue crack growth rate

(a) *Crack growth rates in various zones of welded joints*

The majority of the published work concentrates on specimens with a machined notch situated in the HAZ and the crack propagation direction is through the thickness of the welded plate. Early research (Kobayashi et al, 1980) reported that for a given level of stress intensity range (ΔK) crack growth rate in the HAZ was lower than that in the base metal but the difference between these crack growth rates diminished as (ΔK) increased. They attributed this behaviour to the difference in the mechanical properties of the HAZ and the base metal i.e it was due to the divergence of the fatigue cracks deviated from the harder phase of HAZ towards the softer base metal.

Maddox (1970) studied the fatigue crack growth rates in the weld metal and the HAZ of welded joints. He reported that crack growth rate in HAZ was similar to or less than that of the weld metal. A similar conclusion about crack propagation properties of the HAZ was reported by Ohta et al. (1982). They found that the crack propagation properties of the HAZ were inferior to those of the base metal with a threshold stress intensity factor about one quarter of that of the base metal. This behaviour was explained by the effect of tensile residual stresses in the regions around the crack tip.

Results of a study by Dowse et al. (1971) showed that the crack propagation rates in weld metal for mild steel did not differ significantly from those in the base metal. This conclusion was confirmed later by Sandifer and Bowie (1978). Additionally, they found that the crack propagation rate in the weld metal of the MIG welded joints in A 537 M steel were comparable with those in the HAZ.

Another study on crack propagation in welded joints in several structural steels by Scierski (1985) suggested a similar rate of crack growth in the HAZ and the weld metal deposited by basic electrodes. The rate was independent of the mechanical properties of the parent metal and the electrode used.

(b) *Effect of residual stress and stress ratios on fatigue crack growth rate*

It is well known that the tensile residual stresses perpendicular to the crack surfaces cause an acceleration in the crack growth rate while compressive residual stresses cause the decrease in the crack growth rate (Maddox, 1991).

Considerable work has been carried out on the effect of stress ratio on the fatigue crack growth rate. In general, an increase in the cyclic stress ratio (R) causes a significant increase in the crack growth rate. However, under alternating cyclic loading (R = -1), the crack growth rate tends to be less than the rate under pulsating tensile loading condition (R>0).

Research studies (Pisarski 1976,1977; Lieurade, 1982) have shown that the applied cyclic stress ratio (R) has an important effect at the low level of stress intensity range (ΔK) and as the stress ratio is increased, the differences in the crack growth rates obtained for the HAZ and the base metal disappear.

(c) *Effect of yield stress of the base metal on the crack growth rate*

The yield stress of the base metal was reported to have some effect on fatigue crack growth (Gurney, 1979). He observed a relationship between the material constants of Paris's equation (namely C & m). He noted that "m" slightly increased and "C" decreased as the yield stress of the base metal increased. He also found that "C" and "m" were exponentially related as $C = A/B^m$, where A, B are constants. It was concluded that this relationship was valid for the weld metal, the HAZ and the base metal for welded specimens with thickness less than 20 mm.

A study by Ohta (1986) showed that under repeated tensile loading (R=0) the crack growth rates of welded joints made from steel with yield stresses in the range of 300 MPa to 550 MPa were comparable. However, an earlier study by Lieurade et al. (1982) suggested that the crack growth rates under the same loading condition (R = 0) decreased as the yield stress of the base metal increased from 280 MPa to

515 MPa. They explained this behaviour of the base metal in terms of the increase of compressive residual stresses within the as-welded test specimens as a result of the increased yield strength of the base metal. They suggested that for a given plate thickness and comparable welding conditions, an increase in yield strength of the base metal lead to higher tensile residual stresses. These were the major reasons for the differences in the crack growth rates of the base metal and the HAZ for 20 mm and 40 mm thick plates. They also claimed that the effect of thickness was a result of the higher welding residual stresses in the thicker plate.

(d) Effect of the loading frequency on crack growth rate

A study by Schmidt and Paris (1973) showed that when tested in air the speed of cyclic loading had an insignificant effect on fatigue crack growth in mild steel over a large frequency range (4 Hz to 100 Hz). They noted that at higher frequencies, crack tip heating tended to occur resulting in residual stress relaxation and softening of the material.

Nihei et al. (1982) studied the effect of frequency, plate thickness and types of testing machine on the fatigue of SM50B butt welded joints. They reported that difference in plate thickness had a marked effect whilst other factor such as specimen width, test frequency and testing machine had an insignificant effect on fatigue of welded joints. They suggested that the effect of plate thickness on the fatigue behaviour of welded joints was due to differences in the weld toe stress concentration factors of joints made of different plate thicknesses (9, 20 and 40 mm).

(e) Effect of microstructures on fatigue crack growth rate

In a welded joint fatigue cracks usually propagate through relatively complex microstructures associated with the diluted weld metal, HAZ and the base metal. However, these microstructures rarely have a significant influence on the fatigue strength of the joint. The rate of crack growth is insensitive to the microstructures except in exceptional circumstances where there is a change in the fracture characteristic such that the normal fatigue process (striation formation) is accompanied by static mode of fracture (e.g cleavage) (Maddox, 1991).

Early research workers assumed that microstructures of the weld metal and the HAZ may have a crucial role in reducing the fatigue strength of welded joints. However, later research (Maddox 1972, Braid et. al. 1981) has shown that the microstructures of the weld metal and the HAZ have an insignificant effect. These researches noted that the major reason for the decrease in the fatigue strength was due to the presence of severe stress concentrations induced by joint geometries or weld defects.

In the study by Maddox (1972), he found that the microstructure of the HAZ only had an effect on the fatigue behaviour when the crack growth mode was transgranular. However, he noted that the crack growth rate increased significantly if there were areas of intergranular fracture.

Braid et. al. (1981) carried out the crack growth test on specimens with simulated HAZ microstructure in high strength steel HY80. Their results confirmed the insignificant effect of morphology, inclusion levels and HAZ grain size. They did however find that the crack growth threshold increased as the grain size decreased.

(f) Effect of various welding processes on fatigue crack growth rate

Knight (1979) used the relationship proposed by Maddox (1974) to investigate the fatigue strength of submerged arc butt welds (SAW). He found that there was no significant difference between the fatigue strength of butt joints manufactured by SAW and by other welding processes.

Ohta et. al. (1982) investigated the threshold and mid-range fatigue crack growth rate in butt-joints made from 20 mm thick HT80 steel plates. Two series of specimens were fabricated by Gas Metal Arc Welding (GMAW) and by (SAW). They found that for both processes the fatigue strength of welded joints was inferior to that of the parent metal but the different welding processes had no significant effect on the crack propagation properties of the welded joints.

(g) *Effect of the plastic zone at the crack tip and the crack closure phenomenon*

The crack closure phenomenon was first reported by Elber (1970). He reported that when a fatigue crack propagates in a region subject to elastic stress, it leaves in its wake a plastic zone which induces a field of compressive residual stresses. This field of compressive stress at the crack tip leads to a partial closing of the crack during part of the loading cycle. He suggested that the stress intensity factor, a major driving force during crack propagation, was effective only when the crack tip was completely open. This means that the effective range of stress intensity factor should be evaluated from the opening stress intensity factor (K_{op}) (corresponding to the condition when crack tip was completely open) to the maximum stress intensity factor (K_{max}) i.e. $\Delta K_{eff} = K_{max} - K_{op}$. He further reported that by applying this concept, the results for the crack growth rates with various stress ratio (R) are comparable with that obtained

for the base metal. Using this concept, it was found that the crack growth curves (da/dN vs. ΔK) for various stress ratios tend to converge, and (ΔK_{eff}) tends to be equivalent to (ΔK).

From the studies reviewed in this section, it can be concluded that fatigue crack growth law depends on the loading condition, i.e stress ratio and the residual stresses induced by the plastic deformation at the crack tips. However, it is possible to obtain a single curve for the crack growth subject to various stress ratios and residual stress conditions by using the concept of crack closure.

2.7.2 Fracture mechanics approaches for fatigue evaluation of welded joints

(a) Approaches adopted for the use of crack growth laws

At present, the LEFM based calculation procedure is widely accepted for the evaluation of fatigue behaviour of welded joints. In general, Paris' law (Eq. (2.9)) is used subject to the following conditions for the stress ratio (R) and stress intensity factor range (ΔK):

(i) If $K_{min} > 0$ then $\Delta K = K_{max} - K_{min}$ and $R = K_{min} / K_{max}$

(ii) If $K_{min} < 0$ then $\Delta K = K_{max}$ and $R = 0$

It is worth noting that Paris' law (Eq. 2.9) only represents the linear portion of the log (da/dN) versus log (ΔK) curve. At the lower values of the stress intensity range there is a threshold value $(\Delta K)_{th}$ for which cracks grow more slowly than that predicted by Paris' law. However, approaching final fracture, the crack growth rate accelerates as

the maximum value of the stress intensity factor tends to approach towards the value of the fracture toughness of the material ($K_{max} \rightarrow K_{IC}$). This means that the conditions for fatigue crack growth until failure can be presented as:

$$\Delta K_{th} < \Delta K < K_{IC} \tag{2.10}$$

where K_{IC} - fracture toughness of the material in mode I.

Forman et. al. (1967) postulated the following crack growth law incorporating the condition when the maximum stress intensity factor (K_{max}) approached the fracture toughness of the material (K_{IC}):

$$\frac{da}{dN} = \frac{C \cdot (\Delta K)^m}{(1 - R) \cdot K_{IC} - \Delta K} \tag{2.11}$$

Forman's equation (Eq. 2.11) predicted the crack growth behaviour of an aluminium alloy successfully. However, when applied to mild steel (Branco et al., 1976) and alloy steel (Maddox et al., 1978) it over-predicted the crack growth at high (ΔK) as these material are less sensitive to stress ratio.

The work of Elber (1970, 1971) showed that crack closure commonly occurred and hence the effective range of stress intensity factor (ΔK_{eff}) should be adopted. This was equivalent to the stress intensity range due to the part of the loading cycle during which the fatigue crack was completely open. He suggested that for plane stress conditions, the Paris' law had to be modified to the following form:

$$da / dN = C'. (\Delta K_{eff})^{m'} \tag{2.12}$$

where C', m' - material constants

ΔK_{eff} - the effective range of stress intensity factor ($\Delta K_{eff} = K_{max} - K_{op}$)

K_{op} - the opening stress intensity factor when the crack is fully open.

The effective range of the stress intensity factor can also be expressed in terms of the range of stress intensity factor as follows:

$$\Delta K_{eff} = U.\ \Delta K \qquad (2.13)$$

where U is the effective stress range factor and is defined in terms of the maximum stress (S_{max}), minimum stress (S_{min}) and crack opening stress (S_{op}) as: $U = (S_{max} - S_{op})/(S_{max} - S_{min})$.

Research by Lal et al. (1979, 1980) had shown that U was dependent on the cyclic stress ratio (R), the ratio of applied stress to yield stress (S/S_y) and on the cyclic strain hardening exponent (n).

Underwood et al. (1977) studied the effect of idealised residual stress distributions in both notched and cracked specimens. He suggested that when residual stresses are present the following approaches should be adopted for determining the effective range of the stress intensity factor:

(i) $\Delta K_{eff} = \Delta K_{app} + 2K_r$ for notched specimens

(ii) $\Delta K_{eff} = \Delta K_{app} + K_r$ for cracked specimens

Nelson (1982) had successfully applied the superposition approach for residual stresses in welded joints. He suggested that under this condition, the residual stress intensity factor (K_r) should be calculated and added to the K_{max} & K_{min} and the following condition should be adopted:

(i) If $K_{min} + K_r > 0$ then $\Delta K_{eff} = K_{max} - K_{min}$ and $R = (K_{min} + K_r)/(K_{max}+K_r)$

(ii) If $K_{min} + K_r \leq 0$ then $\Delta K_{eff} = K_{max} + K_r$ and $R = 0$

Similar methods have been successfully used by several other authors (Parker 1982; and Glinka, 1986).

Bignonnet et. al. (1984) suggested another approach to include both residual stress intensity factor (K_r) and the crack opening intensity factor (K_{op}) which remains unchanged for any given material as:

(i) If $K_{min} + K_r < K_{op}$ then $\Delta K_{eff} = K_{max} + K_r - K_{op}$

(ii) If $K_{min} + K_r > K_{op}$ then $\Delta K_{eff} = K_{max} - K_{min}$

(b) Application of fracture mechanics based approaches

Gurney and Maddox (1972) used fracture mechanics to study the fatigue strength of welded joints. They suggested that the fatigue strength at $2x10^6$ cycles was reduced by a factor of approximately 81.5 % when the type of loading switched from pulsating tensile to half tensile loading. Further, the slope of the S-N curves predicted for the lower classes of welded joints i.e D to G (British Standard: BS 5400) is consistent with fatigue crack propagation data. They suggested that the whole fatigue life of

welded joints consists only of crack propagation from a pre-existing small crack-like defect; and the slope of the S-N curve could be considered to be equivalent to the material parameter (m) in the Paris' equation (Paris and Edorgan, 1963).

Lawrence (1973) developed a crack propagation model for perfectly symmetrical double-V butt-welds. He used finite element analysis to calculate the stress field along the plane of the crack for varying weld bead geometries (angles θ and ϕ). Paris' equation and Emery's solution for the stress intensity factor of an edge crack in a semi-infinite body subject to non-uniform arbitrary system of internal stress (Emery et al, 1968) were used in the calculation. He found that the different weld geometries influenced the crack propagation life by as much as a factor of three but the material properties and initial crack size had a much larger effect. He found good agreement between his predicted and fatigue test results for A 36 and A 441 steel weldments. He suggested that for these materials, the crack initiation period was relatively short and could be ignored in calculations based on fracture mechanics. One of the difficulties of his model was that it required an adjustment for the initial crack length in order to fit the theoretical and experimental curves.

Glinka (1979) used the superposition principle to predict the effect of residual stresses on the fatigue behaviour of welded joints assuming that the residual stresses did not diminish under cyclic loading. He argued that even though this assumption over-estimated the effect of residual stress, it was reasonable from a practical point of view and gave satisfactory results. He used Kanazawa's weight function (Kanazawa et al., 1961) to calculate the residual stress intensity factor (K_r) and Forman's crack growth equation (Eq. (2.11) (Forman et. al., 1967) to predict the fatigue life. He claimed that

the effect of residual stresses was dependent on the levels of applied load. He concluded that higher level of the applied load produced a less significant effect on the residual stresses since a higher degree of residual stress relaxation occurred.

Bokalrud (1979) carried out a finite element analysis on the effect of internal defects in butt welds. He compared the number of cycles during crack propagation of joints pre-cracked with 0.1 mm crack at the weld toe or at the root. He reported that the critical crack size for a weld root defect was a function of the plate thickness and flank angle. Under this size, the weld root crack had insignificant effect during fatigue loading as an active crack was initiated at the weld toe.

Maddox (1988) proposed an extensive revision to the fatigue clause: BSI PD 6493 (British Standard BS 5400) based on the fracture mechanics method and the fatigue crack growth data available in the literature. Several recommendations for fatigue assessment of welded joints and structures were:

- The magnitude of tensile residual stresses in welded structures is of the order of 25 % of the yield stress of the parent material
- A sharp undercut at the weld toes deeper than 1.0 mm should be considered as a planar flaw and assessed using a fracture mechanics approach
- The Paris' equation is recommended for calculation of fatigue life of welded joints particularly when the initial crack size is relatively large. Values of material constants in Paris' equation m=3 and C= $3x10^{-13}$ were recommended for crack growth in ferritic steels with a yield stress up to 600 MPa (in air).
- A new relationship for the fatigue crack growth threshold representing 97.9 % probability of survival for ferritic and austenitic steels was recommended:

$$\Delta K_{th} = 170 - 214xR \ [N.mm^{-3/2}] \quad \text{for } 0 \leq R \leq 0.5$$

$$\Delta K_{th} = 63 \ Nmm^{-3/2} \quad \text{for } R \geq 0.5$$

Gurney (1991) investigated the effects of joint geometry on non-load-carrying fillet welded joints using LEFM calculations. A series of fatigue tests were conducted for a range of weld joint geometries with differing thicknesses of stressed members and attachment lengths. In his calculations, he assumed an initial weld toe defect of 0.15 mm and 0.5 times plate thickness as a criterion for final failure. Four loading cases were considered covering axial loading and bend loading. Two crack models i.e straight fronted edge crack and semi-elliptical surface crack were used. He claimed that the fatigue strength of non-load-carrying fillet welds was dependent on both thickness of the stressed member and the attachment length. Under these conditions, the fatigue strength of a given thickness decreased with increasing attachment length until a certain value. Further increases in attachment length produced no further reduction in the fatigue strength. Also the fatigue strength in bending was consistently higher than axial loading although the fatigue strength was still affected by both the plate thickness and the attachment length. He concluded that the results of these fracture mechanics calculations were very sensitive both to the assumed values of the material constants in Paris's equation and the form of the initial weld toe defects.

Janosch et al. (1991) used LEFM and finite element analysis to investigate the effect of lack of penetration in fillet welded joints in E-364 steel under cyclic tensile and bending loads. They used Paris's crack growth law and Sih's strain energy failure criterion (Sih, 1980) to model the crack paths for the single and multiple failure modes which exist at the weld toes and the weld root. They reported that the

propagation phase of short cracks (0.05 mm to 1.0 mm) could account for 30 % to 90 % of the fatigue life of fillet welded joints. The geometrical parameters of fillet welded joints and the evolution of the shape of the crack front were considered in this model. However, the effects of residual stresses and combined loadings were not taken into consideration.

Hentschel (1992) demonstrated that fracture mechanics can be successfully used to model the fatigue behaviour of fillet welded joints in box girder using crack propagation calculations. Using suitable input data for the initial crack size, crack geometry, loading components, residual stress condition and crack propagation properties of the material he predicted the results which lay within the experimental scatter band.

Hobbacher (1992) reviewed the International Institute of Welding (IIW) codes for fatigue design of welded joints. The recommendations in the IIW codes were based on the assumption that the amplitude of the stress in a welded joint and the number of loading cycles have the most pronounced effect on the fatigue strength of weldments and that a welded joint could be considered as a design notch or a manufacturing defect. The codes do not include the effect of stress ratio as they were formulated for large steel welded structures with residual stresses of magnitude of the yield stress. Under these circumstances the fatigue strength is generally independent of the stress ratio of the applied stresses.

In addition, he reported that the codes stated that the fatigue strengths of a large range of materials with yield strengths up to 700 MPa were not dependent on the

static strength of the base metal. The codes recommend the use of Paris's law (with m=3 and $C=3x10^{-13}$) for evaluating the fatigue strength of 28 types of welded joints and considers the concepts of the stress intensity threshold ($\Delta K_{th} = 190 - 144\ R$ and $(\Delta K_{th}) \geq 62$).

Maddox (1993) reviewed fatigue assessment methods for welded joints and structures including fatigue design rules, fracture mechanics calculations and sources of error in their application. He pointed out that apart from the weld toe geometry due to irregular shapes of the weld bead, welding flaws acted as pre-existing cracks and could in effect eliminate the fatigue crack initiation period. He reported that ferritic steels are insensitive to the fatigue behaviour of welded joints, since the crack growth dominates the fatigue life and the crack growth rate is not influenced by material properties. However, he noted that the fatigue crack initiation can be strongly influenced by material properties. Therefore, the adoption of a high-strength steel for extending fatigue life is not a practical solution. He concluded that if reasonable assumptions for input parameters i.e a_i, a_f and C, m in Paris's equation are made, the satisfactory results for fatigue assessment of welded joints can be achieved using fracture mechanics based calculations. Furthermore, this would allow for the conclusion of more detailed information about the weld geometry parameters.

2.8 Conclusions from the Literature Review

The following conclusions can be drawn from the above literature review:

- Considerable research has been conducted on various individual parameters of fatigue of welded joints. However, none has considered the combined effect of these parameters on the fatigue of butt welded joints in structural steels.
- It has been found that the fatigue strength of a welded joint decreases as the plate thickness increases because the effect of plate thickness is greatly affected by the stress concentration factors. The effect of weld geometry parameters i.e weld toe radius, flank angle and plate-edge preparation angle (Fig. 2.1) have been ignored during the experimental investigations on the effect of plate thickness.
- The weld toe radius significantly affects the fatigue strength of a welded joint. The fatigue strength of a welded joint increases as the weld toe radius increases.
- Small cracks in the early stages of fatigue crack propagation grow rapidly in the high stress concentration field at the weld toes. The propagation phase of the short cracks of the order of 0.05 mm to 1.0 mm may account for 30 to 90 % of the fatigue life. If a crack has propagated beyond 1.0 mm, its propagation rate is not affected by the stress concentrations at the weld toes.
- Tensile residual stresses in welded joints are detrimental but compressive residual stresses are beneficial for the fatigue behaviour of the welded joints. The influence of low magnitude residual stresses is less significant than that of the notches at the weld toes.
- The TIG (GTAW) dressing, TIG welding (GTAW), pulsed arc TIG welding (pulsed GTAW) subsequently followed by shot peening are considered to be

effective measures for improving the fatigue strength of butt welded joints. GTAW techniques produce a flat weld seam profile while shot peening produces beneficial compressive residual stresses.

- Fatigue behaviour of welded joints in structural steels is not affected by the yield stress of the parent material or the type of electrode. Hence, the fatigue strength of a welded joint is acceptable for the joints in structural steels with the yield strength in the range of 232 MPa to 850 MPa.
- In air, the cyclic loading frequency has an insignificant effect on the fatigue crack growth rate in mild steel. The specimen width and the type of the testing machine has an insignificant effect on the fatigue strength of butt welded joints.
- The fatigue strength of welded joints are affected by the welding method probably due to the variations in the resultant weld geometry.
- The microstructures of the weld metal and the HAZ have little effect on fatigue of welded joints. The major reason for the decrease in the fatigue strength of welded joints is the presence of severe stress raisers induced by joint geometries or weld defects.
- Welding processes have little effect on the crack propagation of welded joints. Crack propagation rates in the weld metal for mild steels do not differ significantly from those in the base metal. The crack propagation rates in weld metal produced by GTAW or basic electrodes is comparable with that of the HAZ.
- Due to the existence of crack-like defects at the weld toes, the fatigue crack initiation phase becomes less significant and the majority of the fatigue life of the welded components is associated with crack propagation. The fatigue life of these welded components and structures can be satisfactorily predicted by using a suitable crack propagation law.

- Fracture mechanics approaches can be effectively used to assess the fatigue life of welded joints. A sharp undercut at weld toes with a length greater than 1 mm should be considered as a planar flaw.
- Using the local stress range instead of nominal stress range for plotting the S-N curve failed to reduce the scatter of the fatigue test results.
- Weld imperfections i.e undercut at the weld toes, axial misalignment or angular distortions are detrimental to the fatigue strength of welded joints. However, if bending is the only type of loading, the misalignments have no effect on the fatigue strength of the joints.
- There is no consistent influence of the stress ratio except for as-welded joints under zero-compression loading ($R = -\infty$). Test results for stress-relieved joints also showed no consistent influence of positive stress ratio ($R>0$). However, results for $R = -1$ were generally higher than those for cyclic tensile loading.
- The crack growth law depends on the cyclic stress ratio (R) and on the residual stresses induced in the test specimens, particularly at the crack tips. It is possible to obtain a single crack growth curve for various stress ratios and residual stress conditions by using the concept of crack opening and closure.

The following Chapter analyses the theoretical bases for the concepts used in the modelling of fatigue behaviour of butt-joints subjected to various parameters. Throughout this analysis due regard has been given to the important conclusions drawn from this literature survey.

Chapter 3

THEORETICAL ANALYSIS

In this Chapter, the Linear Elastic Fracture Mechanics and Dimensional Analysis concepts are reviewed and used for modelling of the fatigue behaviour of butt-welded joints. Numerical procedures to obtain fatigue life and strength of a butt welded joint subjected to various important parameters are discussed.

3.1 Concepts of Linear Elastic Fracture Mechanics (LEFM)

3.1.1 Introduction

The development of fracture mechanics in the past few decades has provided convenient methods for the analysis of fatigue crack growth. Linear elastic fracture mechanics is a powerful tool for the assessment of flaws and cracks found in service and for the investigations of the fatigue of welded joints and structures containing inherent crack-like flaws at the weld toes or roots (Gurney, 1979; Maddox, 1991).

In fracture mechanics, the growth of fatigue cracks may be due to three physical modes of loading. Mode-I is the opening mode in which a crack failure is caused by the pure tensile loading stress and the direction of crack growth is perpendicular to

the applied stress. Mode-II is the shearing or sliding mode in which the crack advances in the direction parallel to the shear stress. Mode-III is the tearing or anti-plane mode. In the present study, only Mode-I is considered for the theoretical analysis and modelling as it is the dominant failure mode in most service conditions (Broek, 1986). The three basic Modes of fatigue cracks are illustrated in Fig. 3.1

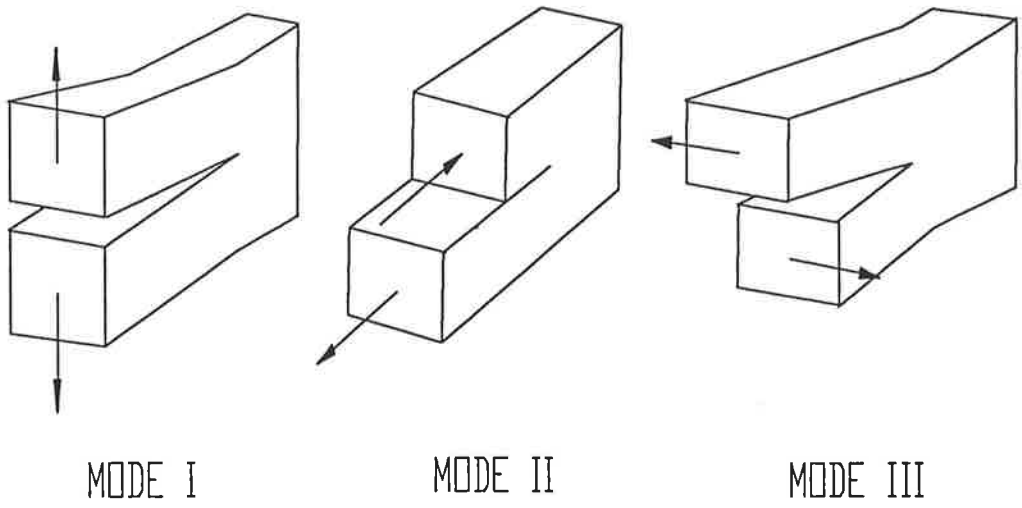

Figure 3.1 Basic Modes of cracks defined in fracture mechanics (Broeck, 1986)

The rate of crack growth under cyclic loading can be expressed in terms of the range of stress intensity factor (ΔK) through Paris's power law (Paris and Erdogan, 1963), as written in Eq. (2.9). If the range of the stress intensity factor (ΔK) of a cracked body is known, fatigue crack propagation life N_p can be calculated by integrating Eq. (2.9) between the initial crack length (a_i) and the final crack length at failure (a_f) as follows:

$$N_p = \int_{a_i}^{a_f} da / C(\Delta K)^m \tag{3.1}$$

The stress intensity factor in mode-I loading has the following form:

$$K = Y.\ S.\sqrt{(\pi a)} \qquad (3.2)$$

where S - remotely applied nominal stress

Y - dimensionless geometry-configuration factor which is a function of crack size, specimen geometry and loading condition i.e Y = f(a/W, loading mode); W - the width of the cracked body

The stress intensity factor for welded joints in Mode-I can be expressed as follows (Maddox, 1991):

$$K = M_k.\ Y_o.\ S.\sqrt{(\pi a)} \qquad (3.3)$$

where Y_o - stress intensity geometry-configuration factor for a finite cracked flat plate or flush-ground welds

M_k - stress intensity magnification factor induced by weld profile geometries ($M_k = Y / Y_o$) and also dependent of crack lengths ($M_k = f(a)$).

Several numerical methods are available for the calculation of elastic stress intensity factor at the crack tip in a finite plate with a particular crack geometry and subjected to certain loading conditions (Parker, 1981). Various solutions for the stress intensity factor can be found in the literature or in handbooks (Sih, 1973; Tada et al. 1973). However, these solutions are limited to certain crack geometries (size & shape), type of specimens and loading conditions.

Using Eq. (3.4) the stress intensity factor for a cracked welded plate can be evaluated if the solution for M_k is known. Some 2D-solutions for cracks at the weld toes of fillet and butt welds are available (Gurney and Johnston, 1979; Smith and Hurworth, 1984). These solutions were obtained by modelling welded joints of various weld profiles with edge-cracks at the weld toes. Recommendations were made in the proposal for revision of BSI PD 6493 (Maddox, 1988) for the use of the 2D-M_k in the assessment of fatigue of welded joints. However, in practice, weld toe flaws and fatigue cracks usually adopt a semi-elliptical shape (Maddox, 1991; Pang 1993) i.e using 2D-M_k in fatigue-fracture mechanics calculations and leads to conservative predictions. Therefore, this method is recognised as an interim approach when three dimensional (3D) solutions for M_k for actual semi-elliptical surface cracks at the weld toes become available (Pang, 1993).

Most of the available solutions for the stress intensity factors of cracked plates either are empirical or approximate solutions. They are not suitable for the advanced modelling of the fatigue of welded joints subjected to a number of parameters e.g weld joint geometries, residual stresses and loading conditions. Therefore, in the present work, an approach for the calculation of the stress intensity factor for a semi-elliptical weld toe surface crack which takes into account the weld geometry, residual stresses and loading conditions was developed using the weight function technique and the superposition principle. More specific details about the weight function technique are discussed in the next section.

3.1.2 Calculation of the stress intensity factor for semi-elliptical surface cracks in butt welded joints.

The behaviour of fatigue cracks at the weld toes can be satisfactory simulated by a semi-elliptical crack model, and this crack model has been adopted in the present study. Figure 3.2 describes the geometry of a weld toe semi-elliptical surface crack initiated at the centre of a butt welded plate under constant amplitude axial loading (where "c" and "a" are half of the major and minor axes of the ellipse respectively, "x" and "y" are the through-thickness and along the plate width directions, "b" and "h" are half the width and length of the welded plate, "r' " is the tip radius at the undercut, "t" is the plate thickness, "r" is the weld toe radius , "θ" is the flank angle, "ϕ_o" is parametric angle of the ellipse, "ϕ" is the edge preparation angle and "S" is the nominal axial loading).

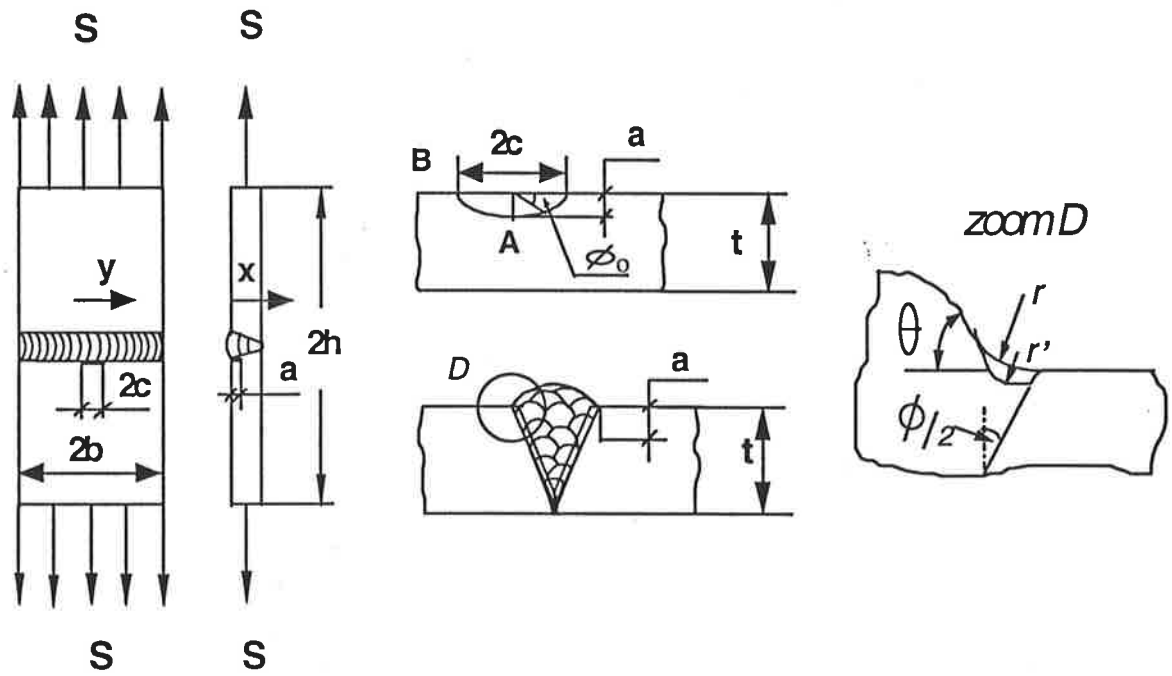

Figure 3.2 A semi-elliptical weld toe surface crack model in a butt welded joint

A new method for calculation of the stress intensity factor for a semi-elliptical surface crack in butt joints was developed in this study and is described here. However, before deriving this new method, the weight function technique used for the calculation of the stress intensity factor for edge and central through-thickness cracks in butt-joints is described.

(a) Weight function technique for calculation of stress intensity factor

Bueckner (1970) demonstrated that a particular function, termed the "Bueckner weight function", is a property of a given crack geometry and is independent of the loading condition. This weight function may be used in the derivation of the stress intensity factor solution provided that the details of the crack line loading are available. The stress intensity factor solutions can be obtained using the following general expression (Parker, 1981):

$$K_I = \int_a p(x).m(a,x)dx \tag{3.4}$$

where p(x) - the stress distribution along x-axis in an uncracked body

m(a,x) - the weight function

a - the crack length

Using this technique the solutions for stress intensity factors under arbitrary loading condition can be found provided p(x) and m(a,x) are known. An illustration of the weight function technique used for calculation of an edge crack in a butt joint is shown in Fig. 3.3. Various crack models in a finite plate and butt joints are shown in Fig. 3.4.

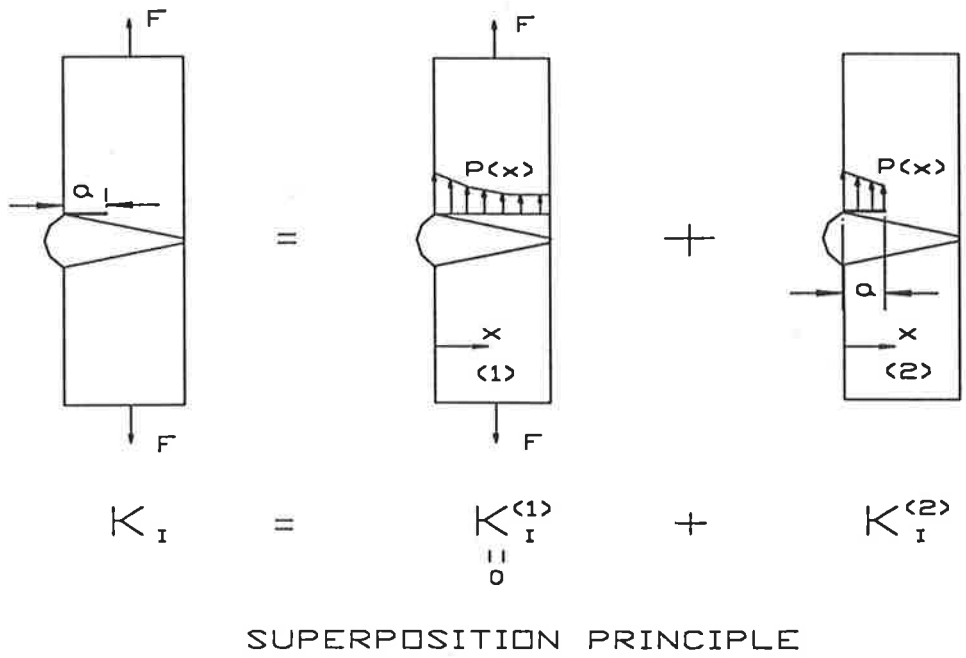

Figure 3.3 The weight function technique used for the calculation of stress intensity factor for an edge crack in a butt welded joint.

In the present study, Bueckner's weight function for an edge crack in a finite plate (Bueckner, 1970) and Kanazawa's weight function for a central through-thickness crack (Kanazawa et al, 1961) were used to obtain the solutions for stress intensity factor subject to the corresponding crack geometry as:

$$K_{ed} = 2.\int_o^a S(x).m(a,x).dx \tag{3.5}$$

$$K_{cen} = 2.\int_o^c S(y).G(c,y).dy \tag{3.6}$$

where K_{ed} - the stress intensity factor for an edge crack (Fig. 3.4)

K_{cen} - the stress intensity factor for a central through- thickness crack (Fig. 3.4).

a - crack length for the edge crack (Fig. 3.4).

c - half crack length for the central through-thickness crack (Fig. 3.4).

S(x), S(y) - the local stress distributions along potential crack directions (x) and (y) (Fig. 3.4).

m(a,x), G(c,y) - Bueckner's and Kanazawa's weight functions (Appendix B).

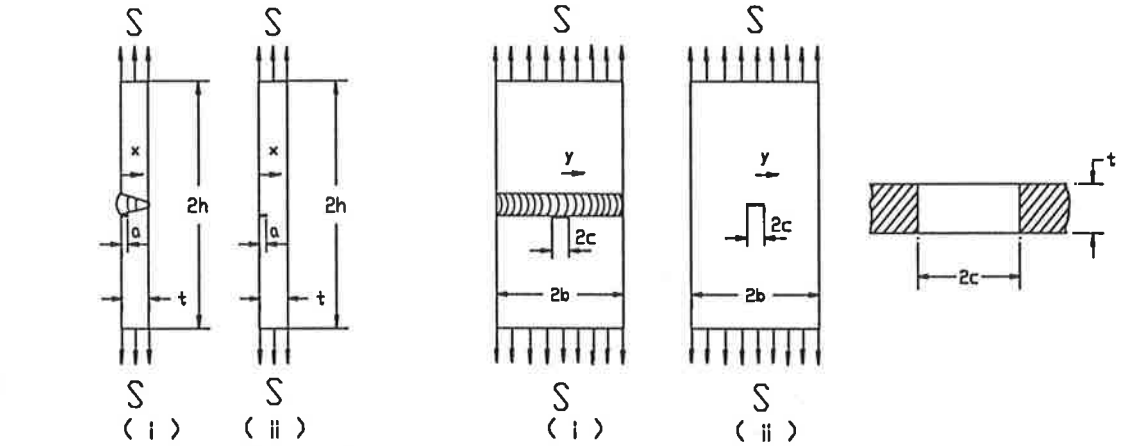

Figure 3.4 Various crack models for a butt welded joint (i) and a finite flat plate (ii)

As S(x) and S(y) are the local stress distributions along potential crack line directions (x) and (y) (Fig. 3.4), each of them should be a resultant stress of the (i) residual

stresses and (ii) the local stresses that are induced by the weld geometry and external loading condition in the corresponding direction. Consequently, based on the superposition principle the following relationships which accounted for weld geometries, residual stresses and combined loading conditions (axial and bending) were derived for butt joints as:

$$S_w(x) = S_{w,a}(x) + S_{w,b}(x) + S_{w,r}(x) \tag{3.7}$$

$$S_w(y) = S_{w,a}(y) + S_{w,b}(y) + S_{w,r}(y) \tag{3.8}$$

where $S_w(x)$, $S_w(y)$ - the range of the local stress along the potential crack line in directions (x) and (y), respectively

$S_{w,a}(x)$, $S_{w,b}(x)$ - the stress components due to the axial load and the bending load in the (x)-direction, respectively

$S_{w,a}(y)$, $S_{w,b}(y)$ - the stress components due to the axial load and the bending load in the (y)-direction, respectively

$S_{w,r}(x)$, $S_{w,r}(y)$ - the stress components due to residual stresses in the (x) and (y)-directions, respectively

Since it is assumed that the butt weld profiles along the (y)-direction are unchanged, the local stress distributions at the surface due to weld geometries and loading conditions in this direction are also unchanged (Fig. 3.4). Hence, the following relationships can be derived:

$$S_{w,a}(y) = S_{w,a}(x=0) = \text{const}$$

$$S_{w,b}(y) = S_{w,b}(x=0) = \text{const}$$

Consequently, the equations (3.8) and (3.9) can be rewritten in terms of the stress concentration factors $K_{t,a}(x)$ and $K_{t,b}(x)$ as follows:

$$S_w(x) = S_A\,(K_{t,a}(x) + K_{t,b}(x).\,R_{ba} + S_{w,r}(x) / S_A\,) \tag{3.9}$$

$$S_w(y) = S_A\,(K_{t,a}(0) + K_{t,b}(0).\,R_{ba} + S_{w,r}(y) / S_A\,) \tag{3.10}$$

where $K_{t,a}(x)$, $K_{t,b}(x)$ - the local stress concentration at a distance (x) from the weld toe due to axial and bending loads ($K_{t,a}(x) = S_{w,a}(x) / S_A$ and $K_{t,b}(x) = S_{w,b}(x) / S_B$)

S_A - axial nominal stress range

S_B - bending nominal stress range

R_{ba} - ratio between bending and axial nominal stress ranges ($R_{ba} = S_B / S_A$)

From the above, the stress intensity factors for a crack in a butt-joint as a function of weld geometries, residual stresses and the combined loading conditions (axial and bending) can be calculated using Eqs (3.5) to (3.10). Hence, Eqs (3.5) and (3.6) can be rewritten in the following form:

$$K^w_{ed} = 2.\int_o^a S_w(x).m(a,x).dx \tag{3.11}$$

$$K^w_{cen} = 2.\int_o^c S_w(y).G(c,y).dy \tag{3.12}$$

where K^w_{ed} - stress intensity factor for an edge crack in a finite welded plate (Fig. 3.4a)

K^{w}_{cen} - stress intensity factor for a central through-thickness crack in a finite welded plate (Fig. 3.4b)

(b) *A new approach for calculation of stress intensity factor of a semi-elliptical surface crack in butt joints*

It was shown in the previous section that Eqs (3.11) and (3.12) provide the solutions for edge cracks and central through-thickness cracks which allow for residual stress, weld geometries and loading conditions. However, the solution for a semi-elliptical surface crack under similar condition can not be obtained using the same technique since no weight function for semi-elliptical surface cracks is available. Therefore, a new approach has been developed in this study to tackle this problem.

This new approach is based on the known solutions of stress intensity factors and assumes that there is a "similarity effect" between the stress intensity values of a notched and an un-notched bodies due to various crack shapes. Therefore, the ratios of stress intensity values for notched and un-notched bodies are the same for surface cracks, edge cracks or central through-thickness cracks (Fig. 3.4). This assumption has been recognised by other researchers (Niu and Glinka 1989, Foth et. al. 1986).

If a welded joint is considered as a notched body due to the stress concentration being raised by the weld profile geometry when the following equations can be derived:

$$K^{w}_{sc,A} / K_{sc,A} = K^{w}_{ed} / K_{ed} = M^{A}_{k,eff} \quad (3.13)$$

$$K^{w}_{sc,B} / K_{sc,B} = K^{w}_{cen} / K_{cen} = M^{B}_{k,eff} \quad (3.14)$$

where $K^{w}_{sc,A}$ - stress intensity factor at point A for a semi-elliptical surface crack in a welded plate (Fig. 3.4c)

$K^{w}_{sc,B}$ - stress intensity factor at the surface front (point B) for a semi-elliptical surface crack in welded plate (Fig. 3.4c)

$K_{sc,A}$ - stress intensity factor at point A for a semi-elliptical surface crack in a flat plate (Fig. 3.4c)

$K_{sc,B}$ - stress intensity factor at the surface front (point B) for a semi-elliptical surface crack in a flat plate (Fig. 3.4c)

$M^{A}_{k,eff}$ - the effective stress intensity magnification factor induced by weld geometry, residual stress and loading conditions in the through-thickness (x -direction) at the deepest point A.

$M^{B}_{k,eff}$ - the effective stress intensity magnification factor induced by weld geometry, residual stress and loading conditions in the plate width (y-direction) at the surface crack front point B.

From Eqs. (3.14) and (3.15) the stress intensity factors for a semi-elliptical weld toe surface crack (Fig. 3.4c) at the deepest point of the crack front (point A), and at the intersection of the crack front with plate surface (point B) can be calculated if the stress intensity solutions for a semi-elliptical surface crack in a finite flat plate and the values of $M^{A}_{k,eff}$ and $M^{B}_{k,eff}$ are known.

An empirical solution for the stress intensity factor of a semi-elliptical surface crack in the centre of a finite plate (Figure 3.4c) in Mode-I loading is provided by Newman and Raju (1981). This was derived from a systematic curve-fitting from their 3-D finite element results. The Newman-Raju's solution has been successfully applied by

many investigators in fatigue crack growth studies and satisfactorily correlates the predicted and experimental results for crack growth observed by Pang (1993). Therefore, this solution was used in the present study to obtain the solutions for the semi-elliptical surface cracks at the weld toes of butt-joints.

The Newman-Raju's solution for the stress intensity factor of a semi-elliptical surface crack at the centre of a finite plate as described in Fig. 3.4c, in Mode-I loading can be expressed as:

$$K_{sc} = S.\sqrt{(\pi a/Q_{sec})}.F(a/t, a/c, c/b, \phi_o) \quad (3.15)$$

where K_{sc} - stress intensity factor of a surface crack in a finite plate

Q_{sec} - shape factor for an elliptical surface crack

($Q_{sec} = 1 + 1.464\,(a/c)^{1.65}$ for $a/c \leq 1.0$)

F - stress intensity boundary correction factor

a/t - ratio of crack depth to plate thickness

a/c - aspect ratio of an elliptical surface crack

c/b - ratio of crack length at the surface to plate width

ϕ_o - parametric angle of the ellipse

Using Eqs (3.5) to (3.15) the solution for the stress intensity factors for the semi-elliptical surface cracks at the weld toes of welded joints at the deepest point of crack front (point A) and at the intersection of the crack front with the plate surface (point B) (Fig. 3.2) taken into account of the effect of weld geometry, residual stresses and the combined loading conditions can be obtained.

3.1.3 Application of LEFM for modelling of the fatigue behaviour of butt joints

In the present study, a semi-elliptical surface crack with an aspect ratio of a/c = 0.2 (Fig. 3.2) is assumed to be located at the weld toe as a result of weld toe undercut of the order of 0.15 mm (a_i = 0.15 mm). This assumption was based on the results of studies carried out by Harrison (1974) and Maddox (1991) on fatigue cracks in welded ferritic steel joints. These cracks propagated from flaws which ranged in depth from 0.05 to 0.5 mm, with an average of 0.15 mm. As a result, the fatigue life of the welded joints was considered as number of cycles needed for the already initiated semi-elliptical surface crack to propagate through the thickness of the welded plate.

Stress intensity factors due to residual stress distributions in welded joints under particular conditions (i.e as-welded or post-weld treated conditions) can be calculated using Bueckner's weight function technique. In the present study, various levels of the residual stress field induced by different post-weld surface treatments such as single or multiple hammer peening, glass or steel shot peening and stress peening and the as-welded conditions were considered. These were based on the results of previous studies on the effect of residual stress (Bellow, Wahab and Faulkner 1986, Maddox 1991 and others). The superposition principle was applied to calculate the effective stress intensity factor as a result of both the applied stress intensity factor and the residual stress intensity factor at a potential crack line as follows (Elber, 1974):

$$K_{eff} = K_{app} + K_{res} \tag{3.16}$$

where K_{eff} - effective stress intensity factor

K_{app} - applied stress intensity factor depending on the weld geometries and loading conditions

K_{res} - residual stress intensity factor

The effect of combined loadings induced by weld imperfections, such as misalignment or angular distortion, was considered in the present study by adopting the relationships for the induced stress concentrations as previously reported (i.e Eqs. (2.4) to (2.7)). Consequently, Eq. (3.16) can be rewritten as follows:

$$K_{eff} = K_A + K_B + K_{res} \tag{3.17}$$

where K_A - stress intensity factor due to axial loading

K_B - stress intensity factor due to bending

K_{res} - residual stress intensity factor

Using Eqs. (3.3) and (3.17) , the effective stress intensity factor resulting from the weld geometry, residual stresses and combined loadings can be calculated as:

$$K_{eff} = Y_{o,a} . M_{k,eff} . S_A . \sqrt{\pi a} \tag{3.18}$$

where

$$M_{k,eff} = (M_{k,a} + \frac{Y_{o,b}}{Y_{o,a}} . M_{k,b} . R_{ba} + M_{k,r} . \frac{S_r}{S_A})$$

and $Y_{o,a}$ - stress intensity geometry-configuration correction factor in axial loading for a flat plate

$Y_{o,b}$ - stress intensity geometry-configuration correction factor in bending for a flat plate

$M_{k,eff}$ - effective stress intensity magnification factor induced by weld profile geometry and residual stresses in combined loadings

$M_{k,a}$ - stress intensity magnification factor induced by the weld profile geometry in axial loading

$M_{k,b}$ - stress intensity magnification factor induced by the weld profile geometry in bending

$M_{k,r}$ - stress intensity magnification factor induced by the weld profile geometry and residual stress

S_r - maximum residual stress at the weld toe surface

In the present work, the range of stress intensity in Paris' equation is replaced by the range of effective stress intensity factor (ΔK_{eff}) which includes the effect of all the influencing parameters on fatigue crack growth rate i.e the rate of fatigue crack growth can be described in Paris's equation as:

$$da / dN_p = C. (\Delta K_{eff})^m \qquad (3.19)$$

If the solution for the stress intensity factor K_{eff} is known the fatigue life and fatigue strength of the welded joint resulting from weld joint geometry, residual stresses and combined loading conditions can be evaluated using Eq. (3.18) and (3.19). For the semi-elliptical surface crack model, the rates of crack-growth at both crack front

directions (x and y in Fig. 3.2) were calculated assuming that Eq. (3.19) is valid independently at points A and B at the crack front. It can be rewritten as:

$$da / dN_p = C_A . (\Delta K^A_{eff})^m \quad (3.20)$$

$$dc / dN_p = C_B . (\Delta K^B_{eff})^m \quad (3.21)$$

where a, c - half length of the minor and major axes of a semi-elliptical surface crack at the weld toe (Fig. 3.2)

C_A, C_B - material constants in Paris's equation at points A and B of the crack front ($C_B = 0.9^m C_A$ as suggested by Newman & Raju (1981)).

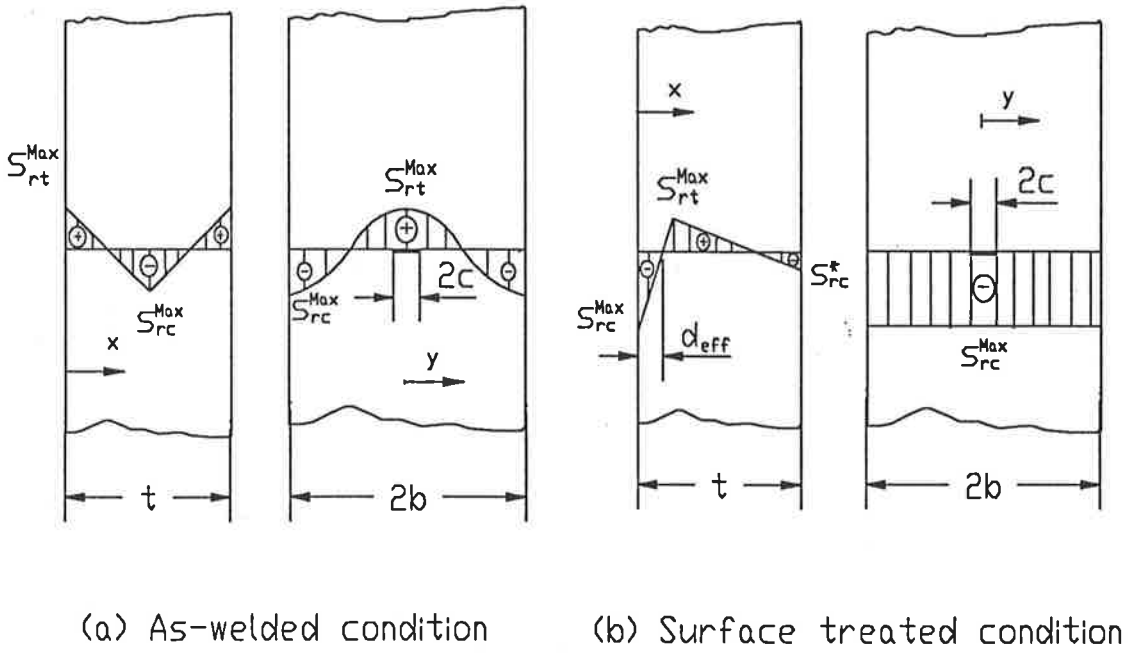

Figure 3.5 Patterns of residual stress fields in butt welded joints

In the present study, during the investigation of the effect of residual stresses, the weld geometry of a butt welded joint is used and assumed that the geometry of the joint is unchanged along the plate width (e.g., r = 1 mm, θ = 30°, t = 6.35 mm). Residual stresses present in the as-welded condition and surface treated condition along (x) and (y) directions were assumed to follow the patterns shown in Figure 3.5 (Gurney 1979, Wahab 1984, Maddox 1991, Lee & Feng 1992).

In the as-welded condition, the pattern of the through thickness residual tensile stress is shown in Fig. 3.5a. The magnitude of the peak compressive residual stress S_{rc}^{max} is assumed to be equivalent to the maximum tensile residual stress and is located at the middle of the plate thickness. This assumption was based on the typical pattern of experimental residual stress distributions in butt joints as reported by Maddox (Maddox 1991) and Lee & Feng (Lee & Feng 1992).

It is well known that the tensile residual stresses in as-welded specimens result from the different levels of heat input during welding process. Theoretically, these tensile residual stresses in welded plates are dependent on the variation of the welding parameters (U, I and v) and can be calculated using heat transfer equations and finite element analysis. However, the calculation of these tensile residual stresses is beyond the scope of the present study.

In the present work, various levels of tensile residual stresses were assumed to be as reported in the literature (Maddox 1991; Lee & Feng 1992, and others). Several levels of maximum tensile residual stresses in as-welded plate were considered in the range from 0.1-1.0 times the yield stress.

In the post-weld surface treated condition, various levels of compressive residual stress (S_r) in butt welded joints induced by post-weld surface treatments were considered on the basis of the available experimental data (Wahab, 1984). The residual stress distribution through the plate thickness after various post-weld surface treatments was assumed to follow two linear paths. These paths range from the peak compressive residual stresses at the treated surfaces to the peak tensile residual stress at a certain depth, then from this point it falls back to the compressive stress region corresponded to the other untreated surface (Fig. 3.5b). The magnitude of the peak tensile residual stress is half of that of the peak compressive residual stress. This conservative assumption was based on the distributions of the induced compressive residual stresses through the plate thickness reported in several experimental studies (Kim and Diesburg 1982, Nelson 1982, Wahab 1984). Using the above assumption, the peak of the self-balanced compressive residual stress at the opposite side of the treated surface can be evaluated as:

$$S^*_{rc} = S_r \,.(t-3.d_{eff}) \,/\, (2.t-3.d_{eff}) \qquad (3.22)$$

where S_{rc}^* - the peak of the self-balanced compressive residual stress at the opposite side of the treated surface (Fig. 3.5)

d_{eff} - effective depth of the surface treatment due to compressive residual stress field (Fig. 3.5)

t - plate thickness of the welded joint

The equations describing the residual stress distribution in as-welded and post-weld surface treated condition assumed in the present study are given in Appendix B.

With the above assumptions the stress intensity magnification factors $M^{A}_{k,eff}$ and $M^{B}_{k,eff}$ due to the combined effect of weld geometry, residual stresses and loading conditions were obtained from which the values of ΔK^{A}_{eff} and ΔK^{B}_{eff} were calculated. By integrating Eqs. (3.21) and (3.22) simultaneously the fatigue life and fatigue strength of as-welded and surface treated butt joint, subjected to various levels of residual stress were evaluated. The material constant used in Paris' equation were assumed to be m=3 and $C_A = 3x10^{-13}$ mm/cycle as recommended in BSI PD 6493 (1991) and the IIW design code (1992) for a wide range of structural steels. The failure criteria was chosen as the instant when the range of the effective stress intensity factor exceeded the fracture toughness of the material ($\Delta K_{eff} > K_{IC}$), or the depth of the semi-elliptical surface crack in the through thickness direction reached half the plate thickness ($a_f = 0.5t$) (whichever occurred first). A computer program was written to facilitate the numerical procedures discussed above and the Simpson's rule was used for the calculation of the integrals in Eqs. (3.21) and (3.22) as given in Appendix C.

As there are many parameters involved in modelling of the fatigue behaviour of butt welded joints, suitable analytical techniques are required to confine the number of variables in order to obtain the appropriate predictive model. The proven concept of dimensional analysis is used for this purpose. To the best of the author's knowledge, this is the first time that the concepts of dimensional analysis have been used to model the fatigue behaviour of welded joints and structures.

3.2 Concept of the Dimensional Analysis Technique

Dimensional analysis has been widely used as an effective and powerful tool for the analysis of physical problems involving large numbers of variables. Although its application can be found in other engineering disciplines there is no established application of dimensional analysis in welding engineering. In the present study, dimensional analysis has been successfully used to model the fatigue behaviour of butt welded joints due to the combined effect of a large number of variables. A review of the basic concept of dimensional analysis follows.

3.2.1 Basic theoretical concept of dimensional analysis

According to the Buckingham Pi-Theorem (Langhaar, 1967) any physical system can be expressed by a dimensionally homogeneous equation of the following form:

$$\pi_d = k.\pi_1^{k_1}.\pi_2^{k_2}\ldots\pi_n^{k_n} \tag{3.23}$$

where $\pi_d, \pi_1, \pi_2, \ldots, \pi_n$ - the terms for a complete set of dimensionless products

π_d - dependent dimensionless product

$\pi_1, \pi_2, \ldots, \pi_n$ - independent dimensionless products

k - proportional constant

$k_1, k_2, \ldots, k_n$ - constants depending on the values of the respective dimensionless terms.

The method used for determining the component equations (Langhaar, 1967) in Eq. (3.23) is described below.

Data obtained from a set of treatments in which only one π-term is varied, say π_i, while all other π-terms are held constant can be used to find a component equation of the following form:

$$\pi_d = A_i \cdot \pi_i^{k_i} \tag{3.24}$$

where k_i - constants corresponding to various π_i-terms

A_i - new proportional constants resulting from the treatments mentioned above

Equation (3.23) can be rewritten in the following form using the transformation equations:

$$\pi_d = k.f(\pi_1).f(\pi_2)...f(\pi_n) \tag{3.25}$$

where $f(\pi_i)$ (for i = 1,2,..,n) - the transformation functions

Consequently, Eq. (3.24) can be rewritten as:

$$\pi_d = A_i \cdot f(\pi_i) \tag{3.26}$$

From Eq. (3.26) the transformation function $f(\pi_i)$ can be found by plotting the values of π_d vs π_i for each set of data. The explicit form of this transformation function can be obtained by using a standard curve fitting procedure. If the dimensionless product

π_i depends on other dimensionless products e.g. on π_j and π_k, then, in this case, it is impossible to hold the products π_j and π_k constant while varying π_i and Eq. (3.25) becomes:

$$\pi_d = A_i^* . f(\pi_j) . f(\pi_k) . f(\pi_i) \tag{3.27}$$

where A_i^* - new proportional constant

If $f(\pi_j)$ and $f(\pi_k)$ are known, the transformation function $f(\pi_i)$ can then be determined by plotting values of $[\pi_d / f(\pi_j)/f(\pi_k)]$ vs π_i. This means that dimensionless products π_j and π_k can be determined before π_i. Subsequently, all the transformation functions corresponding to Eq. (3.25) can be determined by using the concept of component equations. Finally, the proportional coefficient (k) can be obtained by the least-squares method for all the sets of the data fitted to Eq. (3.25).

In the following section, a dimensional analysis for the prediction of fatigue strength and fatigue life of butt welded joints was carried out and the details of this analysis are discussed below.

3.2.2 Dimensional analysis applied in the modelling of the fatigue behaviour of butt-welded joints

All the relevant parameters which may significantly influence the fatigue behaviour of butt welded joints must be defined in order to find a complete set of dimensionless products. In this study, the fatigue strength of butt welded joints "S" is considered as

a dependent variable subject to the notch effect resulted from weld joint geometry, residual stress and loading conditions. The fatigue strength of flush-ground butt joints "S_o" is considered as an initial condition for the fatigue strength of butt joints and free of any possible notch effect. The value of "S_o" is assumed to be equivalent to the fatigue strength of the base metal subject to the same residual stress state and loading conditions (Maddox, 1991).

The independent variables are divided into four main groups: (a) weld geometry parameters, (b) welding parameters, (c) residual stresses and (d) cyclic loadings. In the present study, a single-V butt welded joint was chosen for the fatigue modelling as its shape is also representative of the double-V and K-butt joints. Also it is used in a wide range of industrial applications e.g pipe lines, pressure vessels and ship construction. The independent parameters are defined as follows:

(a) *Weld geometry parameters*

These include the thickness of the welded plate (t), length of the weld (2b), weld bead height or height of weld reinforcement (h), weld bead width (w), undercut tip radius at the weld toe or the depth of undercut (r'), weld toe radius (r), flank angle (θ) and the joint edge preparation angle (ϕ) (Fig. 2.1).

(b) *Welding parameters*

As stated in Chapter 2 only some of the welding parameters strongly influence the fatigue strength of butt welded joints in structural steels. The static strength of the parent material and the type of electrode used in metal arc welding have little effect on the high-cycle fatigue strength (Gurney 1979; Ohta 1986). Among the welding

parameters: current (I), voltage (U) and welding travel speed (v) are the most important parameters that influence the mechanical and microstructural properties of welded joints. These parameters determine the heat input during welding process (e.g. heat input per unit of length for a single pass welded joint: Q = U. I / v) and as a result, influence the level of induced residual stresses. The effect of welding parameters (U, I and v) on the fatigue strength of butt welded joints can be represented by a single parameter Q - the heat input.

(c) *Post-weld residual stresses at the weld toe*

Many studies dealing with the effect of residual stress in welded structures have shown that the fatigue strength of welded structures can be improved by reducing the effect of tensile residual stress in as-welded components by post-weld heat treatments (Haibach 1978, Berge & Eide 1982, Lieurade 1993) or mechanical surface treatments which induce compressive residual stresses at the surface (Masumoto et al 1984; Bellow, Wahab & Faulkner 1984; Thieuleux 1994). However, in practice the majority of welded steel structures are not suitable for heat treatment and are usually put into service in the as-welded condition. In some cases, mechanical surface treatments are used to improve the fatigue performance of welded joints.

In the present study, the effect of residual stresses was investigated in terms of the magnitude of residual stress at the weld toe surface (S_r). The value of (S_r) may represent either the as-welded tensile residual stress or the induced compressive residual stresses. In the surface treated condition, (S_r) is considered to be an independent variable regardless of the level of heat input "Q". However, in the

as-welded condition, (S_r) is reported to be dependent on heat input (Matsuoka et al 1993).

(d) *Cyclic loading parameters*

Early studies (Gurney 1979, Maddox 1991) showed that cyclic loading parameters such as mean stress (S_m) and stress ratio (R) significantly influence the fatigue test results. However, loading frequency and type of fatigue testing machines has an insignificant effect (Schmidt & Paris 1973, Nihei et al 1982). As mean stress and the stress ratio are interrelated ($S_m = 0.5S(1+R)/(1-R)$) only one of them (R) is considered as an independent variable in the present work.

The ratio of nominal bending loads to nominal axial load (R_{ba}), which represents the combined loading condition (axial and bending) due to misalignment and distortion, is considered to be important and is chosen to be an independent variable. The fatigue strength of a welded joint depends on the number of loading cycles (N), therefore, this parameter is also included in the modelling as an independent variable.

A list of all the relevant variables for the dimensional analysis used in the prediction of the fatigue strength of a butt welded joint is given in Table 3.1. A set of 14 dimensionless products are found from all of these variables and these are shown in Table 3.2.

According to the Buckingham Pi-theorem, dimensionless products can be arranged in the following form:

$$S/S_o = f\,(r'/t,\ r/t,\ \theta,\ \phi,\ t/b,\ h/w,\ w/t,\ S_r/S_y,\ S_y/S_o,\ Q/(S_y.t^2),\ R,\ R_{ba},\ N) \qquad (3.28)$$

Two ratios (w/t) and (h/w) are related to the edge preparation angle (ϕ) and the flank angle (θ) ((i.e $w/t = 2 \tan(\phi/2)$ and $h/w = 0.5\tan(\theta/2)$, (Lawrence 1973)), hence they can be omitted from Eq. (3.28).

The term (S_y/S_o) representing the effect of yield stress of the base metal may also be omitted from Eq. (3.28) due to its insignificant effect on the high-cycle fatigue life (Gurney 1979, Ohta 1986). Therefore, only eleven π-terms need to be considered in the present model and Eq. (3.28) becomes

$$S/S_o = f\,(r'/t,\ r/t,\ \theta,\ \phi,\ t/b,\ S_r/S_y,\ Q/(S_y.t^2),\ R,\ R_{ba},\ N) \qquad (3.29)$$

It is well established for the fatigue S-N curves (BSI PD 6493, 1991) that the slope of the S-N curves is related to the material constant "m" in Paris' equation (Maddox, 1991) such that:

$$S^m . N = A \qquad (3.30)$$

where A & m - are proportional constants

Table 3.1 List of Variables used for Dimensional Analysis in terms of Fatigue Behaviour of Butt Welded Joints (* where M = mass, L = length, T = time)

No	Variables	Symbol	Dimension*
	Dependent:		
1	Fatigue strength of butt welded joints	S	$ML^{-1}T^{-1}$
2	Proportional constant "m" (Eq. 3.30)	m	-
3	Proportional constant "A" (Eq. 3.30)	A	-
	Independent:		
1	Tip radius at the weld toe undercut	r '	L
2	Weld toe radius	r	L
3	Length of the welded joint	2b	L
4	Weld reinforcement height	h	L
5	Weld bead width	w	L
6	Thickness of welded plates	t	L
7	Flank angle	θ	-
8	Edge preparation angle	ϕ	-
9	Fatigue strength of the base metal	S_o	$ML^{-1}T^{-1}$
10	Yield stress of the base metal	S_y	$ML^{-1}T^{-1}$
11	Heat input per unit length of weld per weld pass	Q	MLT^{-2}
12	Residual stress at the weld toe surface	S_r	$ML^{-1}T^{-1}$
13	Cyclic stress ratio	R	-
14	Fatigue life or number of loading cycles	N	-
15	Ratio between applied bending and axial stresses	R_{ba}	-

Table 3.2 Set of Dimensionless Products describing various Parameters used for Modelling the Fatigue Behaviour of Butt Welded Joints

No	π-terms	Description
	Dependent :	
1	$\pi_{d1} = S / S_o$	Normalised fatigue strength of butt welded joint
2	$\pi_{d2} = m / m_o$	Normalised "m" constant (Eq. 3.30)
3	$\pi_{d3} = A / A_o$	Normalised "A" constant (Eq. 3.30)
	Independent:	
1	$\pi_1 = r' / t$	Ratio of undercut tip radius to plate thickness
2	$\pi_2 = r / t$	Ratio of weld toe radius to plate thickness
3	$\pi_3 = \theta$	Flank angle of welded joint geometry
4	$\pi_4 = \phi$	Edge preparation angle for single-V butt weld
5	$\pi_5 = t / b$	Ratio of plate thickness to half the weld length
6	$\pi_6 = h / w$	Ratio of weld reinforcement height to bead width
7	$\pi_7 = w / t$	Aspect ratio of butt weld cross section
8	$\pi_8 = S_y / S_o$	Normalised yield stress of the base metal
9	$\pi_9 = S_r / S_y$	Normalised residual stress at the weld toe surface
10	$\pi_{10} = Q / (S_y.t^2)$	Normalised heat input level used during welding
11	$\pi_{11} = R$	Cyclic stress ratio
12	$\pi_{12} = R_{ba}$	Ratio between applied nominal bending and axial stresses
13	$\pi_{13} = N$	Number of loading cycles

From Eqs. (3.29) and (3.30) it can be seen that "m" and "A" are the functions of the weld geometry, residual stresses, heat input and loading conditions. Therefore, the functions for "A" and "m" can be expressed in the following form:

$$m / m_0 = f_m (r'/r, r/t, \theta, \phi, t/b, S_r/S_y, R_{ba}, R, Q/(S_y.t^2)) \quad (3.31)$$

$$A / A_0 = f_A (r'/r, r/t, \theta, \phi, t/b, S_r/S_y, R_{ba}, R, Q/(S_y.t^2)) \quad (3.32)$$

where $m_0 = 3$ and $A_0 = f(t/b)$ are the values of "m" and "A" in Eq. (3.30) for residual stress-free flush-ground butt joints under axial loading.

Using dimensional analysis and transformation functions as described in section 3.2.1, Eqs. (3.31) and (3.32) can be rewritten as follows:

$$m/m_0 = k_m.f_m(r'/r).f_m(r/t).f_m(\theta).f_m(\phi).f_m(t/b).f_m(S_r/S_y).f_m(R_{ba}).f_m(R).f_m(Q/(S_y.t^2)) \quad (3.33)$$

$$A/A_0 = k_A.f_A(r'/r).f_A(r/t).f_A(\theta).f_A(\phi).f_A(t/b).f_A(S_r/S_y).f_A(R_{ba}).f_A(R).f_A(Q/(S_y.t^2)) \quad (3.34)$$

Once Eqs. (3.33) and (3.34) have been determined, the fatigue behaviour of butt joints subject to combined effect of all the important parameters can be evaluated by substituting values of "m" and "A" into Eq. (3.30).

3.2.3 Description of the dimensionless products obtained for fatigue modelling of butt-welded joints

A brief discussion on the individual dimensionless products and the methodology to obtain various transformation equations corresponding to Eqs. (3.29), (3.33) and (3.34) is described as follows:

(a) Dependent dimensionless products

- The first dependent π_d-terms ($\pi_{d1} = S/S_o$) represents the normalised fatigue strength of butt welded joints. This term is the inverse of the fatigue notch factor or fatigue strength reduction factor ($K_f = S_o/S$). This means that any model which is developed for S/S_o can be used to predict the fatigue notch factor of butt welded joints.

- The second and the third dependent π-terms ($\pi_2 = m / m_o$ and $\pi_3 = A / A_o$) describe how various parameters affect the slope of the S-N curve.

(b) Independent dimensionless products

- The first independent π-term ($\pi_1 = r' / t$) represents the effect of the undercut at the weld toes. This parameter is one of the most important geometrical parameters and it is reported to have a significant role in determining the notch severity (Jubb, 1981 and Petershagen, 1990). As the variation in (r') does not affect any other π-terms, this π_1-term can be investigated by plotting π_d vs. π_1 to find the corresponding transformation function $f(\pi_1)$.

- The second independent π-term ($\pi_2 = r / t$) represents the effect of weld toe radius. This determines the local stress concentrations at the weld toes and is the key parameter influencing the fatigue behaviour of welded joints. The value of this term can be changed either by varying the weld toe radius (r) or the plate thickness (t). As the variation of (r/t) affects the π_1-term, the corresponding transformation function $f(\pi_2)$ is obtained by plotting $\pi_d/f(\pi_1)$ vs. π_2.

- The third independent π-term ($\pi_3 = \theta$) describes the effect of the shape of the weld reinforcement (weld bead) on the fatigue behaviour. As the variation of the flank angle (θ) is independent of the other π-terms the transformation function $f(\pi_2)$ is obtained by plotting the values of π_d vs. π_3.

- The fourth independent π-term ($\pi_4 = \phi$) represents the effect of the edge preparation angle in a single-V butt joint on its fatigue behaviour. The variation of this angle results in the variation of other weld geometry parameters such as weld toe radius (r) and flank angle (θ). Therefore, the transformation function $f(\pi_4)$ is found by plotting the values of $[\pi_d / f(\pi_2) / f(\pi_3)]$ vs. π_4. However, this parameter (φ) was omitted in the later stages of the present modelling because its effect on the fatigue of butt joints was shown to be insignificant.

- The fifth independent π-term ($\pi_5 = t / b$) describes the effect on the fatigue behaviour of the plate thickness (t) for constant weld length or the effect of weld length (2b) for constant plate thickness. The corresponding transformation

function $f(\pi_5)$ is obtained by plotting $[\pi_d / f(\pi_1) / f(\pi_2)]$ vs. π_5 since π_1 and π_2 terms are dependent on the thickness term (t/b).

- The sixth independent π-term ($\pi_6 = h / w$) also represents the effect of weld reinforcement shape. This π-term is related to the flank angle (θ) (Lawrence, 1973) and hence it was not taken into account in the present model.

- The seventh independent π-term ($\pi_7 = w / t$) represents the aspect ratio of the butt joint cross section but was also omitted in the present model as it is similar to that of the edge preparation angle (ϕ) (Lawrence 1973).

- The eighth independent π-term ($\pi_8 = S_y / S_o$) represents the effect of the yield stress of the base metal. However, this term is also omitted in this model as it was reported to have an insignificant effect (Maddox, 1991; and other).

- The ninth independent π-term ($\pi_9 = S_r / S_o$) represents the effect of residual stress. The value of S_r in as-welded condition is closely related to the heat input level Q. However, when post-weld thermal or mechanical surface treatments are applied, S_r becomes independent of the heat input Q. Some of the weld joint geometry parameters (e.g. r', r and θ) are also affected by the post-weld mechanical treatments. Therefore, the corresponding transformation function $f(\pi_7)$ is found by plotting the values of $[\pi_d / (f(\pi_1) / f(\pi_2). f(\pi_3)]$ vs. π_9.

- The tenth independent π-term ($\pi_{10} = Q / (S_y.t^2)$) represents the effect of welding process parameters. If the welded joints are fabricated from plates of the same thicknesses using a structural steel (S_y = constant), then the π_{10}-term depends only on the heat input Q. The value of Q can then be varied by varying one of the welding parameters (U, I or v). However, the variation in the heat input Q also affects the other weld geometry parameters such as undercut tip radius (r'), weld toe radius (r), flank angle (θ) and the levels of the as-welded residual stresses at the weld toe (S_r). Therefore, the transformation function $f(\pi_{10})$ can be found experimentally by plotting the values of $[\pi_d / (f(\pi_1).f(\pi_2).f(\pi_3).f(\pi_5).\ f(\pi_9))]$ vs. π_{10}.

As the level of the as-welded residual stresses at the weld toe (S_r) depends on the heat input levels Q, either the π_9-term or the π_{10}-term may be omitted from Eqs. (3.29), (3.33) and (3.34). In the present study, π_9-term was selected as the preferred variable for the numerical modelling and π_{10}-term was omitted.

- The eleventh independent π-term ($\pi_{11} = R$) represents the effect of the cyclic stress ratio. The cyclic stress ratio (π_{11}-term) is independent of the other previously mentioned π-terms. Therefore, the transformation function $f(\pi_{11})$ is obtained by plotting values of π_d vs. the variation of the π_{11}-term.

- The twelfth independent π-term ($\pi_{12} = R_{ba}$) represents the effect of the combined loading conditions. This term, to some extent, also represents the effect of the induced bending stresses resulting from misalignment and angular distortions in actual welded joints. As it does not depend on the other previously mentioned π-

terms, then the corresponding transformation function $f(\pi_{12})$ is obtained by plotting values of π_d vs. π_{12}-term.

With the above consideration, the equations (3.33) and (3.34) can be rewritten as:

$$m / m_o = k_m . f_m (r'/r) . f_m(r/t) . f_m(\theta) . f_m(t/b) . f_m(S_r/S_y) . f_m(R_{ba}) . f_m(R) \quad (3.35)$$

$$A / A_o = k_A . f_A (r'/r) . f_A (r/t) . f_A (\theta) . f_A (t/b) . f_A(S_r/S_y) . f_A(R_{ba}) . f_A(R) \quad (3.36)$$

Based on Eqs. (3.35) and (3.36) and the dimensional analysis carried out in the previous sections numerical concepts for the present model of the fatigue behaviour of butt welded joint are developed and described in detail in the following section.

3.3 Numerical Modelling Concepts

3.3.1 Methods to obtain various groups of transformation functions

In the present study, an attempt has been made to reduce the number of experiments to minimise expense and time without loosing sight of the main objectives. In Eqs. (3.35) and (3.36), the first five transformation functions represent the effect of weld geometry on the fatigue strength of welded joints. These functions can be obtained by numerical methods if it is assumed that the residual stresses are either zero or remain unchanged, and the combined loading ratio (R_{ba}) and the cyclic stress ratio (R) are kept constant.

In practice, residual stresses in machined and small sized welded test specimens are negligible as a result of stress relieving resulted from machining. If cyclic stress ratio (R) is held constant during the fatigue tests (e.g R = 0), only the effect of weld geometry parameters are significant. The corresponding equations for the prediction of the fatigue behaviour can be rewritten in the following form:

$$m / m_o = k_{mG}. f_m(r'/t). f_m(r/t). f_m(\theta). f_m(t/b) \quad (3.37)$$

$$A / A_o = k_{AG}. f_A(r'/t). f_A(r/t). f_A(\theta). f_A(t/b) \quad (3.38)$$

where k_{mG}, k_{AG} - proportional constants representing the effects of weld joint geometry.

A procedure to calculate the fatigue strength (S) and fatigue life (N) of a butt welded joint due to the variations of weld geometry were developed using LEFM and Finite Element methods. From these values of (S) and (N) using Eq. (3.30) the corresponding values of "m" and "A" can be found. Once the value of "m" and "A" are known the various transformation functions representing weld geometry parameters in Eqs. (3.37) & (3.38) can be obtained.

Further, in the actual welded joints, fatigue cracks are usually initiated at the weld toes, the region of high stress concentration, and propagate through the plate thickness during the fatigue life of the joints (Gurney 1979, Maddox 1991). It is generally assumed in LEFM that a semi-elliptical surface crack is initiated at the center of the welded plate along the weld toes (Fig. 3.2). The modified Paris' equation

(Eq. 3.19) was used to evaluate the fatigue behaviour of butt joints due to variations of all the weld geometry parameters concerned.

The second group of important parameters for modelling the fatigue behaviour related to post-weld residual stresses and are represented by the transformation functions $f_m(S_r/S_y)$ & $f_A(S_r/S_y)$ in Eqs. (3.35) & (3.36). These functions can be obtained by assuming that a residual stress field pattern corresponding to a surface treated or as-welded condition is unchanged for a particular weld geometry. In the present study, residual stress distributions were not experimentally measured but determined from several available experimental studies (Wahab 1984, Maddox 1991, and other). Under a certain loading condition and for a particular weld geometry, the influence of residual stresses on the stress intensity factors is evaluated using the semi-elliptical surface crack model as described above. The superposition principle is applied for residual stress and local stress fields along the potential crack line. Subsequently, the effect of residual stresses on the fatigue strength of the welded joints can be evaluated.

A third group of parameters for the prediction of fatigue strength and fatigue life of butt-welded joints considers the combined loading conditions represented by the transformation functions $f_m(R_{ba})$ & $f_A(R_{ba})$ in Eqs. (3.35) & (3.36). The effect of (R_{ba}) can be evaluated if the level of residual stresses, weld geometry and the stress ratio (R = 0) are held constant whilst varying the value of (R_{ba}).

The remaining transformation functions ($f_m(R)$, $f_A(R)$) in Eqs. (3.35) and (3.36) related to the cyclic stress ratio can be found experimentally from fatigue test results

or by using an appropriate crack growth law which incorporates the effect of stress ratio.

Using these procedures, the experimental and calculated fatigue data are then curve-fitted using a curve-fitting software (TABLECURVE, v.3.03, 1991) to find the corresponding transformations functions in equations (3.35) and (3.36). The proportional coefficients (k_m and k_A) are then found by the standard least squares method. More details about the numerical methods used in the present model are described in the following section.

3.3.2 Numerical methods

The numerical methods used to calculate the fatigue life of butt welded joints for various levels of the stress range, under repeated tensile loading (R=0) and subject to various weld geometries, residual stresses and combined loading conditions are described as follows:

Step # 1. The stress distributions along the potential crack line of various uncracked butt weld profiles under pure axial and pure bending loads are calculated using a finite element package ANSYS 5.0 (Ansys User's Manual, 1992). Several sets of weld profiles were chosen on the basis of the dimensional analysis discussed previously. These are shown in Table B.1 (Appendix B). A typical finite element mesh used for the finite element analysis was generated for each butt weld profile as shown in Fig. 3.6.

Step # 2. A curve-fitting technique was used to find the following representative mathematical expression for the stress distributions along the potential crack line as:

$$S(x)/S = p(x)=(a_1 + a_3.\, x + a_5.\, x^2 + a_7.x^3)/(1+ a_2.x+ a_4.x^2 + a_6.x^3+ a_8.x^4) \qquad (3.39)$$

where $p(x)$ - the local stress at a distance (x) from the weld toe surface along the potential crack line where $p(x) = K_{t,a}(x)$ for pure axial loading or $p(x) = K_{t,b}(x)$ for pure bending load.

S - the remote membrane stress where if P is the applied tensile load and M is the applied bending moment then $S = P / (2tb)$ for pure axial loading or $S = 3M / (bt^2)$ for pure bending load.

a_k - regression constants (for k = 1 to 8)

Step # 3. The range of the effective stress intensity factors corresponding to each level of the stress range, crack geometry, residual stresses and loading conditions was calculated using Eqs. (3.5) to (3.15) as described in section 3.1.2.

Step # 4. The fatigue life and the fatigue strength of butt joints was calculated using the modified Paris' equation (Eqs. (3.20) and (3.21)).

Step # 5. After calculating the fatigue life and fatigue strength of butt welded joints subjected to variations of weld geometry parameters, residual stresses and the combined loadings, the corresponding transformation functions in Eq. (3.35) and (3.36) were found using standard curve fitting techniques.

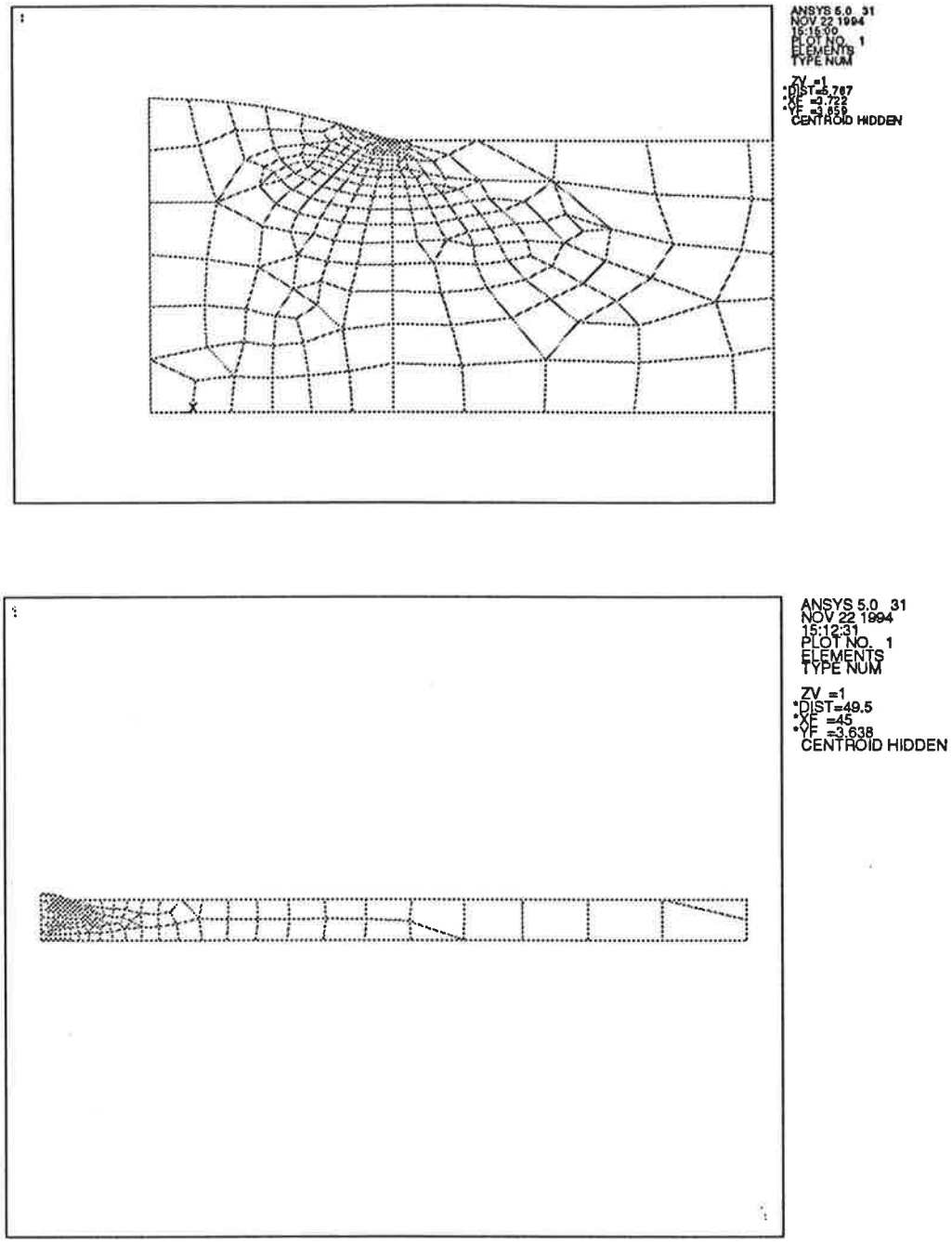

Figure 3.6 Typical finite element meshes generated for a butt-weld profile

All the aforementioned modelling procedures for the prediction of fatigue life and strength of butt joints are summarised in a flow-chart as shown in Fig. 3.7.

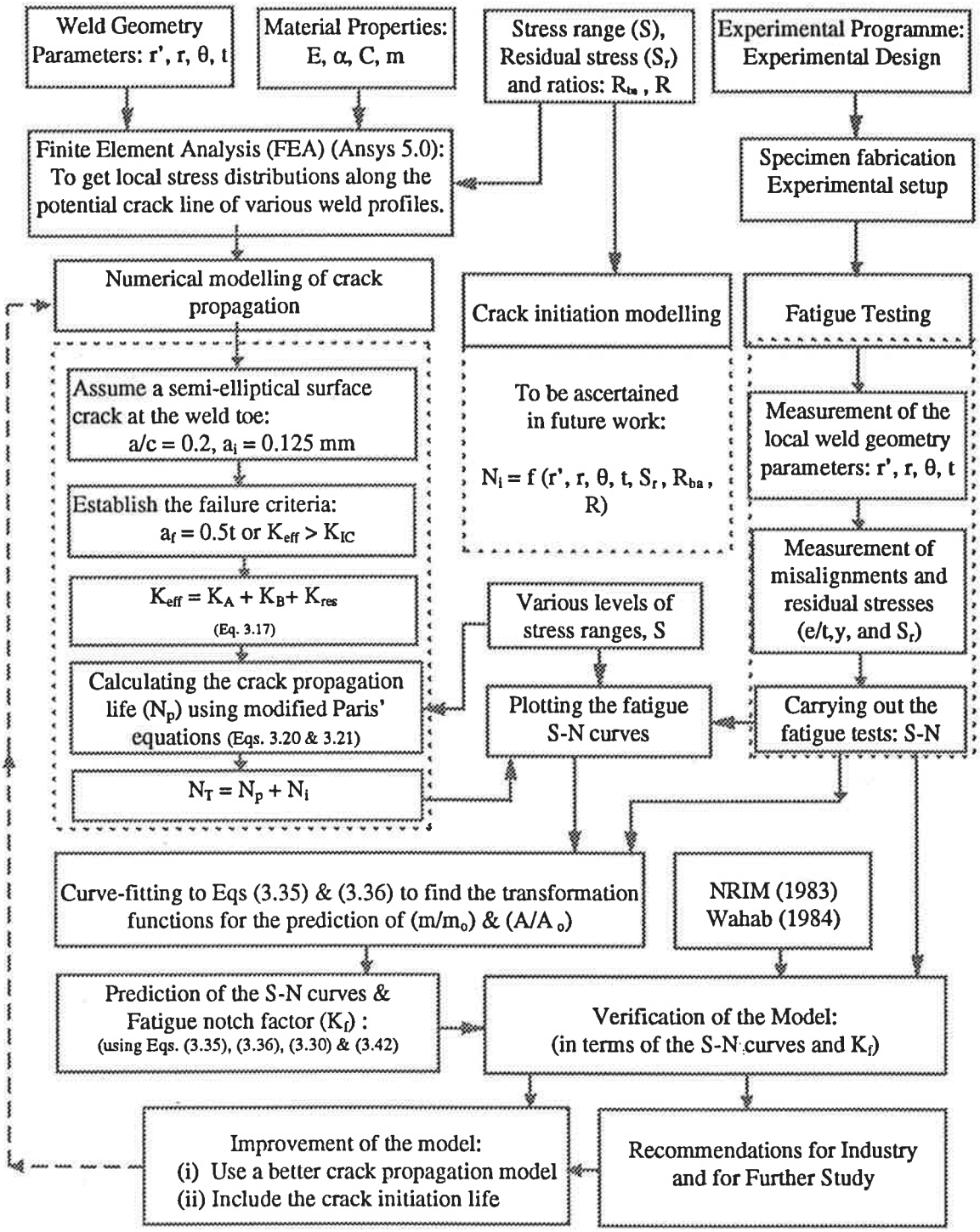

Figure 3.7 General structure for the modelling of the fatigue behaviour of butt-joints.

3.4 Calculation of the Fatigue Notch Factor

In order to assess the influence of the stress concentrations on the fatigue strength it is usually needed to compare the S-N curves of un-notched and notched specimens. The magnitude of the reduction in fatigue strength resulting from the stress concentration factor (K_t) is expressed in terms of the fatigue notch factor (K_f). The fatigue notch factor (K_f) is defined as the ratio of the fatigue strengths of un-notched specimens to notched specimens, obtained under the same test conditions and at the same number of loading cycles.

In general, a material is regarded as more sensitive to a "fatigue notch" if the value of K_f is larger for a given value of K_t. Therefore, to understand the "fatigue notch sensitivity" of welded joints, the value of K_f for various weld geometry parameters, residual stress and the combined loading conditions are calculated in the present study.

Amongst the equations in the literature for the calculation of the fatigue notch factor (K_f) of the notched body the following equation (Peterson, 1959) is one of the most widely used:

$$K_f = 1 + (K_t - 1) / (1 + a^* / \rho) \qquad (3.40)$$

where ρ - the notch root radius

a^* - experimentally determined material parameter

K_t - theoretical elastic stress concentration factor

Another equation for (K_f) (Buch, 1988) is :

$$K_f = K_t \, [(1 - 2.1h / (\rho + \rho_o)] / B \qquad (3.41)$$

where B & h are material constants which are dependent on materials and the type of loading but independent of the notch radius and specimen size e.g B = 1.1, h = 0.25 mm for rolled sheet specimens under pulsating tension and $\rho_o = 6.3\ h / (3-B)$.

It should be noted that both of the above equations do not take into account the variations in the relevant weld geometry, residual stresses and the loading conditions but only the notch root radius (ρ) and (K_t) and are therefore, not suitable for achieving the objectives of the present work. Hence, a new equation for (K_f) which included all of the above factors were developed in this study.

The fatigue notch factor (K_f) is the inverse of the value of the dependent dimensionless product (S/S_o) i.e ($K_f = S_o / S$); therefore, the equations already developed for the dimensionless products listed in Table 3.2 can be used. Alternatively, the following equation for fatigue notch factor can be easily derived from Eq. (3.30):

$$K_f = \left(\frac{A}{N_f}\right)^{\frac{1}{m_o} - \frac{1}{m}} \cdot \left(\frac{A}{A_o}\right)^{-\frac{1}{m_o}} \qquad (3.42)$$

A detailed derivation of this equation is given in Appendix E.

In the present study, the fatigue notch factors due to weld geometry, residual stresses and loading conditions are calculated using Eq. (3.42), (3.35) and (3.36) and are compared with that predicted by Peterson's and Buch's equations i.e Eqs. (3.40) & (3.41).

In the following Chapter, a fatigue testing program was carried out to validate the numerical modelling of the fatigue behaviour of butt-welded joints.

Chapter 4

FATIGUE TESTS

4.1. Introduction

The reliability of the present model can be verified using experimental data available in the literature (NRIM 1983, Wahab 1984). A fatigue testing program of butt welded specimens was carried out to validate the numerical results and was designed to meet the following objectives:

(i) To verify the effects of weld geometry on the fatigue behaviour of butt welded joints as predicted by the present model.

(ii) To obtain fatigue data to verify the predicted fatigue S-N curves and fatigue notch factor (K_f) due to the variations in the weld geometry, residual stresses and combined loading conditions.

Details of the experimental program are described in the following sections.

4.2 Test Specimens and Materials

The welded specimens used for fatigue tests were fabricated from structural steel plate grade 250 (AS 3678) (grade A36, ASTM A568M-88). Small scale specimens were

designed for constant amplitude axial loading fatigue tests according to ASTM Standard E466-82 (ASTM, 1990). The test specimens were machined from the 12 mm thick welded plates which had been fabricated using Submerged Arc Welding (SAW) and Metal Inert Gas (MIG) welding from steel plates with heat input levels ranging from 1.0 kJ/mm to 4.0 kJ/mm to ensure the different shapes of the weld profiles. The direction of welding was perpendicular to the rolling direction of the parent material. The welding parameters used during fabrication of the welded plates are listed in Table 4.1.

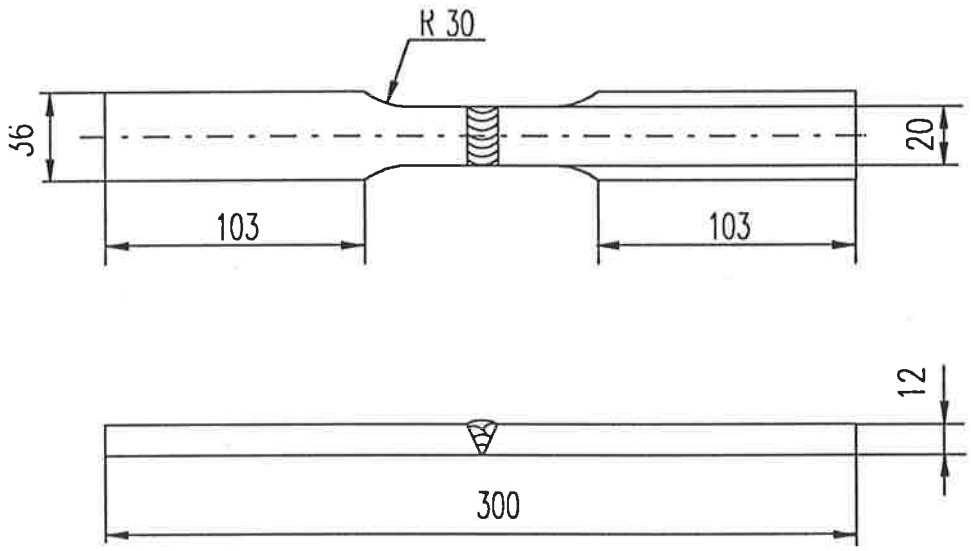

Figure 4.1 Dimensions of the fatigue test specimens (all dimensions are in mm)

All welded plates were X-rayed for possible weld defects and only sound portions of the plates were used for specimen fabrication. The dimensions of the small scale fatigue specimens are shown in Fig. 4.1.

Table 4.1. Welding parameters and specifications used for the fabrication of welded plates.

Set No	Weld Pass No.	Cur -rent I (A)	Volt -age U (V)	Speed v (mm/ min)	Heat Input Q_i (kJ/mm)	Aver. Heat Input, Q kJ/mm	Elect -rode Dia. (mm)	Elect -rode Type	Flux or Gas	Gas Flow (l / min)	Weld. Pro- cess
# 4.	1 2 3 4 5 6	190 258 240 240 242 246	23.5 28 27 27 27 26	225 312 492 476 455 526	1.19 1.39 0.79 0.82 0.86 0.73	0.96	1.2	V/ COR 3XP	CO_2	15	MIG
#5a.	1 2 3 4 5	503 449 495 498 497	30.3 30.2 30.2 30.0 30.1	452 450 450 452 451	2.02 2.01 1.99 1.98 1.99	2.0	3.2	EM1 2K- 61	780 YH 10	N/A	SAW
#6.	1 2 3	490 475 490	32 32 31.5	300 310 297	3.14 2.94 3.12	3.07	3.2	EM1 2K- L61	780 YH 10	N/A	SAW
#7.	1 2	450 458	32.0 31.8	213 215	4.06 4.06	4.06	3.2	EM1 2K- L61	780 YH 10	N/A	SAW

Measurements of the local weld geometry parameters (i.e the tip radius at the undercut (r'), the weld toe radius (r) and the flank angle (θ)) were carried out on macrographs of the rectilinear weld bead cross-sections taken for each set of specimens. The weld toe radius and flank angle were measured using the method of

least radius (IIW/IIS Doc. XIII-1090-90). Circles of different diameters drawn on transparent paper are superimposed on the macrographs of the weld toes at 5x magnification. The smallest circle fitting into the weld toe defines the value of the weld toe radius (r) and then the flank angle (θ) is defined at the point at which the circle becomes tangential to the weld toe. This method proved to be accurate and reproducible. An illustration of this method is shown in Figure 4.2. If an undercut is present at the weld toe, the undercut tip radius (r') is also measured on the macrograph and is defined as being the depth of the undercut.

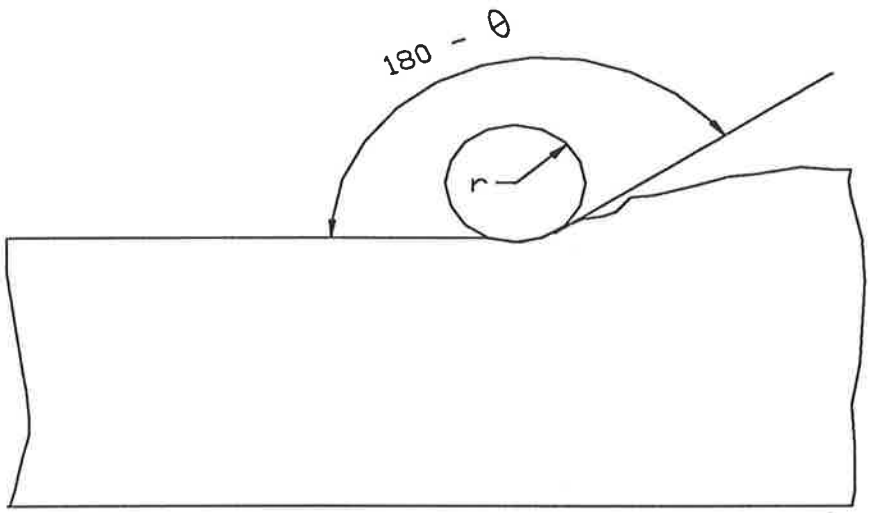

Figure 4.2 An illustration of the method of the least radius for the measurement of the weld toe radius and the flank angle (IIW/IIS Doc. XIII-1090-90).

In the present study, the measurements of weld toe radii and flank angles were carried out on the weld toes on both sides of the weld bead cross section. For each weld cross section, the smaller value of the two measured weld toe radii and the higher value of

the two measured flank angles were considered to be representative for that section. This assumption was adopted on the basis that smaller weld toe radii and higher flank angles are more detrimental to the fatigue behaviour of butt welded joints. For each set of test specimens, the average of the measured values of weld geometry parameters (θ, r and r') obtained for all the cross sections were considered to be representative for that set. The values for the weld geometry parameters obtained for various sets of test specimens are shown in detail in Table 4.2 and Table D.3 (Appendix D). The chemical composition and mechanical properties of the base metal used in the fabrication of various sets of welded specimens are given in Tables 4.3 and 4.4.

Table 4.2. Specimen joint geometry and treatments used for fatigue tests

Set No.	r' (mm)	r (mm)	θ (deg)	ϕ (deg)	t (mm)	2b (mm)	Stress ratio, R	No. of spec.	Notes
# 0.	0	∞	0	-	12	20	0.1	8	Flat unwelded plate
# 7.	as weld.	2.1	22.3	60	12	20	0.1	8	Low profile (SAW)
# 5a.	as weld	1.4	33.9	60	12	20	0.1	11	Medium profile (SAW)
# 6.	as weld	1.1	37.4	60	12	20	0.1	9	High profile (SAW)
# 4.	0	4.75	28.5	60	12	20	0.1	9	Medium profile with ground weld toes (MIG)

Table 4.3 Chemical composition of the base metal (steel grade 250-AS 3678) (% wt)

C	Mn	Si	P	S
0.08	1.47	0.19	0.01	0.005

Table 4.4 Mechanical properties of the base metal (steel grade 250-AS 3678)

S_y (MPa)	S_u (MPa)	Elongation (%)	Reduction of area (%)
287	457	38.5	62 %

4. 3 **Test Procedures**

4.3.1 **Fatigue test setup**

A dynamic computer-controlled servo-hydraulic universal MTS-testing machine with a maximum capacity of 250 kN was used for both static and fatigue testing. This system is able to digitally record all the dynamic test conditions, i.e., loading, displacement, strains, frequency and number of fatigue cycles onto a computer hard disk. A range of frequencies from 10 to 20 Hz were used for fatigue tests. The particular frequency was dependent on the magnitude of the applied loads and all the fatigue tests were carried out under constant stress ratio R=0.1. A load cell of 125 kN was used for all

the fatigue tests. An X-Y plotter was also connected to the computer for necessary graphical output during the fatigue test (e.g oil temperature vs. time).

Two tensile tests were conducted on test specimens taken randomly from each set to determine the static properties of the specimens for that set. The remaining specimens in each set were used for load-controlled constant amplitude fatigue tests at several loading levels. Strain gauges were bonded to the weld toes of some specimens from each set to determine the level of the bending stresses induced by misalignments. These strain gauges were also used to detect the crack initiation period and their analogue outputs were connected to external channels of the MTS-machine via a dynamic strain-gauge amplifier (KYOWA, DPM-6CT Model CO-50CT). The strain gauges were calibrated by running a calibration program during the first-loading cycle (C.3, Appendix C).

All the fatigue tests were run using Test-Star Software R. 2.0A with a program written and adapted for each load level (Appendix C). TestStar allows for the adjustment of the load levels while the test is in progress. The program monitored the output levels of load and displacement and the machine switched off automatically if the specimen failed or the preset limits were reached. Sinusoidal wave form was selected for the load input control and it was also monitored through the TestStar computer program. The overall view of the fatigue test setup and the instrumentation is shown in Fig. 4.3. A welded specimen with the strain gauges bonded at the toes of the weld is shown in Fig. 4.4.

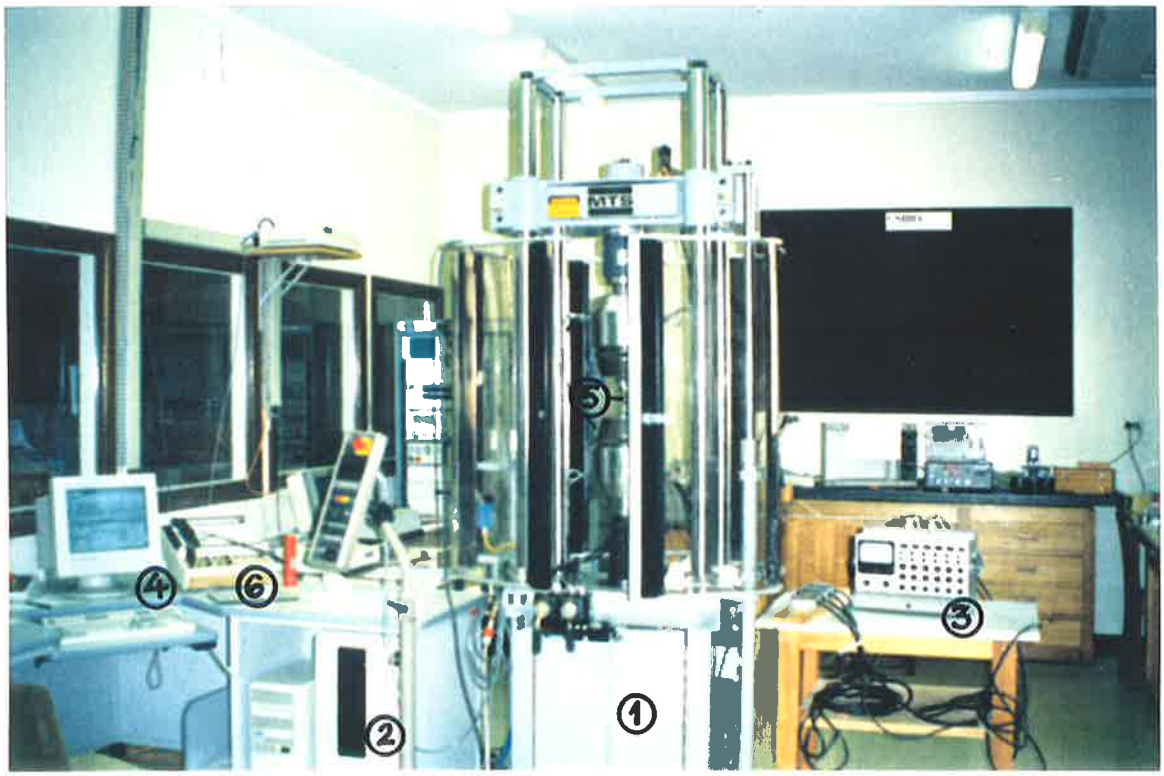

Figure 4.3 Fatigue test setup and instrumentation for butt welded specimens: (1) MTS-testing machine, (2) A/D acquisition system, (3) KYOWA strain amplifier, (4) PC, (5) Specimen, (6) X-Y plotter

Figure 4.4 Test specimens with strain gauges bonded at the weld toes

The input load level was controlled by the computer which was pre-programmed to give a constant-load amplitude. Normally, four stress levels were used for each set of specimens. Replications at some stress ranges were conducted depending on the availability of welded specimens for each set. Eight to eleven specimens were used from each set to get the fatigue data needed for the construction of the S-N curve. The failure criteria were chosen as the final rupture of the specimens or when the number of loading cycles exceeded two millions. However, if a specimen had not broken after two millions cycles, the test was stopped and a higher level of load was applied to break the specimen. After the test, the equivalent fatigue life was calculated using Miner's cumulative damage rules as recommended in BSI PD 6493 (1991). The description of the fatigue testing procedure is discussed in the following section.

4.3.2 **Data collection during fatigue tests**

In the present study, the dynamic local strains at the weld toes during each fatigue test were recorded in order to detect the crack initiation period. The peak values of the applied load and the corresponding ram displacements, elapsed time and number of the loading cycles were also recorded for later assessment. The rate of data collection of the response of the strain gauges during fatigue tests was a trigger of 10 data points for every 5000 cycles. This provided sufficient information needed for the crack initiation period to be detected. The output data file which contained the elapsed time, load range, number of cycles, frequency, peak ram displacements and the peak output voltages of the strain gauges were recorded by TestStar and stored on the hard disk. A total number of 45 test specimens were used in five sets of fatigue tests as follows:

- 28 welded specimens representing three typical weld bead profiles: low, medium and high i.e Set # 7, # 5a, # 6 respectively (Tab. 4.2).
- 9 specimens with ground weld toes (undercut-free) (Set # 4)
- 8 specimens of flat parent material (Set # 0)

Cyclic strains experienced at the weld toes during fatigue tests were recorded using strain gauges bonded to within 0.5 mm of weld toes. The gauges showed an increase in the micro-strain reading when a crack initiated at the weld toe. Further growth of the crack resulted in an increase in the strain reading until the crack extended beneath the gauges. After that, the strain gauge reading began to decrease as the material below the gauge could not be strained further. In the present study, crack initiation was defined as the number of cycles needed to produce a ± 5 % change in the strain gauge reading. This small change was found to correspond to the presence of a crack (approximately 0.25 mm) initiated at the weld toe (Mattos and Lawrence, 1977).

The following test procedures were adopted during the fatigue tests:

1. Local weld geometry parameters represented for each set of welded specimens were measured directly from the macrographs using the method of the least radius (IIW/IIS Doc. XIII-1090-90) and this data was recorded for latter assessment (Table D.3, Appendix D).

2. Monotonic tensile tests were used to determine the static properties of the parent material (set # 0) and the welded specimens (Set # 4, 5a, 6, 7). Two specimens were randomly selected from each set and used for tensile tests. The average value of these

two tests was taken as the test result. These values were used as a reference for selecting the loading levels for the fatigue tests.

3. Load-controlled constant amplitude fatigue tests were conducted for each set of the specimens at various levels of applied stress and at a constant stress ratio (R=0.1). The S-N curves were plotted from which the endurance limit S_e (in air) was determined. This was considered to be the applied stress range which would produce failure at $2x10^6$ loading cycles (AS 4100-1990).

4. Depending on the number of specimens in each set, repetitions of the fatigue tests were carried out for each stress level. Those specimens which did not fail after $2x10^6$ cycles were tested again at a higher stress level to produce failure. The equivalent fatigue data was obtained using Miner's rule of cumulative damage as recommended in BSI PD 6493 (1991).

4.4 **Test Evaluation**

Generally, a series of standard specimens were tested and the data used for plotting the S-N curve on log-log scales. The endurance limit was difficult to determine exactly because of the scatter in the fatigue data due to the variations in the specimen geometries, residual stresses, loading and test conditions (e.g in-air or in-sea water).

In design practice, the fatigue strength is considered to be the stress range corresponding to a particular number of cycles. In the high-cycle fatigue regime, this is of the order of 10^5 to 10^7 cycles. The British Standard (BSI PD 6493, 1991) and the Australian Standard AS-4100-1990 (1990) specify the fatigue endurance limit at $2x10^6$

cycles while European Standards use 10^7 cycles. In the present study, the fatigue endurance limit was assumed to be at $2x10^6$ cycles.

A mathematical model for the S-N curve is expressed in Eq. (3.30). Since fatigue test data were plotted on log-log scales and represented by straight lines obtained using regression analysis (i.e. log N = log A - m log S), the following procedures were adopted to evaluate the fatigue test results :

1. Fatigue data obtained from each set of specimens were taken for plotting the mean S-N curve on a log-log graph. The coefficients "m" and "A" of Eq. (3.30) were obtained by regression analysis using Excel 5.0. The standard deviations for log(N) and log(S) were calculated for each set of specimens and are reported in Table D.1 (Appendix D).

2. Fatigue strengths for each set of specimens were interpolated from the corresponding mean of the S-N curves at $5x10^5$, $2x10^6$ and 10^7 cycles. These are reported in Table D.2 (Appendix D). These values were latter used for the calculation of the fatigue notch factor at various levels of the fatigue life.

3. Predicted values of the fatigue strength, fatigue life and fatigue notch factor of butt welded joints using equations developed for the model in the present study were plotted against the test results to verify the validity of the model.

In the following Chapter, the numerical and experimental results obtained from this work are reported.

Chapter 5

RESULTS AND DISCUSSION

Firstly, the effect of the most important weld geometry parameters on the stress concentrations and the stress intensity factor at the weld toes under axial and bending load conditions are discussed. Subsequently, an explanation for the effect of weld geometry on the fatigue behaviour of butt joints is reported. This includes the effect of weld geometry parameters on the fatigue life, fatigue strength and fatigue notch factors of the joints.

The effects of residual stresses on the fatigue behaviour of butt joints in the as-welded and post-weld surface treated conditions are discussed in relation to weld geometry parameters. The effect of the combined axial and bending loading is discussed in terms of the various levels of the bending stress induced by misalignments of butt joints. At the end of this Chapter, the combined effect of several important weld geometry parameters, residual stresses and the combined loading ratio (R_{ba}) on the fatigue strength and fatigue notch factor of butt welded joints are also discussed. Subsequently, the numerical results are compared with the fatigue test results obtained during the present study and from the literature.

5.1 Effect of Butt Weld Geometry on Stress Concentration Factor

Stress distributions along the potential crack line, which originates at the weld toe and propagates through the thickness of the welded plate, were calculated for various butt weld profiles (Table B.1, Appendix B), under axial and bending loads. A 2D-finite element mesh with a condensed region at the weld toe zone was generated for each butt weld profile (Fig. 3.6). Stress distributions were calculated for all the chosen weld profiles (Table B.1, Appendix B) using a finite element package, ANSYS 5.0 (Ansys User's Manual, 1992). The corresponding normalised stress distributions through the thickness of the welded plates under axial and bending load conditions ($K_{t,a}$ and $K_{t,b}$) were obtained and shown in Figures 5.1 to 5.5.

Figure 5.1a showed the effect of the tip radius at the undercut of the weld toe (r') on the stress concentration factor along the potential crack line in pure axial loading ($K_{t,a}$) condition (subscript "a" refers to axial loading and other weld geometry parameters are constant: r = 1 mm, θ = 30°, ϕ = 60° and t = 12 mm). This figure shows that the presence of an undercut at the weld toe increases the values of ($K_{t,a}$) significantly from a typical value of 3 for a weld geometry without undercut (Maddox, 1991) to the value between 4.3 and 5.7 for levels of (r') ranging from 0.35 mm to 0.05 mm. However, the stress concentration factors gradually decrease as the depth from the weld toe increases. Therefore, the stress concentration factor is significantly affected by the presence of an undercut at the weld toes at a distance approximately 5 % of the plate thickness from the weld toes.

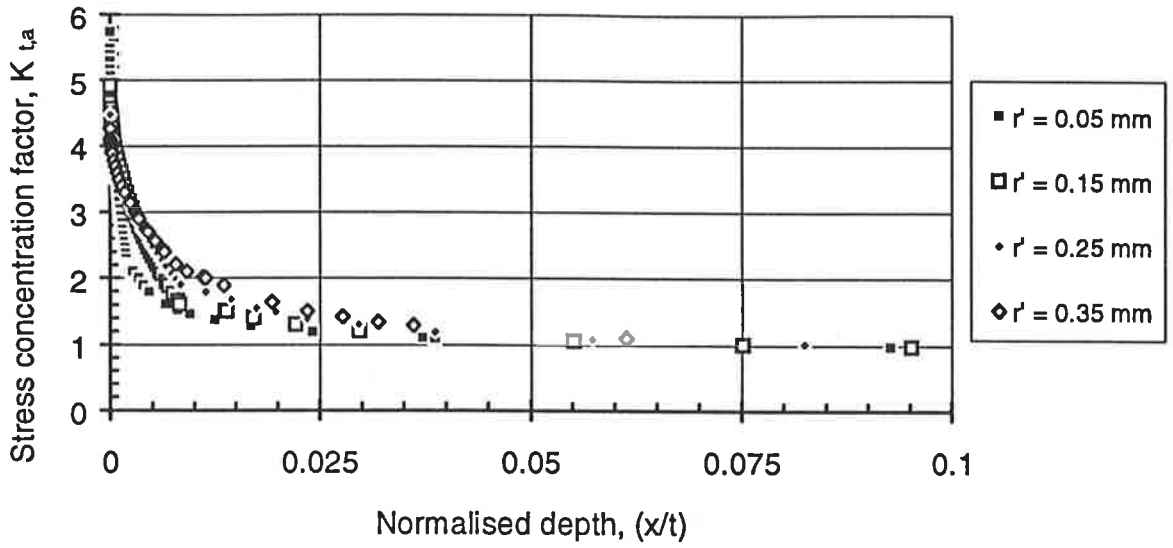

(a) Stress concentration factor under pure axial load ($K_{t,a}$)

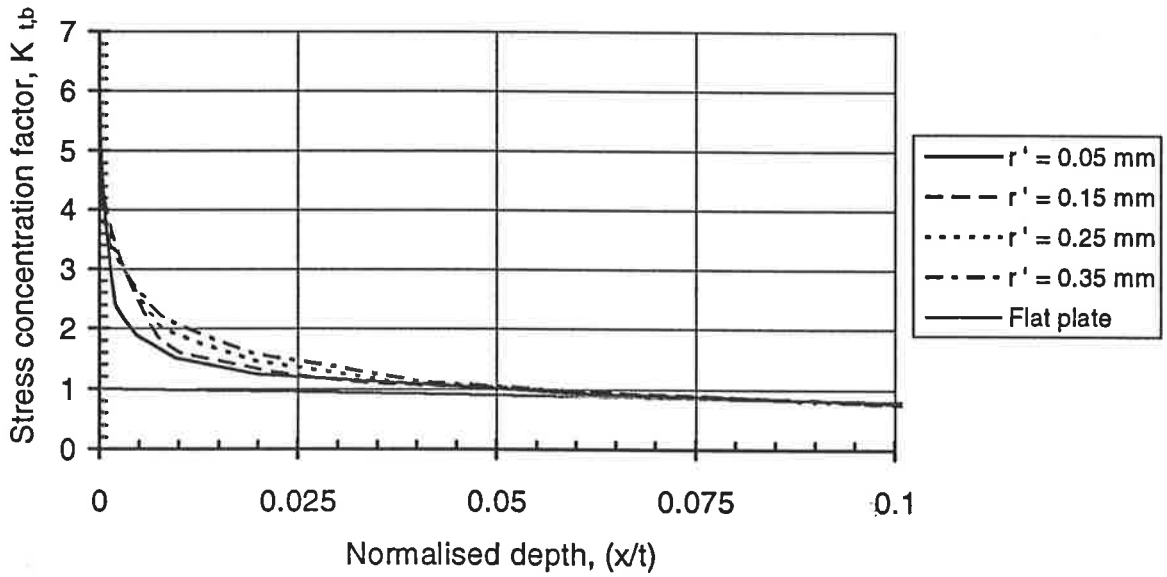

(b) Stress concentration factor under pure bending ($K_{t,b}$)

Figure 5.1 Effect of the tip radius at the undercut (r') on the stress concentration factor in butt welded joints along the potential crack line (constant parameters: r = 1 mm, $\theta = 30°$, $\phi = 60°$ and t = 12 mm).

Figure 5.1b showed the effect of (r') on the stress concentration factor along the potential crack line in pure bending ($K_{t,b}$) (subscript "b" refers to bending loading and other weld geometry parameters are constant: r = 1 mm, θ = 30°, ϕ = 60° and t = 12 mm). The effect of (r') on ($K_{t,b}$) is similar to that in pure axial loading except the values of $K_{t,b}$ at the weld toe surface are increased up to 6.1 for r' = 0.05 mm and 4.3 for r'=0.35 mm. The values of the stress concentration factor also gradually decreased as the distance from the weld toe increased. The increase of ($K_{t,b}$) due to the presence of an undercut was only found up to a distance of 5 % of the plate thickness, beyond that no significant increase of ($K_{t,b}$) was found.

Figure 5.2a showed the effect of the weld toe radius (r) on the stress concentration factor ($K_{t,a}$) under pure axial loading condition (other geometrical parameters are unchanged: r' = 0, θ = 30°, ϕ = 60° and t = 12 mm). It shows that the weld toe radius significantly affected the values of the stress concentration factor along the potential crack line, particularly in the vicinity of the weld toes. The stress concentration factor at the weld toe increased sharply with a small decrease in weld toe radius. The value of the stress concentration factor at the weld toe ($K_{t,a}$) was increased by 70 % (from 1.27 to 2.16) as the weld toe radius decreases from 5.0 mm to 0.0 mm. However, the values of the stress concentration factors due to variations in the weld toe radii gradually decreased as the distance from the weld toe increased. Therefore, the stress concentration factor was significantly affected by the weld toe radius within a depth of 3.5 % of the plate thickness (0.035t) from the weld toe. Beyond this depth, variations in the weld toe radius had an insignificant effect on the stress concentration factor.

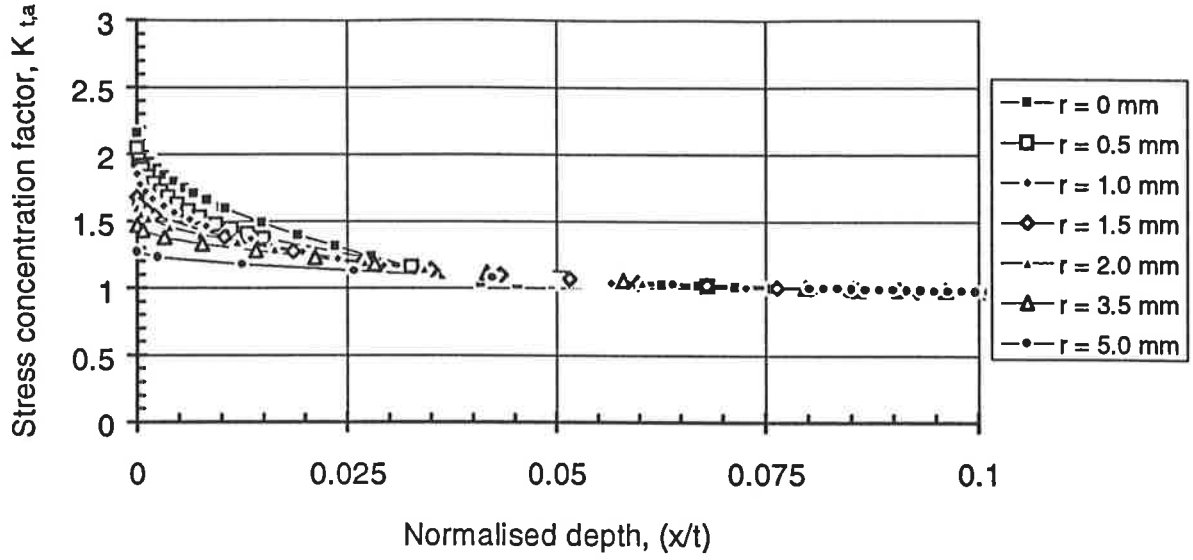

(a) Stress concentration factor under pure axial loading ($K_{t,a}$)

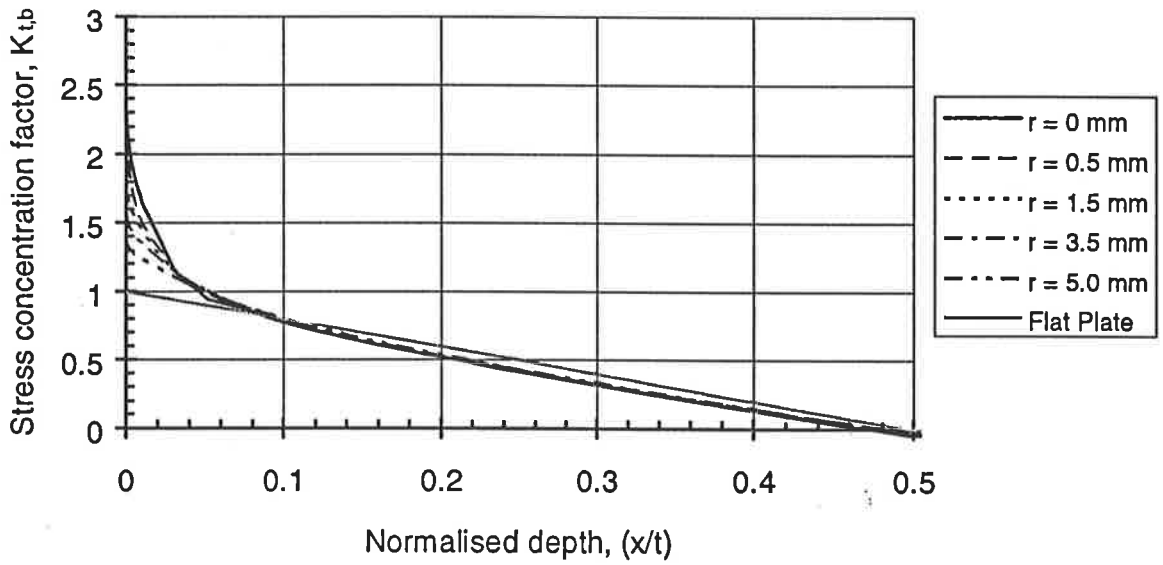

(b) Stress concentration factor under pure bending ($K_{t,b}$)

Figure 5.2 Effect of the weld toe radii on the stress concentration factors in butt welded joints under axial and bending loads along the potential crack line (constant parameters: r' = 0, θ = 30°, ϕ = 60° and t = 12 mm).

Figure 5.2b showed the values of the stress concentration factor ($K_{t,b}$) due to the variations in the weld toe radius (r) under pure bending (other geometrical parameters are constant: r' = 0, $\theta = 30°$, $\phi = 60°$ and t = 12 mm). The effect of the weld toe radius on the stress concentration factor under pure bending was similar to that under pure axial loading. The values of ($K_{t,b}$) at the weld toe surface were increased by 69 % (from 1.37 to 2.32) due to a decrease in the weld toe radius (r) from 5.0 mm to 0.0 mm. However, as the distance from the weld toe increased the values of the stress concentration factor gradually decreased. Beyond a distance of 3.5 % of the plate thickness (0.35t), no noticeable effect of the weld toe radius on the stress concentration factor was found.

Figure 5.3a showed the values of the stress concentration factor ($K_{t,a}$) resulting from the variations in the weld flank angle (θ) under pure axial loading (other weld geometry parameters are constant: r' = 0 mm, r = 1 mm, $\phi = 60°$ and t = 12 mm). The stress concentration factor through the plate thickness increased as the weld flank angle increased from 5° to 60°. The stress concentration factor at the weld toe increased by 66 % (from 1.24 to 2.06) with an increase in the flank angle from 5° to 60°. However, when compared with the flush-ground welded plate or flat plate of parent metal the stress concentration at the weld toe increased by up to 106 % as the flank angle increased from 0° to 60° (0° refers to the flush-ground welded plate or the flat plate of the base metal). Fig. 5.3a also showed that as the distance from the weld toe increases the stress concentration factor gradually decreased. Suggesting, that the effect of the flank angle on the stress concentration factor was only significant for the depths up to 6.5 % of the plate thickness (0.065t) from the weld toe surface.

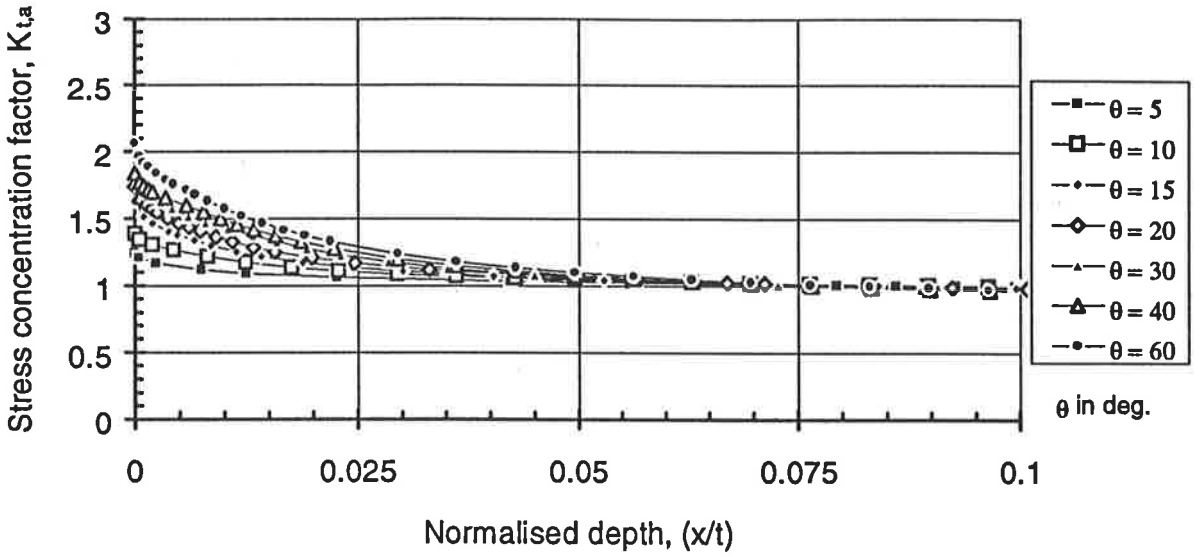

(a) Stress concentration factor under pure axial loading ($K_{t,a}$)

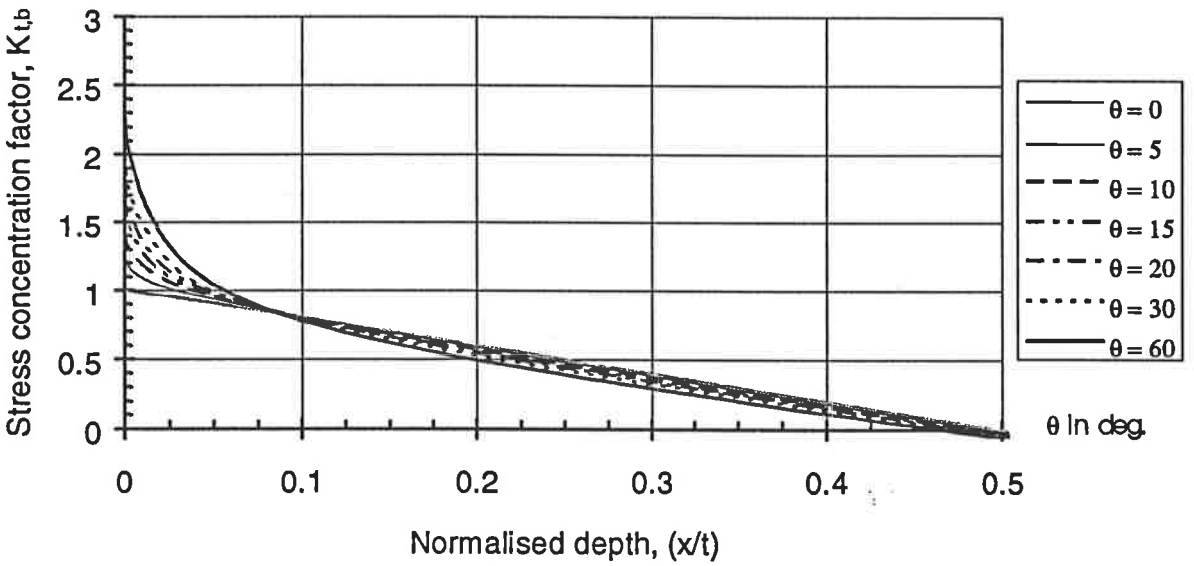

(b) Stress concentration factor under pure bending ($K_{t,b}$)

Figure 5.3 Effect of the flank angle on the stress concentration factor in butt welded joints along the potential crack line (constant parameters: r' = 0, r = 1 mm, ϕ = 60° and t = 12 mm).

Figure 5.3b showed the values of the stress concentration factor ($K_{t,b}$) due to the variations in the weld flank angle (θ) under pure bending (other weld geometry parameters are constant: r' = 0, r = 1 mm, ϕ = 60° and t = 12 mm). The stress concentration factor at the weld toe increased by 82 % (from 1.25 to 2.28) as the flank angle increased from 5° to 60°. However, if the flush-ground weld is considered, the stress concentration factor increases by up to 128 % as the flank angle increased from 0 to 60°. Figure 5.3b also showed that as the distance from the weld toe increased the stress concentration factor gradually decreased. The effect of the flank angle on the stress concentration factor was significant only for depths up to 7.5 % of the plate thickness (0.075t). Beyond that depth, the variations in the flank angle had a small effect on the stress concentration factor of butt joints.

Figure 5.4a showed the values of the stress concentration factor ($K_{t,a}$) for the variations in the plate thickness (t) under pure axial loading (other weld geometry parameters are constant: r' = 0, r = 1 mm, θ = 30° and ϕ = 60°). The values of the stress concentration factor at the weld toe surface increased by 96 % (from 1.61 to 3.16) as the plate thickness increased from 6.3 to 100 mm. This behaviour of the stress concentration factor due the plate thicknesses offers an explanation for the well known effect of plate thickness reducing the fatigue strength of welded joints (Gurney, 1979; Ohta et al., 1990; Maddox, 1991; and others).

Figure 5.4 showed that the values of the stress concentration factor gradually decreased as the depth from the weld toe surface increased. However, the effect of the plate thickness on stress concentration factor through the thickness of the welded

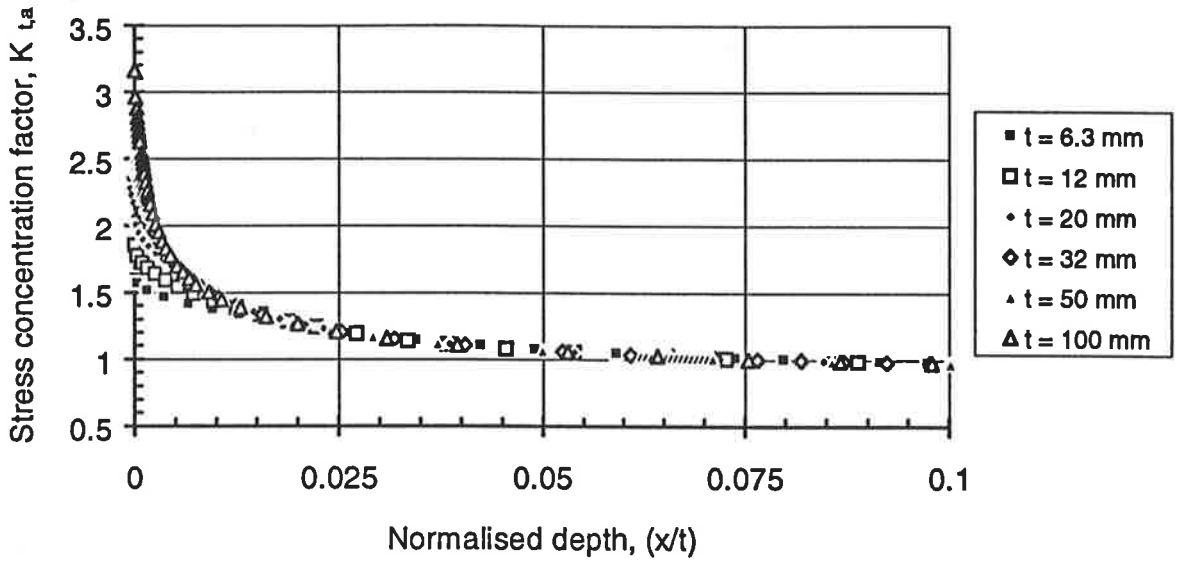

(a) Stress concentration factor under pure axial loading ($K_{t,A}$)

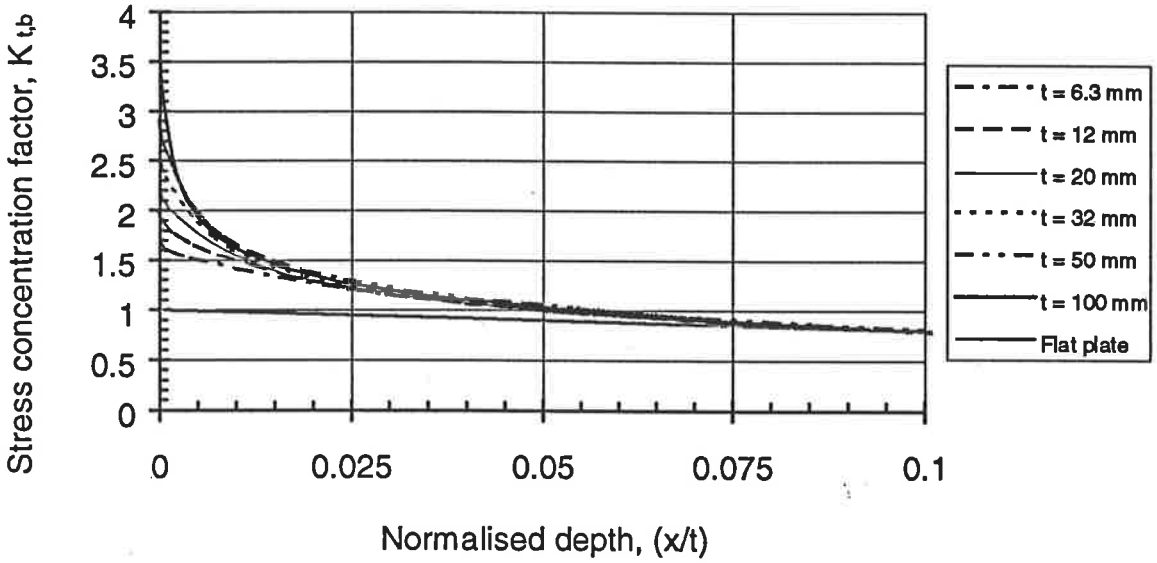

(b) Stress concentration factor under pure bending ($K_{t,B}$)

Figure 5.4 Effect of the plate thickness on the stress concentration factor in butt welded joints along the potential crack line (constant parameters: r' = 0, r = 1 mm, $\theta = 30°$ and $\phi = 60°$).

plate was insignificant when the distance from the weld toes increased beyond the 2.5 % of the plate thickness (0.025t). Hence the plate thickness may only influence the fatigue behaviour of butt joints during the crack initiation period and in the early stages of crack propagation.

Figure 5.4b showed the values of the stress concentration function ($K_{t,B}$) for variations in the plate thickness (t) under pure bending (other weld geometry parameters are constant: r' = 0, r = 1 mm, $\theta = 30°$ and $\phi = 60°$). The stress concentration factors at the weld toe surface increased by 114 % (from 1.70 to 3.64) as the thickness of the welded plate increased from 6.3 to 100 mm. This behaviour of the plate thickness under bending was similar to that under pure axial loading but slightly stronger. Fig. 5.4b also showed that the stress concentration factor gradually decreased as the distance from the weld toe surface increased. The effect of the plate thickness on the stress concentration factor became insignificant when the distance from the weld toes increased further beyond 3.5 % of the plate thickness (0.035t).

Figure 5.5a showed the values of the stress concentration function ($K_{t,A}$) subject to the variations in the edge preparation angle (ϕ) under pure axial loading (other weld geometry parameters are constant: r' = 0, r = 1 mm, $\theta = 30°$ and t = 12 mm). The values of the stress concentration factor at the weld toe increased by 10 % (from 1.58 to 1.74) as the preparation angle (ϕ) increased from 45° to 90°. The effect of (ϕ) on the stress concentration factor was less significant than that of the other weld geometry parameters (i.e r', r, t or θ). The values of the stress concentration factor again gradually decreased as the depth from the weld toe surface increases. However,

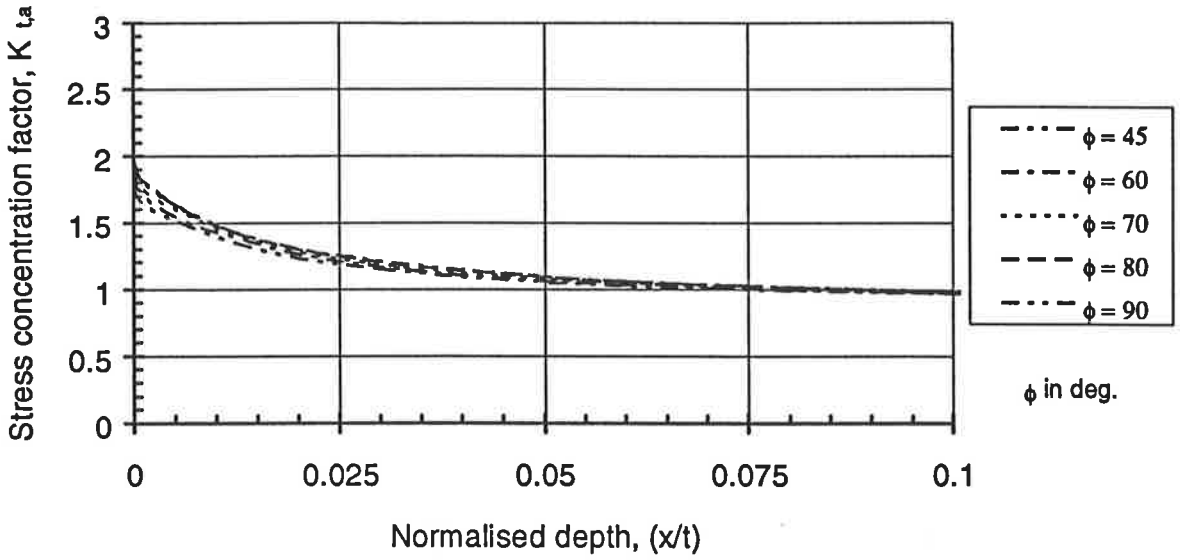

(a) Stress concentration factor under pure axial loading ($K_{t,a}$)

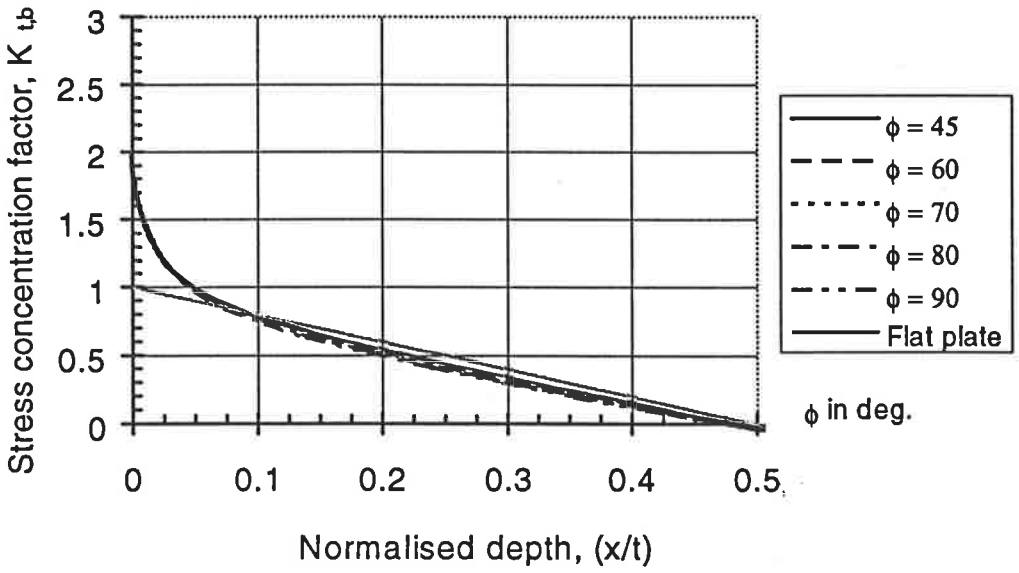

(b) Stress concentration factor under pure bending ($K_{t,b}$)

Figure 5.5 Effect of the edge preparation angle on the stress concentration factor in the butt joints along the potential crack line (constant parameters: r' = 0, r = 1 mm, $\theta = 30°$ and $\phi = 60°$).

the effect of (ϕ) on the stress concentration factor was insignificant when the depth from the weld toes increased beyond 2.5 % of the plate thickness (0.025t).

Figure 5.5b showed the values of stress concentration function ($K_{t,B}$) subject to the variations in the angle (ϕ) under pure bending load (other weld geometry parameters are constant: r' = 0, r = 1 mm, θ = 30° and t = 12 mm). There was a little difference between the values of the stress concentration factor despite the variations in the edge preparation angle from 45° to 90°. Therefore, the edge preparation angle had insignificant effect on the stress concentration factor along the potential crack line under pure bending.

5.2 **Effect of Butt-Weld Geometry on the Stress Intensity Factor (K)**

In this section, the effect of the butt-weld geometry on the stress intensity factor is discussed in terms of the geometry-configuration factor (Y) (Eq. 3.2) and stress intensity magnification factor (M_k) (Eq. 3.3). Subsequently, the effect of the butt-weld geometry on the stress intensity factor (K) is discussed at the end of this section.

5.2.1 **Effect of butt-weld geometry on the geometry-configuration factor (Y)**

Figures 5.6 to 5.10 showed the effect of various butt weld geometry parameters (r', r, θ, t and ϕ) on stress intensity factor (K) in terms of the geometry-configuration factor (Y) (Eq. (3.3)). These figures show that the values of geometry-configuration factor (Y) are significantly influenced by the combined effects of butt weld geometry parameters. However, this behaviour of (Y) due to the variations in the geometrical

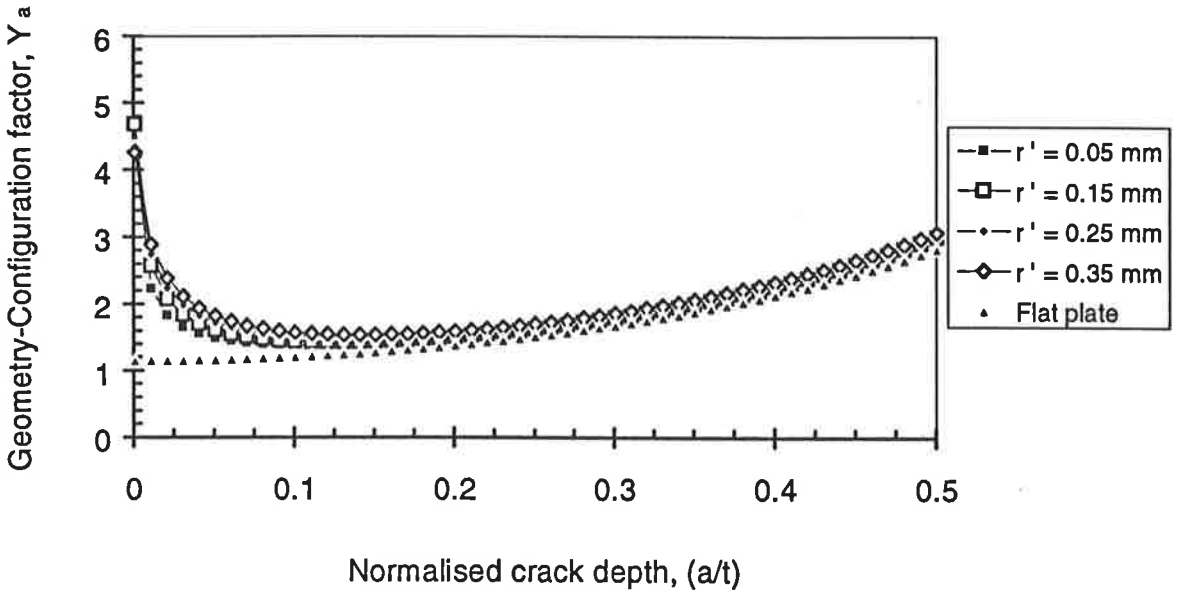

(a) Pure axial loading condition

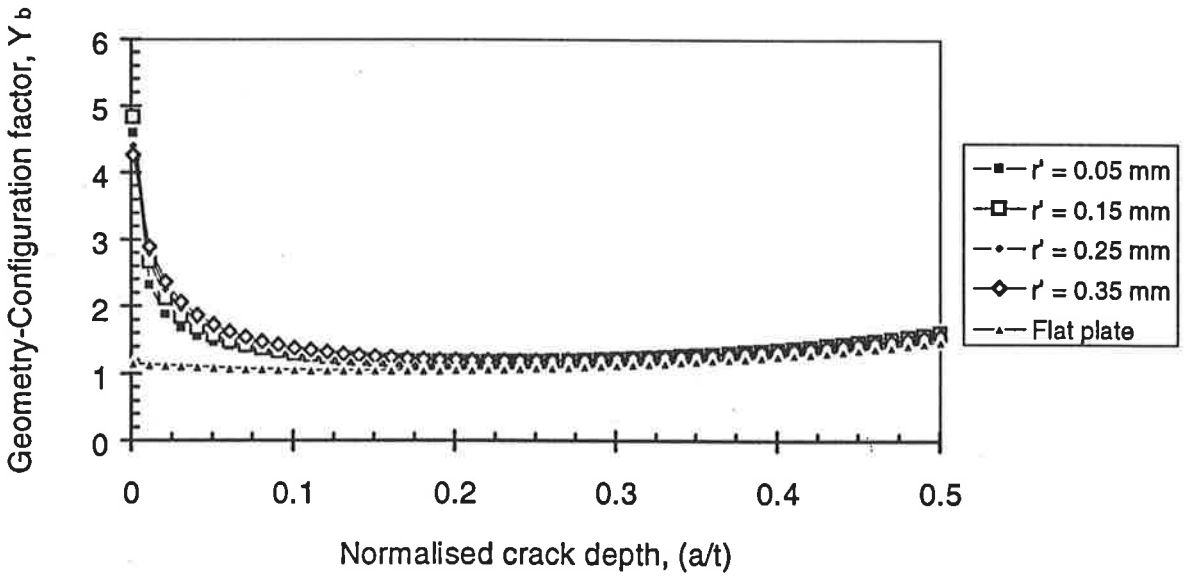

(b) Pure bending load condition

Figure 5.6 Effect of the tip radius of undercut (r ') on the stress intensity geometry-configuration factor (Y) (constant parameters: r = 2 mm, t = 12 mm, $\theta = 30°$ and $\phi = 60°$).

parameters is noticeable only for the crack lengths up to approximately 15 % of the plate thickness (a = 0.15t). Furthermore, each of the weld geometry parameter had a different effect on the factor (Y) depending on the particular loading conditions (Fig. 5.6 to 5.10).

Figure 5.6a showed the effect of the tip radius at the undercut on the stress intensity geometry-configuration factor under pure axial loading (Y_a). This figure shows that the values of (Y_a) are strongly influenced by the variations in the tip radius at the undercut (r'). The values of (Y_a) at the surface were increased significantly from 1.12 for a flat plate to up to 4 or 5 due to the presence of the weld toe undercut. At an early stage of crack growth corresponding to a crack length up to 20 % of the plate thickness (0.2t), the values of (Y_a) increased as (r') increased from 0.05 mm to 0.35 mm. However, beyond that crack length (0.2t), there was an insignificant effect of the (r') on the values of (Y_a) i.e the values of (Y_a) due to variations in the (r') were of the same order as those of a flat plate. A similar trend of the effect of the tip radius at the undercut on the stress intensity geometry-configuration factor (Y_b) under bending load is shown in Fig. 5.6b. The values of (Y_b) at the surface increased significantly from 1.12 for a flat plate up to 4 or 5 when an undercut was present. At an early stage of crack growth corresponding to a crack length of 20 % of the plate thickness (0.2t), the values of (Y_b) increase as (r') increases from 0.05 mm to 0.35 mm. Beyond that crack length, the effect of the tip radius at the undercut on the values of (Y_b) was insignificant. It is worth noting that for crack lengths of more than 0.2 times plate thickness (Fig. 5.6b) the values of (Y_b) are lower than those of (Y_a) for the same crack length (Fig. 5.6a). This behaviour of the geometry-configuration factor suggests that it is associated with the effect of the loading conditions.

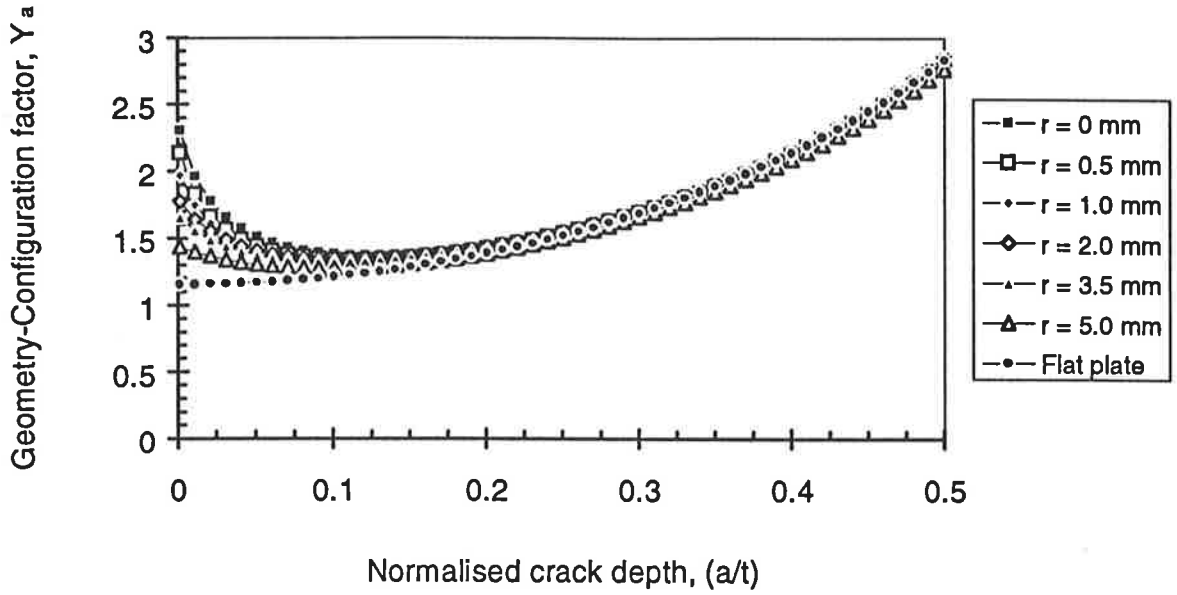

(a) Pure axial loading condition

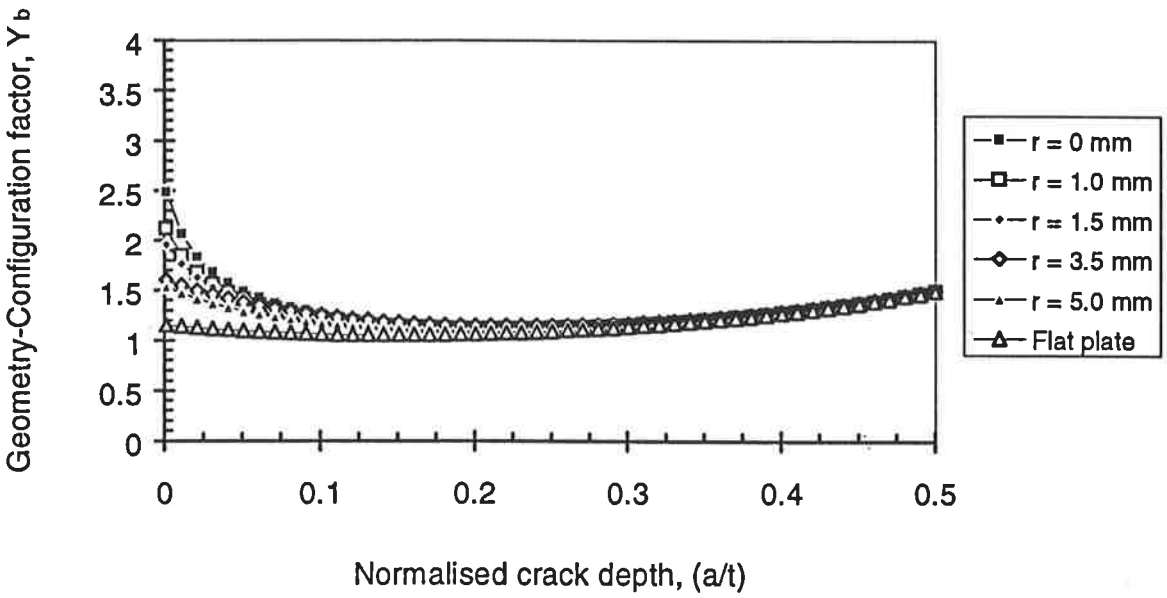

(b) Pure bending load condition

Figure 5.7 Effect of weld toe radius to the stress intensity geometry-configuration factor (Y) (constant parameters: r ' = 0, t = 12 mm, $\theta = 30°$ and $\phi = 60°$).

Figure 5.7a showed the effect of the weld toe radius on the stress intensity geometry-configuration factor under pure axial loading. The values of (Y_a) are strongly influenced by the variations in the weld toe radius. The values of (Y_a) at the surface increased significantly from 1.12 for a flat plate to between 1.5 and 2.5 subject to the variations in the weld toe radius (r) from 0.5 mm to 5 mm. At an early stage of the crack growth corresponding to a crack length of 15 % of the plate thickness (0.15t), the values of (Y_a) decreased as (r) increased from 0.5 mm to 5 mm. However, beyond that crack length (0.15t), there was little difference between the values of (Y_a) due to the variations in the weld toe radius.

Fig. 5.7b showed a similar effect of the weld toe radius on the stress intensity geometry-configuration factor under pure bending. The values of (Y_b) at the weld toe surface increased significantly from 1.12 for a flat plate to between 1.5 and 2.5 subject to the variations in (r). At the early stage of crack growth due to a crack length of 15 % of the plate thickness(0.15t), the values of (Y_b) decreased as (r) increased from 0.5 mm to 5 mm. Beyond that crack length the effect of the weld toe radius on the values of (Y_b) was insignificant. Furthermore, the values of (Y_b) due to the crack lengths greater than (0.15t) (Fig. 5.7b) were lower than those of (Y_a) (Fig. 5.7a). This behaviour of the geometry-configuration factor suggests it was due to the effect of loading conditions.

Figure 5.8a showed the effect of the flank angle (θ) on the stress intensity geometry-configuration factor under pure axial loading. The values of (Y_a) were significantly influenced by variations in the flank angle. The values of (Y_a) at the weld toe surface increased significantly from 1.12 for a flat plate to between 1.4 to 2.3 due to the

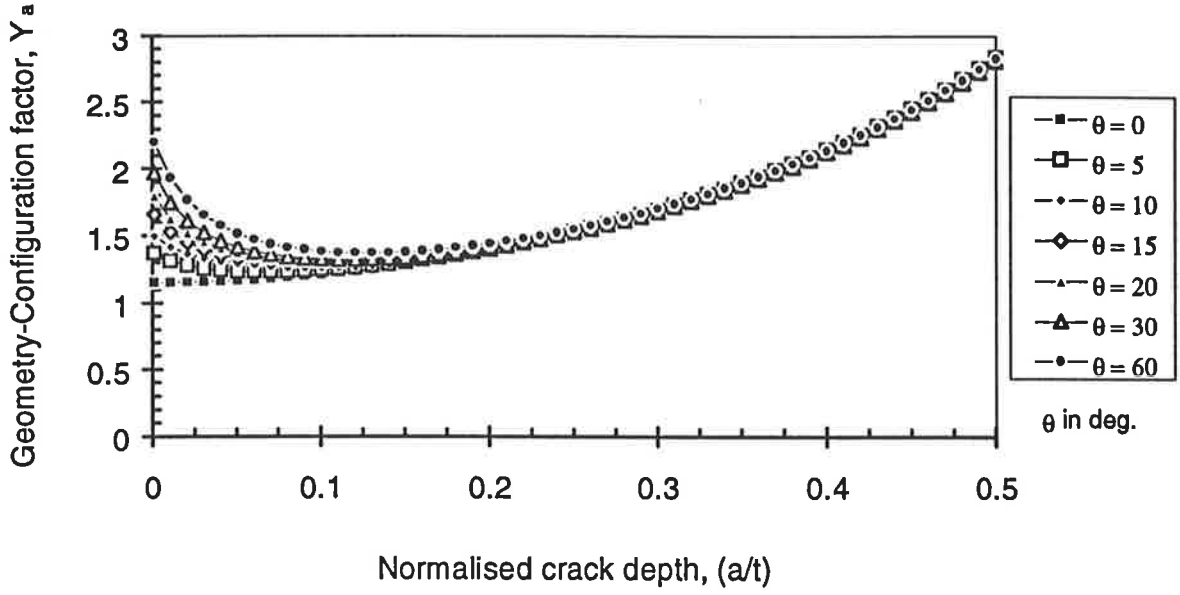

(a) Pure axial loading condition

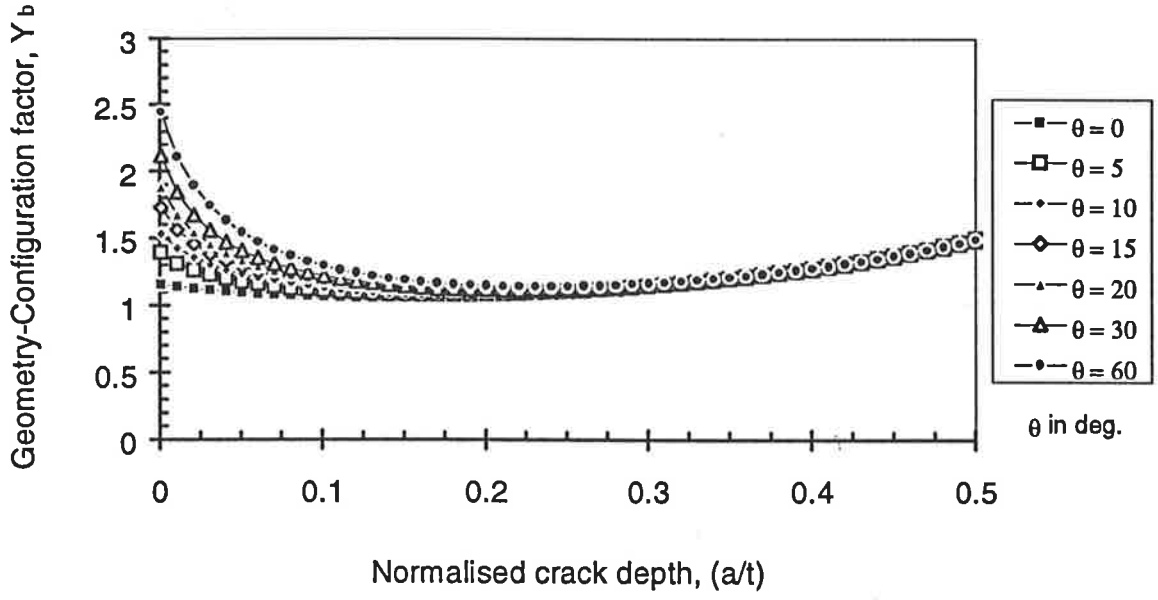

(b) Pure bending load condition

Figure 5.8 Effect of weld flank angle (θ) on the stress intensity geometry-configuration factor (Y) (constant parameters: r ' = 0 mm, r = 1 mm, t = 12 mm and $\phi = 60^{\circ}$).

variations in the flank angle from 5° to 60°. At the early stage of the crack growth corresponding to a crack length of 15 % of the plate thickness (0.15t), the values of (Y_a) increased as (θ) increased from 5° to 60°. However, beyond that crack length (0.15t), there was some difference between the values of (Y_a) due to variations in the flank angle.

Fig. 5.8b showed the similar effect of the flank angle on the stress intensity geometry-configuration factor under bending load. The values of (Y_b) at the weld toe surface increased significantly from 1.12 for a flat plate to between 1.4 and 2.5 for variations in the flank angle (θ) from 5° to 60°. At the early stage of the crack growth corresponding to a crack length of 20 % of the plate thickness (0.2t), the values of (Y_b) increased as the flank angle increased from 5° to 60°. Beyond that crack length, the flank angle had a little effect on the values of (Y_b). In addition, the values of (Y_b) for crack lengths of more than (0.2t) (Fig. 5.8b) were lower than those of (Y_a) (Fig. 5.8a) for the same crack length. Again, it suggested that this behaviour of the factor (Y) for crack lengths of more than (0.2t) was associated with the loading conditions.

Figure 5.9a showed the effect of the plate thickness (t) on the stress intensity geometry-configuration factor under axial loading. The values of (Y_a) are significantly influenced by the variations in the plate thickness from 6.3 mm to 100 mm. The values of (Y_a) at the weld toe surface increased from 1.12 for a flat plate to between 1.8 and 2.8 for variations in the plate thickness from 6.3 mm to 100 mm. At the early stage of the crack growth corresponding to a crack length of up to 5 % of the plate thickness (0.05t), the values of (Y_a) increased as the plate thickness (t) increased. However, after the crack had propagated beyond that length (0.05t), there was an insignificant

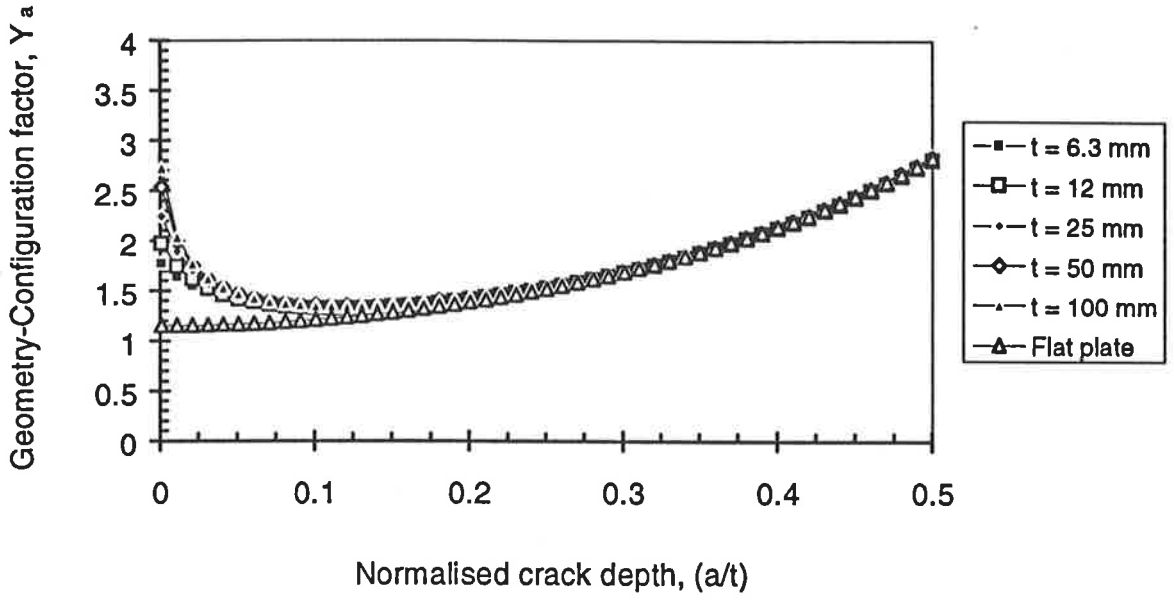

(a) Pure axial loading condition

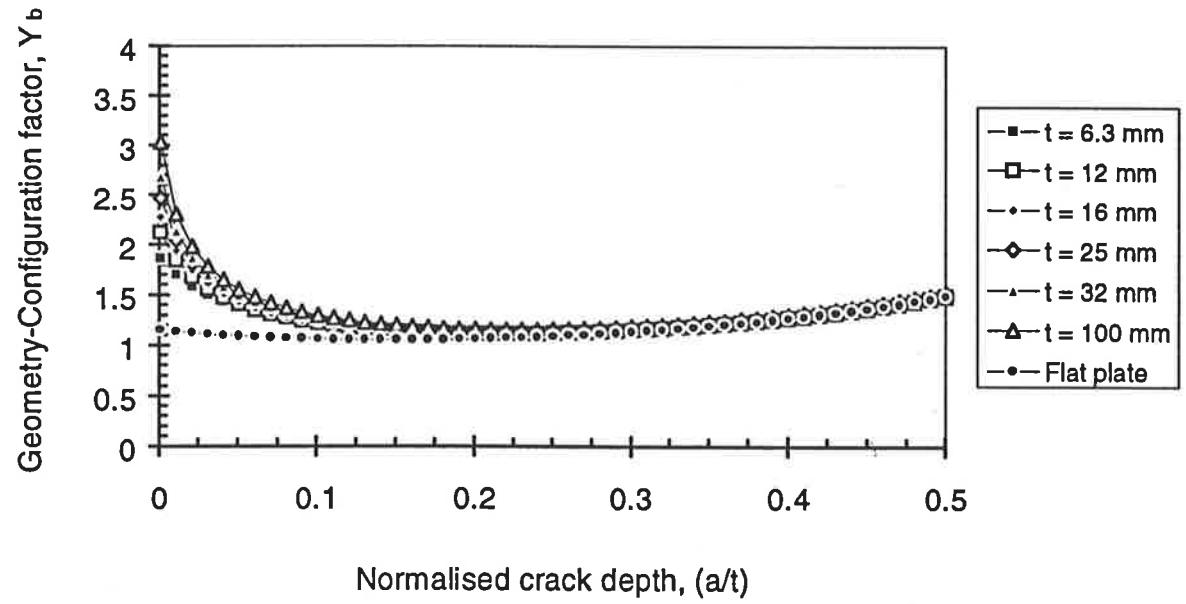

(b) Pure bending load condition

Figure 5.9 Effect of plate thickness (t) on the stress intensity geometry-configuration factor (Y) (constant parameters: r ' = 0, r = 1 mm, $\theta = 30°$ and $\phi = 60°$).

effect of the plate thickness on the values of (Y_a). Furthermore, for the crack lengths of up to 15 % of the plate thickness (0.15t) the values of (Y_a) due to variations in the plate thickness are higher than those for a flat plate. However, beyond that length (0.15t), the values of (Y_a) for variations in the plate thickness and for a flat plate were the same. Hence, the behaviour of the factor (Y) corresponding to a crack length of more than (0.15t) was associated with the axial loading condition.

Fig. 5.9b showed the similar effect of the plate thickness on the stress intensity geometry-configuration factor under bending and under axial loading. The values of (Y_b) at the weld toe surface increased from 1.12 for a flat plate to between 1.8 and 3 due to the variations in the plate thickness from 6.3 mm to 100 mm. At the early stage of the crack growth corresponding to a crack length of 15 % of the plate thickness (0.15t), the values of (Y_b) increased as the plate thickness increased from 6.3 mm to 100 mm. However, beyond that crack length, there was a little effect of the plate thickness on the values of (Y_b). Fig. 5.9b also shows that the values of (Y_b) due to crack lengths of more than (0.15t) (Fig. 5.9b) were lower than those of (Y_a) (Fig. 5.9a). This means that the behaviour of the factor (Y) corresponding to a crack length of more than (0.15t) was due to the type of loading.

Figure 5.10a showed the effect of the edge preparation angle (ϕ) on the stress intensity geometry-configuration factor under axial loading. It shows that the values of (Y_a) slightly increased as the values of angle increased from 45° to 90°. This behaviour suggested that the effect of the edge preparation angle on the stress intensity geometry-configuration factor was less significant than that of the other weld

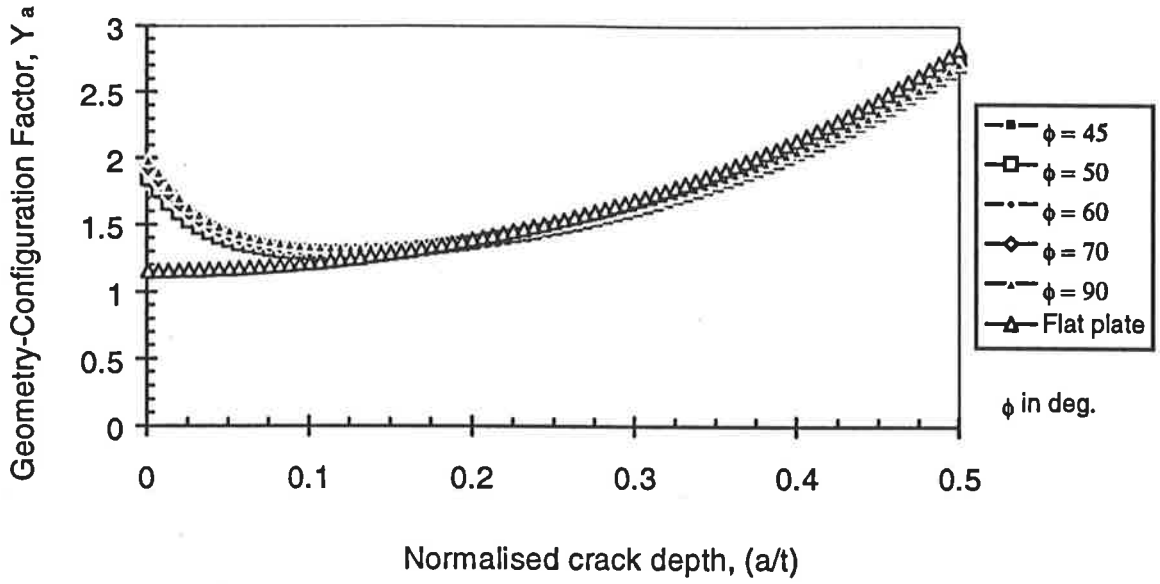

(a) Pure axial loading condition

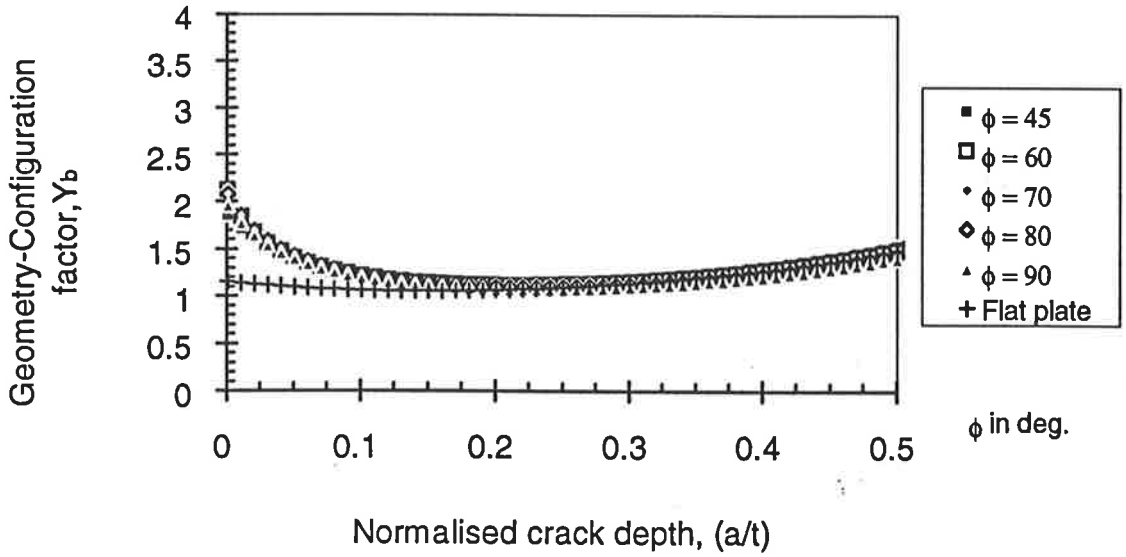

(b) Pure bending load condition

Figure 5.10 Effect of edge preparation angle (ϕ) on the stress intensity geometry-configuration factor (Y) (constant parameters: r ' = 0, r = 1 mm, θ = 30° and t = 12 mm).

geometry parameters previously discussed (r', r, θ and t). Fig. 5.10a also showed that the effect of the edge preparation angle was only significant for crack lengths of up to 15 % of the plate thickness (0.15t). However, beyond that length, there was an insignificant difference between the values of (Y_a) due to the variations in the edge preparation angle and all these values were of the same order as those for a flat plate. This means that there was no effect of weld geometry on the (Y_a) when a crack had propagated beyond the length of (0.15t). The effect of the edge preparation angle on the factor (Y) under bending (Fig. 5.10b) was similar to that under axial loading (Fig. 5.10a). However, the values of (Y_a) corresponding to crack lengths beyond (0.15t) (Fig. 5.10a) were higher than the those of (Y_b) (Fig. 5.10b). This behaviour of the geometry-configuration factors due to the crack lengths beyond (0.15t) was also attributed to the type of loading. It is worth noting here that, all of the important weld geometry parameters only affected the stress intensity geometry-configuration factor of a cracked butt-joint at small crack lengths of the order of 15 to 20 % of the plate thickness (0.15t and 0.2t). This means that the effect of the weld geometry parameters only influenced the fatigue behaviour of butt welded joints at an early stage of the crack propagation.

5.2.2 Effect of weld geometry on the stress intensity magnification factor (M_k)

Figure 5.11a showed the effect of the tip radius at the undercut (r') on the stress intensity magnification factor ($M^A_{k,a}$) under axial loading. This figure shows that the values of ($M^A_{k,a}$) were strongly influenced by variations in (r'). The values of ($M^A_{k,a}$) at the weld toe surface increased significantly from 1.0 for a flat plate to between 3.5 and 4 when an undercut at the weld toe was present. At the early stage of the crack

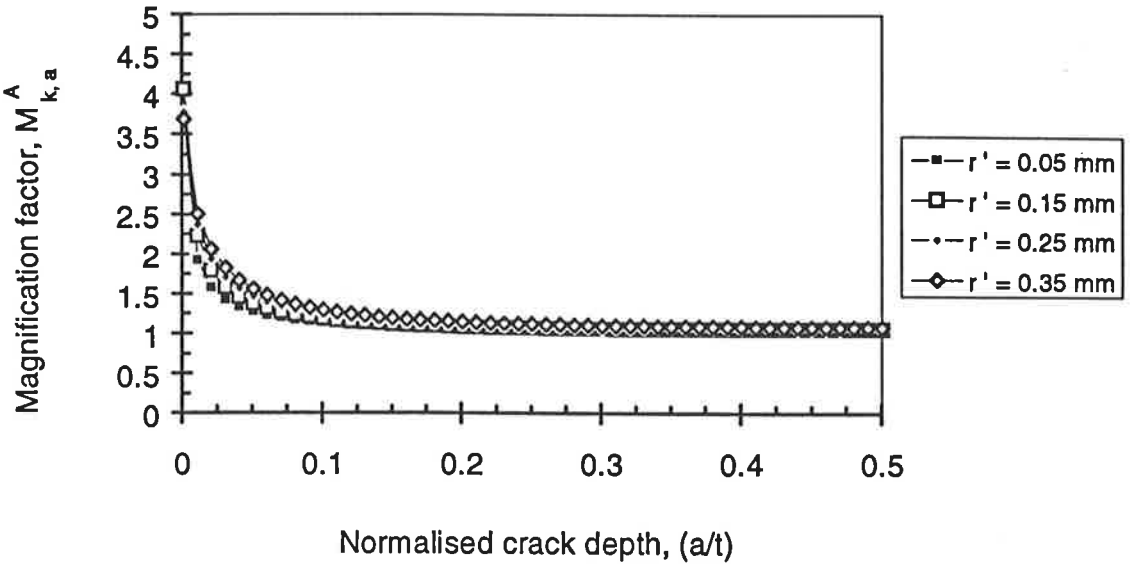

(a) Pure axial loading condition

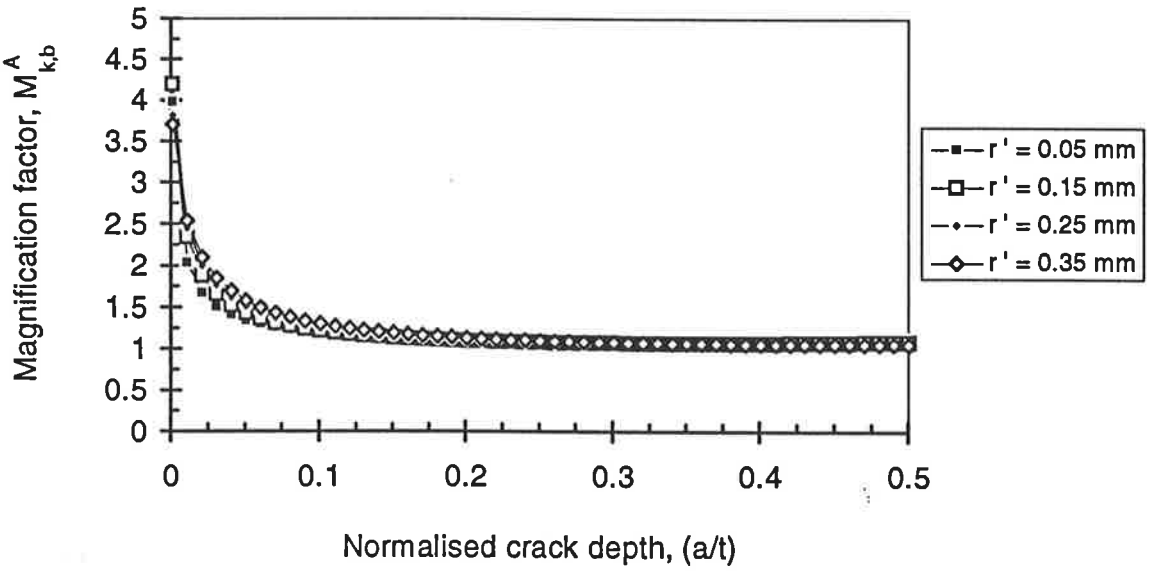

(b) Pure bending load condition

Figure 5.11 Effect of the tip radius of undercut on the stress intensity magnification factor (M_k) (constant parameters: r = 1 mm, $\theta = 30°$, $\phi = 60°$ and t = 12 mm).

growth (corresponding to a crack length less than 10 % of the plate thickness) the values of ($M^{A}_{k,A}$) increased as the (r') increased from 0.05 mm to 0.35 mm. However, beyond that crack length (0.1t), there was an insignificant difference between the values of ($M^{A}_{k,A}$) for variations in the tip radius at the undercut and for a flat plate.

A similar behaviour of the (r') on the stress intensity magnification factor ($M^{A}_{k,B}$) under bending is shown in Fig. 5.11b. The values of ($M^{A}_{k,B}$) at the surface increased significantly from 1.0 for a flat plate to between 3.7 and 4.5 for variations in the weld toe undercut. At an early stage of the crack growth (i.e. for a crack length less than 10 % of the plate thickness) the values of ($M^{A}_{k,B}$) increased as (r') increased from 0.05 mm to 0.35 mm. Furthermore, beyond that crack length (0.1t), there was a little effect of the tip radius at the undercut on the values of ($M^{A}_{k,B}$).

Figure 5.12a showed the effect of the weld toe radius (r) on the stress intensity magnification factor ($M^{A}_{k,A}$) under axial loading. The values of ($M^{A}_{k,A}$) were strongly influenced by variations in the weld toe radius. The values of ($M^{A}_{k,A}$) at the weld toe surface were increased significantly from 1.0 for a flat plate to between 1.2 and 2.0 for variations of the weld toe radius. At an early stage of the crack growth, for a crack length less than 10 % of the plate thickness (0.1t), the values of ($M^{A}_{k,A}$) decreased as (r) increased from 0.0 mm to 5.0 mm. However, beyond that crack length, there was an insignificant difference between the values of ($M^{A}_{k,A}$) for the variations of the weld toe radius.

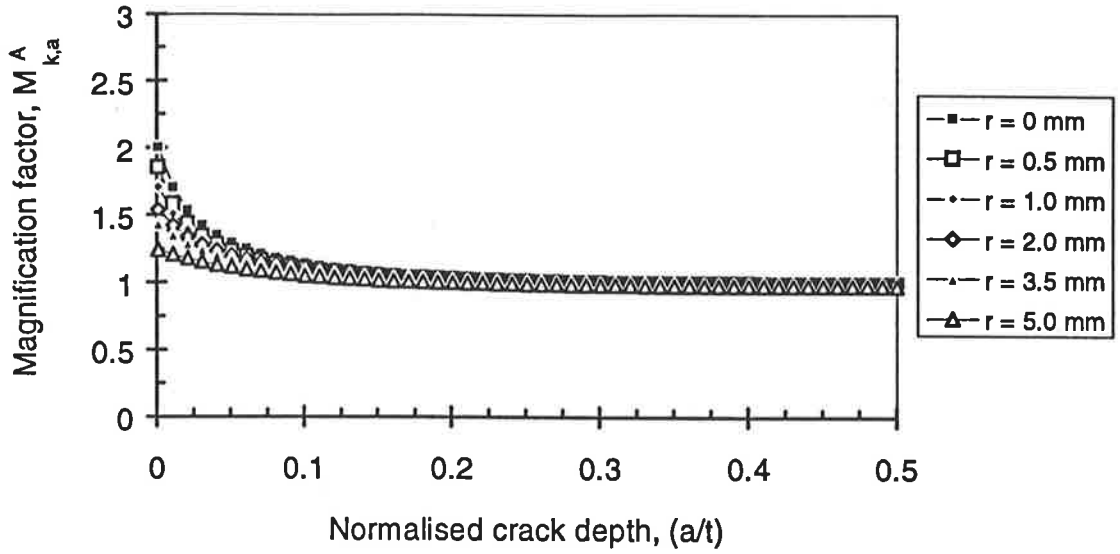

(a) Pure axial loading condition

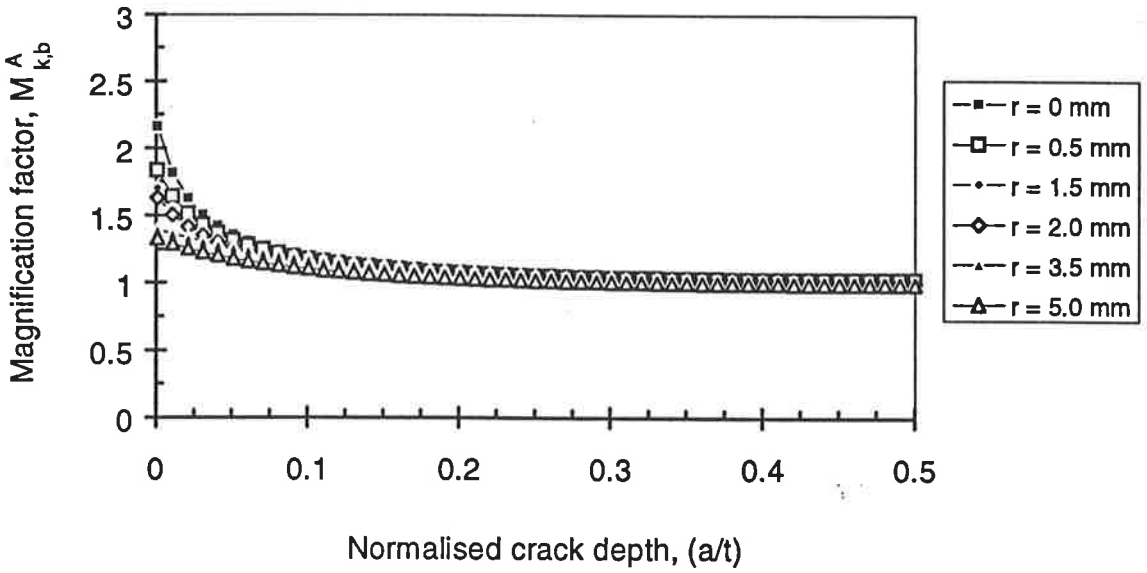

(b) Pure bending load condition

Figure 5.12 Effect of the weld toe radius on the stress intensity magnification factor (M_k) (constant parameters: r ' = 0, $\theta = 30°$, $\phi = 60°$ and t = 12 mm).

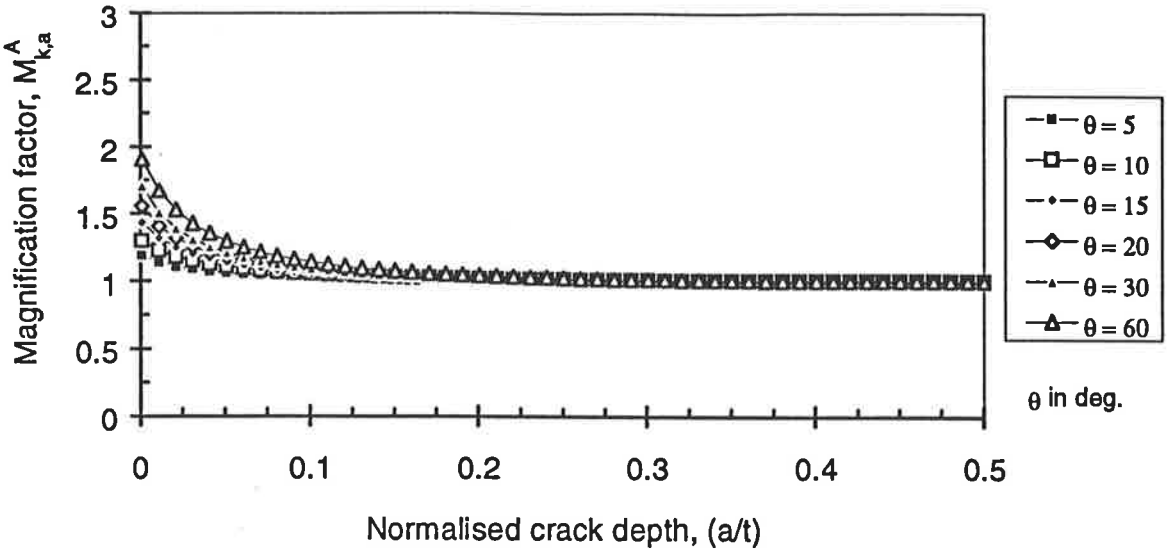

(a) Pure axial loading condition

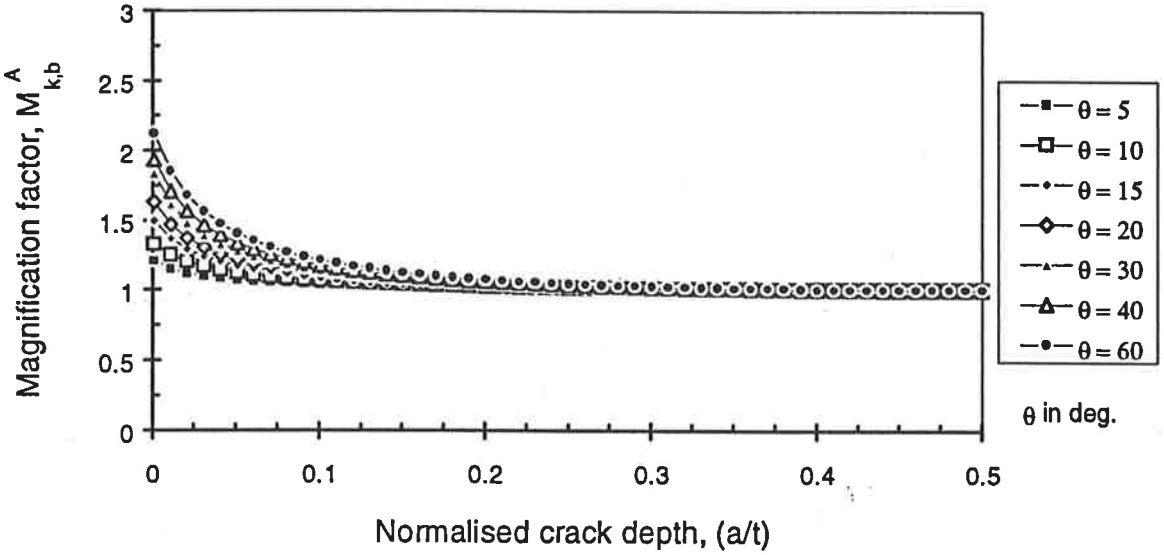

(b) Pure bending load condition

Figure 5.13 Effect of the flank angle on the stress intensity magnification factor (M_k) (constant parameters: r ' = 0, r = 1 mm, $\phi = 60°$ and t = 12 mm).

A similar behaviour of the effect of the weld toe radius on the stress intensity magnification factor ($M^{A}_{k,B}$) under bending is shown in Fig. 5.12b. The values of ($M^{A}_{k,B}$) at the surface increased significantly from 1.0 for a flat plate to between 1.2 to 2.2 due to the presence of the weld toe undercut. At an early stage of the crack growth (i.e. for a crack length of less than 10 % of the plate thickness) the values of ($M^{A}_{k,B}$) increased as the (r) increased from 0.0 mm to 5.0 mm. However, beyond that crack length (0.1t), there was an insignificant effect of the weld toe radius on the values of ($M^{A}_{k,B}$).

Figure 5.13a showed the effect of the flank angle (θ) on the stress intensity magnification factor ($M^{A}_{k,A}$) under axial loading. The values of ($M^{A}_{k,A}$) were strongly influenced by the variations in the flank angle. The values of ($M^{A}_{k,A}$) at the weld toe surface increased significantly from 1.0 for a flat plate or for flush-ground weld ($\theta = 0°$) to between 1.2 and 2.0 for variations of the flank angle from 5° to 60°. At the early stage of the crack growth corresponding to a crack length less than 15 % of the plate thickness (0.15t), the values of ($M^{A}_{k,A}$) increased as (θ) increased from 5° to 60°. However, beyond that crack length, there was an insignificant effect of the flank angle on the values of ($M^{A}_{k,A}$). Therefore, the flatter the weld bead profile the smaller the stress intensity factor. Consequently, this will result in increased fatigue life.

Figure 5.13b showed the effect of the flank angle (θ) on the stress intensity magnification factor ($M^{A}_{k,B}$) under bending. The values of ($M^{A}_{k,B}$) were strongly influenced by the variations of the flank angle. The values of ($M^{A}_{k,B}$) at the weld toe surface were increased significantly from 1.0 for a flat plate to between 1.2 and 2.2 for variations of the flank angle (θ) from 5° to 60°. At the early stage of the crack

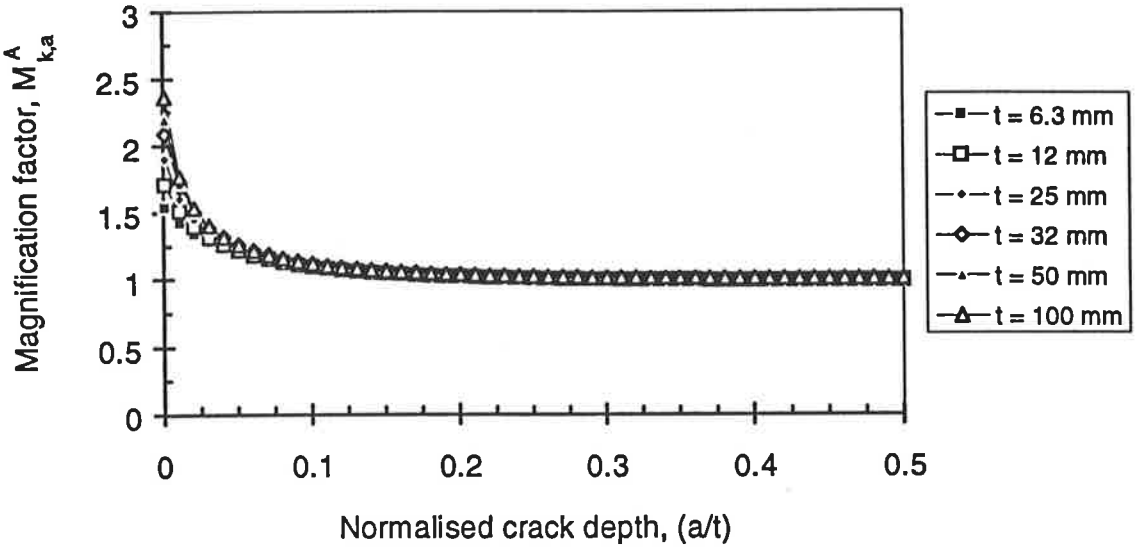

(a) Pure axial loading condition

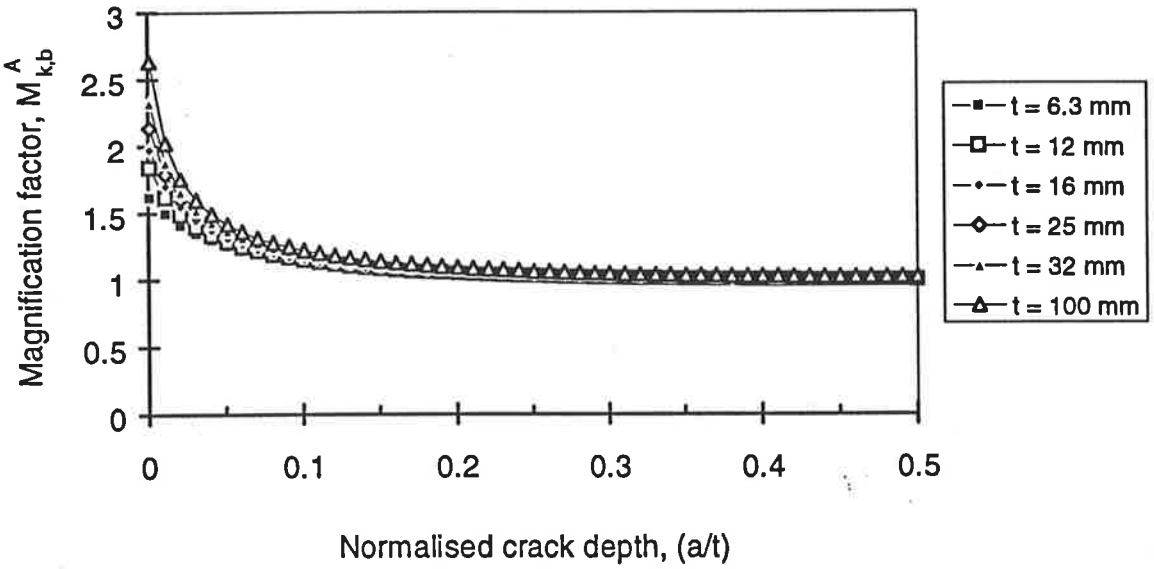

(b) Pure bending load condition

Figure 5.14 Effect of the plate thickness on stress intensity magnification factor (M_k) (constant parameters: r ' = 0, r = 1 mm, $\theta = 30°$ and $\phi = 60°$).

growth (corresponding to a crack length less than 15 % of plate thickness) the values of ($M^{A}_{k,B}$) increased as the (θ) increased from 5° to 60°. However, beyond that crack length (0.15t), the flank angle had an insignificant effect on the values of ($M^{A}_{k,B}$).

Figure 5.14a showed the effect of the plate thickness on the stress intensity magnification factor ($M^{A}_{k,A}$) under axial loading. The values of ($M^{A}_{k,A}$) were strongly influenced by the variations in the plate thickness. The values of ($M^{A}_{k,A}$) at the weld toe surface increased significantly from 1.0 for a flat plate to between 1.5 and 2.5 for the variations of the plate thickness from 6.3 to 100 mm. At the early stage of the crack growth (corresponding to a crack length less than 5 % of the plate thickness) the values of ($M^{A}_{k,A}$) increased as (t) increased from 6.3 mm to 100 mm. However, beyond that crack length (0.05t), there was an insignificant effect of the plate thickness on the values of ($M^{A}_{k,B}$). Figure 5.14b showed that the effect of the plate thickness on the stress intensity magnification factor ($M^{A}_{k,B}$) under bending was similar to that under axial loading (Fig. 5.14a). The values of ($M^{A}_{k,B}$) shown in Fig. 5.14b were strongly influenced by the variations of the plate thickness. The values of ($M^{A}_{k,B}$) at the weld toe surface increased significantly from 1.0 for a flat plate to between 1.5 and 2.6 for variations of the plate thickness from 6.3 mm to 100 mm. At the early stages of the crack growth (corresponding to crack lengths less than 5 % of the plate thickness) the values of ($M^{A}_{k,B}$) increased as the (t) increased from 6.3 mm to 100 mm. Beyond that crack length (0.05t), there was an insignificant effect of the plate thickness on the values of ($M^{A}_{k,B}$).

The effect of the plate thickness shown in Figs 5.14a and 5.14b suggested that the thicker welded plate produces the higher values of (M_k) and therefore the fatigue life

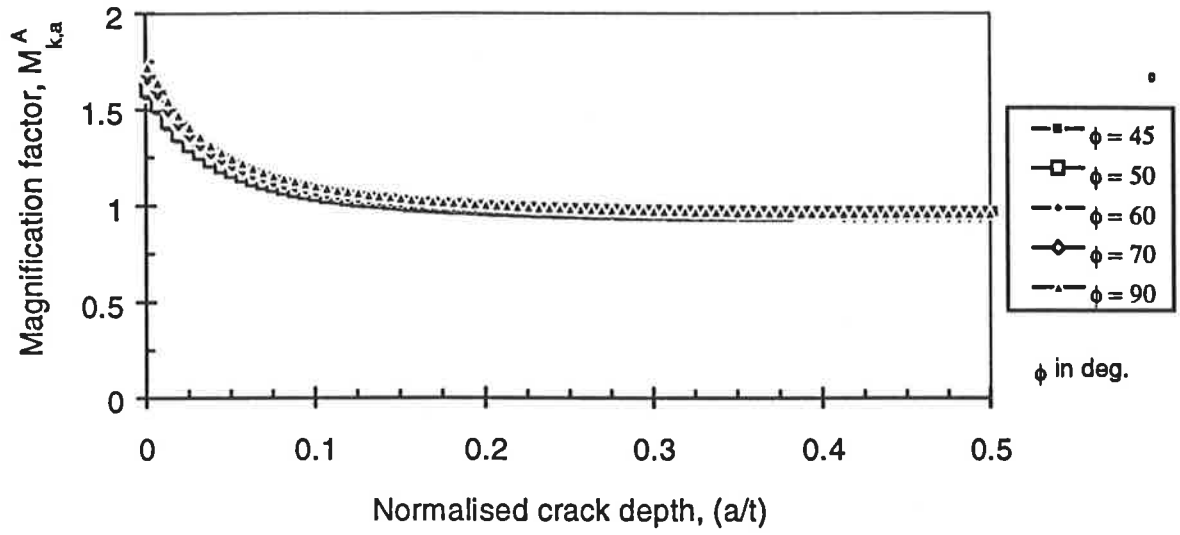

(a) Pure axial loading condition

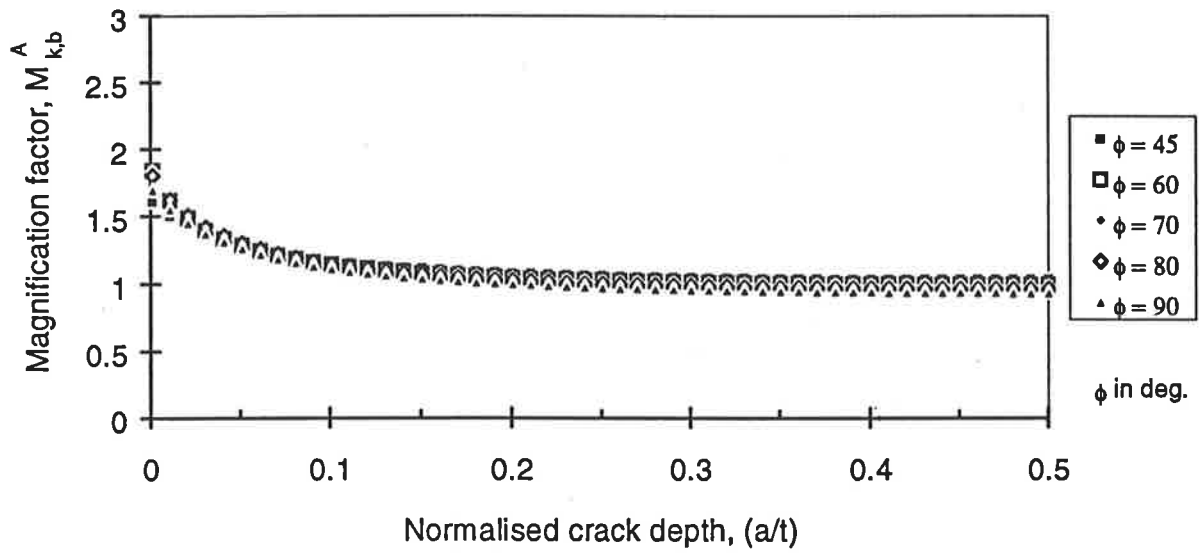

(b) Pure bending load condition

Figure 5.15 Effect of the edge preparation angle on stress intensity magnification factor (M_k) (constant parameters: r ' = 0, r = 1 mm, θ = 30° and t = 12 mm).

of a thick welded plate would be less than that of a thin one. This conclusion was consistent with the size effect of plate thickness on fatigue strength of welded joints as reported by other researchers (Gurney 1979, Yee et al 1988, Ohta et al 1990, Maddox 1991). However, the effect of plate thickness is shown to be significant for very small crack lengths (less than 0.05 and 0.1 times the plate thickness) under axial and bending loads. This suggests that for a welded joint with defects at the weld toes of 0.5 mm, there would be no effect of thickness for welded plates of less than 10 mm thick. In this case, other weld geometry parameters such as tip radius at the undercut, weld toe radius and flank angle are significant factors which determine the effect of weld geometry on the fatigue behaviour of welded joints.

Figure 5.15a showed the effect of the edge preparation angle (ϕ) on the stress intensity magnification factor ($M^{A}_{k,a}$) under axial loading. The values of ($M^{A}_{k,a}$) are slightly influenced by variations in the edge preparation angle. The values of ($M^{A}_{k,a}$) at the weld toe surface slightly increased from 1.0 for a flat plate to between 1.5 to 1.7 for variations of the edge preparation angle (ϕ) from 45° to 90°. At the early stage of the crack growth (corresponding to a crack length less than 5 % of the plate thickness) the values of ($M^{A}_{k,a}$) increased as (ϕ) increased from 45° to 90°. However, beyond that crack length (0.05t), the edge preparation angle had an insignificant effect on the values of ($M^{A}_{k,a}$).

A similar the effect of the edge preparation angle on the stress intensity magnification factor under bending is shown in Fig. 5.15b. There is an insignificant difference between the values of ($M^{A}_{k,b}$) for the variations in the angle (ϕ). However, the values of ($M^{A}_{k,b}$) for the crack lengths less than (0.1t) subject to variations in angle (ϕ) are

higher than that for a flat plate. This behaviour was due to the co-influence effect of the edge preparation angle and all the other butt weld geometry parameters (r, θ & t).

The effect of the edge preparation angle shown in Figs. 5.15a and 5.15b suggests that the fatigue performance of butt welded joints can be improved by decreasing the value of the edge preparation angle (ϕ). However, this method is often impractical since the value of the angle (ϕ) is dependent on the design requirements and welding techniques involved.

5.2.3 A mathematical model for (M_k)

A curve-fitting technique has been used to find the most suitable mathematical expression to represent the calculated values of (M_k) in terms of the normalised crack length (a/t). The resulting mathematical model is as follows:

$$M_k = A_1 + A_2 \,.\, \exp(a/t) + A_3 \,.\, \ln^2(a/t) + A_4 / \sqrt{(a/t)} \qquad (5.1)$$

where a, t - crack length and plate thickness respectively

A_i - constants depending on the weld geometry parameters:

where $A_i = K_i \,.\, f_i(r/t) \,.\, f_i(\theta) \,.\, f_i(t/b) \,.\, f_i(\phi)$

and K_i and $f_i(...)$ are as described below:

K_i - proportional constants (i = 1 to 4) as given in Table B.3 (Appendix B).

$f_i(...)$ - transformation functions of the concerned dimensionless product (i = 1 to 4) as given in Table B.3 (Appendix B).

5.2.4 Effect of weld geometry on the stress intensity factor of butt joints

As has been discussed in the previous section, the effect of butt weld geometry on the stress intensity geometry-configuration factor (Y) and magnification factor (M_k) under both loading conditions (axial and bending) are very similar except that their degree of influence is slightly different. Therefore, in the following sections, only the results obtained for the pure axial loading condition are reported.

Effect of undercut at the weld toe

Figure 5.16a showed the effect of the tip radius at the undercut (r') on the stress intensity factor $K^{w}_{sc,A}$ calculated for the constant stress range S = 80 MPa (other weld geometry parameters are kept constant: r = 2 mm, $\theta = 30°$, $\phi = 60°$ and t=12 mm). It shows that the values of $K^{w}_{sc,A}$ are slightly increased as the value of (r ') increased from 0.05 mm to 0.5 mm. This effect of (r ') on $K^{w}_{sc,A}$ can be used to explain the detrimental effect of the weld toe undercut on fatigue behaviour of welded joints. However, when a crack propagates beyond the length of 0.3 times the plate thickness (0.3t) the value of $K^{w}_{sc,A}$ decreased as the value of (r ') increased. This means that the effect of the weld toe undercut diminishes after that length, and the tip radius of undercut acts as the weld toe radius.

Figure 5.16b showed the effect of (r') on the stress intensity factor $K^{w}_{sc,B}$ calculated for the constant stress range S = 80 MPa (other weld geometry parameters are kept constant: r = 2 mm, $\theta = 30°$, $\phi = 60°$ and t=12 mm). At the early stages of the crack growth (c/b < 0.05), the values of the stress intensity factor $K^{w}_{sc,B}$ increased as the tip

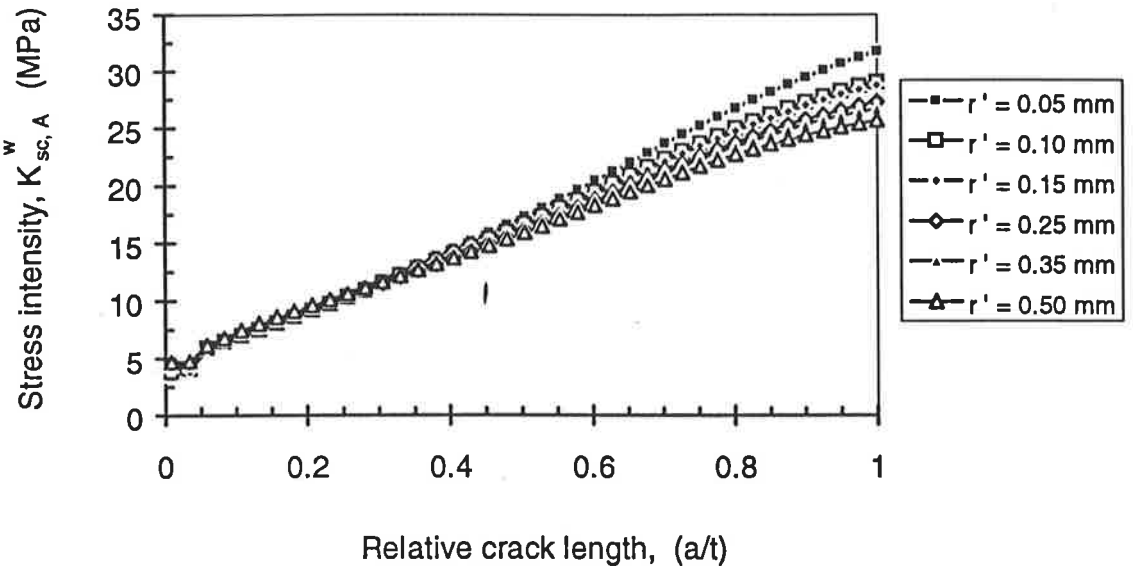

(a) Effect of tip radius of undercut at weld toe (r') on $K^{w}_{sc,A}$

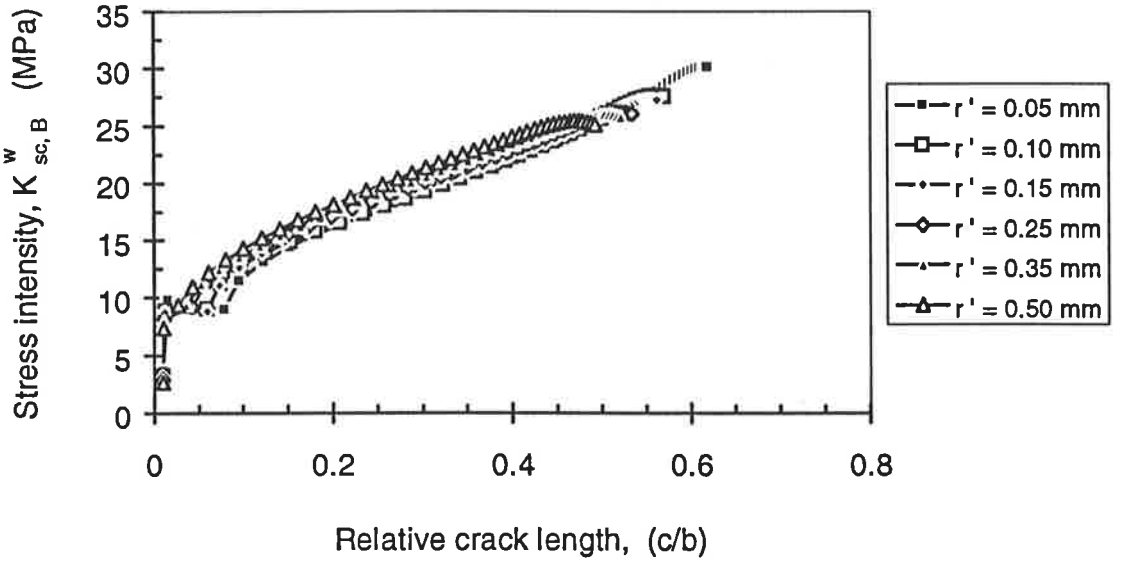

(b) Effect of tip radius of undercut at weld toe (r') on $K^{w}_{sc,B}$

Figure 5.16 Effect of the tip radius at the undercut on the stress intensity factor of butt-joints (constant parameters: r = 2 mm, $\theta = 30°$, $\phi = 60°$ and t = 12 mm).

radius at the undercut decreases. This effect of (r') is similar to that of the weld toe radius as shown later in Fig. 5.17b. However, beyond that crack length (c/b >0.05) the values of the stress intensity factor $K^{w}_{sc,B}$ decreased as the tip radius at the undercut decreased. It suggests that the fatigue behaviour of butt joints can be improved by eliminating the undercuts at the weld toes.

Effect of the weld toe radius

Figure 5.17a showed the effect of the weld toe radius (r) on the stress intensity factor $K^{w}_{sc,A}$ calculated for the constant stress range S = 80 MPa (other weld geometry parameters are kept constant: r ' = 0, $\theta = 30°$, $\phi = 60°$ and t = 12 mm). It shows that the values of $K^{w}_{sc,A}$ decreased as the weld toe radius (r) increased. There is a significant difference between the values of $K^{w}_{sc,A}$ due to the variations in the weld toe radii from 0.3 mm to 2.0 mm. However, there is a less significant difference between the values of $K^{w}_{sc,A}$ due to the variations in the weld toe radii from 2.0 mm to 2.5 mm.

Figure 5.17b showed the effect of the weld toe radius (r) on the stress intensity factor $K^{w}_{sc,B}$ calculated for the constant stress range S = 80 MPa (other weld geometry parameters were kept constant: r ' = 0, $\theta = 30°$, $\phi = 60°$ and t = 12 mm). It shows that the values of $K^{w}_{sc,B}$ decreased as the weld toe radius increased. It suggests that the fatigue behaviour of butt joints can be improved by increasing the weld toe radii .

Effect of the flank angle

Figure 5.18a showed the effect of the flank angle (θ) on the stress intensity factor $K^{w}_{sc,A}$ calculated for the constant stress range S = 80 MPa (other weld geometry

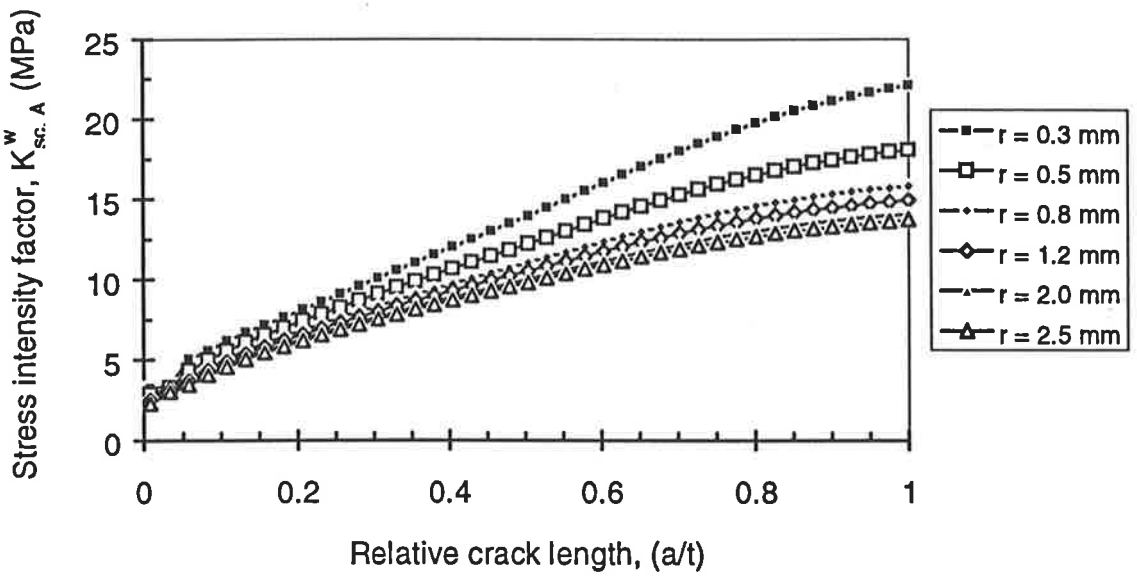

(a) Effect of weld toe radius (r) on $K^{w}_{sc,A}$

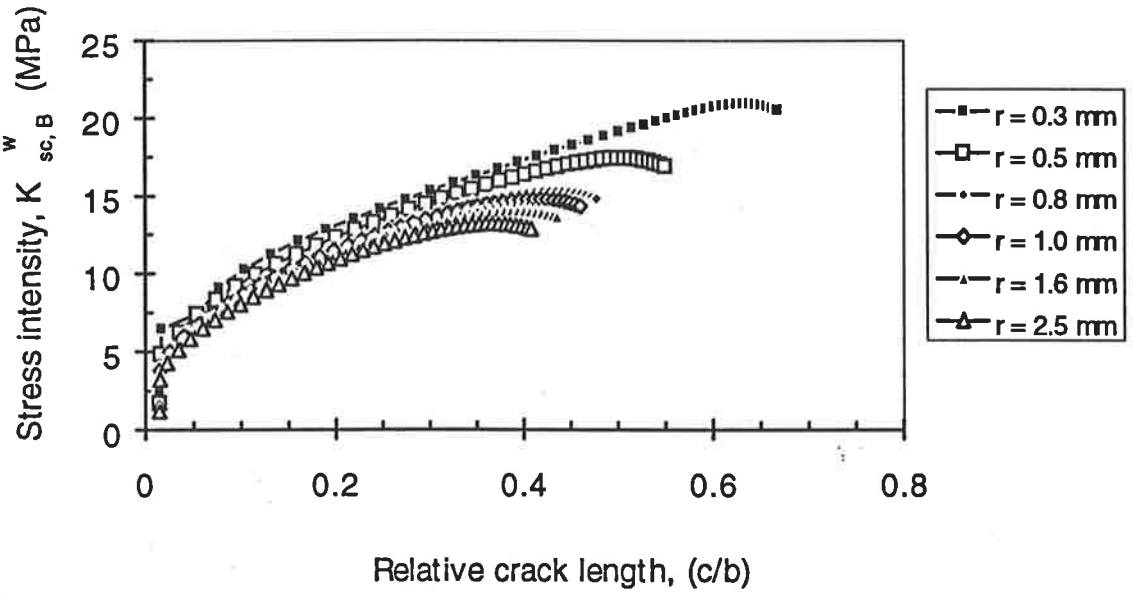

(b) Effect of weld toe radius (r) on $K^{w}_{sc,B}$

Figure 5.17 Effect of weld toe radius on the stress intensity factor of butt-joints (constant parameters: r ' = 0, $\theta = 30°$, $\phi = 60°$ and t = 12 mm).

parameters are kept constant: r ' = 0, r = 1 mm, ϕ = 60° and t = 12 mm). It shows that the values of $K^{w}_{sc,A}$ decreased as the flank angle decreased. There was a significant difference between the values of $K^{w}_{sc,A}$ due to the variations in the flank angles from 20° to 0°. However, there was a small difference between the values of $K^{w}_{sc,A}$ corresponding to the values of flank angle from 20° to 60°.

Figure 5.18b showed the effect of the flank angle (θ) on the stress intensity factor $K^{w}_{sc,B}$ calculated for the constant stress range S = 80 MPa (other weld geometry parameters are kept constant: r ' = 0, r = 1 mm, ϕ = 60° and t = 12 mm). It showed that the values of $K^{w}_{sc,B}$ decreased as the flank angle decreased from 60° to 0°. Fig. 5.18b also showed that there was a small difference between values of $K^{w}_{sc,B}$ was observed due to the variations in the flank angle from 20° to 60°.

Effect of the plate thickness

Figure 5.19a showed the effect of the plate thickness (t) on the stress intensity factor $K^{w}_{sc,A}$ calculated for the constant stress range S = 80 MPa (other weld geometry parameters are kept constant: r ' = 0, r = 1 mm, θ = 30° and ϕ = 60°). It shows that the values of $K^{w}_{sc,A}$ increased as the plate thickness increased. Based on this behaviour of the $K^{w}_{sc,A}$, the known effect of the plate thickness in reducing the fatigue life of weld joints (which are reported in the literature (Gurney 1979, Ohta et al. 1990, Maddox 1991)) can be well-explained.

Figure 5.19b showed the effect of the plate thickness (t) on the stress intensity factor $K^{w}_{sc,B}$ calculated for constant stress range S = 80 MPa (other weld geometry

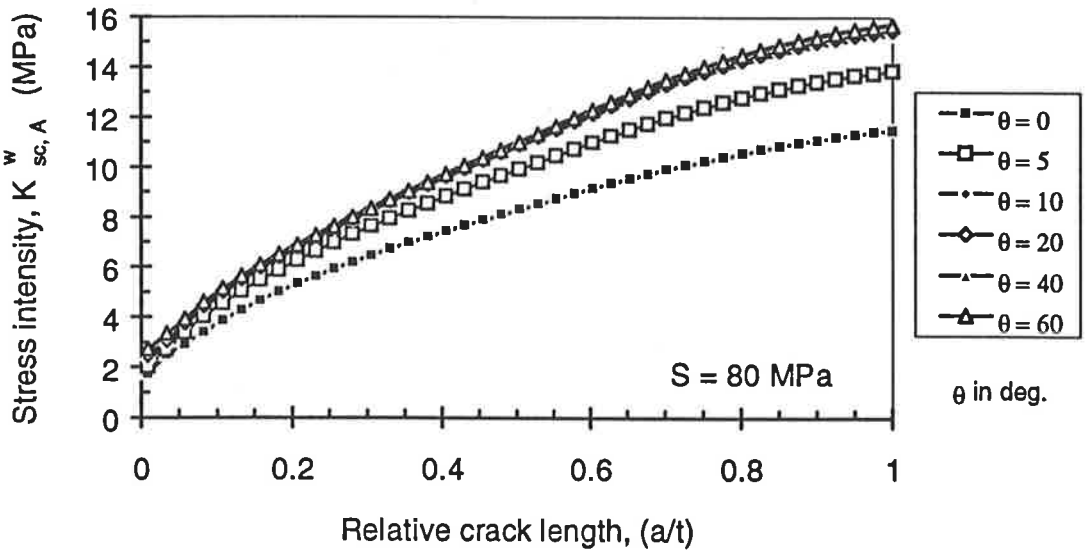

(a) Effect of (θ) on $K^{w}_{sc,A}$

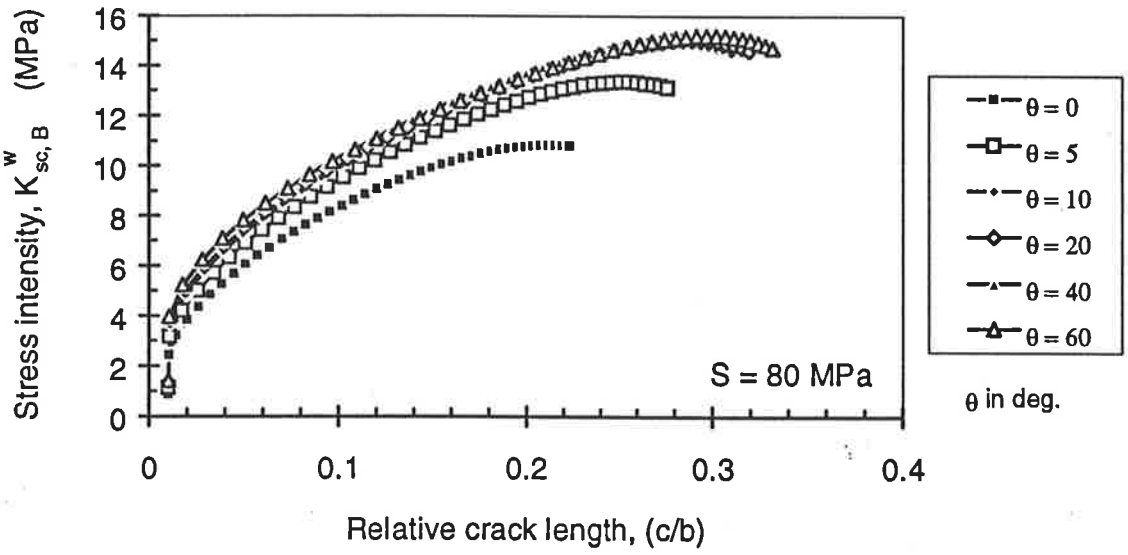

(b) Effect of (θ) on $K^{w}_{sc,B}$

Figure 5.18 Effect of flank angle on the stress intensity factor of butt-joints (constant parameters: r ' = 0, r = 1 mm, $\phi = 60^{\circ}$ and t = 12 mm).

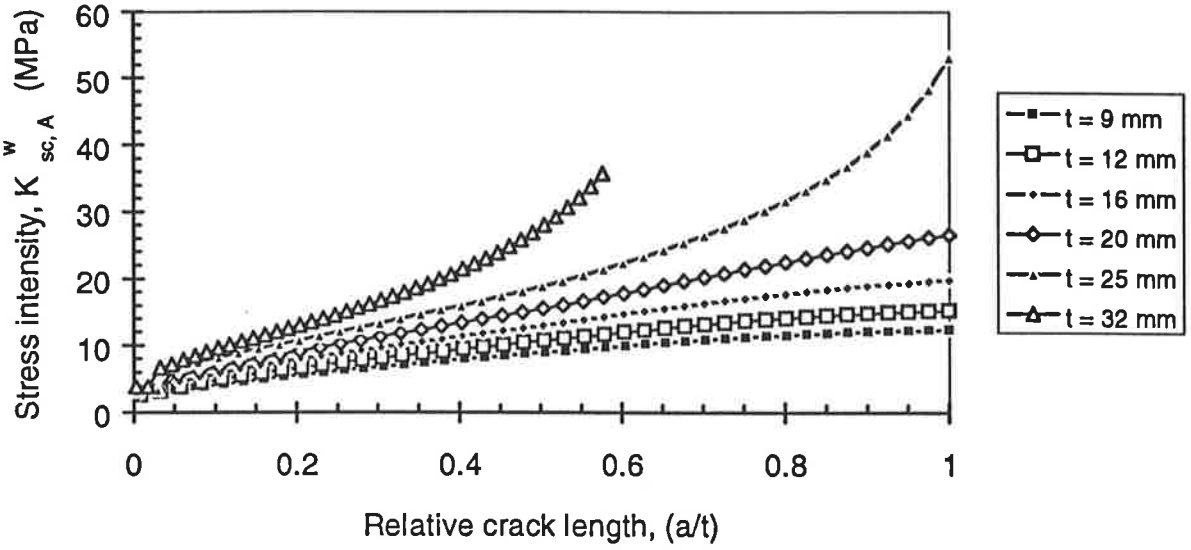

(a) Effect of (t) on $K^{w}_{sc,A}$

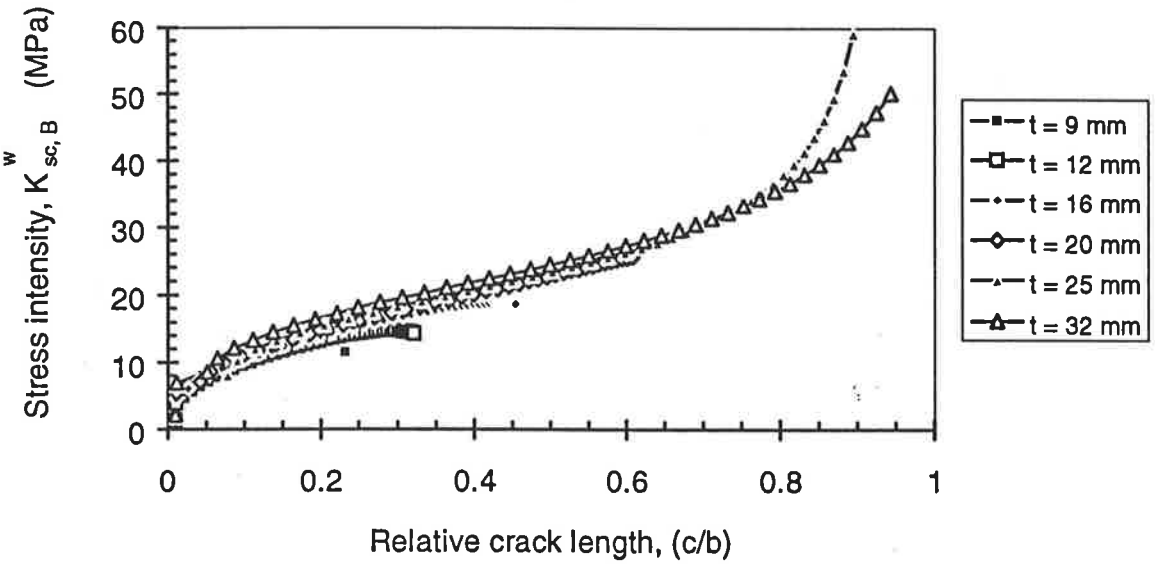

(b) Effect of (t) on $K^{w}_{sc,B}$

Figure 5.19 Effect of the plate thickness on the stress intensity factor of butt-joints (constant parameters: r ' = 0, r = 1 mm, $\theta = 30°$ and $\phi = 60°$).

parameters were kept constant: r ' = 0, r = 1 mm, θ = 30° and ϕ = 60°). Fig. 5.19b shows that the values of the $K^{w}_{sc,B}$ increased as the plate thickness increased. This behaviour of the $K^{w}_{sc,B}$ was similar to that of the $K^{w}_{sc,A}$ except that the effect of the plate thickness on the $K^{w}_{sc,A}$ was far more significant.

Effect of the edge preparation angle

Figure 5.20a showed the effect of the edge preparation angle (ϕ) on the stress intensity factor $K^{w}_{sc,A}$ calculated for the constant stress range S = 80 MPa (other weld geometry parameters were kept constant: r ' = 0, r = 1 mm, t = 12 mm and θ = 30°). It shows that the values of the $K^{w}_{sc,A}$ slightly increase as the edge preparation angle increases from 45° to 90°. However, this effect of the angle (ϕ) was more significant in the later stages of the crack propagation when the crack had propagated beyond the 40 % of the plate thickness (a/t > 0.4).

Figure 5.20b showed the effect of the edge preparation angle (ϕ) on the stress intensity factor $K^{w}_{sc,B}$ calculated for constant stress range S = 80 MPa (other weld geometry parameters are kept constant: r ' = 0, r = 1 mm, t = 12 mm and θ = 30°). This figure also shows that the values of the $K^{w}_{sc,B}$ slightly increased as the edge preparation angle increased from 45° to 90°. It was observed that the effect of the angle (ϕ) on the $K^{w}_{sc,B}$ became more distinguishable after the crack has propagated beyond the crack length of 20 % of the width of welded plate (c/b > 0.2).

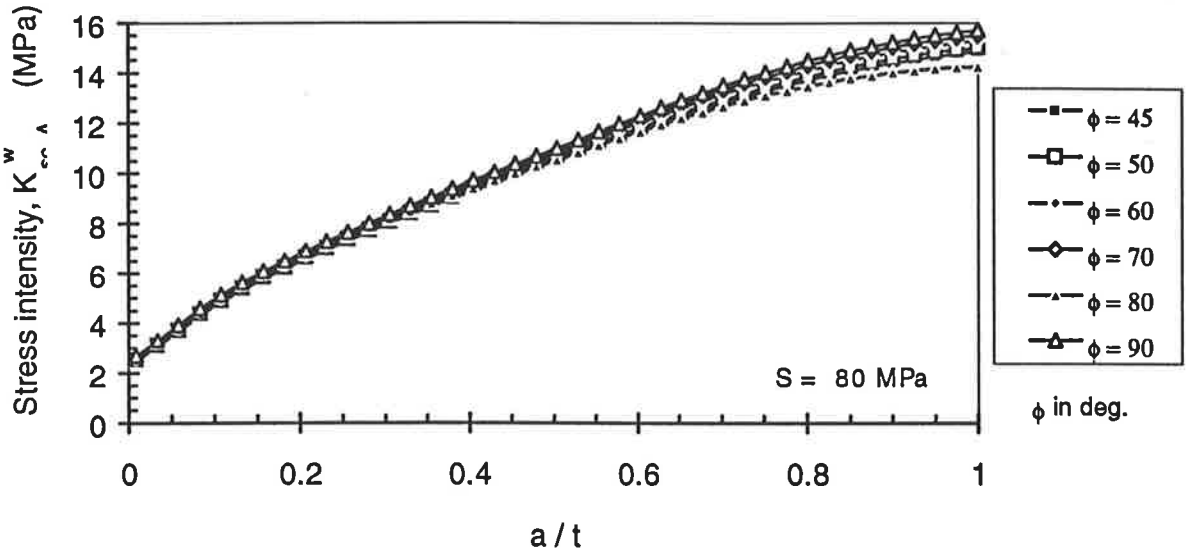

(a) Effect of (ϕ) on $K^w_{sc,A}$

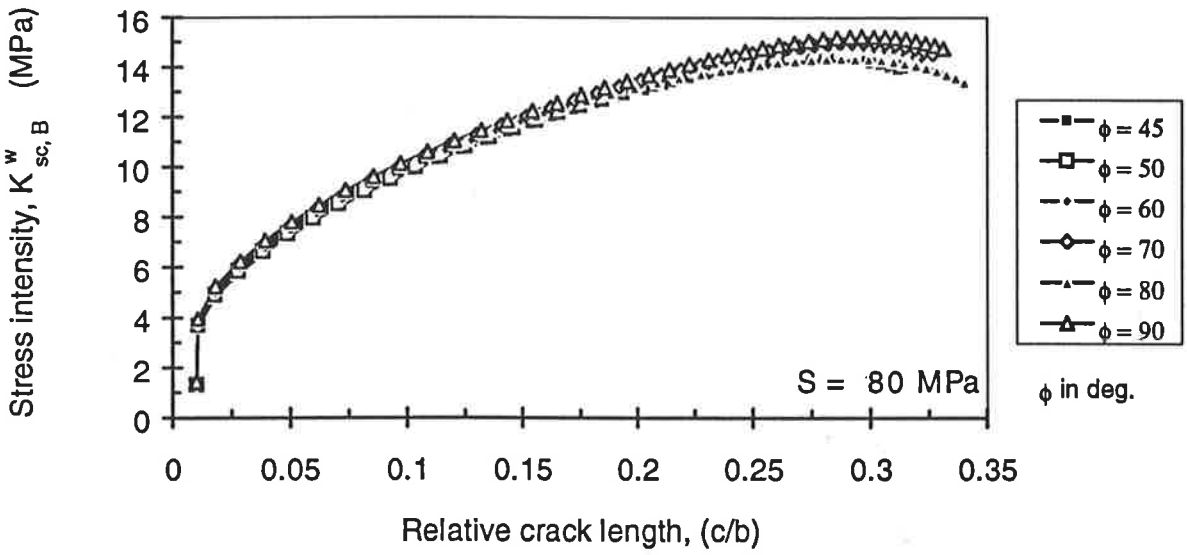

(b) Effect of (ϕ) on $K^w_{sc,B}$

Figure 5.20 Effect of the edge preparation angle (ϕ) on the stress intensity factor of butt-joints (constant parameters: r ' = 0, r = 1 mm, $\theta = 30°$ and t = 12 mm).

Effect of the initial crack shape aspect ratio

The effect of the initial crack shape aspect ratio $(a/c)_o$ (Fig. 3.2) on the fatigue behaviour of a butt welded joint was investigated by keeping all the relevant butt-weld geometry parameters constant and varying the values of $(a/c)_o$.

Figure 5.21a showed the effect of the ratio $(a/c)_o$ on the stress intensity factor $K^w_{sc,A}$ calculated for constant stress range S = 80 MPa (other weld geometry parameters are kept constant: r' = 0.15 mm, r = 2 mm, $\theta = 30°$, $\phi = 60°$ and t = 12 mm). It shows that the values of $K^w_{sc,A}$ decreased as the ratio $(a/c)_o$ increased from 0.1 to 1.0. However, this trend tended to be significant during the early stages of the crack growth ($a/t < 0.1$) only.

Figure 5.21b showed the effect of the ratio $(a/c)_o$ on the stress intensity factor $K^w_{sc,B}$ calculated for constant stress range S = 80 MPa (other weld geometry parameters are kept constant: r' = 0.15 mm, r = 2 mm, $\theta = 30°$, $\phi = 60°$ and t = 12 mm). It showed that the values of the $K^w_{sc,B}$ increased as the ratio $(a/c)_o$ increased from 0.1 to 1.0. This behaviour of the $K^w_{sc,B}$ was observed only during the early stages of the crack growth ($c/b < 0.15$), beyond that limit there was an insignificant effect of the ratios $(a/c)_o$ on the values of $K^w_{sc,B}$. However, some fluctuations of the values of $K^w_{sc,B}$ were found during the early stages of the crack growth ($c/b < 0.1$).

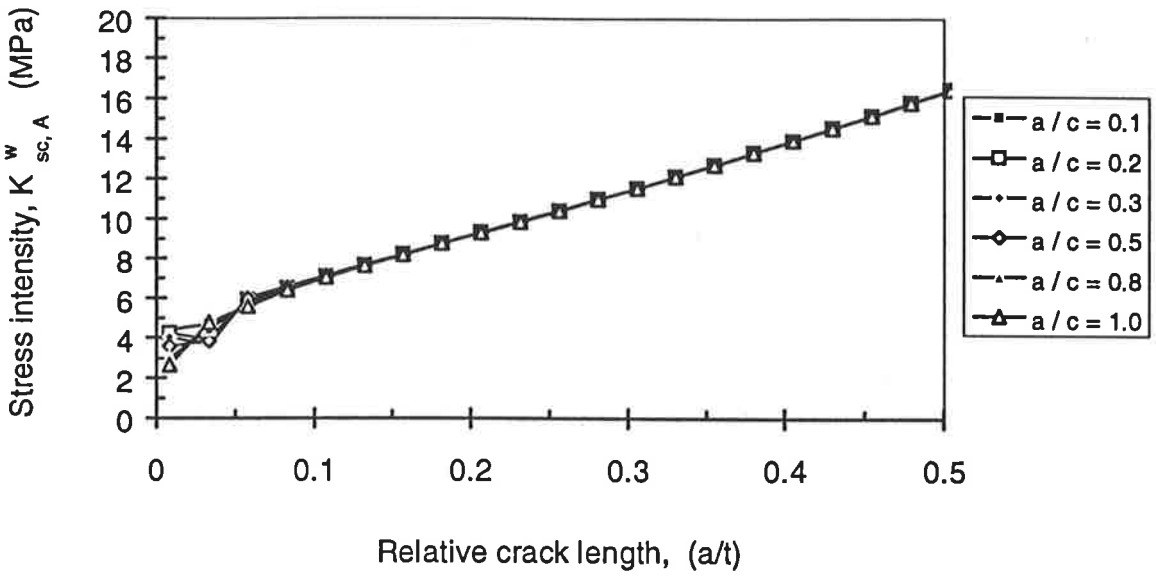

(a) Effect of $(a/c)_o$ on $K^{w}_{sc,A}$

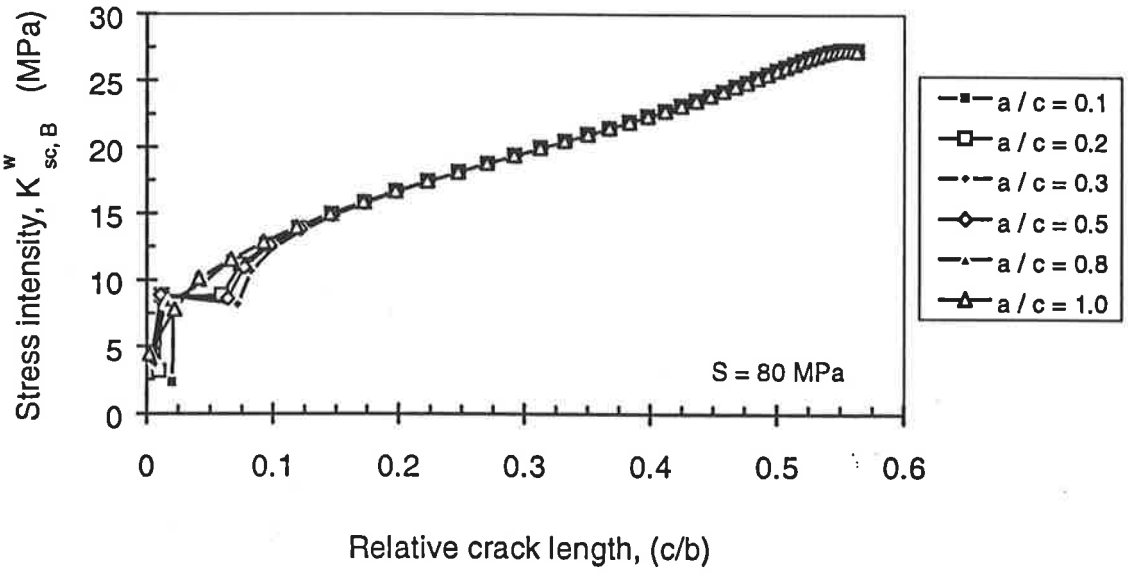

(b) Effect of $(a/c)_o$ on $K^{w}_{sc,B}$

Figure 5.21 Effect of the edge preparation angle on the stress intensity factor of butt-joints (constant parameters: r ' = 0, r = 1 mm, $\theta = 30°$ and t = 12 mm).

5.3 Effect of Weld Geometry on the Fatigue Behaviour of Butt Joints

In this section, the effect of various weld geometry parameters on the fatigue behaviour of butt-welded joints in terms of the evolution of crack shape, crack growth a-N curve and fatigue S-N curve are discussed.

5.3.1 Effect of weld geometry on the crack shape evolution

Effect of the undercut at the weld toe

Figure 5.22 showed the effect of the tip radius at the weld toe undercut (r') on the crack aspect ratio (a/c). It shows that the semi-elliptical surface crack with a higher value of (r') when propagated in a butt-welded joint tended to develop the crack shape with a higher value of (a/c) i.e approaching towards the semi-circle shape. At the early stage of the crack growth ($a/t < 0.1$), the semi-elliptical surface crack tended to reach the shape with a higher value of (a/c) during crack propagation life i.e close to the shape of the semi-circular crack. However, the ratio of (a/c) decreased as the crack propagated further.

Effect of the weld toe radius

Figure 5.23 shows the effect of weld toe radius on the crack shape aspect ratio (a/c). It shows that a semi-elliptical surface crack with a larger weld toe radius when propagates in butt welded joints tended to develop a crack shape with the higher value of (a/c) during crack propagation life. At the early stage of the crack growth ($a/t < 0.1$), surface crack tended to reach the semi-elliptical shape with a higher value

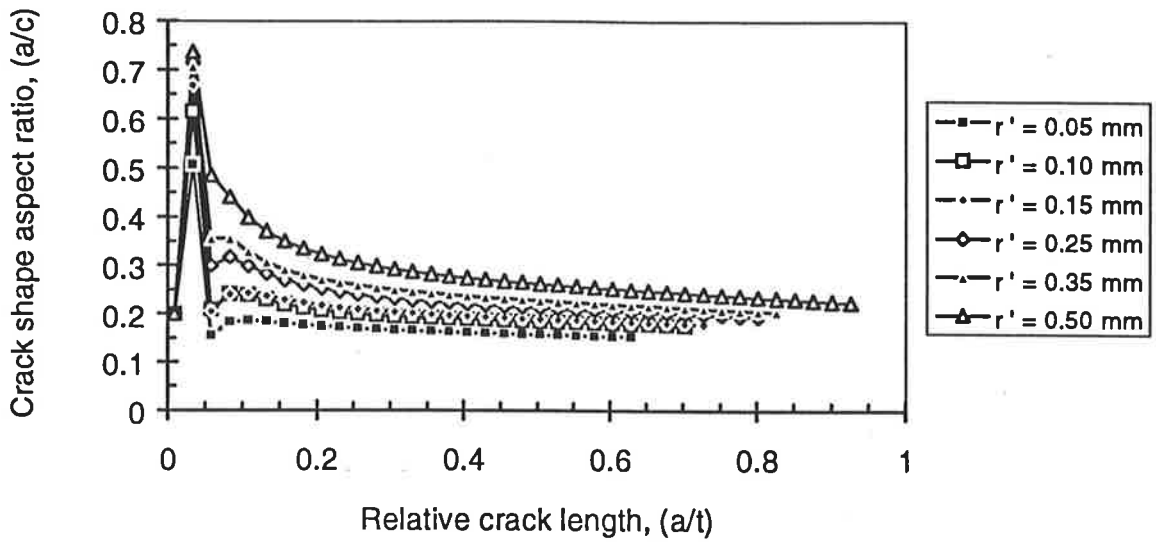

Figure 5.22 Effect of the tip radius at the weld toe undercut on the evolution of the crack shape aspect ratio (a/c) (constant parameters: r = 2 mm, θ = 30°, ϕ = 60°, t = 12 mm, R=0).

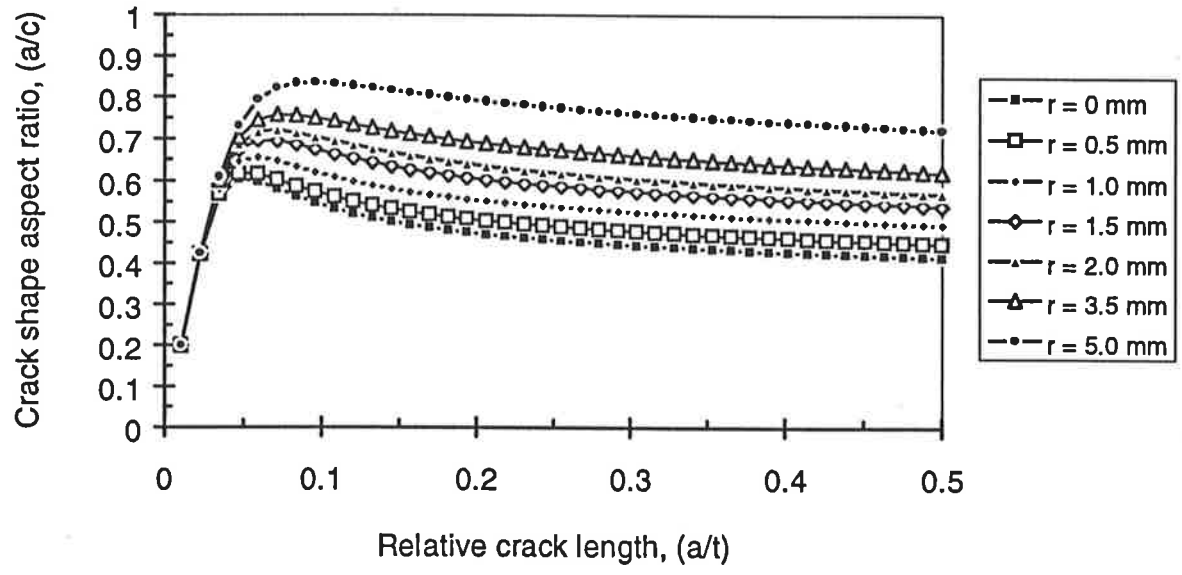

Figure 5.23 Effect of weld toe radius on the evolution of the crack shape aspect ratio (a/c) (constant parameters: r' = 0, θ = 30°, ϕ = 60°, t = 12 mm, R=0).

of (a/c) i.e approaching towards the shape of the semi-circular crack. However, the ratios (a/c) tend to decrease as the crack propagates further.

Effect of the flank angle

Figure 5.24 showed the effect of the flank angle on the crack shape aspect ratio (a/c). It shows that semi-elliptical surface cracks with smaller flank angle when propagated in butt-welded joints, tended to develop the semi-elliptical crack shape with a higher value of (a/c) during crack propagation life. At the early stage of the crack growth ($a/t < 0.1$), the surface crack tended to reach the semi-elliptical shape with a higher value of (a/c) i.e close to the shape of the semi-circular crack. However, for the base plate or the flush-ground welded plate (with $\theta = 0$), the initial semi-elliptical crack became semi-circular after a few cycles. The ratio (a/c) decreased as the crack propagated further.

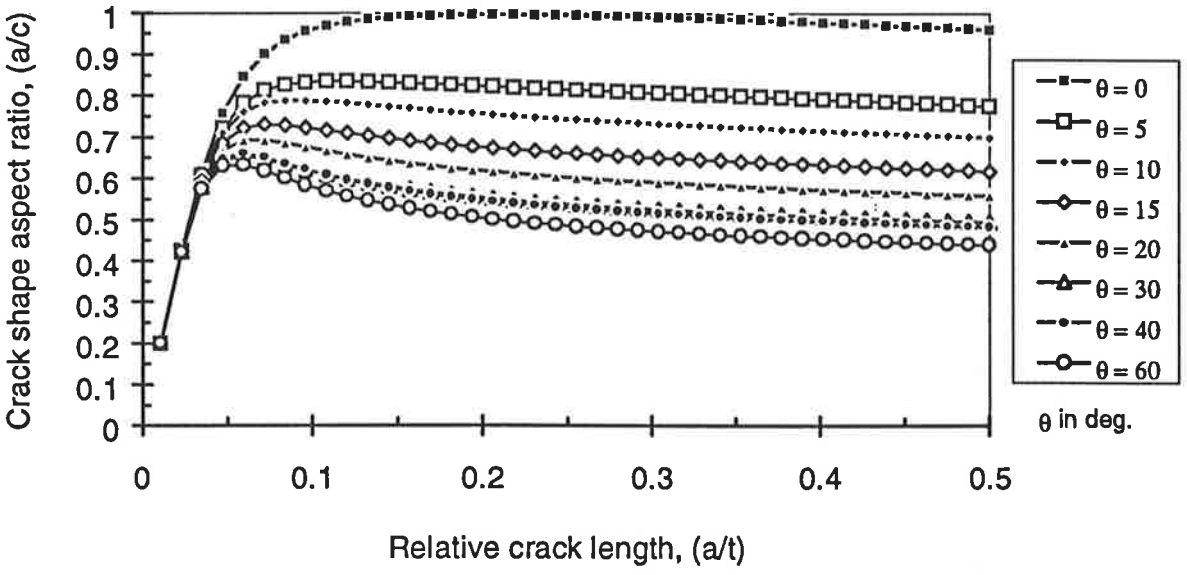

Figure 5.24 Effect of the flank angle on the evolution of the crack shape aspect ratio (a/c) (constant parameters: r' = 0, r = 1 mm, $\phi = 60°$, t = 12 mm, R=0).

Effect of the plate thickness

Figure 5.25 showed the effect of the plate thickness on the ratio (a/c). It shows that semi-elliptical surface cracks with a certain initial crack shape ($(a/c)_o$ = const) propagate through butt-welded joints made from thin plate tend to develop a semi-elliptical crack shape with a higher value of (a/c). During the early stage of the crack growth ($a/t < 0.1$), the surface crack tends to approach towards a crack shape with a higher value of (a/c) i.e close to the shape of the semi-circular crack. However, the ratio of (a/c) decreases as the crack propagates further.

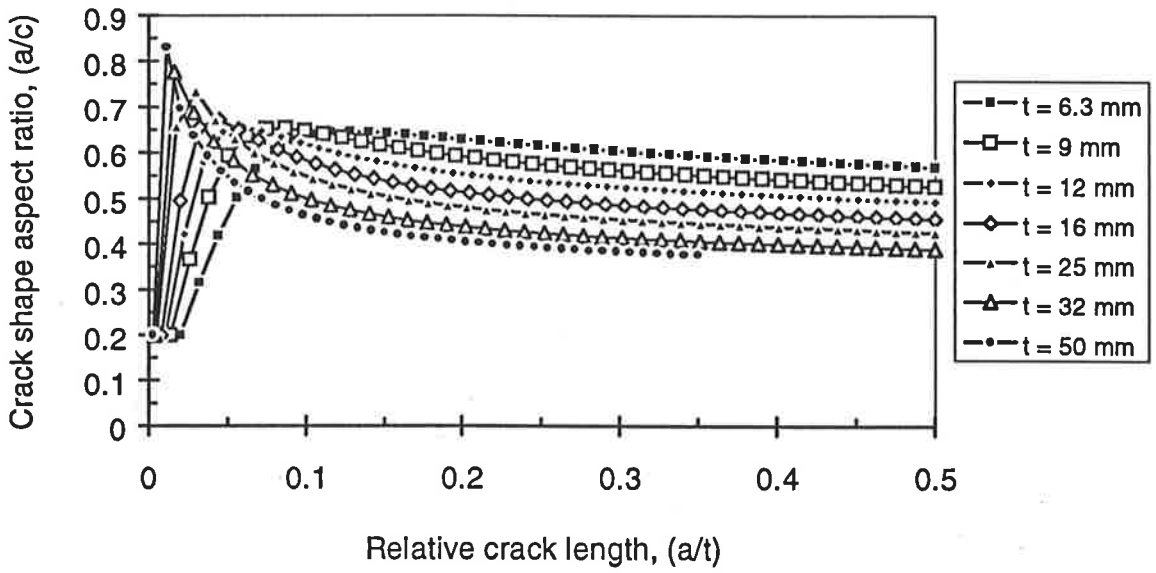

Figure 5.25 Effect of the plate thickness on evolution of the crack shape aspect ratio (a/c) (constant parameters: r' = 0, $\theta = 30°$, $\phi = 60°$, r = 1 mm, R=0).

Effect of the edge preparation angle

Figure 5.26 showed the effect of the edge preparation angle on the ratio (a/c). It shows that semi-elliptical surface cracks with a lower value of the angle (ϕ) propagate through butt welded joints tend to develop the semi-elliptical crack shape with higher

value of (a/c) during crack propagation life. At the early stage of the crack growth (a/t < 0.1), the surface crack tends to reach the crack shape with a higher value of (a/c) i.e close to the shape of the semi-circular crack. However, as the crack propagates further the ratio (a/c) decreases.

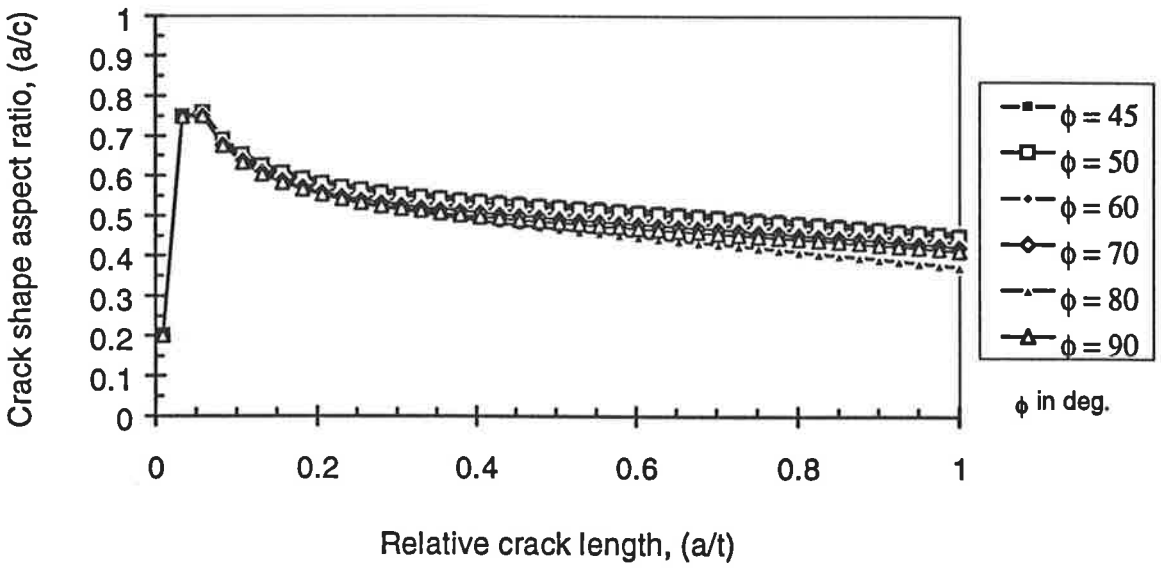

Figure 5.26 Effect of the edge preparation angle on the evolution of the crack shape aspect ratio (a/c) (constant parameters: r' = 0, r = 1 mm, θ = 60°, t = 12 mm, R=0).

Effect of the initial crack shape aspect ratio

Figure 5.27 showed the effect of the initial crack aspect ratio $(a/c)_o$ on the evolution of the crack shape during crack propagation. It shows that semi-elliptical surface cracks with various values of $(a/c)_o$ tend to develop the crack shape similar to the shape that developed by the initial semi-circular surface crack during the crack propagation life. However, this effect of the initial crack shape ratio was significant only during the early stages of the crack propagation (a/t < 0.1). Some fluctuations of the value of (a/c) were observed in this figure. Further, the values of (a/c) due to

various values of $(a/c)_o$ follow the same curve as expected from the initial semi-circular surface crack.

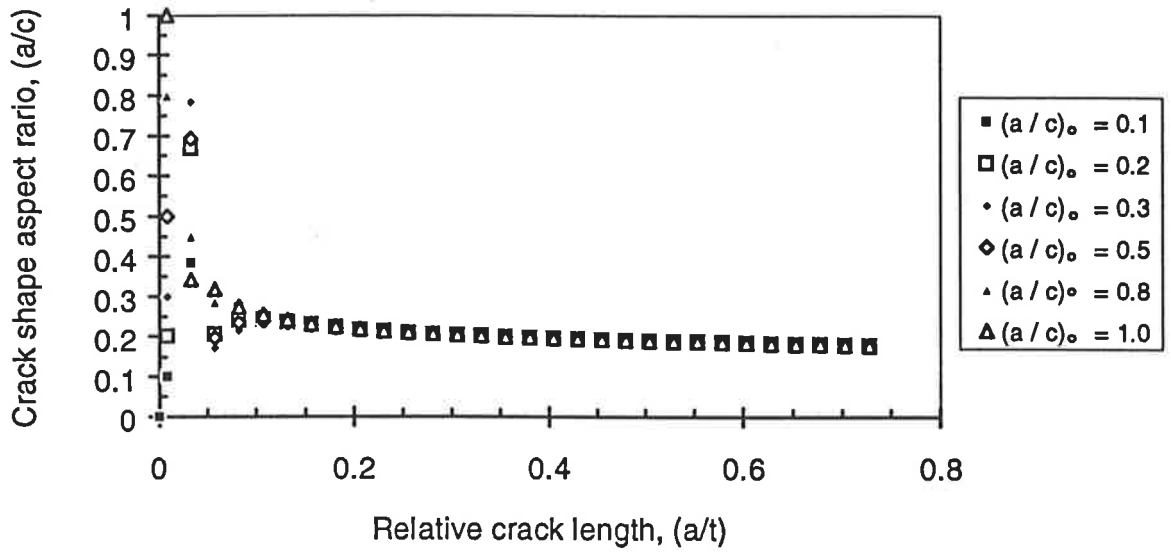

Figure 5.27 Effect of the initial crack aspect ratio $(a/c)_o$ on the evolution of crack shape (a/c) (constant parameters: r' = 0, r = 1 mm, $\theta = 60°$, $\phi = 60°$, t = 12 mm, R=0).

5.3.2 Effect of weld geometry on the fatigue crack growth curve (a vs. N) and on the S-N curve

Effect of the undercut at the weld toe

Figure 5.28a showed the effect of the tip radius at the undercut at the weld toe (r') on fatigue crack propagation life. It is obvious that the fatigue crack propagation life increased as the value of (r') decreased. It means that the fatigue life of the butt-welded joints can be improved by decreasing the value of (r') or by eliminating the undercut at weld toe by grinding or some other post-weld surface finishing

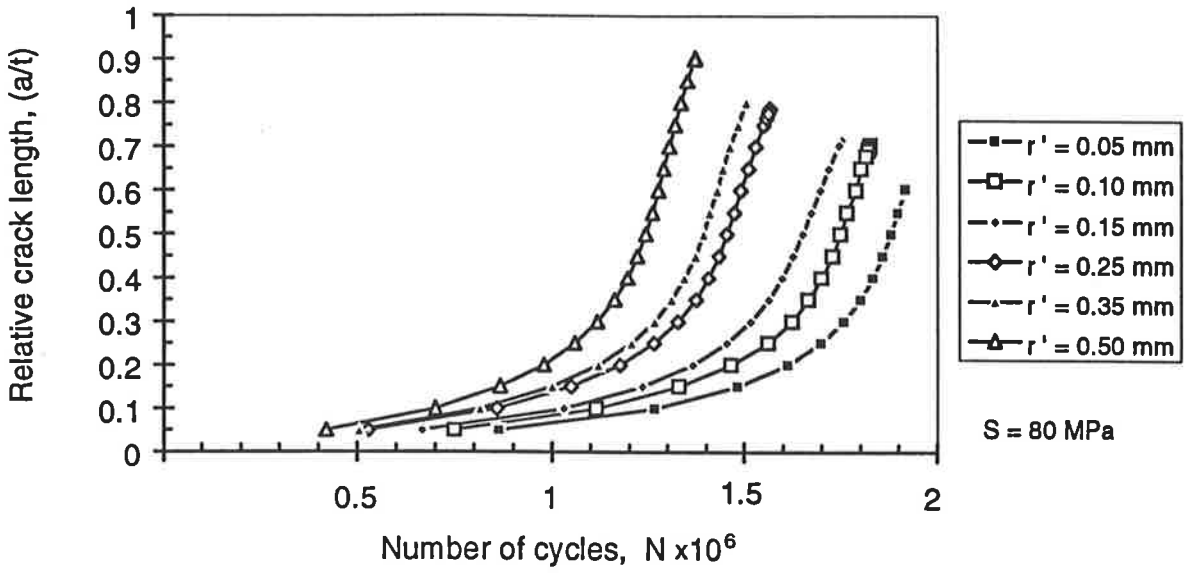

(a) Effect of (r') on crack growth curve (a vs. N)

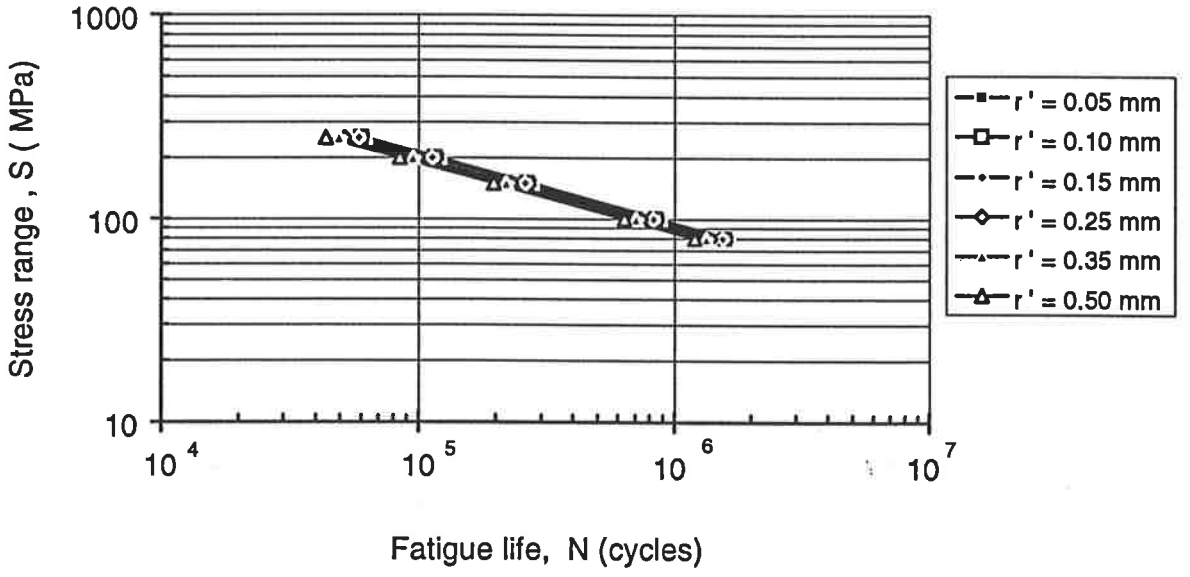

(b) Effect of (r') on fatigue S-N curve

Figure 5.28 Effect of the tip radius of undercut at the weld toe on crack growth curve (a vs. N) and S-N curve (constant parameters: r = 2 mm, θ = 30°, ϕ = 60°, t = 12 mm, R=0).

technique. Under the constant axially applied stress range (e.g. S=80 MPa), the improvement of the crack propagation life due to the decrease of (r') from 0.5 mm to 0.05 mm was of the order of $1.7x10^6$ cycles while that due to variation of (r), (θ), (t) and (ϕ) was $4.5x10^6$, $14x10^6$, $3x10^6$ and $1x10^6$ cycles respectively. This means that the degree of the influence of the tip radius at the undercut on the fatigue behaviour of butt-welded joints was less than that of (r), (θ) and (t) but stronger than that of (ϕ).

Figure 5.28b showed the effect of (r') on the S-N curve. It showed that the S-N curve tended to move from the left to the right as the value of (r') decreased. It means that the fatigue strength and fatigue life of butt-welded joints could be improved by either partly or totally removing the weld toe undercut. This figure also shows that the fatigue strength of a butt-joint at $2x10^6$ cycles (fatigue limit) was increased by 12 % as the tip radius at the undercut decreased from 0.5 mm to 0.05 mm.

Effect of the weld toe radius

In Fig. 5.29a it is shown how the fatigue crack propagation life increased as the value of the weld toe radius (r) increased. This means that the fatigue life of butt-welded joints can be improved by increasing the value of the weld toe radius (e.g. by grinding or other post-weld surface finishing technique). This conclusion was consistent with the results claimed by several other researchers (Lawrence et al 1973, Gurney 1979, Maddox 1991). This figure also showed that the improvement of the crack propagation life was due to an increase of (r) from 0.3 mm to 2.5 mm was of the order of $4.5x10^6$ cycles for constant axially applied stress range (S=80 MPa).

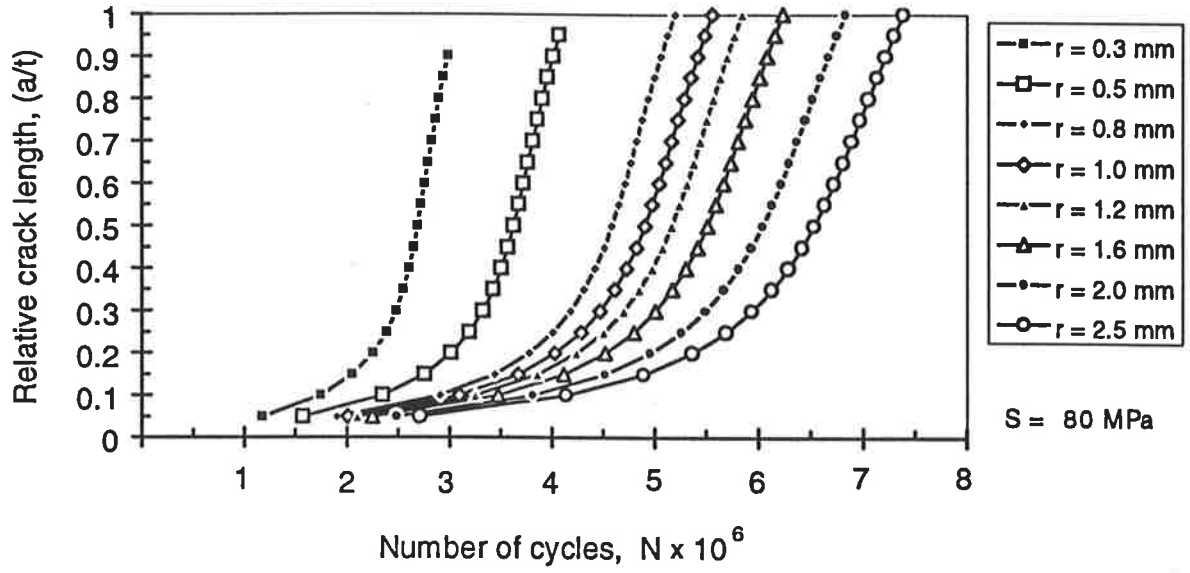

(a) Effect of (r) on crack growth curve (a vs. N)

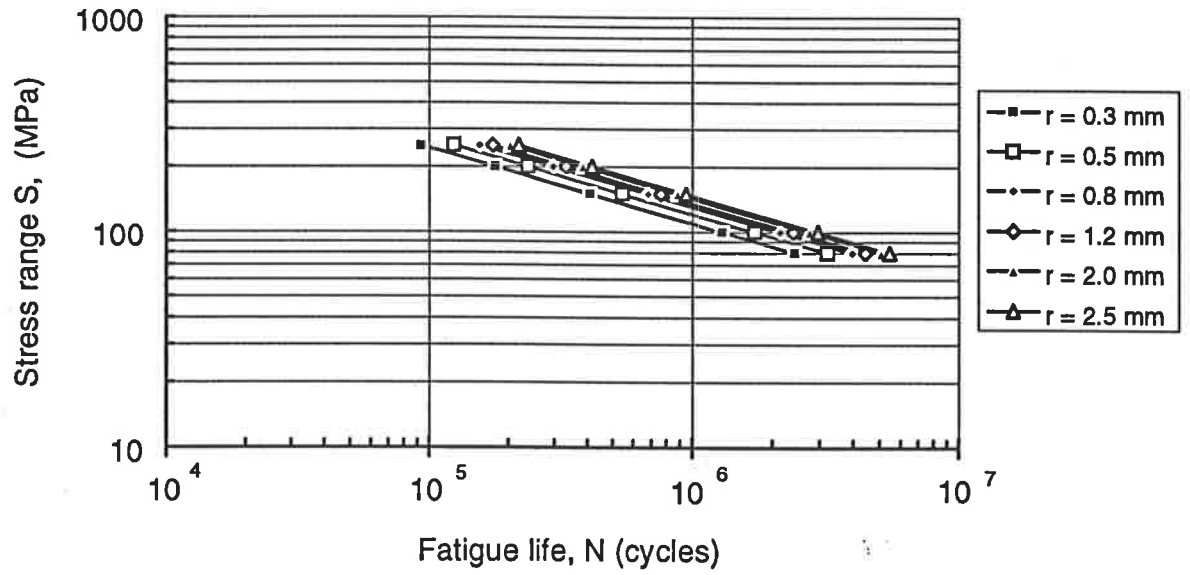

(b) Effect of (r) on fatigue S-N curve

Figure 5.29 Effect of the weld toe radius on the crack growth curve (a vs. N) and fatigue S-N curve (constant parameters: r' = 0, $\theta = 30°$, $\phi = 60°$, t = 12 mm, R=0).

Figure 5.29b showed the effect of the weld toe radius on the S-N curve. It showed that the S-N curve tended to move from the left to the right as the value of the weld toe radius increased. As a result, fatigue strength and fatigue life of butt welded joints can be improved correspondingly. This figure also showed that the fatigue strength of butt-joint at $2x10^6$ cycles was increased by 34 % as the weld toe radius increased from 0.3 mm to 2.5 mm.

Effect of the flank angle

Figure 5.30a showed the effect of the flank angle (θ) on the fatigue crack propagation life. It is obvious that the fatigue crack propagation life increased as the value of (θ) decreased. This means that the fatigue life of the butt-welded joint can be improved by decreasing the value of the flank angle (e.g. by grinding or other post-weld surface finishing technique). This conclusion is consistent with those of other researchers (Lawrence et al 1973, Gurney 1979, Maddox 1991). For a constant nominal applied stress range (S=80 MPa), the improvement of the fatigue crack propagation life due to the decrease of (θ) from 60° to 0° is of the order of $14x10^6$ cycles while that due to the variation of (r) is of $4.5x10^6$ cycles (Fig. 5.29a). It means that the degree of influence of flank angle on fatigue crack propagation life is more significant than that of the weld toe radius.

Figure 5.30b showed the effect of the flank angle on the S-N curve. It showed that the S-N curve tended to move from the left to the right as the value of flank angle decreased. As a result, the fatigue strength and fatigue life of butt welded joints can be improved by modifying the weld profile with smaller flank angle i.e smoother weld

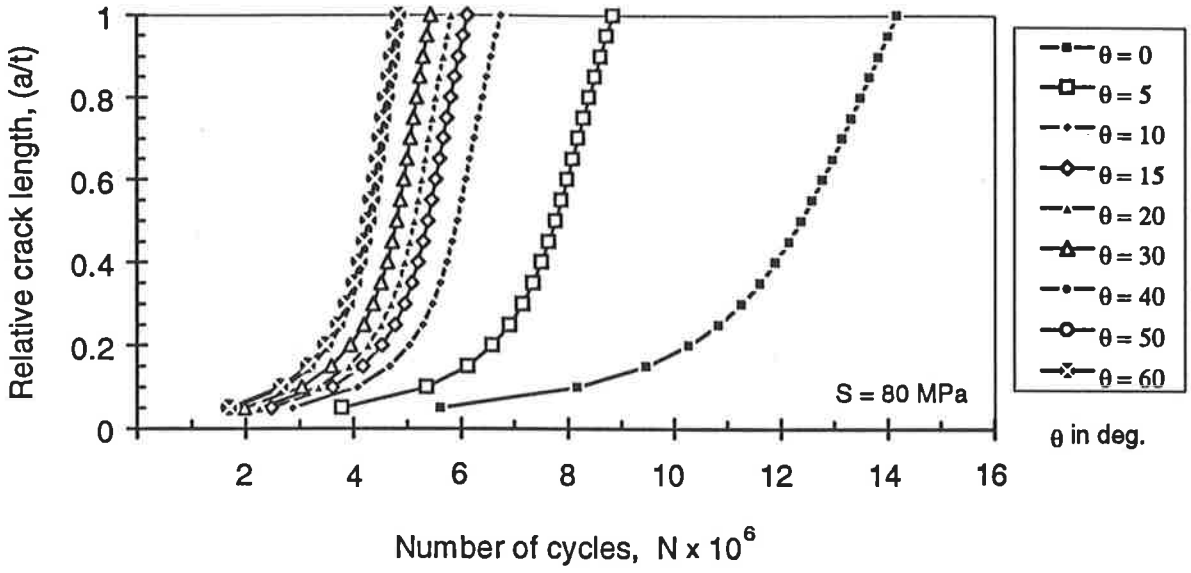

(a) Effect of (θ) on crack growth curve (a vs. N)

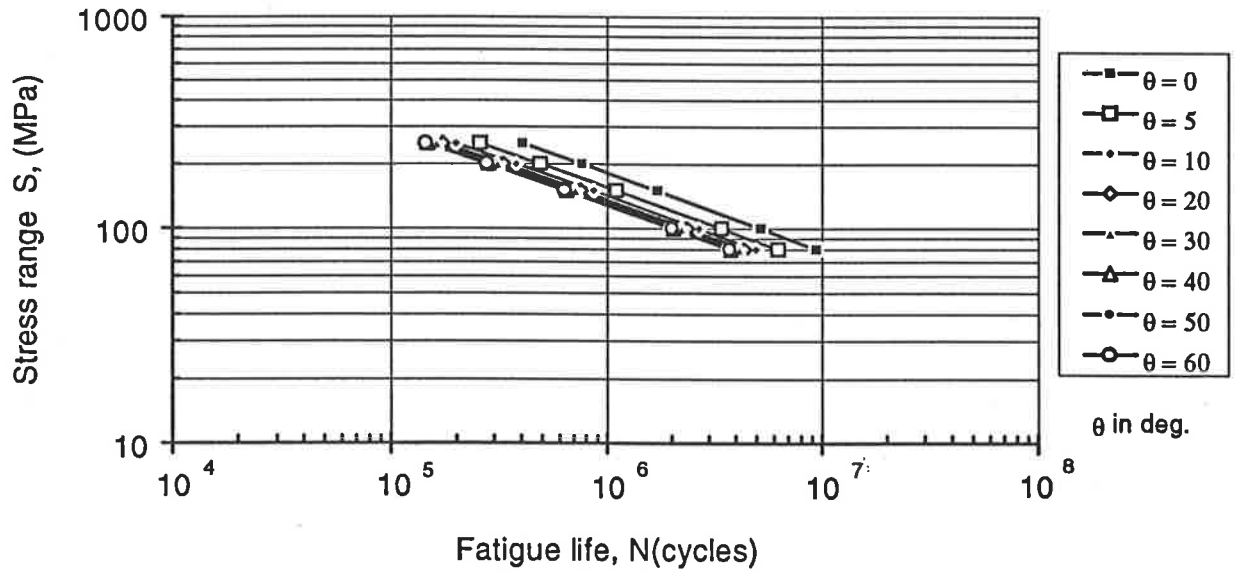

(b) Effect of (θ) on fatigue S-N curve

Figure 5.30 Effect of the flank angle on crack growth curve (a vs. N) and fatigue S-N curve (constant parameters: r' = 0, r = 1 mm, $\phi = 60°$, t = 12 mm, R=0).

bead. The flush-ground welded plate will have the highest fatigue strength and this is reported to be equivalent to the fatigue strength of the parent plate (Maddox, 1991). This figure also shows that the fatigue strength of butt-joints at $2x10^6$ cycles was increased by 21 % as the flank angle decreased from 60° to 5°. However, the fatigue strength of the butt-joint would be increased by up to 54 % as the flank angle decreases further up to the level of the base plate (θ=0°).

Effect of the plate thickness

Figure 5.31a showed the effect of the plate thickness (t) on the fatigue crack propagation life. It is obvious that the fatigue crack propagation life decreased as the value of (t) increased. This conclusion was consistent with the experimental results obtained by several other researchers (Gurney 1979, Berge 1985, Yee et al 1988, Ohta et al 1990, Maddox 1991). The improvement of the fatigue crack propagation life due to the decrease of (t) from 32 mm to 9 mm was of the order of $3x10^6$ cycles under the constant axially applied stress range (S=80 MPa) while the improvement of the fatigue life due to the variations of (r) and (θ) were of the order of $4.5x10^6$ and $14x10^6$ respectively. This means that the degree of influence of the plate thickness was less significant than that of both weld toe radius and flank angle.

Figure 5.31b shows that the fatigue life is significantly increased as the plate thickness decreased from 32 mm to 9 mm. However, the improvement of the fatigue life due to the decreased of the plate thickness from 20 mm to 9 mm was insignificant. It means that for the lower range of the plate thicknesses (less than 20 mm), the effect of plate thickness was ignorable. It is also clear from this figure that thicker plate tended

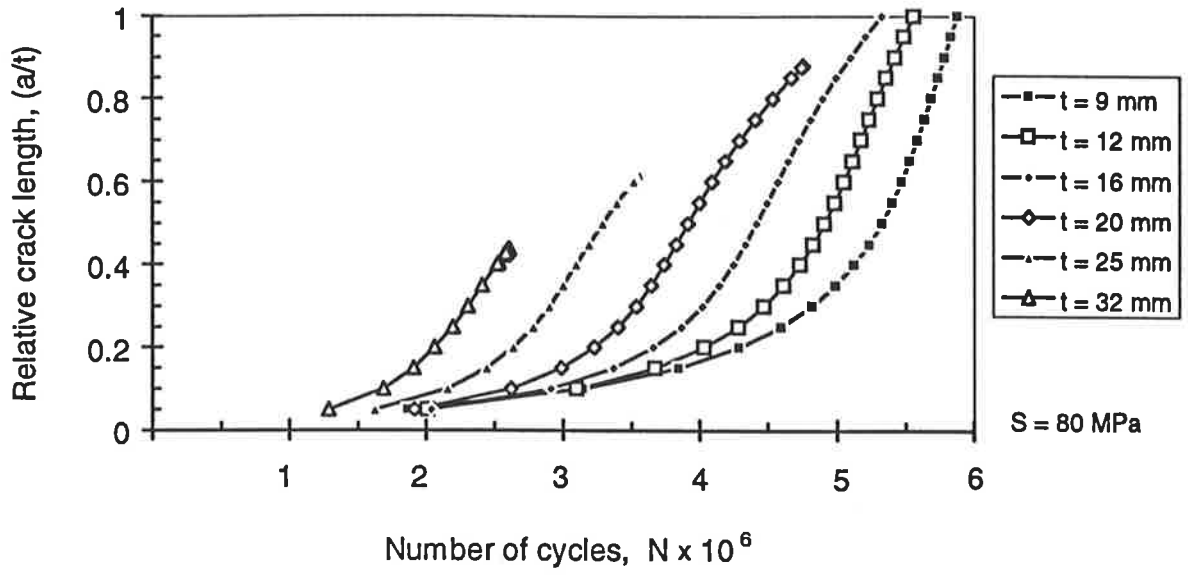

(a) Effect of (t) on crack growth curve (a vs. N)

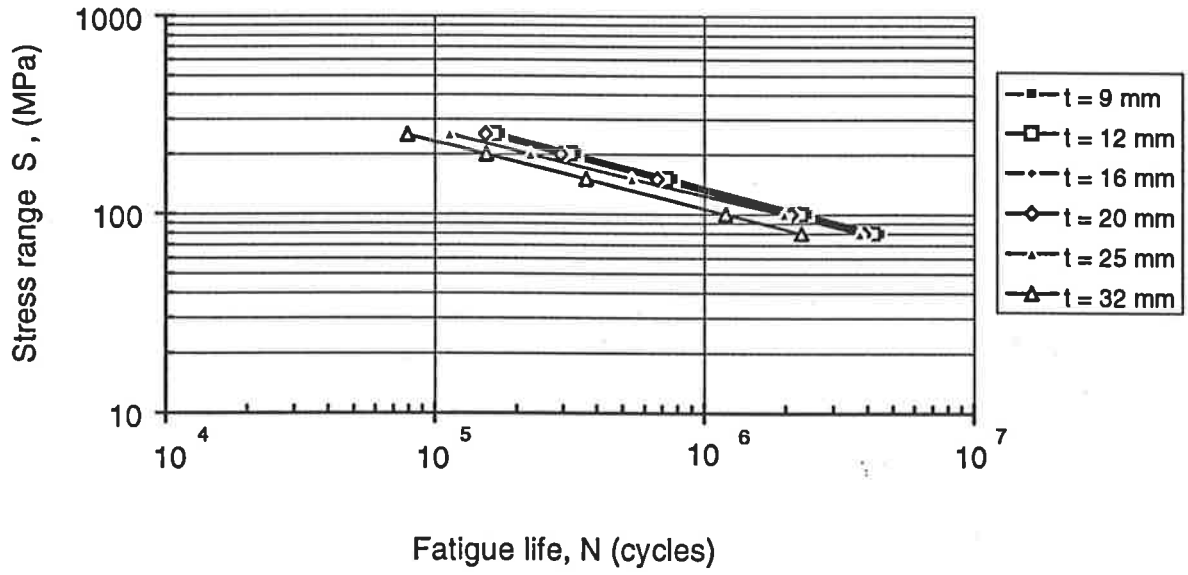

(b) Effect of (t) on fatigue S-N curve

Figure 5.31 Effect of the plate thickness on the crack growth curve (a vs. N) and fatigue S-N curve (constant parameters: r' = 0, r = 1 mm, $\theta = 60°$, $\phi = 60°$, R=0).

to move the S-N curve from the right to the left. This means that the fatigue life and fatigue strength of welded joints decreased with the increased value of the plate thickness. This figure also showed that the fatigue strength of a butt joint at $2x10^6$ cycles was decreased by up to 21 % as the plate thickness increased from 9 mm to 32 mm.

Effect of the edge preparation angle

Figure 5.32a showed the effect of the edge preparation angle (ϕ) on the fatigue crack propagation life. It is obvious from this figure that the crack propagation life increased as the value of (ϕ) decreased from 90° to 45°. The improvement of the fatigue crack propagation life due to the decrease of angle (ϕ) from 45° to 90° was of the order of $1x10^6$ cycles for a constant axially applied stress range (S=80 MPa) while the improvement of the fatigue life due to variation of (r), (θ) and (t) were of $4.5x10^6$, $14x10^6$ and $3x10^6$ cycles respectively. This means that the degree of the influence of the edge preparation angle was less significant than that of the other weld geometry parameters i.e weld toe radius, flank angle and plate thickness.

Figure 5.32b showed the effect of the edge preparation angle (ϕ) on the S-N curve. It shows that the S-N curve slightly moved from the left to the right as the value of angle (ϕ) decreased. However, a slight improvement of the fatigue strength and fatigue life of butt-welded joints due to the variation of angle (ϕ) was considered to be insignificant (S-N curves almost overlap). This figure also showed that the fatigue strength of butt-joints at $2x10^6$ cycles was increased by 7 % as the angle (ϕ) deceased

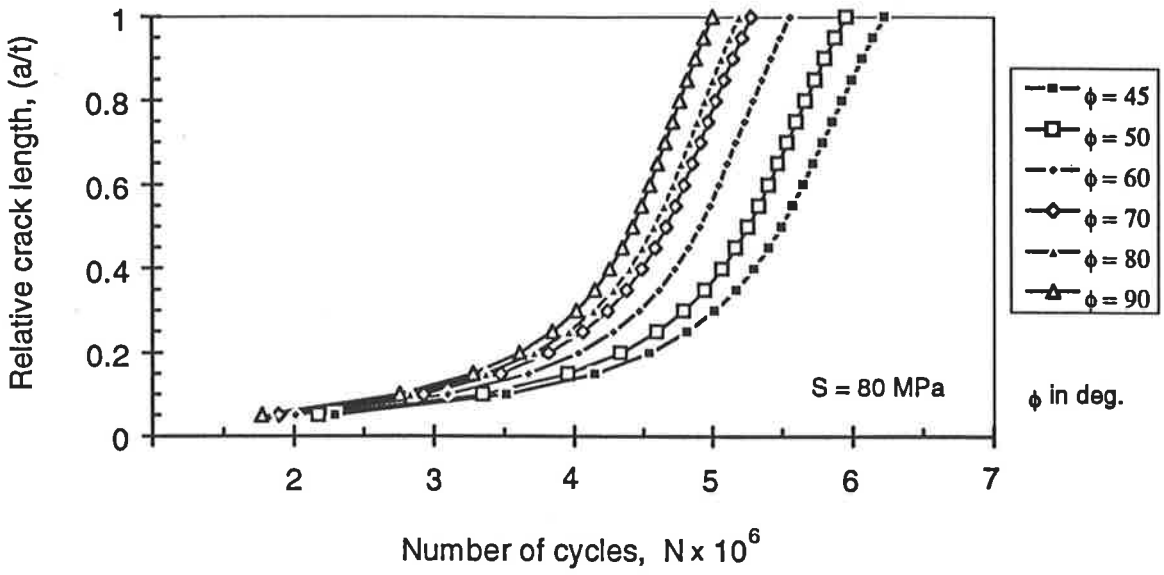

(a) Effect of (ϕ) on crack growth curve (a vs. N)

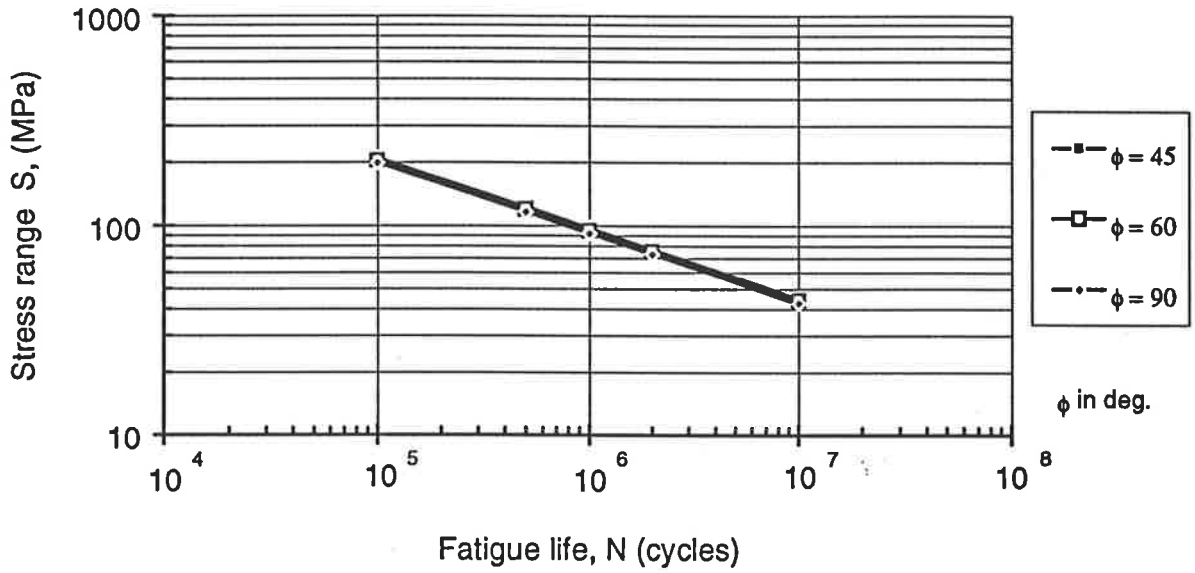

(b) Effect of (ϕ) on fatigue S-N curve

Figure 5.32 Effect of the edge preparation angle on the crack growth curve (a vs. N) and fatigue S-N curve (constant parameters: r' = 0, r = 1 mm, θ = 60°, t = 12 mm, R=0).

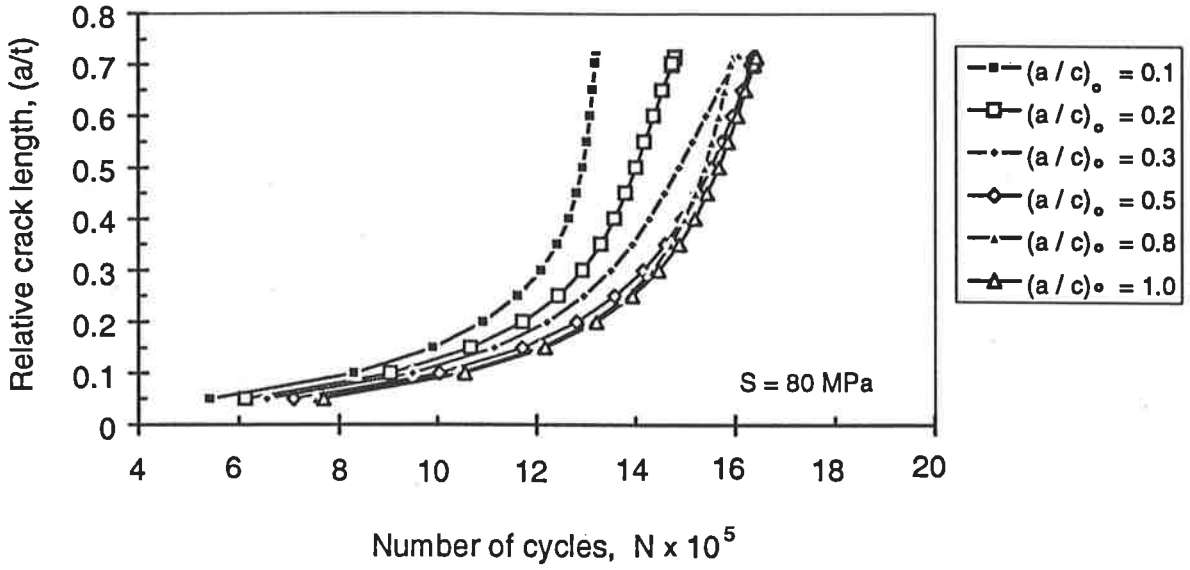

(a) Effect of $(a/c)_o$ on crack growth curve (a vs. N)

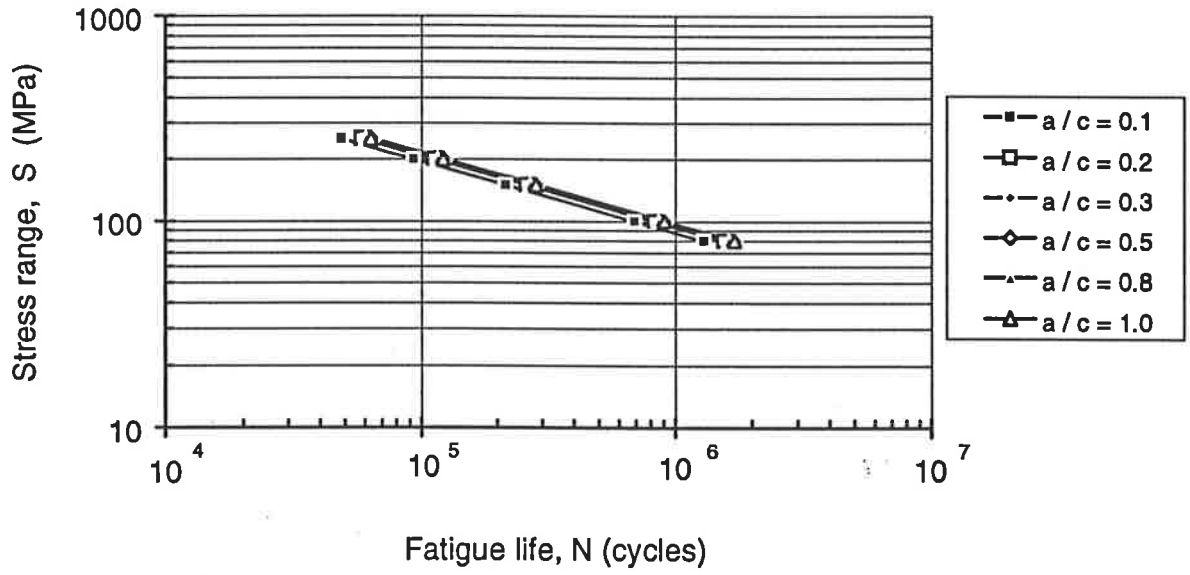

(b) Effect of $(a/c)_o$ on fatigue S-N curve

Figure 5.33 The effect of the initial crack shape aspect ratio $(a/c)_o$ on the crack growth curve (a vs. N) and S-N curve (constant parameters: r' = 0, r = 1 mm, θ = 60°, ϕ = 60°, t = 12 mm, R=0).

from 90° to 45°. This improvement was ignorable considering a large scatter of the fatigue data occurs in the testing practice.

Effect of the initial crack shape aspect ratio

Figure 5.33a showed the effect of the initial crack shape aspect ratio $(a/c)_o$ on the fatigue crack propagation life. It is obvious from this figure that the crack propagation life increased as the value of $(a/c)_o$ increased. This means that an initiated fatigue crack with lower initial crack shape aspect ratio tended to be more detrimental to the fatigue life of butt-joints than that with higher initial crack shape aspect ratio. This suggested that a semi-circular shape of a surface crack was less harmful than the other shapes of the surface crack like a semi-elliptical or edge crack.

Figure 5.33b showed the effect of the initial crack shape aspect ratio $(a/c)_o$ on the S-N curve. It showed that the S-N curve tended to move from the left to the right as the value of $(a/c)_o$ increased from 0.1 to 1.0. This figure also showed that there was an insignificant difference between the effect of $(a/c)_o$ on S-N curve for a large range of the initial crack shape aspect ratio from 0.2 to 1.0. Therefore, it suggested that when using a semi-elliptical crack propagation model to evaluate the fatigue behaviour of butt-welded joints, an initial crack with aspect ratio of 0.2 could be adopted.

5.4 Effect of the Residual Stresses on the Fatigue Behaviour of Butt-Joints

In the present study, the effect of the post-weld residual stresses on the fatigue behaviour of butt-welded joints is investigated for three cases: (i) the post-weld surface treated condition, (ii) the as-welded condition and (iii) the stress-relieved condition.

It has been mentioned earlier that the post-weld surface residual stresses have not been measured but are assumed on the basis of experimental data (Wahab, 1984, Maddox 1991 and others). In the post-weld surface treated condition, several levels of the induced compressive residual stresses at the weld toe surface are assumed to simulate the post-weld surface treated conditions e.g single or multiple point hammer peening (S_r = -152 MPa and -172 MPa), glass or steel shot peening (S_r= -62 MPa and -110 MPa) and stress peening (S_r=-172 MPa) (Wahab, 1984). In the as-welded condition, for simulation of the state of residual stress of the actual welded structures, several levels of the tensile residual stresses at the weld toes were assumed. These levels ranged from a fraction of the yield stress of the base metal up to its yield stress (S_r= 300 MPa) (Maddox 1991). In the stress-relieved condition, the magnitude of the tensile residual stresses was assumed to be zero (S_r = 0, refers to the "perfectly stress-relieved" state) or as low as S_r = 14 MPa (Wahab, 1984). An idealised pattern of the residual stress fields in the as-welded and post-weld treated conditions is shown in Figure 3.5 (Chapter 3). The values of the effective depth of the surface treatments d_{eff} (shown in Fig. 3.5) were assumed to be 0.2 mm and 0.43 mm for glass and steel shot peening; 0.76 mm and 0.69 mm for single-point and multiple-point hammer peening and 0.7 mm for stress peening (Wahab, 1984).

For the as-welded condition, the magnitude of the peak compressive residual stresses (S_{rc}^{max}) was assumed to be equivalent to the maximum tensile residual stress at the weld toe surface and located at the middle of the plate thickness ($S_{rc}^{max} = S_r$). The distribution of the surface residual stresses along the plate width (y-direction) was assumed to be constant for each type of surface treatment. In the as-welded condition it follows a cosine pattern with the peak tensile residual stress located in the middle of the welded plate (Fig. 3.5, Chapter 3). The explicit form of the equations used to describe the residual stress distributions for the as-welded and the surface-treated conditions are given in Appendix B.

Effect of the residual stresses on the stress intensity factor

Figures 5.34a and 5.34b show the variation of the stress intensity magnification factors $M^A_{k,r}$ and $M^B_{k,r}$ due to the combined effect of the weld geometry and residual stresses calculated for an assumed butt-weld geometry (r ' = 0 mm, r = 1 mm, $\theta = 30°$, t = 6.35 mm) respectively. Figure 5.34a shows that the compressive residual stresses reduce the value of the stress intensity magnification factor $M^A_{k,r}$ at the early stage of the crack growth while tensile residual stresses tend to increase it. However, the effect of the lower level of the compressive residual stresses of the order of -62 MPa on $M^A_{k,r}$ is similar to that of the residual stresses in the stress-relieved condition (S_r=0 and S_r=14 MPa).

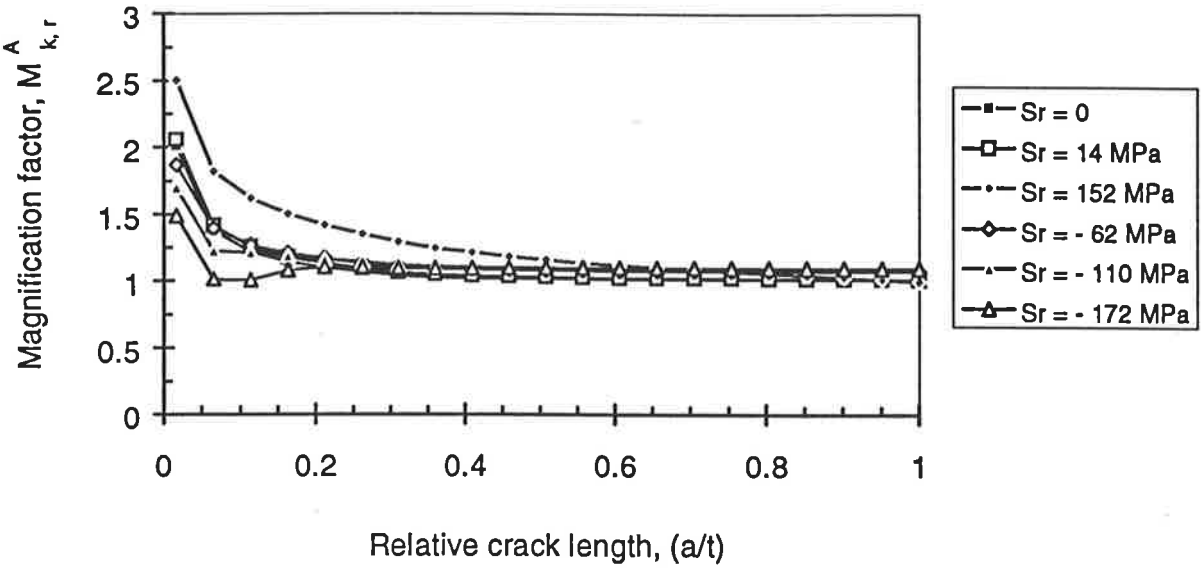

(a) Effect of residual stress on stress intensity magnification factor $M^A_{k,r}$

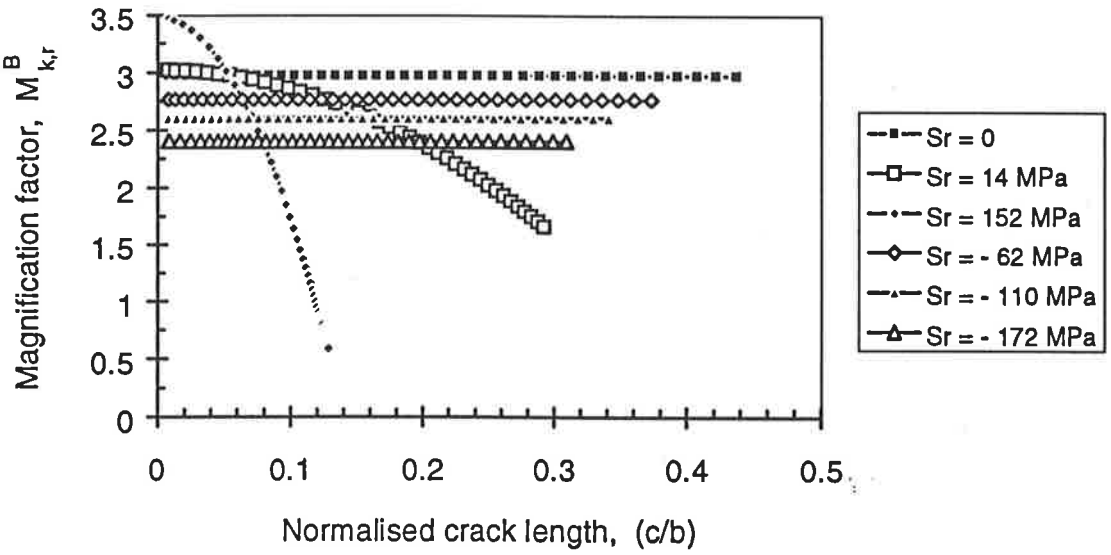

(b) Effect of residual stress on stress intensity magnification factor $M^B_{k,r}$

Figure 5.34 Effect of the residual stresses and weld geometry on the stress intensity magnification factors $M^A_{k,r}$ and $M^B_{k,r}$.

Figure 5.34b shows the effect of the residual stresses on the stress intensity magnification factor $M^B_{k,r}$ across the width of the welded plate. The values of $M^B_{k,r}$ for each surface treatment are constant resulting from the same level of compressive residual stresses introduced at the plate surface. However, the values of $M^B_{k,r}$ are reduced compared with that in "perfectly stress-relieved" condition ($S_r = 0$) due to the particular level of the induced compressive residual stresses. In the as-welded condition, due to the presence of the tensile residual stress, the values of $M^B_{k,r}$ are increased in the early stages of the crack growth compared with that in "perfectly" stress-relieved condition ($S_r = 0$) but decreased after the crack reaches the length of 0.06 times the width of the welded plate (c/b = 0.06).

Figure 5.35(a) and (b) show the values of the stress intensity factors $K^w_{sc,A}$ and $K^w_{sc,B}$ for the applied stress of S = 150 MPa. Figure 5.35a shows that when compared with the "perfectly" stress-relieved condition, the stress intensity factor $K^w_{sc,A}$ was increased with tensile residual stresses and decreased with compressive residual stresses in the early stages of the crack growth. As a result, the compressive residual stresses improve the fatigue life of butt-welded joint while tensile residual stresses reduce it. This conclusion is consistent with the results reported by many authors (Toyooka et al 1985, Bellow et al 1986, Cooper et al 1986, Desvignes et al 1986, Heeschen et al 1986, etc.). However, after the crack length increased to 0.45 times the plate thickness (0.45t), the stress intensity value $K^w_{sc,A}$ begins to decrease as the level of the tensile residual stress increases. This behaviour is due to the portion of the compressive residual stress through the plate thickness which balances the tensile residual stresses at the weld toe surface. However, beyond the crack length of (0.45t)

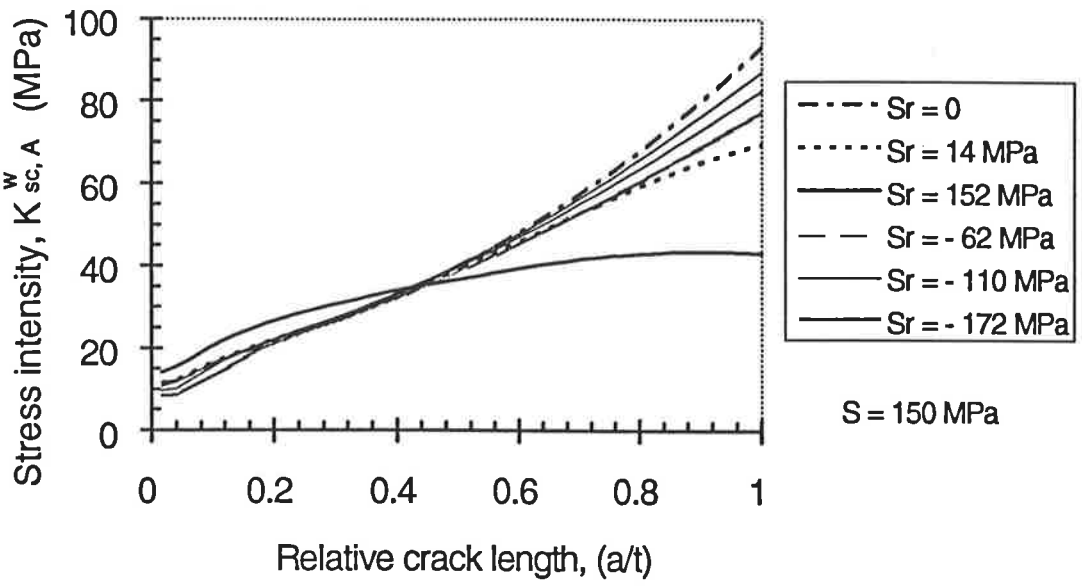

(a) Effect of the residual stress on the stress intensity factor $K^{w}_{sc,A}$

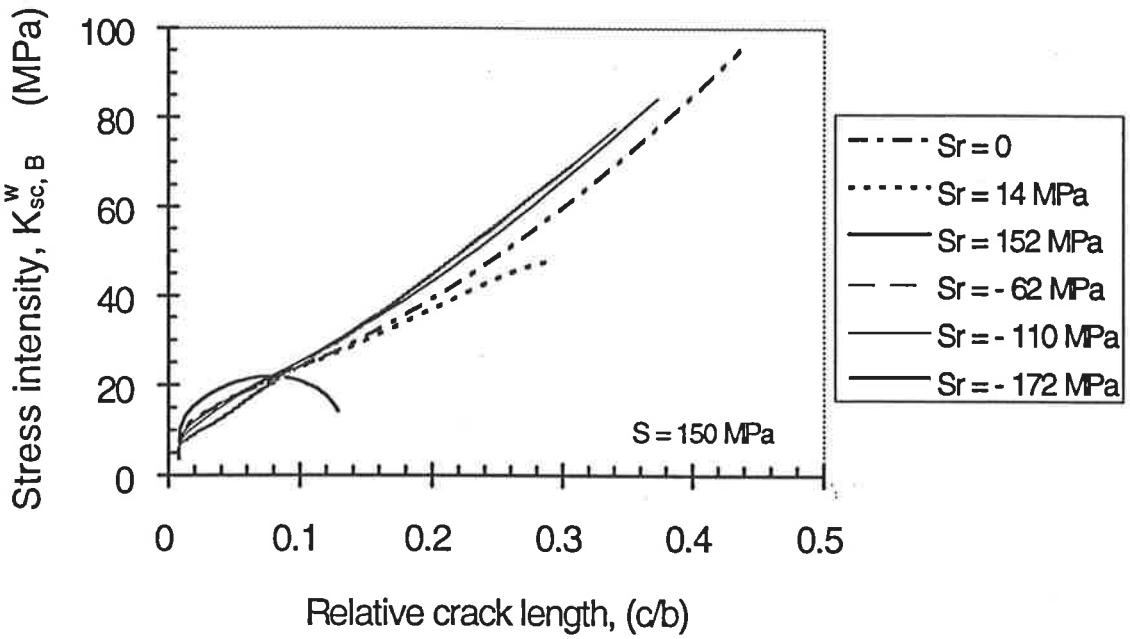

(b) Effect of the residual stress on the stress intensity factor $K^{w}_{sr,B}$

Figure 5.35 Effect of the residual stresses on stress intensity factors $K^{w}_{sr,A}$, $K^{w}_{sr,B}$

the compressive residual stresses continue to decrease the value of $K^{w}_{sc,A}$ compared with that in the stress-relieved state. It means that the fatigue crack growth during the early stage (crack length less than 0.45 times plate thickness) dominate the major part of the fatigue life.

Figure 5.35a also showed that there was a little difference between the effects of low levels of tensile residual stresses corresponding to the stress-relieved state (S_r=0 and S_r=14 MPa) and low levels of compressive residual stresses of the order of -62 MPa. This means that the effect of low levels of compressive residual stresses (e.g less than -62 MPa) and the effect of stress-relieving processes (e.g. annealing) on the fatigue behaviour of butt welded joints were almost equivalent.

Figure 5.35b shows the effect of residual stresses on stress intensity factor $K^{w}_{sc,B}$ is similar to its effect on $K^{w}_{sc,A}$ i.e. its value is increased by tensile residual stresses and decreased by compressive residual stresses. However, after a transition point at the crack length of 0.08 times plate width (0.08b), the effect of residual stress on $K^{w}_{sc,B}$ has a new feature. The values of $K^{w}_{sc,B}$ begin to increase by the induced compressive residual stresses and decrease by tensile residual stresses compared with that in "perfectly stress-relieved" condition. This is due to the change of the sign of the residual stresses at the transition point i.e from compressive to tensile in surface treated condition and from tensile to compressive in as-welded condition.

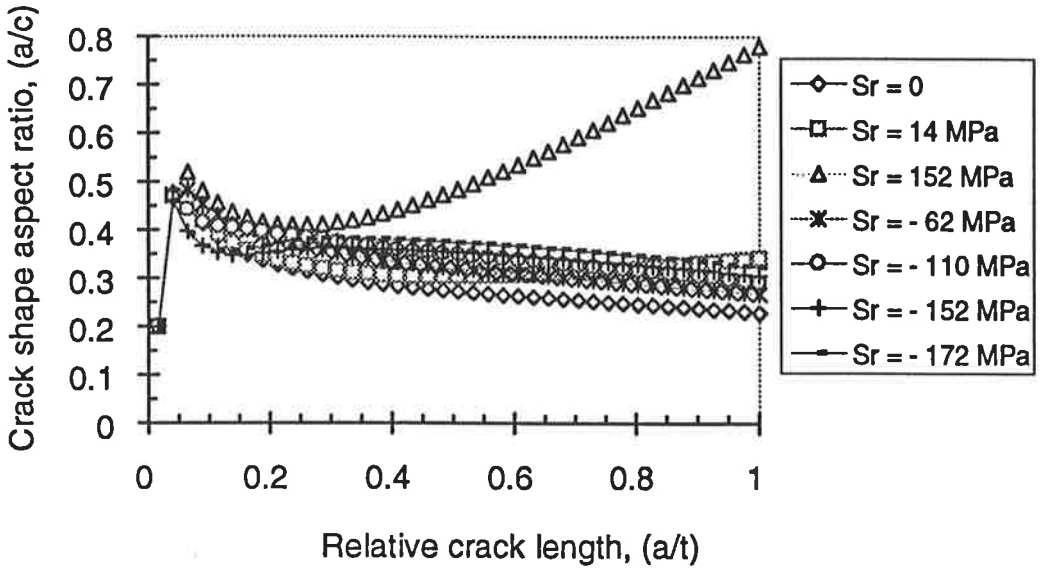

Figure 5.36 Effect of residual stresses on the evolution of crack shape aspect ratio (r'= 0, r = 1 mm, $\theta = 30°$, $\phi = 60°$, t = 6.3 mm, R = 0, S = 150 MPa)

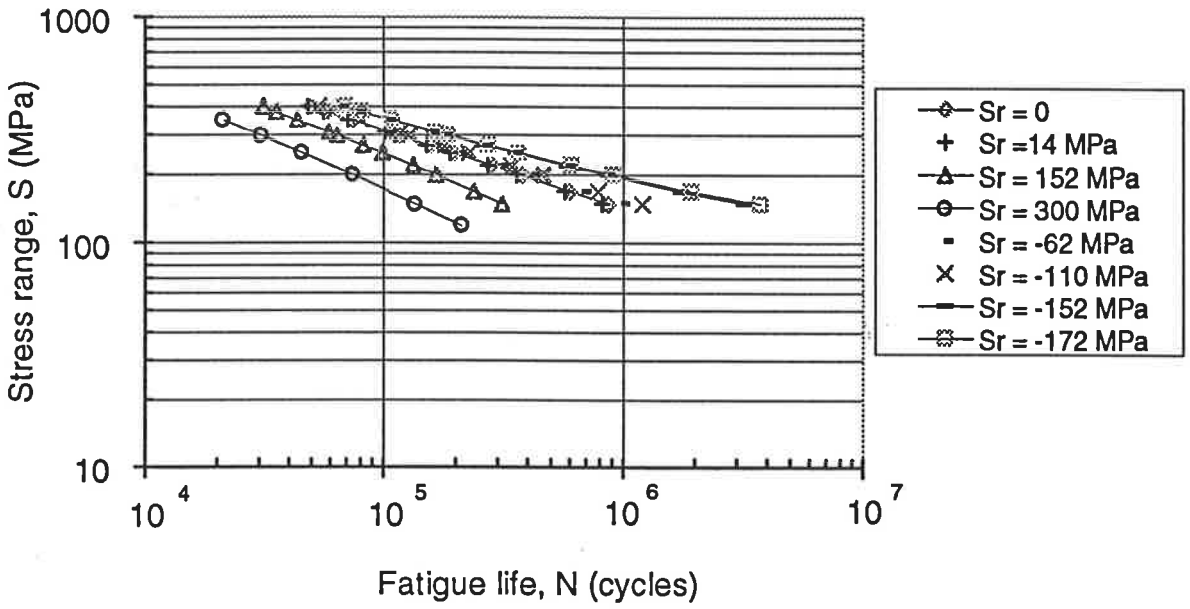

Figure 5.37 Effect of residual stresses on S-N curve of butt-joints

Effect of residual stresses on the evolution of crack shape aspect ratio

Figure 5.36 shows the effect of residual stresses on the evolution of crack shape aspect ratio (a/c). It shows that at the early stage of the crack growth ($a < 0.25t$), the values of crack shape aspect ratio (a/c) increased as the level of the tensile residual stresses increased or level of the compressive residual stresses decreased. However, beyond that length, the values of (a/c) increased as the level of the compressive residual stresses increased. This means that after a fatigue crack has propagated beyond the 25 % of the plate thickness, the behaviour of the crack shape evolution in the induced compressive residual stresses condition is similar to that in the tensile residual stresses condition. The sign of the surface residual stresses at the weld toes influenced the crack shape aspect ratios during the early stage of the crack growth only. A high level of tensile residual stresses at the weld toes tended to develop a crack with a higher aspect ratio of the crack shape whilst a high level of compressive residual stresses tends to develop a crack with a lower crack shape aspect ratio.

Effect of residual stresses on the S-N curve

Figure 5.37 shows the fatigue S-N curves in terms of the effect of residual stresses in butt-welded joints. It is obvious from this figure that the fatigue strength is improved by compressive residual stresses whilst it was reduced by tensile residual stresses. The effect of the residual stress-relieved process and that of the low level of compressive residual stresses (e.g less than -62 MPa) was shown in the same scatter band.

5.5 Effect of the Combined Axial and Bending Load Conditions

The effect of the combined loadings on the stress intensity factor

Figures 5.38a and 5.38b show the effect of the combined loading condition in terms of the ratio R_{ba} ($R_{ba} = S_b / S_a$) on the stress intensity factor of a butt-joint with a semi-elliptical surface crack. A constant weld geometry profile subjected to the axially loaded stress range S_a = 150 MPa in the "perfectly stress-relieved" condition was assumed for the calculation (r' = 0, r = 1 mm, $\theta = 30°$, $\phi = 60°$, t =12 mm, $S_r = 0$ and R=0).

Figure 5.38a shows that the values of $K^w_{sc,A}$ increased as the ratio R_{ba} increased from 0 to 1.5 ($R_{ba} = 0$ represents the pure axial loading case). This behaviour of the stress intensity factor at the deepest point (A) (Fig. 3.2) with respect to the combined loading condition resulted in a decrease in the fatigue life and fatigue strength of butt-joints (as shown latter in Fig. 5.40). A similar behaviour of the stress intensity factor is also observed at the point (B) (Fig. 3.2) as shown in Fig. 5.38b. It shows that the values of $K^w_{sc,B}$ increased as the ratio R_{ba} increased from 0 to 1.5. This means that a higher magnitude of the nominal bending stress in a combined loading case results in a higher value of the stress intensity factor which determines the fatigue behaviour of the joints under consideration.

The effect of combined loading ratio on the evolution of the crack shape

Figure 5.39 shows the evolution of the crack shape aspect ratio under combined loading conditions. This figure shows that the combined loading ratio (R_{ba}) has a little

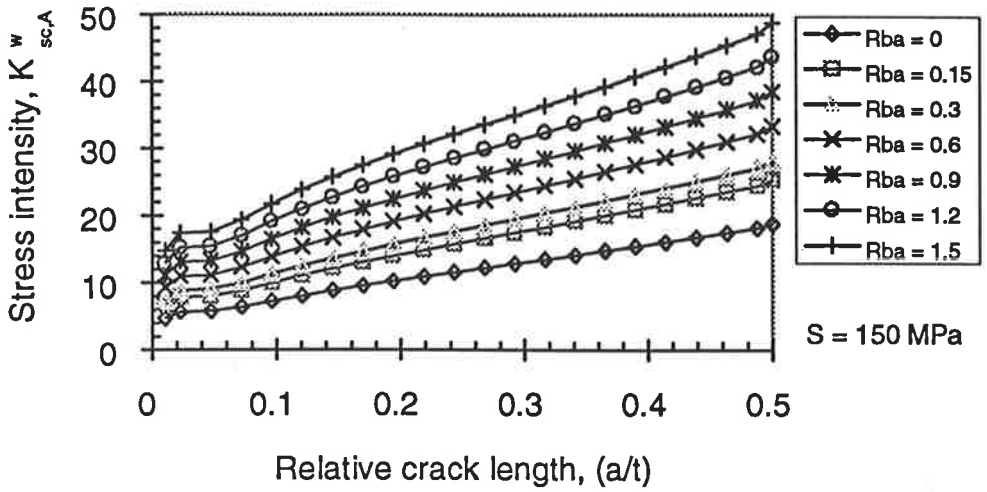

(a) Effect of (R_{ba}) on $K^{w}_{sc,A}$

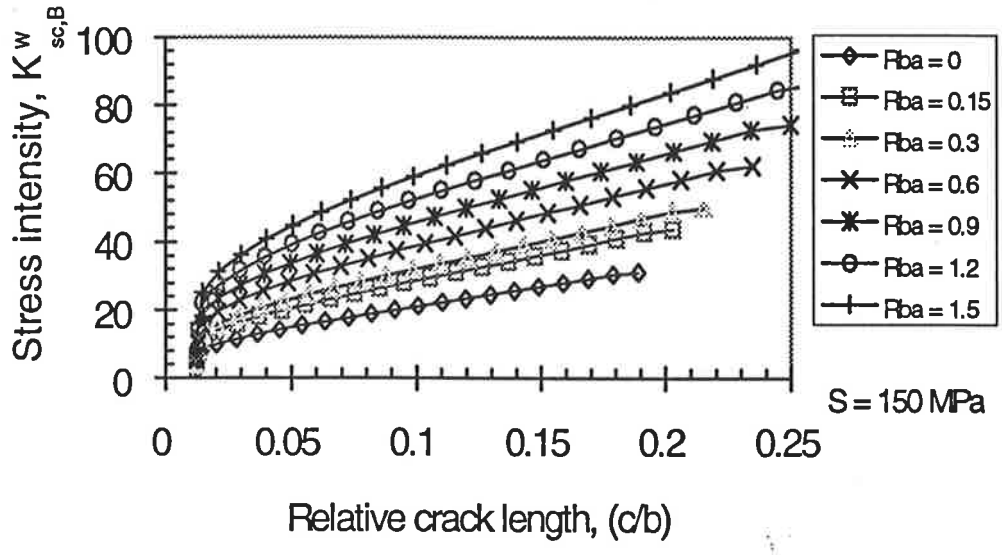

(b) Effect of (R_{ba}) on $K^{w}_{sc,B}$

Figure 5.38 Effect of the combined loading ratio (R_{ba}) on the stress intensity factor

influence on the evolution of the crack shape. There is an insignificant difference between the values of (a/c) for changes in (R_{ba}) from 0 to 1.5 suggesting that the evolution of the crack shape in the combined loading case is similar to that expected under pure axial loading.

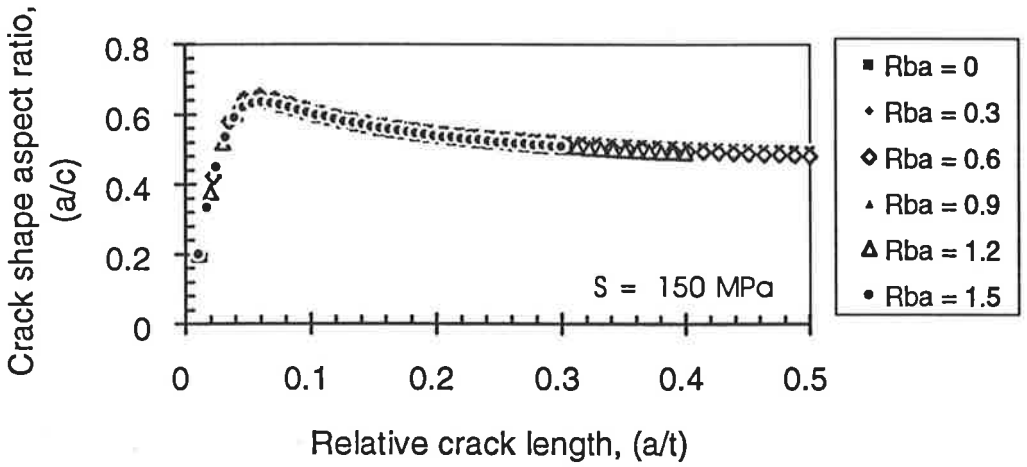

Figure 5.39 Effect of the combined loading ratio (R_{ba}) on the crack shape aspect ratio

The effect of the combined loading ratio on the S-N curve

Figure 5.40 shows the effect of the combined loading ratio (R_{ba}) on the fatigue S-N curve. It shows that the S-N curve tends to move from the right to the left as the values of (R_{ba}) increased from 0 to 1.5. Showing that the fatigue strength and fatigue life of butt joints decreased as the values of (R_{ba}) increased. This behaviour of the S-N curve under combined loading gives a clear explanation for the effect of misalignments (axial and angular) in butt joints. The misalignment induced bending stresses are combined with the nominal axial stresses in the actual loading condition. There are some useful relationships that can be used to relate the levels of axial or angular

misalignments with the (R_{ba}) as described in Eqs. (2.5) to (2.7) (Berge and Myhre, 1977; Petershagen and Zwick, 1982). Using these equations, the effect of the misalignment on fatigue behaviour of butt-joints can be considered to be equivalent to that under combined loading conditions.

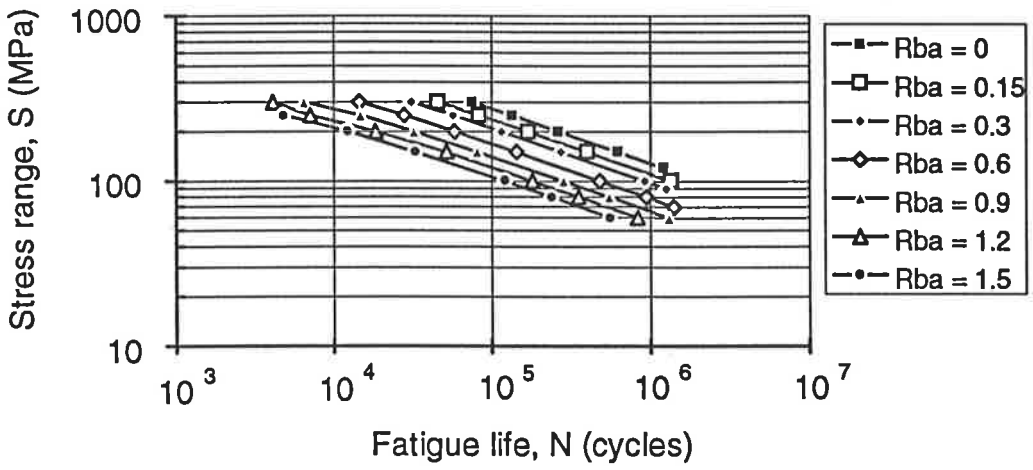

Figure 5.40 Effect of the combined loading ratio (R_{ba}) on the S-N curve

5.6 The Combined Effect of Undercut, Misalignment and Residual Stresses

The effect of undercut on the fatigue behaviour of butt joints

The effect of the tip radius at the undercut at the weld toe (r') on the *S-N* curves of the aligned and misaligned joints (e/t = 0.1) is shown in Figure 5.41a and 5.41b.

Figure 5.41a shows that the *S-N* curves tend to move from the left to the right side as the values of (r') decrease (other parameters are unchanged: r=1 mm, θ=30^o, ϕ=60^o, t=12 mm, R = 0, R_{ba} = 0 and S_r = 0). It suggests that the fatigue strength and fatigue

life of butt-welded joints can be improved by either partly or totally removing the weld toe undercut. It is shown from Fig. 5.41a that the fatigue limit of a welded joint with undercut is decreased by 58 % (from 120 MPa to 50 MPa) compared with that of undercut-free joint and by up to 75 % (from 200 MPa to 50 MPa) compared with that of flush-ground welded plate or parent material. The fatigue limit of the undercut-free joint is decreased by only 40 % (from 200 MPa to 120 MPa) when compared with flush-ground welded plate or parent material. The fatigue limit of the undercut joint can be improved by up to 140 % (from 50 MPa to 120 MPa) and 300 % (from 50 MPa to 200 MPa) by eliminating the undercut at the weld toe or by flush-grinding the weld bead to the level of the parent plate respectively.

Figure 5.41b shows that the effects of tip radius of the undercut (r') on the *S-N* curve of the misaligned joint (e/t = 0.1) and *S-N* curve of the aligned joint are similar (other parameters are kept unchanged: r=1 mm, θ=30^o, ϕ=60^o, t=12 mm, and S_r=0). However, the fatigue limits of the undercut misaligned joint, misaligned joint without an undercut and flush-ground misaligned joint move towards a lower position. Fig. 5.41b also shows that the fatigue limit of an undercut misaligned joint was decreased by 56 % (from 90 MPa to 40 MPa) and by 73 % (from 150 MPa to 40 MPa) compared with that of the misaligned joint without an undercut and flush-ground joint respectively. Furthermore, the fatigue limit of the misaligned joint without an undercut is decreased by only 40 % (from 150 MPa to 90 MPa) compared with that of the flush-ground joint.

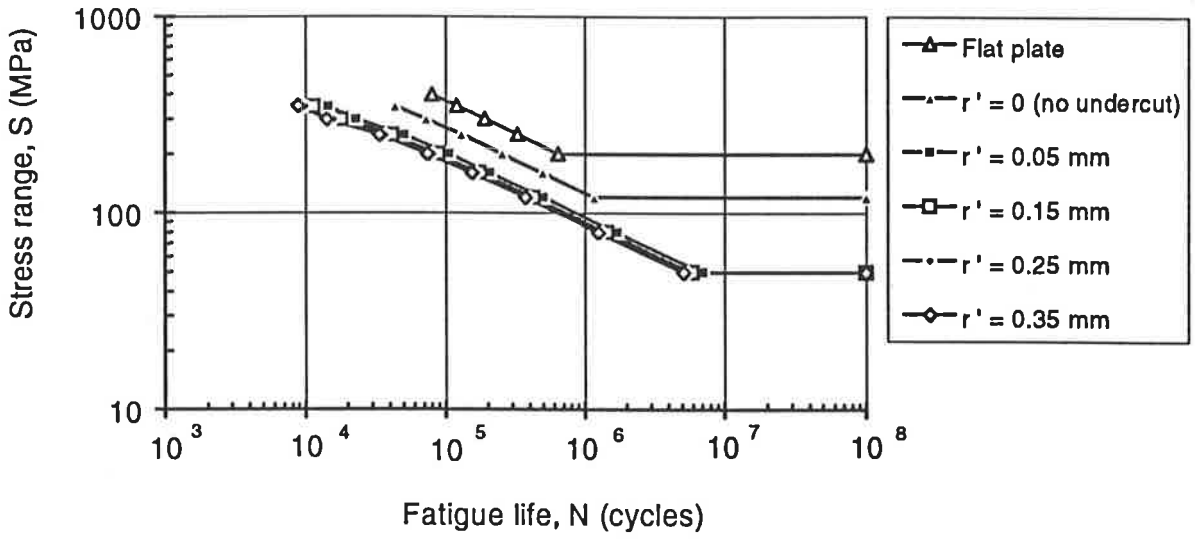

(a) S-N curves of the aligned joint

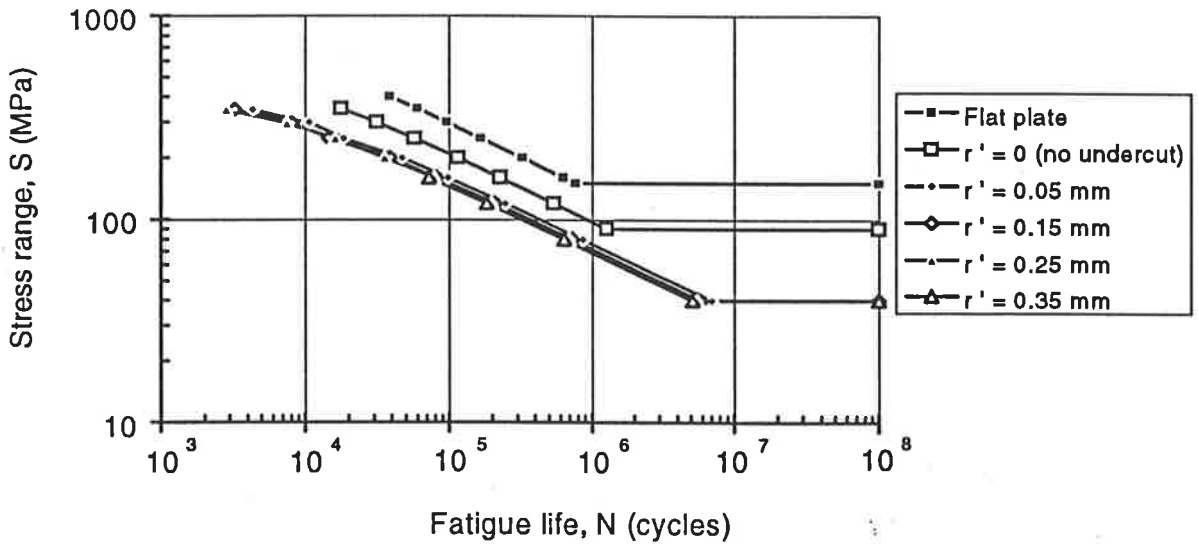

(b) S-N curves of the misaligned joint (e/t = 0.1 or y = 0.6 mm)

Figure 5.41 Effect of the tip radius of the weld toe undercut on S-N curves of the aligned and misaligned joint (constant parameters: r = 1 mm, θ = 30°, ϕ = 60°, t = 12 mm, R = 0 and S_r = 0).

It is also obvious from Figs. 5.41a and 5.41b that the undercut is one of the most significant weld geometric parameters to influence the fatigue behaviour of butt-joints and the effect of the tip radius at the undercut is governed by the other weld geometric parameters.

The effect of misalignment on fatigue behaviour of butt joints

Figure 5.42a shows that for an undercut-free welded joint in a "perfectly stress-relieved" condition the fatigue strength and fatigue life of butt joints are decreased with the increasing levels of misalignments (increasing values of *e/t* or *y*). It shows that the *S-N* curves of the misaligned joints move to the left side of the graph. And that the fatigue limit of the misaligned joints decreased by up to 17 % (from 120 MPa to 100 MPa) and by 58 % (from 120 MPa to 50 MPa) subject to levels of misalignment from 5 % and 50 % of the plate thickness (e/t from 0.05 to 0.5) respectively when compared with that of the aligned joints. This also means that the fatigue limits of the misaligned joint can be improved by from 20 % to 140 % due to the elimination of misalignments from 5 % to 50 % respectively. Figure 5.42b also shows that when an undercut is present in the "perfectly stress-relieved" condition, the fatigue strength and fatigue life of butt-joints decreased with increasing levels of misalignment (increasing value of *e/t* or *y*). However, the reduction in the fatigue limit of the undercut joint (r' = 0.25 mm) ranged from 10 % to 60 % subject to the levels of misalignment from 5 % to 50 % respectively. This suggests that the fatigue limits of the undercut misaligned joint can be improved by from 11 % to 150 % due to the elimination of misalignments from 5 % to 50 % respectively.

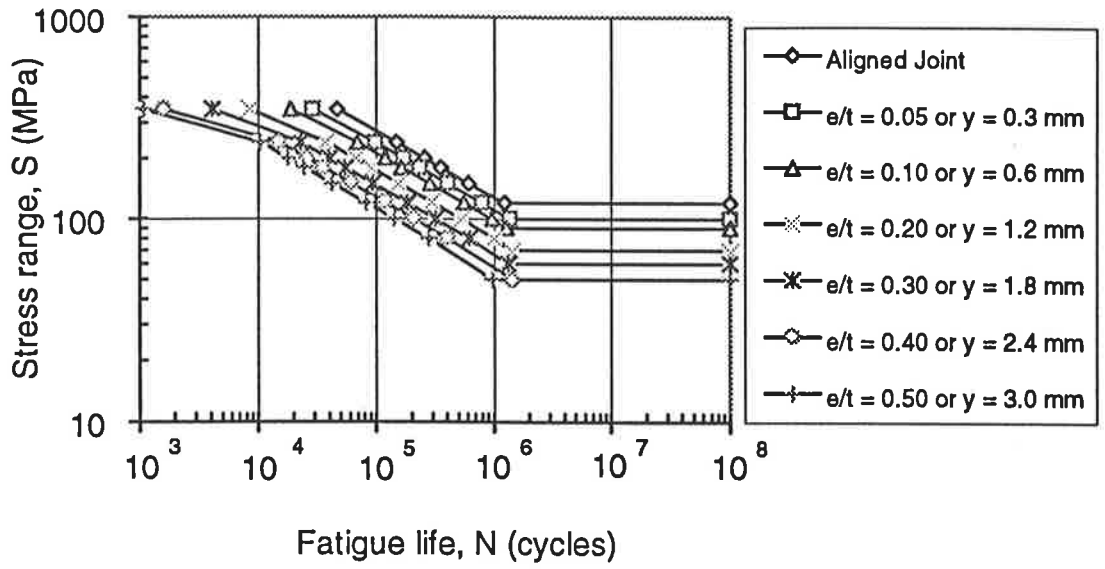

(a) *S-N* curves of the undercut-free joint

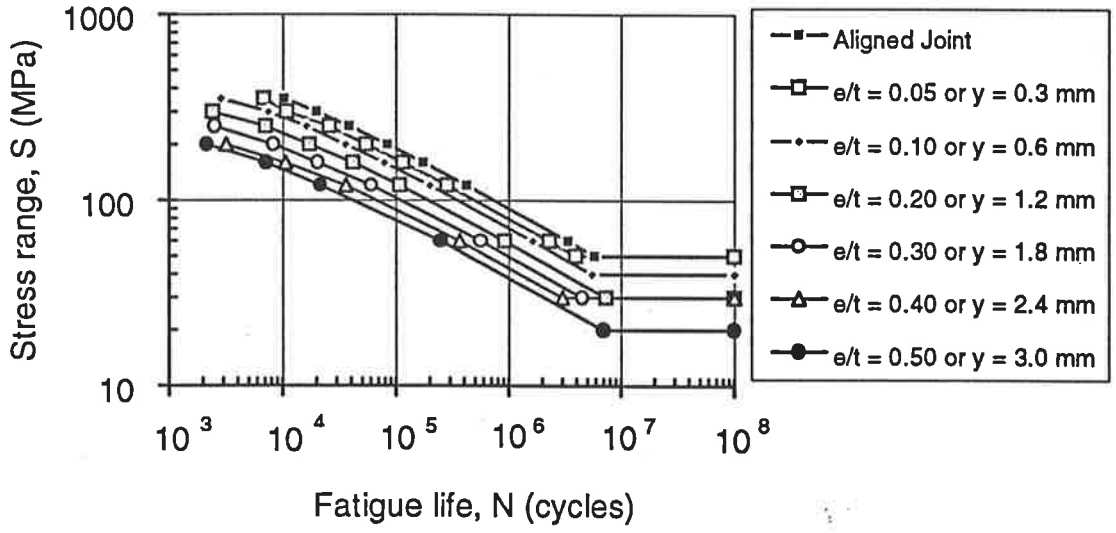

(b) *S-N* curves of the undercut joint

Figure 5.42 Effect of the misalignment on the *S-N* curves of the undercut-free and undercut butt-joints (constant parameters: r = 1 mm, $\theta = 30°$, $\phi = 60°$, t = 12 mm, R = 0 and $S_r = 0$).

The combined effect of the undercut, misalignment and residual stresses on the fatigue behaviour of but- joints

Figures 5.43a and 5.43b show the effect of residual stresses on the *S-N* curves of the misaligned undercut-free and misaligned undercut joints. It is obvious from these figures that the fatigue life was improved by the compressive residual stresses whilst reduced by the tensile residual stresses. This conclusion is consistent with the results reported by many other authors as already reported in section 5.4 of this Chapter.

Figure 5.43a shows the effect of residual stresses on the *S-N* curves of undercut-free misaligned joint. It shows that under the condition of high tensile residual stresses the effect of misalignment on the *S-N* curves becomes more severe. The effect of residual tensile stresses on *S-N* curves of aligned and misaligned joint are similar in a way such that it significantly reduced the fatigue life of the joints. On the contrast, the effect of compressive residual stresses showed a similar trend for the misaligned and aligned joints but the fatigue life of the joints was improved.

Furthermore, fatigue limits of the treated misaligned and aligned joints (S_r = - 172 MPa) were improved by 78 % (from 90 MPa to 160 MPa) and by 75 % (from 120 MPa to 210 MPa) when compared with that under stress-relieved condition (S_r = 0) respectively. Figure 5.43a also shows that the fatigue limit of the misaligned and aligned joint subjected to high tensile residual stresses of the yield stress magnitude (S_r = 300 MPa) could be considerably improved by relieving the tensile residual stresses alone. Under this condition, the fatigue limits of the misaligned and

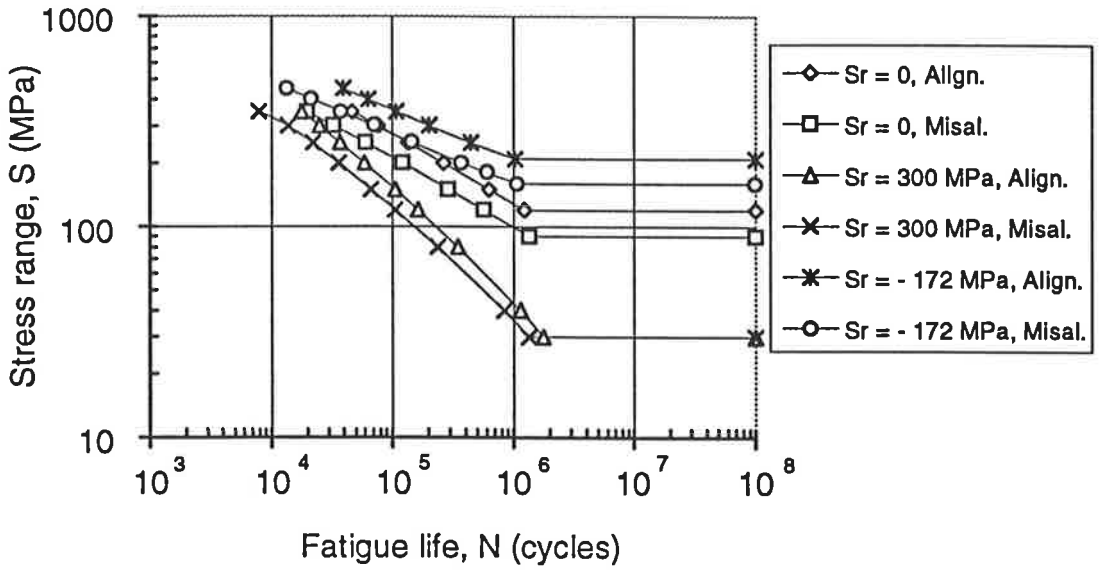

(a) *S-N* curves of undercut-free joint

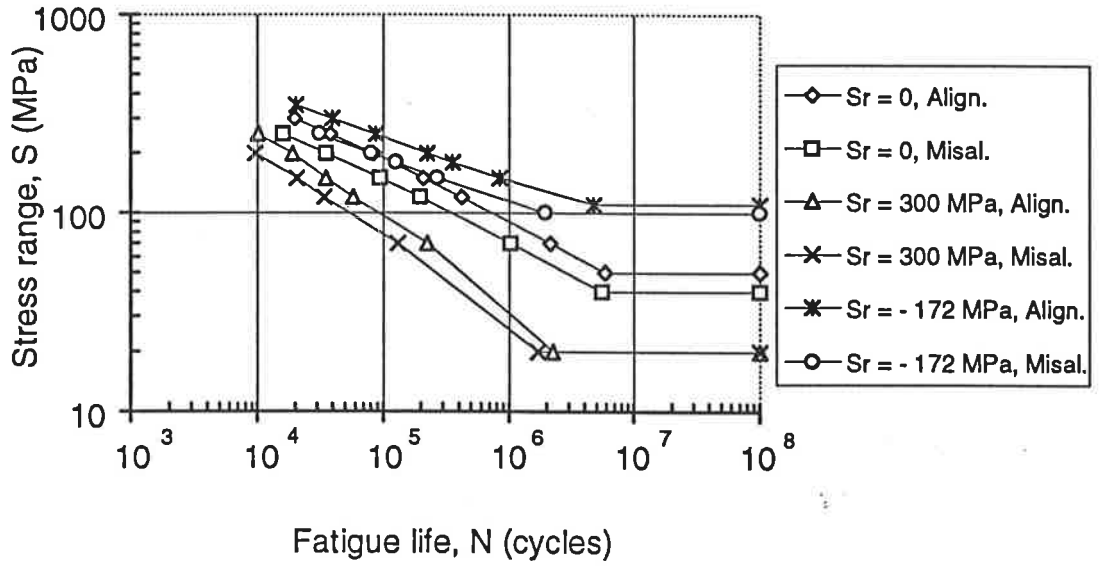

(b) *S-N* curves of undercut joint

Figure 5.43 Effect of residual stresses on the *S-N* curves of the misaligned butt joints (constant parameters: r = 1 mm, $\theta = 30°$, $\phi = 60°$, t = 12 mm, R = 0 and $S_r = 0$).

aligned joints are improved by up to 300 % (from 30 MPa to 90 MPa) and by 400 % (from 30 MPa to 120 MPa) respectively. However, when a surface treatment is applied (with S_r = -172 MPa), the improvement of the fatigue limits of the misaligned and aligned joints can be expected by up to 433 % (from 30 MPa to 160 MPa) and by 600 % (from 30 MPa to 210 MPa) respectively.

Figure 5.43b shows that when an undercut of 0.25 mm is present at the weld toe (r' = 0.25 mm), the improvement of the fatigue limit by surface treatment (S_r = - 172 MPa) of the misaligned and aligned joint significantly decreased by 38 % (from 160 MPa to 100 MPa) and by 48 % (from 210 MPa to 110 MPa) respectively. Using a surface treatment alone the fatigue limit of the undercut misaligned and aligned joint can be increased by up to 150 % (from 40 MPa to 100 MPa) and by 120 % (from 50 MPa to 110 MPa) when compared with that of under stress-relieved condition (S_r = 0) respectively. If the undercut at the weld toes is eliminated after the surface treatments, the fatigue limits of the misaligned and aligned joints can be expected to be improved by up to 300 % (from 40 MPa to 160 MPa) and by 320 % (from 50 MPa to 210 MPa) respectively. The fatigue limit of the undercut misaligned and aligned joint (r' = 0.25 mm) subjected to high tensile residual stresses of the yield stress magnitude (S_r = 300 MPa) can be considerably improved by relieving the tensile residual stresses alone. As a result, the fatigue limits of the misaligned and aligned joints improve by up to 100 % (from 20 MPa to 40 MPa) and by 150 % (from 20 MPa to 50 MPa). When the undercut is eliminated, the improvement of the misaligned and aligned joint can be up to 700 % (from 20 MPa to 160 MPa) and by 950 % (from 20 MPa to 210 MPa).

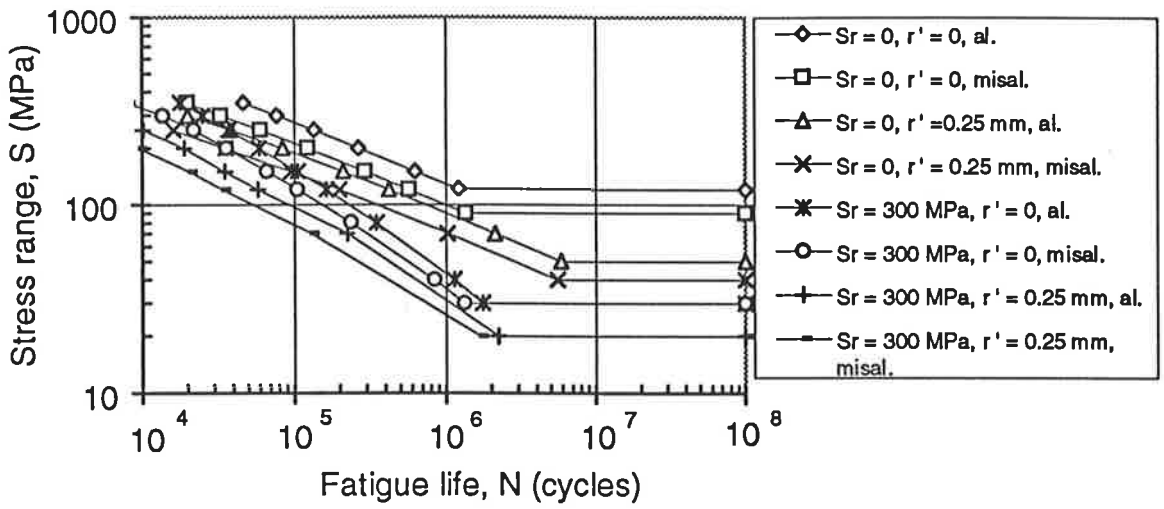

Figure 5.44 Effect of the undercut and misalignment on *S-N* curves of butt-joints due to tensile residual stress field (constant parameters: r = 1 mm, θ = 30°, ϕ = 60°, t = 12 mm, R = 0).

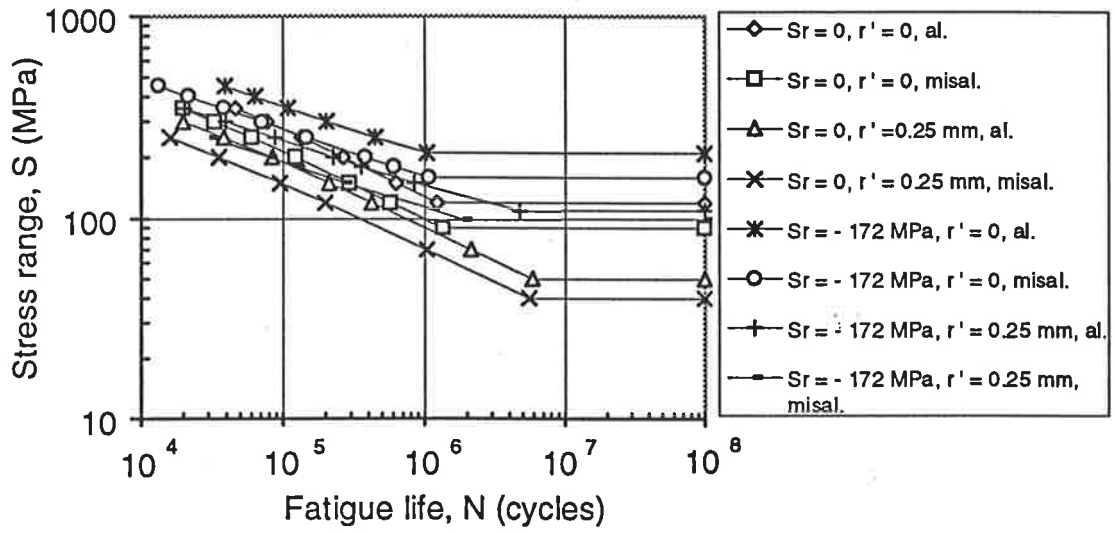

Figure 5.45 Effect of the undercut & misalignment on *S-N* curves of butt-joint subjected to compressive residual stress field (constant parameters: r = 1 mm, θ = 30°, ϕ = 60°, t = 12 mm, R = 0).

Figure 5.44 shows the effect of the undercut and misalignment on *S-N* curves of a butt-joint under the condition of tensile residual stresses. It is obvious from this figure that the effect of an undercut of 0.25 mm in a high tensile residual stress condition (S_r = 300 MPa) on fatigue curve (S-N curve) was more significant than that of the axial misalignment of 5 % of plate thickness. However, the effect of undercut of 0.25 mm in the aligned joint under perfectly stress-relieved condition (S_r = 0 MPa) is similar to the effect of undercut-free misaligned joint of 5 % of plate thickness. However, the fatigue limit of the undercut-free misaligned joint is higher than that of the aligned undercut joint. This figure also shows that under a high tensile residual stress of the magnitude of the yield stress (S_r = 300 MPa), fatigue limits of the undercut-free and undercut aligned joint were decreased by 75 % (from 120 MPa to 30 MPa) and 60 % (from 50 MPa to 20 MPa) when compared with that under perfectly stress-relieved condition respectively. Furthermore, if an axial misalignment (e/t = 0.05) is present, fatigue limits of the undercut-free and undercut joint (r' = 0.25 mm) are decreased by 67 % (from 90 MPa to 30 MPa) and by 50 % (from 40 MPa to 20 MPa) when compared with that of under perfectly stress-relieved condition respectively. It means that the sole effect of high tensile residual stress is less significant when undercut or misalignment is present in the joints.

Figure 5.45 shows the effect of an undercut and misalignment on the *S-N* curves of butt-joints subjected to the compressive residual stresses that were induced by surface treatment (S_r = - 172 MPa). It is obvious from this figure that the fatigue strength and fatigue life of butt joints were improved by the induced compressive residual stress. However, the level of the improvement depended on the particular level of undercut and misalignments. Fig. 5.45 shows that the effect of undercut of the 0.25 mm on the

S-N curve was more significant than that of the misalignment of the order of 5 % of plate thickness under surface treated condition (S_r = - 172 MPa). It also shows that due to the induced compressive residual stresses (S_r = -172 MPa), the fatigue limits of the aligned undercut-free and undercut joint (r' = 0.25 mm) were improved by 75 % (from 120 MPa to 210 MPa) and by 120 % (from 50 MPa to 110 MPa) respectively. However, if an axial misalignment (e/t = 0.05) is present, the improvements of fatigue limits in undercut-free and undercut joint (r' = 0.25 mm) were increased by 78 % (from 90 MPa to 160 MPa) and by 150 % (from 40 MPa to 100 MPa) respectively. This suggests that the surface treatment is more effective for the improvement of the fatigue behaviour of undercut and misaligned joints than that of aligned joints without an undercut.

From the above discussion it can be emphasised that with high induced compressive residual stresses, the individual effect of undercut is more significant than that of the misalignment. The influence of the undercut can be explained by the effect of the threshold range of stress intensity factor (ΔK_{th}) and stress concentrations. Under high compressive residual stresses at the weld toe surface, the applied stress range which is needed for a crack to overcome the threshold value (ΔK_{th}) to propagate further, is increased. As a result, high stress concentrations which are accompanied by an undercut at the weld toes would play the more significant role than the secondary bending stresses induced by the misalignment.

Figure 5.45 also shows that the improvement of the fatigue limit of surface treated joints can be increased by eliminating the undercut at the weld toes. For the aligned undercut joint, the improvement obtained by the same level of surface treatment

(S_r = -172 MPa) can be increased by up to 320 % (from 50 MPa to 210 MPa) if the undercut is eliminated but only by 120 % of improvement (from 50 MPa to 110 MPa) if the undercut is present. For the misaligned joint (e/t = 0.1 or y = 0.6 mm), the improvement obtained by the same level of surface treatment (S_r = -172 MPa) can be increased by up to 300 % (from 40 MPa to 160 MPa) if the undercut is eliminated but only by 150 % (from 40 MPa to 100 MPa) when the undercut is present.

5.7 A Mathematical Model to Predict S-N Curve and Fatigue Notch Factor (K_f)

Table 5.1 shows the transformation functions f_m (...), f_A (...) and proportional constants k_m and k_A for various dimensionless products taking into account the weld geometry parameters (r', r, θ and t), normalised residual stresses (S_r/S_y) and combined loading ratios (R_{ba}) as described in Eqs. (3.35) and (3.36). The value of A_o is given in Table 5.1 as a function of the normalised plate thickness. The values of the constants "m" and "A" in Eq. (3.30) can be calculated by substituting these transformation functions and suitable constants (k_m and k_A) into Eqs. (3.35) and (3.36). The S-N curves which take into account variations in the butt-weld geometry parameters, residual stresses and the combined loading conditions can then be plotted using Eq. (3.30). The fatigue notch factor (K_f) for a certain fatigue life corresponding to the various weld geometry parameters, residual stresses and the combined loading condition can also be easily calculated from Eqs. (3.35), (3.36) and (3.42).

The valid ranges of the dimensionless products of the relevant parameters for the transformation functions as shown in Table 5.1 are: (r'/t) from 0.0 to 0.029, (r/t) from 0.0 to 0.417, flank angle (θ) from 0° to 60°, plate thickness (t/b) from 0.126 to 1.0, (S_r/S_y) from -0.573 to 1.0 and R_{ba} from 0.0 to 1.5.

Furthermore, in order to evaluate the effect of the theoretical stress concentration factor (K_t) on the fatigue notch factor (K_f) a mathematical model for (K_t) as a function of the weld geometry parameters (r', r, θ and t) was found using a dimensional analysis technique as shown in the following Eq. (5.2).

Table 5.1 Transformation functions f_m (...), f_A (...) and proportional constants k_m and k_A for various dimensionless products of weld geometry parameters, residual stresses and combined loading ratio as described in Eqs. (3.35) and (3.36).

No.	Transformation Functions	k_A & k_m	r^2
1	$f_m(r'/t) = 1.0202 + 0.2077(r'/t)^{0.3172}$		0.9992
2	$f_m(r/t) = 0.9994 + 0.0239 \exp(-r/0.1035t)$		0.9982
3	$f_m(\theta) = (0.9996 + 0.0087\theta)/(1 + 0.0082\theta)$		0.9996
4	$f_m(t/b) = -4.8892 - 6.1809(t/b) - 3.8325(t/b)^{2.5} + 5.8762 \exp(t/b)$	$k_m = 0.9929$	0.9921
5	$f_m(R_{ba}) = 0.9015 + 0.0816 \exp(R_{ba} / 2.0745)$		0.9960
6	$f_m(S_r/S_y) = 208.5398 + 113.9884(S_r/S_y)^2 - 101.4969 \exp(S_r/S_y) -$ $- 105.6686 \exp(-S_r/S_y)$ for $S_r <$ 0		0.9957
	$f_m(S_r/S_y) = 0.0037 + 0.1642(S_r/S_y)^2 + 1.0036 \exp(-S_r/S_y)$ for $S_r \geq 0$		0.9989
1	$f_A(r'/t) = 1.1665 + 605.1324(r'/t)^{1.5} - 2359.4361(r'/t)^2 - 7.5657(r'/t)^{0.5}$		0.9999
2	$f_A(r/t) = 0.8167 + 10.6842(r/t)^{2.5} - 12.1409(r/t)^3 + 0.2053(r/t)^3$		0.9972
3	$f_A(\theta) = 0.9911 - 0.085\theta + 0.0192\theta^{1.5} - 0.0012\theta^2$		0.9924
4	$f_A(t/b) = [0.8123 - 1.1884(t/b) + 0.6013(t/b)^2]/[1 - 2.2647(t/b) +$ $+ 1.8548(t/b)^2]$		0.9985
5	$f_A(R_{ba}) = 0.3666 + 1.3564 \exp(-R_{ba}/0.3313)$	$k_A = 1.1051$	0.9995
6	$f_A(S_r/S_y) = [0.5508 + 2.3203(S_r/S_y) + 4.8020(S_r/S_y)^2] / [1 +$ $+ 3.6984(S_r/S_y) + 3.4123(S_r/S_y)^2]$ for $S_r < 0$		0.9999
	$f_A(S_r/S_y) = [0.553773 - 2.285794(S_r/S_y) + 3.523719(S_r/S_y)^2 -$ $- 1.594448(S_r/S_y)^3] / [1 - 50.217416(S_r/S_y) + 1123.602(S_r/S_y)^2 -$ $- 4877.0156(S_r/S_y)^3 + 8142.0423(S_r/S_y)^4]$ for $S_r \geq 0$		0.9999
	$A_o = [4.7776 + 18.4503(t/b)^{3.5437}] \times 10^{12}$ (for b = 50 mm)		0.9981

$$K_t = 0.9992 \cdot f_{kt}(r'/t) \cdot f_{kt}(r/t) \cdot f_{kt}(\theta) \cdot f_{kt}(t/b) \qquad (5.2)$$

where $f_{kt}(r'/t)$, $f_{kt}(r/t)$, $f_{kt}(\theta)$ and $f_{kt}(t/b)$ are the corresponding transformation functions for the mathematical model of (K_t) (Table B.4, Appendix B)

Equation (5.2) is valid if the weld geometry parameters are within the range indicated earlier and if the values of the flank angle (θ) and the tip radius at the undercut (r') are not simultaneously equal to zero ($\theta = 0$ and $r' = 0$). In the latter case, the value of K_t is independent of (r) and (t) since it is always equal to one ($K_t = 1$).

However, for residual stresses and combined loadings, the effective stress concentration factor $K_{t,eff}$ is used and is defined as follows:

$$K_{t,eff} = K_t (1+R_{ba}) + S_r / S_e \qquad (5.3)$$

where S_e - the corresponding fatigue strength at a fatigue life of 2×10^6 cycles (known as the fatigue limit).

5.7.1 The co-influence effect of weld geometry parameters on the fatigue notch factor of butt joints

(a) Effect of various weld geometry parameters on the scatter band of (K_f) and (K_t)

Figures 5.46 to 5.49 show the effect of various weld geometries on the stress concentration factor and the fatigue notch factor of butt joints which have been predicted using Eqs. (3.35), (3.36), (3.42), (5.2) and (5.3)). These figures show the maximum and minimum boundaries of the scatter bands of (K_f) and (K_t) due to the variations in the weld geometry parameters (r', r, θ and t) under two types of boundary conditions which were considered to be representative of the butt joints and are described as follows:

(i) A misaligned as-welded butt-joint (S_r = 30 MPa, R_{ba} = 0.15)

(ii) A perfectly stress-relieved aligned butt-joint (S_r = 0, R_{ba} = 0).

These figures indicate that the scatter band of the fatigue notch factors of butt-joints (K_f) increased as the values of (r'), (θ) or (t) increased and decreased as the weld toe radius (r) increased. The influence of these weld geometry parameters on the scatter band of (K_f) are closely reflected in the behaviour of (K_t).

Figure 5.46 shows the scatter band of (K_f) at 2×10^6 cycles and that of (K_t), generated from Eqs. (3.35), (3.36), (3.42), (5.2) and (5.3) for as-welded and stress-relieved conditions for butt welded joints with the normalised tip radius of undercut (r'/t) varying from 0.0 to 0.029 and the other weld geometry parameters (r, θ, t) maintained within the valid range.

For the as-welded condition, Fig. 5.46 shows that as (r'/t) varies from 0.0 to 0.029 the maximum boundary of (K_f) increases by 41 % (from 3.62 to 5.10) and the minimum boundary of (K_f) increases by 48 % (from 1.10 to 1.63). However, over the whole range of the scatter band of (K_f), the value of (K_f) can be increased by up to 364 % when the effect of (r') is combined with the effects of other parameters (r), (θ) and (t) whilst (r'/t) remains within the same valid range of 0.0 to 0.029. This conclusion was obtained by comparing the minimum and the maximum points of the respective scatter band. This also means that the combined effect of the tip radius at the undercut (r') and other weld geometry parameters (r, θ and t) in the as-welded condition can reduce the fatigue limit (S_e) of butt joints by up to 79 % (corresponding to an increase in (K_f) from 1.10 to 5.10).

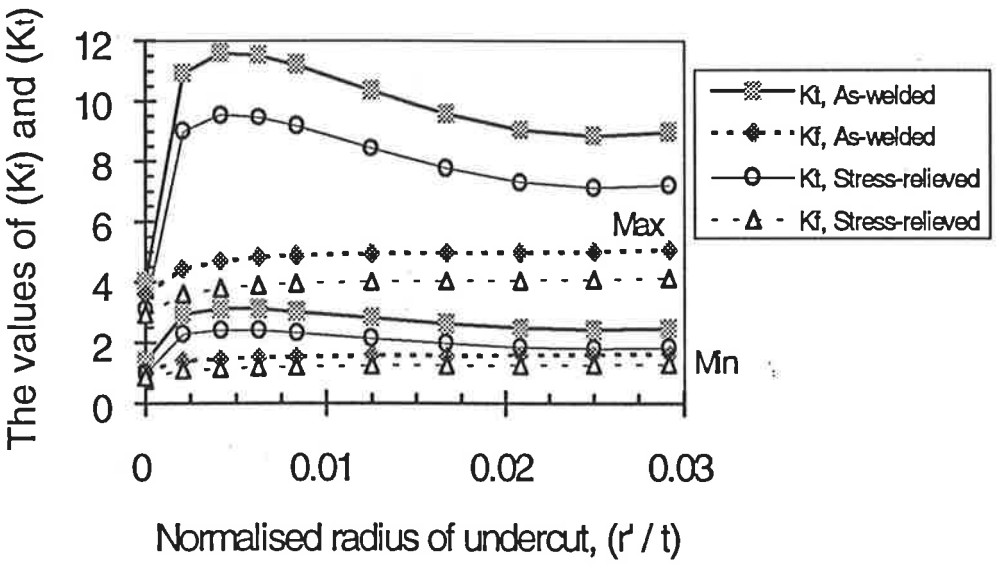

Figure 5.46 Effect of the tip radius of undercut (r') on the scatter bands of (K_f) and (K_t) in the as-welded and stress-relieved conditions.

In the perfectly stress relieved condition, Fig. 5.46 shows that as (r'/t) varies from 0 to 0.029 the maximum and minimum boundary of (K_f) increases by 42 % (from 2.94 to 4.16) and by 30 % (from 1.0 to 1.30) respectively. However, regarding the whole range of (K_f) scatter band, the value of (K_f) can be increased by up to 316 % due to the combined effect of (r') with (r), (θ) and (t) whilst (r'/t) varying in the same valid range from 0.0 to 0.029. This suggests that the combined effect of the tip radius of undercut and other weld geometry parameters (r, θ and t) in perfectly stress relieved condition can reduce the fatigue limit (S_e) of butt joints by up to 76 % (corresponding to an increase in (K_f) from 1.0 to 4.16).

The behaviour of the scatter band of (K_f) described above is reflected in the behaviour of scatter band of (K_t) when the effect of (r') is combined with the effect of other geometry parameters (r, θ and t). However, the values of (K_f) are only a small fraction of the stress concentration factor (K_f / K_t from 0.41 to 0.94).

From Fig. 5.46 it is seen that there is a turning point in the behaviour of the stress concentration factor (K_t) due to the tip radius at the undercut (r'/t). Before that point (r'/t < 0.005) the values of K_t rapidly increase as (r'/t) increases. But, beyond the turning point (r'/t > 0.005) the values of (K_t) decrease as (r'/t) increases. As the tip radius at the undercut of the weld toe increases, it becomes identical to the weld toe radius (r), and hence its effect on K_t is similar to that of weld toe radius (r) as shown latter in Fig. 5.47. Figure 5.46 also shows that the scatter band of (K_f) and (K_t) move downwards as a result of the residual stress-relieving.

Figure 5.47 shows the scatter band of (K_f) at $N_f = 2x10^6$ cycles and the scatter band of (K_t) calculated for butt welded joints with a weld toe radius (r/t) varying from 0.0 to 0.417 whilst other weld geometry parameters (r', θ, t) are maintained within the range valid for Eqs. (3.35), (3.36), (3.42), (5.2) and (5.3) in the as-welded and stress-relieved conditions.

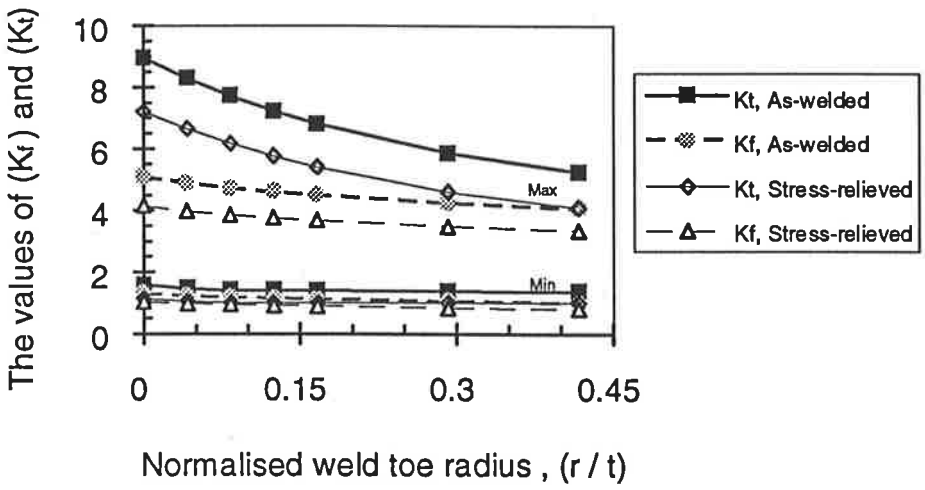

Figure 5.47 Effect of the weld toe radius (r) on the scatter band of (K_f) and (K_t) in the as-welded and stress relieved conditions.

In the as-welded condition, it can be seen from Fig. 5.47 that as (r/t) varies from 0 to 0.417 the maximum boundary of (K_f) was decreased by 20 % (from 5.09 to 4.06) and minimum boundary of (K_f) was decreased by 24 % (from 1.31 to 1.0). However, for the whole range of (K_f) scatter band, the value of (K_f) can be decreased by up to 80 % when the effect of (r) is combined with the other parameters (r'), (θ) and (t) whilst (r/t) maintained within the same valid range of 0.0 to 0.417. This conclusion was also obtained by comparing the maximum and the minimum points in the respective scatter band. This also means that the combined effect of the weld toe radius and other weld

geometry parameters (r', θ and t) in the as-welded condition can improve the fatigue limit (S_e) of butt-joints by up to 409 % (corresponding to a decrease in (K_f) from 5.09 to 1.0).

In the "perfectly" stress relieved condition, Fig. 5.47 shows that as (r/t) varies from 0.0 to 0.417 the maximum boundary of (K_f) are decreased by 20 % (from 4.15 to 3.34) and the minimum boundary of (K_f) are decreased by 4 % (from 1.04 to 1.0). But for the whole range of the scatter band of (K_f), the value of (K_f) can be decreased by up to 81 % when the effect of (r) is combined with other weld geometry parameters (r', θ and t) whilst (r/t) remains in the same valid range of 0.0 to 0.417. This suggests that the combined effect of the weld toe radius and other weld geometry parameters (r', θ and t) in the as-welded condition, can improve the fatigue limit (S_e) of butt-joints by up to 315 % (corresponding to a decrease in (K_f) from 4.15 to 1.0).

It can be noticed from Fig. 5.47 that the values of (K_f) is closely influenced by the behaviour of (K_t) values when the effect of (r) is combined with other geometry parameters (r', θ and t). However, the slopes of the (K_t) vs. (r/t) curves are steeper than those of the (K_f) vs. (r/t) curves. Again the values of the fatigue notch factor are only a small fraction of the stress concentration factor (K_f / K_t from 0.57 to 0.95).

Figure 5.48 shows the variation in (K_f) at $N_f = 2x10^6$ cycles and the values of (K_t) calculated for butt-welded joints with the flank angle (θ) varied between 5° to 60° whilst other weld geometry parameters (r', r and t) are held within a range valid for

Eqs. (3.35), (3.36), (3.42), (5.2) and (5.3) in the as-welded and stress-relieved conditions.

For the as-welded condition, it can be seen from Fig. 5.48 that as (θ) varies from 0° to 60° the maximum boundary of (K_f) increased by 34 % (from 3.80 to 5.10) and the minimum boundary of (K_f) are increased by 43 % (from 1.09 to 1.56). However, for the whole range of the scatter band of (K_f), the value of (K_f) can be increased by up to 368 % when the effect of (θ) is combined with (r'), (r) and (t) whilst (θ) maintained in the same valid range of 0° to 60°. This conclusion was also obtained by comparing the minimum and the maximum points in the respective scatter band. This means that the combined effect of the flank angle and other weld geometry parameters (r', r and t) in the as-welded condition can reduce the fatigue limit (S_e) of butt-joints by up to 79 % (corresponding to an increase in (K_f) from 1.09 to 5.10).

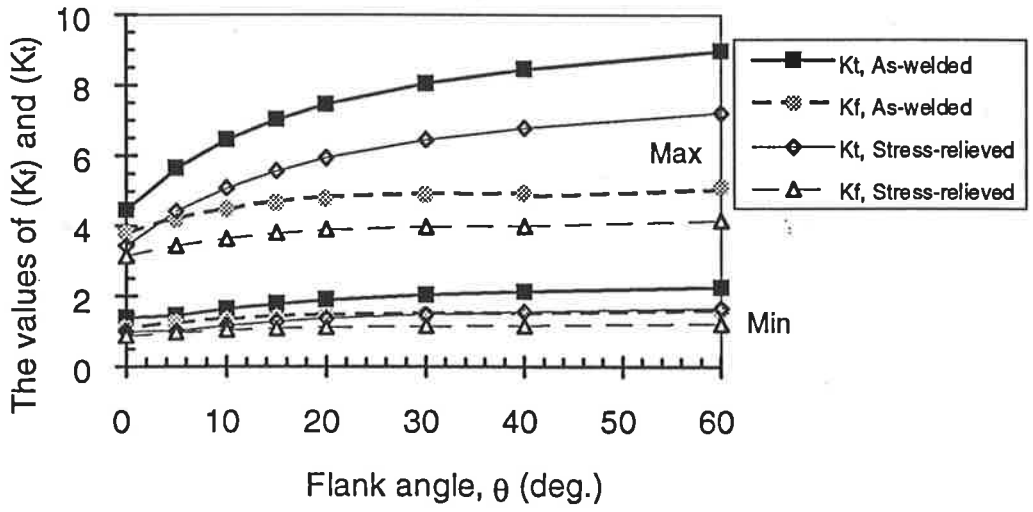

Figure 5.48 Effect of the flank angle (θ) on the scatter band of (K_f) and (K_t) in the as-welded and stress-relieved conditions.

For the "perfectly" stress relieved condition, this figure shows that as (θ) varied from 0° to 60° the maximum boundary of (K_f) increased by 32 % (from 3.15 to 4.16) and the minimum boundary of (K_f) increased by 21 % (from 1.0 to 1.21). However, for the whole range of the scatter band of (K_f), the value of (K_f) can be increased by up to 316 % when the effect of (θ) is combined with other geometry parameters (r', r and t) whilst (θ) remained in the same range from 0° to 60°. It also means that the combined effect of the flank angle (θ) with other geometry parameters (r', r and t) in the perfectly stress-relieved condition can reduce the fatigue limit (S_e) of butt joints by up to 76 % (corresponding to an increase in (K_f) from 1.0 to 4.16).

It is also noticeable from Fig. 5.48 that the behaviour of (K_f) scatter band is closely reflected in the behaviour of (K_t) scatter band due to combining the effect of (θ) with the effects of the other geometry parameters (r', r and t). However, the slopes of the (K_t) vs. (r/t) curves are steeper than those of the (K_f) vs. (r/t) curves. Again the absolute values of the fatigue notch factor are only a small fraction of the stress concentration factor (K_f / K_t from 0.57 to 0.95).

Figure 5.49 shows the scatter band of (K_f) at $N_f = 2x10^6$ cycles and the scatter band of (K_t) calculated for butt-welded joints when the normalised plate thickness (t/b) was varied from 0.126 to 1.0 whilst other parameters (r', r and θ) are held within the range valid for Eqs. (3.35), (3.36), (3.42), (5.2) and (5.3) in the as-welded and stress-relieved conditions.

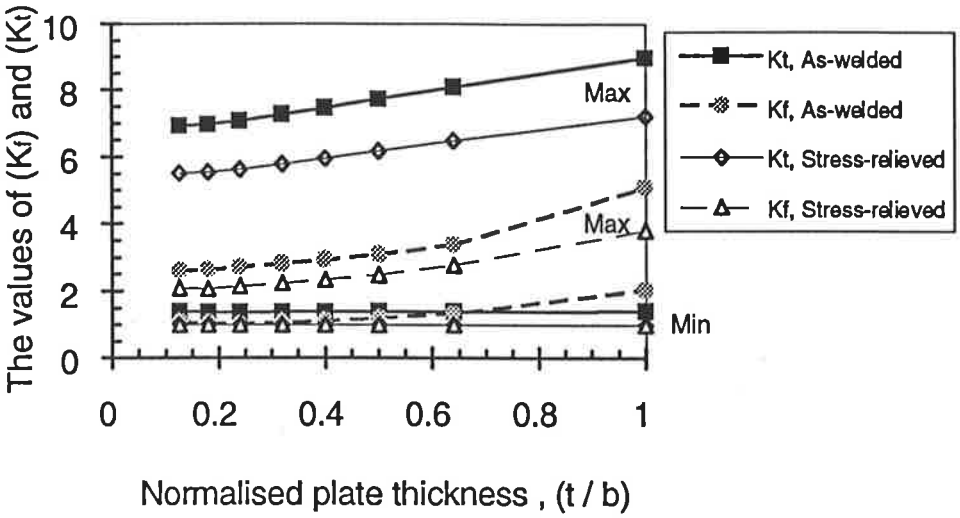

Figure 5.49 Effect of the plate thickness (t/b) on the scatter band of (K_f) and (K_t) in the as-welded and stress-relieved conditions.

For the as-welded condition, Fig. 5.49 shows that as (t/b) varied from 0.126 to 1.0 the maximum boundary of (K_f) increased by 96 % (from 2.60 to 5.10) and the minimum boundary of (K_f) increased by 86 % (from 1.10 to 2.04). But, for the whole range of (K_f) scatter band, the value of (K_f) can be increased by up to 364 % when the effect of (t) is combined with (r'), (r) and (θ) whilst (t/b) are held in the same valid range of 0.126 to 1.0. This conclusion was also obtained by comparing the minimum and the maximum points in the respective scatter band. This means that the combined effect of the plate thickness with other weld geometry parameters (r', r and θ) in the as-welded condition can reduce the fatigue limit (S_e) of butt-joints by up to 78 % (corresponding to an increase in (K_f) value from 1.1 to 5.10).

For perfectly stress relieved condition, this figure shows that as (t/b) varies from 0.126 to 1.0 the maximum boundary of (K_f) increased by 83 % (from 2.08 to 3.81)

whilst the minimum boundary of (K_f) remained unchanged (K_f =1). However, for the whole range of the (K_f) scatter band, the value of (K_f) can be increased by up to 281 % when the effect of (t) is combined with (r'), (r) and (θ) whilst (t/b) varied in the same valid range of 0.126 to 1.0. It also means that the combined effect of plate thickness with other weld geometry parameters (r', r and θ) in the perfectly stress-relieved condition can reduce the fatigue limit (S_e) of butt-joints by up to 74 % (corresponding to an increase in (K_f) value from 1 to 3.81). This figure also shows that thicker the welded plate larger the scatter band of (K_f) is expected.

Fig. 5.49 shows that the behaviour of (K_f) scatter band is closely influenced by the behaviour of (K_t) scatter band in terms of the combined effect of (t) with other geometry parameters (r', r and θ). However, the slopes of the (K_t) vs. (t/b) curves are steeper than those of the (K_f) vs. (t/b) curves. Again the absolute values of the fatigue notch factor are only a small fraction of the stress concentration factor (K_f / K_t from 0.37 to 1.0) in the stress-relieved condition.

(b) Co-influence effect of the weld toe radius and the flank angle on (K_t) and (K_f)

In reality, the values of the plate thickness (t) and plate-edge angle (ϕ) for a butt-welded joint are usually selected by design. As the transformation functions corresponding to these geometrical parameters do not change, Eqs. (3.49) and (3.40) can be rewritten in a more simplified form as a function of three independent variables (r', r and θ). Furthermore, if the weld toe is ground off or TIG-remelting (GTAW-remelting) to eliminate the possibility of the undercuts at the weld toes, then Eqs. (3.39) and (3.40) become the functions of two independent variables (r and θ). For

example when a single-V butt-welded joint is fabricated from 12 mm thick plate with an edge preparation angle of $\phi = 60°$, at a given residual stress level and loading condition (S_r/S_y = const. and R_{ba} = const.) Eqs. (3.35) and (3.36) become:

$$m / m_o = k^*_{mG} .f_m(r/t). f_m(\theta) \quad (5.4)$$

$$A / A_o = k^*_{AG} .f_A(r/t). f_A(\theta) \quad (5.5)$$

where $f_m(r/t)$, $f_m(\theta)$, $f_A(r/t)$ and $f_A(\theta)$ are transformation functions, and

k^*_{mG} , k^*_{AG} - proportional constants

Using Eqs. (5.2) to (5.5) and (3.42) the combined effect of the weld toe radius and flank angle on the stress concentration factor (K_t) and the fatigue notch factor (K_f) at $2x10^6$ cycles have been investigated in the following two representative cases:

(i) An aligned butt-joint in a perfectly stress-relieved condition without an undercut ($S_r = 0$, $R_{ba} = 0$ and r' = 0)

(ii) A misaligned butt-joint in the as-welded condition with an undercut ($S_r /S_y = 0.1$, $R_{ba} = 0.15$ and r' = 0.05 mm)

(i) An aligned butt-joint in a perfectly stress-relieved condition without an undercut

Figure 5.50 shows the co-influence effect of the weld toe radius and flank angle on the stress concentration factor of the aligned butt-joints in the stress-relieved condition (r' = 0, t = 12 mm, $S_r = 0$ and $R_{ba} = 0$). This figure shows that the stress concentration of butt-joints increased significantly due to the combined influence of the weld toe radius

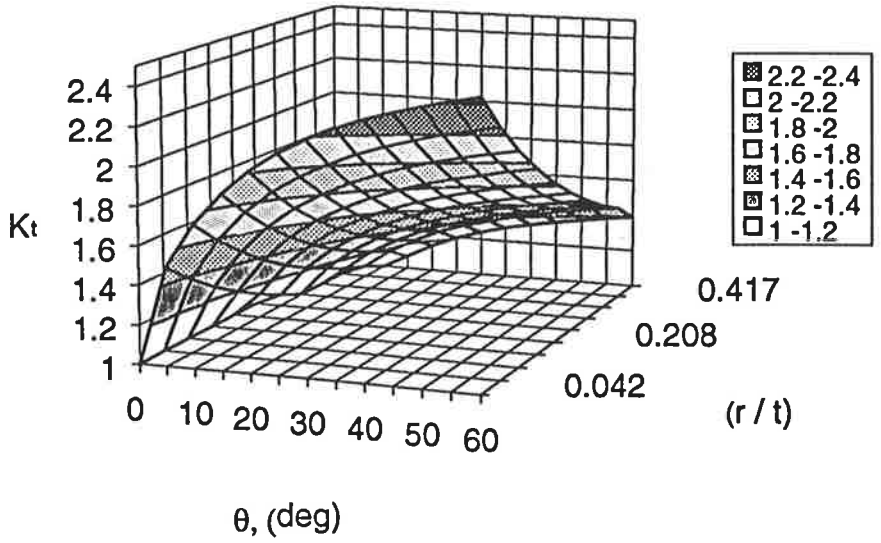

Figure 5.50 Co-influence effect of (r) and the flank angle (θ) on the stress concentration factor of aligned butt-joints in the stress-relieved condition (r'=0).

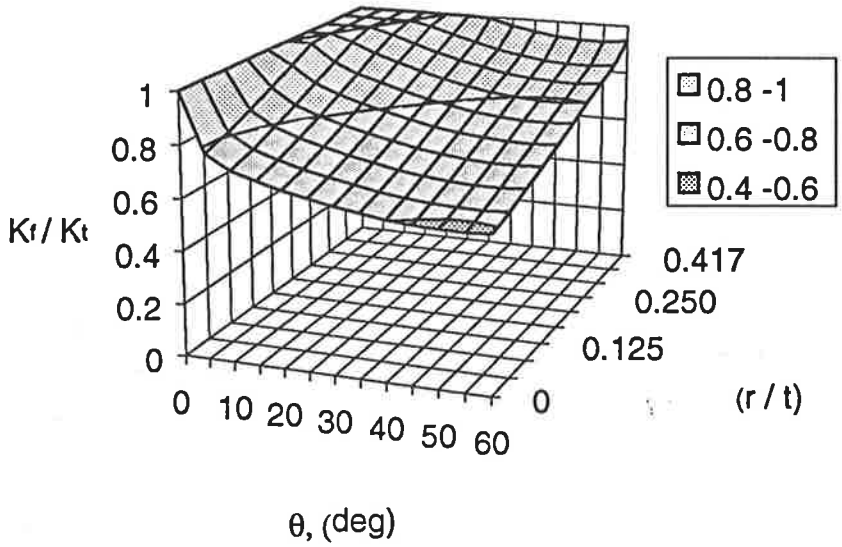

Figure 5.51 The co-influence effect of the weld toe radius and flank angle on the (K_f/K_t) ratio of aligned butt-joints in the stress-relieved condition (r' = 0).

and the flank angle. It shows that the values of (K_t) increased as (θ) increased from 0° to 60° or (r/t) decreased from 0.417 to 0.0. Also the values of (K_t) can be increased by up to 240 % from 1.0 (corresponding to θ = 0° and (r/t) = 0.417) to 2.4 (corresponding to θ = 60° and (r/t) = 0). This behaviour of (K_t) due to variations in (r) and (θ) determines the behaviour of (K_f) as shown in Fig. 5.51.

Figure 5.51 shows the combined effect of the weld toe radius and flank angle on the (K_f/K_t) ratio which represents the fatigue notch sensitivity of the aligned butt-joints in the stress-relieved condition (r' = 0, t = 12 mm, S_r = 0 and R_{ba} = 0). It shows that the values of the (K_f/K_t) ratio decreased as the flank angle (θ) increased (from 0° to 60°) or the values of (r/t) decreased (from 0.417 to 0.0). Further, it shows that the values of (K_f) is only a small fraction of the value of (K_t) for any given weld toe radius and flank angle.

(ii) A misaligned butt-joint in the as-welded condition with an undercut

Figure 5.52 shows the co-influence effect of the weld toe radius and flank angle on the stress concentration factor of a misaligned butt-joints in the as-welded condition with an undercut (r' = 0.05 mm, t = 12 mm, S_r = 30 MPa, R_{ba} = 0.15). This figure shows that the values of the effective stress concentration factor ($K_{t,eff}$) increased significantly when an undercut, residual stresses and misalignment are all present. However, the behaviour of ($K_{t,eff}$) subjected to variations in the flank angle and weld toe radius were similar to that of the aligned joints in the stress-relieved condition

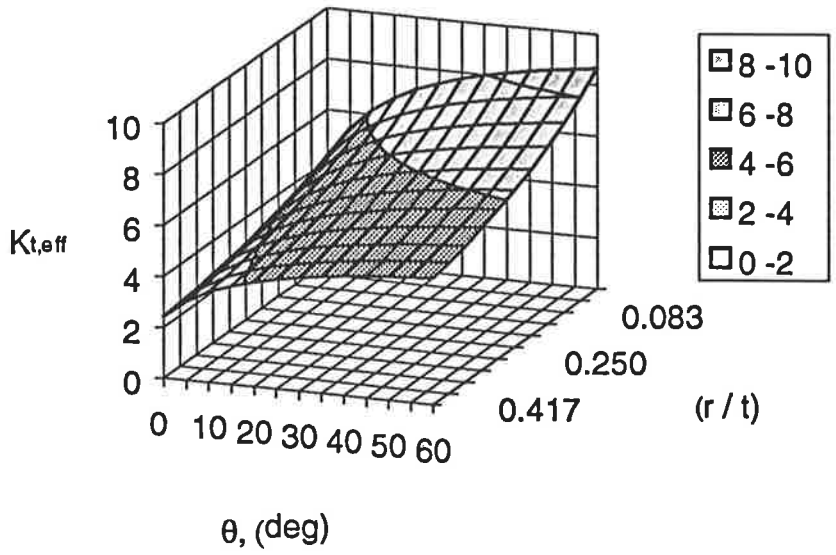

Figure 5.52 Co-influence effect of (r) and (θ) on the stress concentration factor of a misaligned butt-joint in the as-welded condition (r' = 0.05 mm).

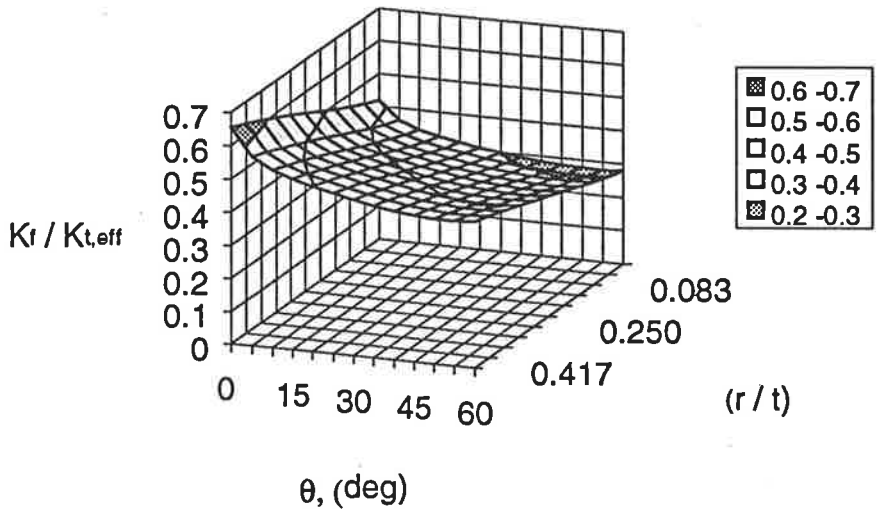

Figure 5.53 The co-influence effect of (r) and (θ) on the (K_f / $K_{t,eff}$) for an as-welded misaligned butt-joints (constant parameters: r' = 0.05 mm, t = 12 mm, S_r = 30 MPa, R_{ba} = 0.15).

without an undercut as shown in Fig. 5.50. Furthermore, the values of ($K_{t,eff}$) increased as the flank angle increased or the weld toe radius decreased.

Figure 5.53 shows the co-influence effect of the weld toe radius and flank angle on (K_f / $K_{t,eff}$) of the misaligned butt joints in the as-welded condition (r' = 0.05 mm, t = 12 mm, S_r = 30 MPa, R_{ba} = 0.15). It shows that the values of (K_f / $K_{t,eff}$) decreased as the flank angle (θ) increased (from 0° to 60°) or (r/t) decreased (from 0.417 to 0).

It can also be seen from this figure that the behaviour of (K_f / $K_{t,eff}$) due to variations in (θ) and (r/t) is similar to that of (K_f / K_t) for the aligned butt-joint in the stress-relieved condition without an undercut (Fig. 5. 51). Also, the value of (K_f) was only a small fraction of the ($K_{t,eff}$) for a given weld toe radius and flank angle. The magnitude of the ratio (K_f /$K_{t,eff}$) was much smaller in this case than for the aligned butt-joint in the stress-relieved condition without an undercut (Fig. 5. 51).

5.7.2 The effect of residual stresses and combined loadings on the fatigue notch factor of butt-joints

In this section, the effect of residual stresses and the combined loading ratio (R_{ba}) on the variations of the fatigue notch factor (K_f) of butt-welded joints are discussed simultaneously with that on the scatter band of the effective stress concentration factor ($K_{t,eff}$).

(a) Effect of residual stress and the ratio (R_{ba}) on the values of ($K_{t,eff}$) and (K_f)

Figure 5.54 shows the effect of the combined loading ratio (R_{ba}) on the values of (K_f) & ($K_{t,eff}$) which have been calculated for butt welded joints in the as-welded and stress-relieved conditions using Eqs. (3.35), (3.36), (3.42) and (5.2) & (5.3). For these calculations, the combined loading ratio (R_{ba}) was varied between from 0.0 to 1.5 and the other weld geometry parameters were maintained within the valid ranges. This range of (R_{ba}) was selected on the basis of the acceptable levels of the misalignment for butt-joints Class D-Q1 and Class D-Q7 (BSI PD 6493, 1991) respectively.

In the as-welded condition, it can be seen from Fig. 5.54 that as (R_{ba}) increases from 0 to 1.5 the maximum boundary of (K_f) are increased by 110 % (from 4.49 to 9.44) and the minimum boundary of (K_f) are increased by 136 % (from 1.0 to 2.36). However, for the whole range of the scatter band of (K_f), the value of (K_f) can be increased by up to 844 % (from 1.0 to 9.44) when the effect of (R_{ba}) is combined with the other geometry parameters (r', r, t and θ) whilst (R_{ba}) remains in the same valid range of 0.0 to 1.5. This conclusion was obtained by comparing the minimum and the maximum points in the respective ranges.

This also means that the combined effect of the combined loading ratio (R_{ba}) with other weld geometry parameters (r', r , t and θ) in the as-welded condition can reduce the fatigue limit (S_e) of butt-joints by up to 89 % (corresponding to an increase in (K_f) value from 1.0 to 9.44).

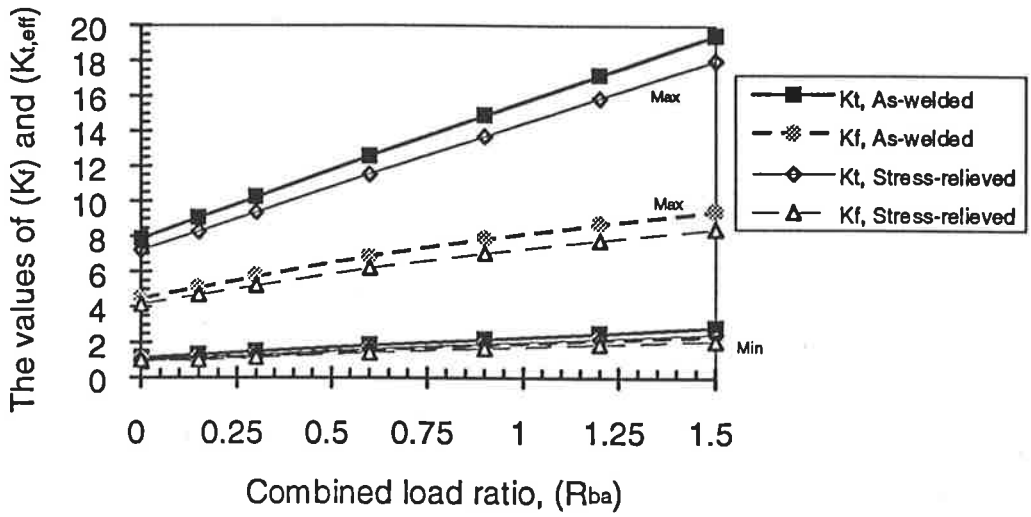

Figure 5.54 Effect of (R_{ba}) when combined with the other weld geometry parameters on the values of ($K_{t,eff}$) & (K_f) for the as-welded and stress relieved conditions.

In the "perfectly" stress relieved condition, Fig. 5.54 shows that as (R_{ba}) increased from 0 to 1.5, the maximum boundary of (K_f) were increased by 103 % (from 4.16 to 8.46) and the minimum boundary of (K_f) were increased by 109 % (from 1.0 to 2.09). However, for the whole range of (K_f) values, the value of (K_f) can be increased by up to 746 % when the effect of (R_{ba}) is combined with the effects of other weld geometry parameters (r', r , t and θ) whilst (R_{ba}) maintained in the same valid range of 0.0 to 1.5. This also means that the combined effect of (R_{ba}) with other weld geometry parameters (r', r, t and θ) in the perfectly stress-relieved condition can reduce the fatigue limit (S_e) of butt-joints by up to 88 % (corresponding to an increase in (K_f) value from 1.0 to 8.46).

Figure 5.54 also shows that the behaviour of (K_f) is closely influenced by the behaviour of ($K_{t,eff}$) due to the combined effect of (R_{ba}) with other geometry parameters (r', r, t and θ). However, the slopes of the ($K_{t,eff}$) vs. (R_{ba}) curves are

steeper than those of the (K_f) vs. (R_{ba}) curves. Furthermore, the values of ($K_{t,eff}$) are only a small fraction of the stress concentration factor (K_f / K_t from 0.49 to 0.87 in the as-welded condition and from 0.47 to 1.0 in the stress-relieved condition).

Figure 5.55 shows the combined effect of the residual stresses (S_r/S_y) on the values of (K_f) and ($K_{t,eff}$) calculated for the aligned and misaligned butt-joints (R_{ba}= 0 and R_{ba}= 0.15 respectively) whilst other weld geometry parameters were varied within the range valid for Eqs. (3.35), (3.36), (3.42), (5.2) and (5.3).

For the misaligned butt-joints, Fig. 5.55 shows that as (S_r / S_y) varied from -0.57 to 1.0 the maximum boundary of (K_f) were increased by 676 % (from 2.70 to 20.94) and the minimum boundary of (K_f) were increased by 921 % (from 0.53 to 5.41). This suggests that for a particular residual stress condition the fatigue notch factor of the misaligned butt-joints can be decreased up to 81 % (from 2.70 to 0.53 for S_r / S_y = -0.57) and 74 % (from 20.94 to 5.41 for S_r / S_y = 1.0) by modifying the weld geometry parameters (r', r, t and θ) alone. Thus improves the fatigue limit (S_e) up to 409 % and by 287 % respectively.

However, for the whole range of the (K_f), the value of (K_f) can be decreased up to 98 % (from 20.94 to 0.53) by using post-weld surface treatments as well as modifying geometry parameters (r', r, t and θ) of the joints. This conclusion was obtained by comparing the minimum and the maximum values of (K_f).

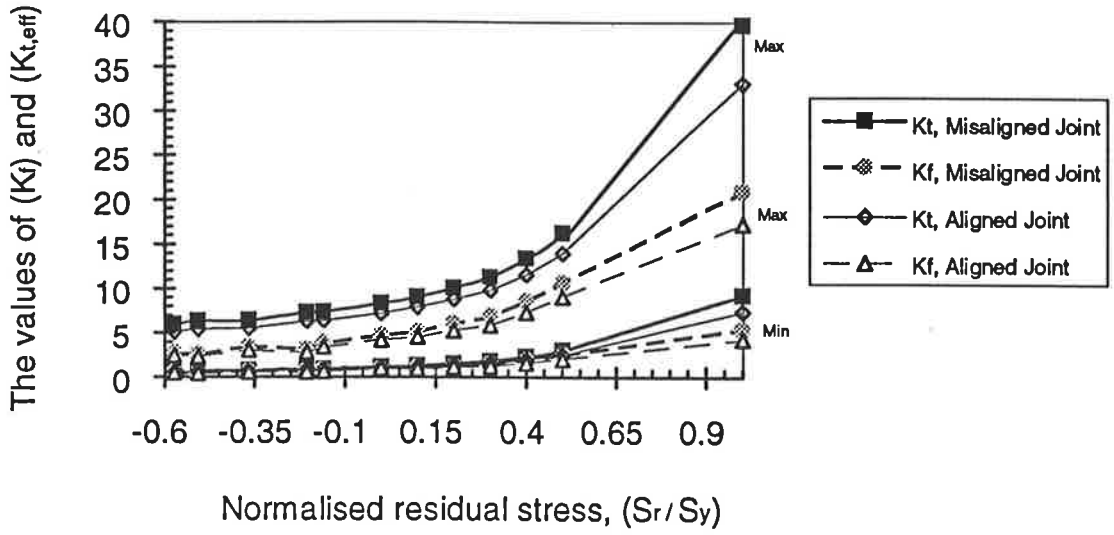

Figure 5.55. Effect of the residual stresses (S_r/S_y) on the values of ($K_{t,eff}$) & (K_f) in aligned and misaligned butt-joints.

For the aligned butt-joints, Fig. 5.55 shows that as (S_r / S_y) varies from -0.57 to 1.0, the maximum boundary of (K_f) were increased by 608 % (from 2.44 to 17.28) and the minimum boundary of (K_f) were increased by 809 % (from 0.47 to 4.27). For the particular residual stress condition the fatigue notch factor of aligned butt joints can be decreased by up to 81 % (from 2.44 to 0.47 for S_r / S_y = -0.57) and 75 % (from 17.28 to 4.27 for S_r / S_y = 1.0) by modifying the weld geometry parameters (r', r, t and θ) alone. Thus improves the fatigue limit (S_e) up to 419 % and by 305 % respectively. However, for the whole range of (K_f) values, (K_f) may be decreased by 97 % (from 17.28 to 0.47) using post-weld surface treatments as well as modifying the geometry parameters (r', r, t and θ). This conclusion was reached after comparing the minimum and the maximum values of (K_f).

Figure 5.55 shows that the behaviour of (K_f) is closely influenced by the variation of ($K_{t,eff}$) when subjected to the combined effect of (S_r / S_y) and other geometry parameters (r', r, t and θ) for both aligned and misaligned joints. However, the slopes of the ($K_{t,eff}$) vs. (S_r / S_y) curves are steeper than those of the (K_f) vs. (S_r / S_y) curves. The values of the fatigue notch factor are only a fraction of the stress concentration factor (K_f / K_t from 0.41 to 0.90 for the misaligned butt-joints and from 0.43 to 1.0 for the aligned butt-joints).

(b) Combined effect of the residual stress and combined axial and bending loadings on ($K_{t,eff}$) and (K_f)

The effect of residual stresses and the combined loading conditions were investigated in the present study in terms of the two parameters (S_r) and (R_{ba}). The effect of each of these two parameters was investigated whilst holding the other weld geometry parameters (r', r, θ and t) unchanged. Transformation functions were evaluated for (S_r) and (R_{ba}) corresponding to Eqs. (3.35) and (3.36) were obtained (Table 5.1). Equations (3.35) and (3.36) could then be rewritten in the following form:

$$m / m_o = k^*_{m,RL} . f_m (S_r/S_y). f_m (R_{ba}) \quad (5.6)$$

$$A / A_o = k^*_{A,RL} . f_A (S_r/S_y). f_A (R_{ba}) \quad (5.7)$$

where $f_m (S_r/S_y)$, $f_m (R_{ba})$, $f_A (S_r/S_y)$, $f_A (R_{ba})$ are the transformation functions for (m) and (A) due to residual stresses and the combined axial and bending loadings;

$k^*_{m,RL}$ and $k^*_{A,RL}$ are proportional constants due to residual stresses and the combined axial and bending loadings.

Using Eqs. (5.2), (5.3), (5.6), (5.7) and (3.42) the combined effect of residual stresses (S_r) and combined loadings (R_{ba}) on ($K_{t,eff}$) and on (K_f) at $2x10^6$ cycles were investigated for the following two representative cases of a butt joint with the same weld geometry:

(i) The 12 mm thick butt-joint without an undercut at the weld toe

($r' = 0$, $r = 1$ mm, $\theta = 30°$ and $t = 12$ mm)

(ii) The 12 mm thick butt-joint with an undercut at the weld toe

($r' = 0.05$ mm, $r = 1$ mm, $\theta = 30°$ and $t = 12$ mm)

(i) The 12 mm thick butt-joint without an undercut at the weld toe (r'=0.0 mm)

Figure 5. 56 shows the effect of the residual stress (S_r/S_y) and the combined loading ratio (R_{ba}) on ($K_{t,eff}$) of the undercut-free butt-joints ($r' = 0$, $r = 1$ mm, $\theta = 30°$, $t = 12$ mm). It shows that for a particular residual stress condition (S_r/S_y = const.) the values of ($K_{t,eff}$) increased as the ratio (R_{ba}) increased. Furthermore, the values of ($K_{t,eff}$) increased much more rapidly at the higher levels of tensile residual stresses but more slowly at the lower level of tensile residual stresses or higher level of compressive residual stresses.

Figure 5. 56 also shows that the effect of the residual stresses and the combined loading ratio can increase the value of ($K_{t,eff}$) up to 35.8. However, the effect of compressive residual stresses in the aligned joints ($R_{ba} = 0$) can decrease the value of ($K_{t,eff}$) up to 1.3. It means that the effect of tensile residual stresses and the combined loading ratio results in a more detrimental stress distribution while the presence of compressive residual stresses in the aligned joints results in a less harmful stress

distribution in the welded joints. This also reflects the effect on the fatigue notch factor (K_f) of the welded joints as shown in Fig. 5.57.

Figure 5. 57 shows the effect of residual stress (S_r/S_y) and (R_{ba}) on the (K_f) at $2x10^6$ cycles of the undercut-free butt welded joints (r' = 0, r = 1 mm, θ = 30°, t = 12 mm) . The behaviour of (K_f) when subject to the effect of (S_r/S_y) and (R_{ba}) was similar to that of ($K_{t,eff}$). Figure 5.57 also shows that for a particular residual stress condition (S_r/S_y = const.) the values of (K_f) increased as the ratio (R_{ba}) increased.

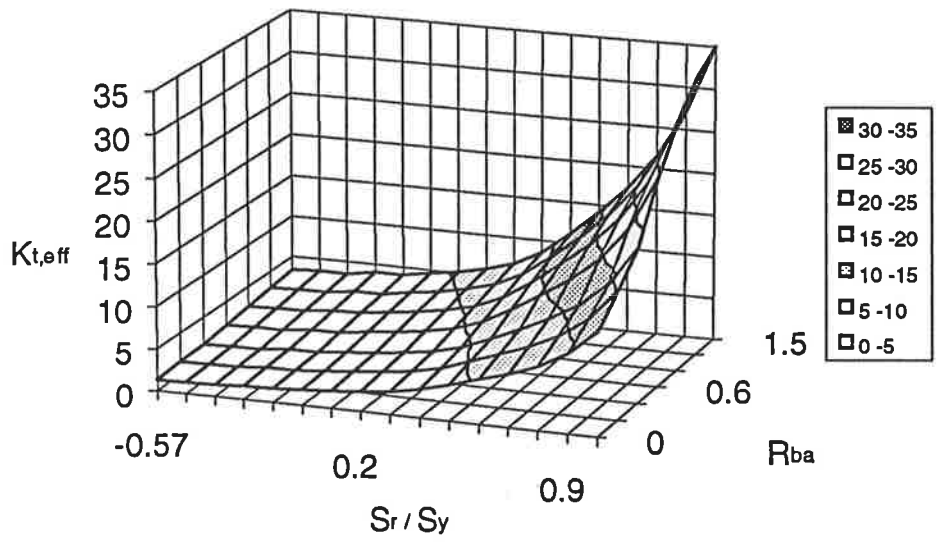

Figure 5.56 The effect of residual stresses and the combined loading ratio on ($K_{t,eff}$) of the undercut-free butt-joints (constant parameters: r' = 0, r = 1 mm, θ = 30°, t = 12 mm).

However, the increase in (K_f) occurred much more rapidly at the higher levels of tensile residual stresses than at the lower levels of tensile residual stresses or higher levels of compressive residual stresses. Furthermore, the effect of residual stresses and

the combined loading ratio can increase the value of (K_f) up to 20.8. The effect of compressive residual stresses in the aligned joints (R_{ba} = 0) can decrease the value of (K_f) beyond the value of 1.0 (which represents the fatigue behaviour of the un-notched plate) to 0.64. This suggests that the fatigue limit (S_e) can be decreased by as much as 95 % due to the co-influence effect of tensile residual stresses and the combined loading ratio, but it can be increased by up to 56 % compared to the fatigue limit of the flat (unwelded) plate. This also suggests that the effect of tensile residual stresses and the combined loading ratio is detrimental to the fatigue behaviour of welded joints but the presence of compressive residual stresses in aligned joints is beneficial to the fatigue behaviour of the joints.

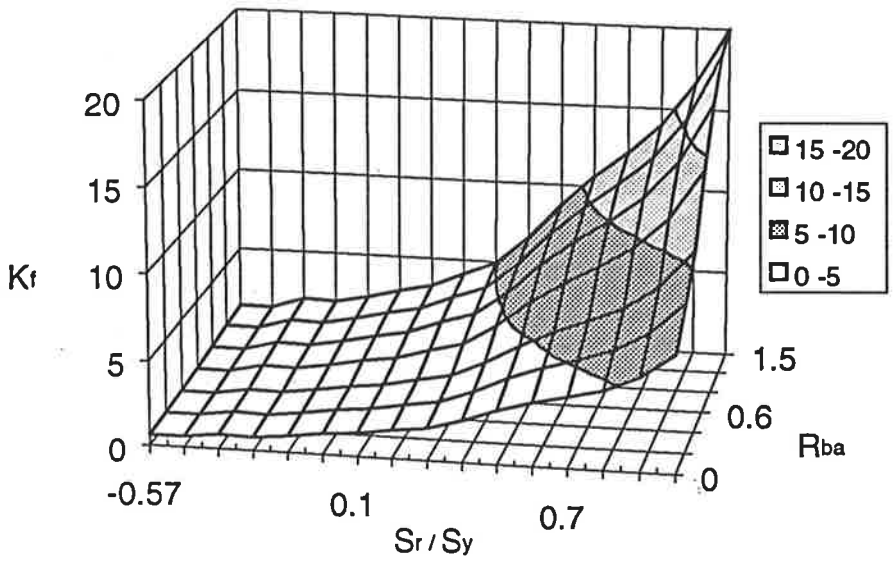

Figure 5.57 The effect of the residual stress and combined loading ratio on (K_f) of the undercut-free butt-joints (constant parameters: r' = 0, r = 1 mm, θ = 30°, t = 12 mm).

(ii) The 12 mm thick butt-joint with an undercut at the weld toe (r'=0.05 mm)

Figure 5. 58 shows the effect of the residual stress (S_r/S_y) and the combined loading ratio (R_{ba}) on ($K_{t,eff}$) of the undercut butt-joints (r' = 0.05 mm, r = 1 mm, θ = 30°,

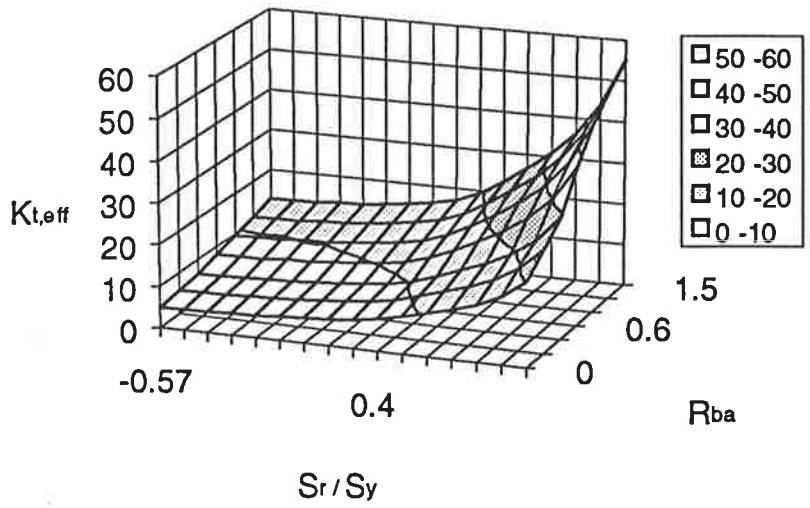

Figure 5.58 The effect of the residual stress and combined loading ratio on ($K_{t,eff}$) of the undercut butt-joints (constant parameters: r' = 0.05 mm, r = 1 mm, θ = 30°, t = 12 mm).

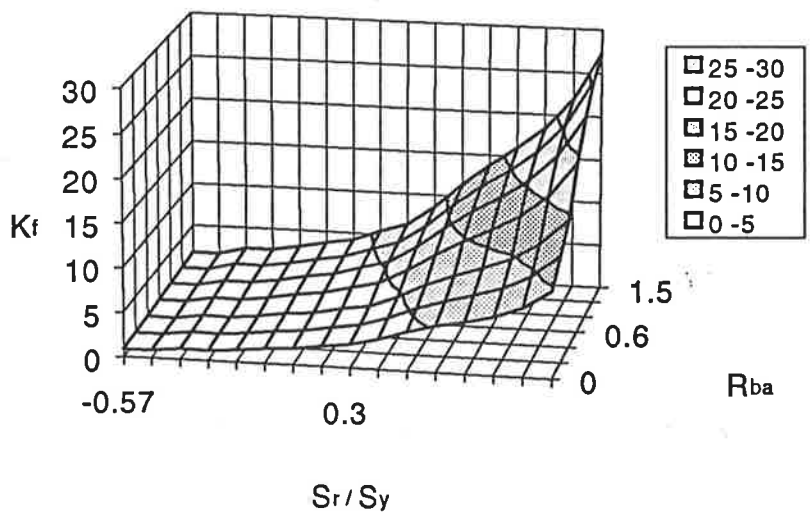

Figure 5.59 The effect of residual stress and the combined loading ratio on (K_f) of the undercut butt-joints (constant parameters: r' = 0.05 mm, r = 1 mm, θ = 30°, t = 12 mm).

t = 12 mm). It shows that the behaviour of ($K_{t,eff}$) when subject to the effect of (S_r/S_y) and (R_{ba}) was similar to that of the undercut-free joints except that the magnitude of ($K_{t,eff}$) was much higher due to presence of the undercut.

Figure 5.58 also shows that for a particular residual stress condition (S_r/S_y = const.) the values of ($K_{t,eff}$) increased as the ratio (R_{ba}) increased. Furthermore, the values of ($K_{t,eff}$) increased much more rapidly at higher levels of tensile residual stresses but more slowly at lower levels of tensile residual stresses or higher levels of compressive residual stresses. However, the effect of residual stresses and the combined loading ratio on the undercut butt-joints can increase the values of ($K_{t,eff}$) up to 55.1.

The effect of compressive residual stresses in the aligned welded joints with an undercut (R_{ba} = 0, r' = 0.05 mm) can decrease the value of ($K_{t,eff}$) up to 4.95. This means that the effect of tensile residual stresses and the combined loading ratio result in a more detrimental stress distribution whilst the effect of the compressive residual stresses in the aligned joints resulted in a more beneficial stress distribution in welded joints. This is also reflected in the effect of residual stresses and the combined loading ratio on (K_f) of the undercut welded joints as shown in Fig. 5.59.

Figure 5. 59 shows the effect of residual stress (S_r/S_y) and the combined loading ratio(R_{ba}) on (K_f) at $2x10^6$ cycles of the undercut butt-joints (r' = 0.05 mm, r = 1 mm, θ = 30°, t = 12 mm). It shows that the behaviour of (K_f) of the undercut joints when subject to the effect of (S_r/S_y) and (R_{ba}) is similar to that of the undercut-free joints except that the magnitude of (K_f) of the undercut joints is much higher than that of undercut-free joints. Furthermore, for a particular residual stress condition (S_r/S_y =

const.) the values of (K_f) increased as the ratio (R_{ba}) increased. However, the values of (K_f) increased much more rapidly at the higher tensile residual stresses and more slowly at lower tensile residual stresses or higher compressive residual stresses.

Figure 5.59 also shows that the effect of residual stresses and the combined loading ratio can increase the value of (K_f) for the undercut joints to 27.2. The effect of compressive residual stresses on the aligned joints (R_{ba} = 0) decreased the value of (K_f) beyond 1.0 to 0.85. Thus, the fatigue limit (S_e) of the undercut joints can be decreased by as much as 96 % due to the effect of tensile residual stresses and the combined loading ratio but it can also be increased by 18 % compared to the fatigue limit of the flat unwelded plate (S_o).

By comparing these results with those made from Fig. 5.57 for the undercut-free joints, it can be concluded that the presence of an undercut can significantly increases the harmful effect of tensile residual stresses and combined loading ratio and reduce the effectiveness of the beneficial compressive residual stresses.

5.8 Verification of the Model

In this section, the model developed in this study is verified in terms of the fatigue notch factor, the effect of residual stresses, undercut and misalignments; and the fatigue S-N curves.

5.8.1 Verification of the fatigue notch factor

The above mathematical model has been verified by comparing the predicted values of the fatigue notch factor (K_f) with the author's fatigue test results and fatigue test data published by the National Research Institute for Metal in Tokyo-Japan (NRIM Fatigue Data Sheet, 1983). The values of (K_f) predicted by other models used for calculations of (K_f) (Peterson 1959, Buch & Switek 1988) are also plotted on the same graphs for comparison.

Figure 5.60 shows the values of the fatigue notch factor (K_f) predicted by the author's model, the author's fatigue test results and available fatigue data (NRIM Fatigue Data Sheet, 1983). The (K_f) values predicted by Peterson's and Buch-Switek's equations (Eqs. (3.40) and (3.41)) which accounted for the effect of the weld toe radius (r) and stress concentration factor (K_t) are also shown in Fig. 5.60.

The range of the scatter band of (K_f) corresponding to the lower and upper boundaries for the weld geometry parameters, welding residual stress and loading condition is shown in Fig. 5.60. The aligned, undercut-free, butt-joints in perfectly stress-relieved condition were selected for the lower boundary condition (r' = 0, R_{b_a} = 0, S_r = 0). In

this case, only three weld geometry parameters namely weld toe radius (r), flank angle (θ) and plate thickness (t) were varied. However, for the upper boundary condition three parameters i.e (r', R_{ba} and S_r) were selected so as to simulate the conditions in the test specimens. Consequently, the value of (r') was selected at r' = 0.05 mm since it was representative of values of (r') seen on the majority of the weld profile micro-graphs. The representative values for (R_{ba}) and (S_r) were estimated at R_{ba} = 0.15 and S_r/S_y= 0.1 based on the experimental results obtained from strain gauge outputs during fatigue tests.

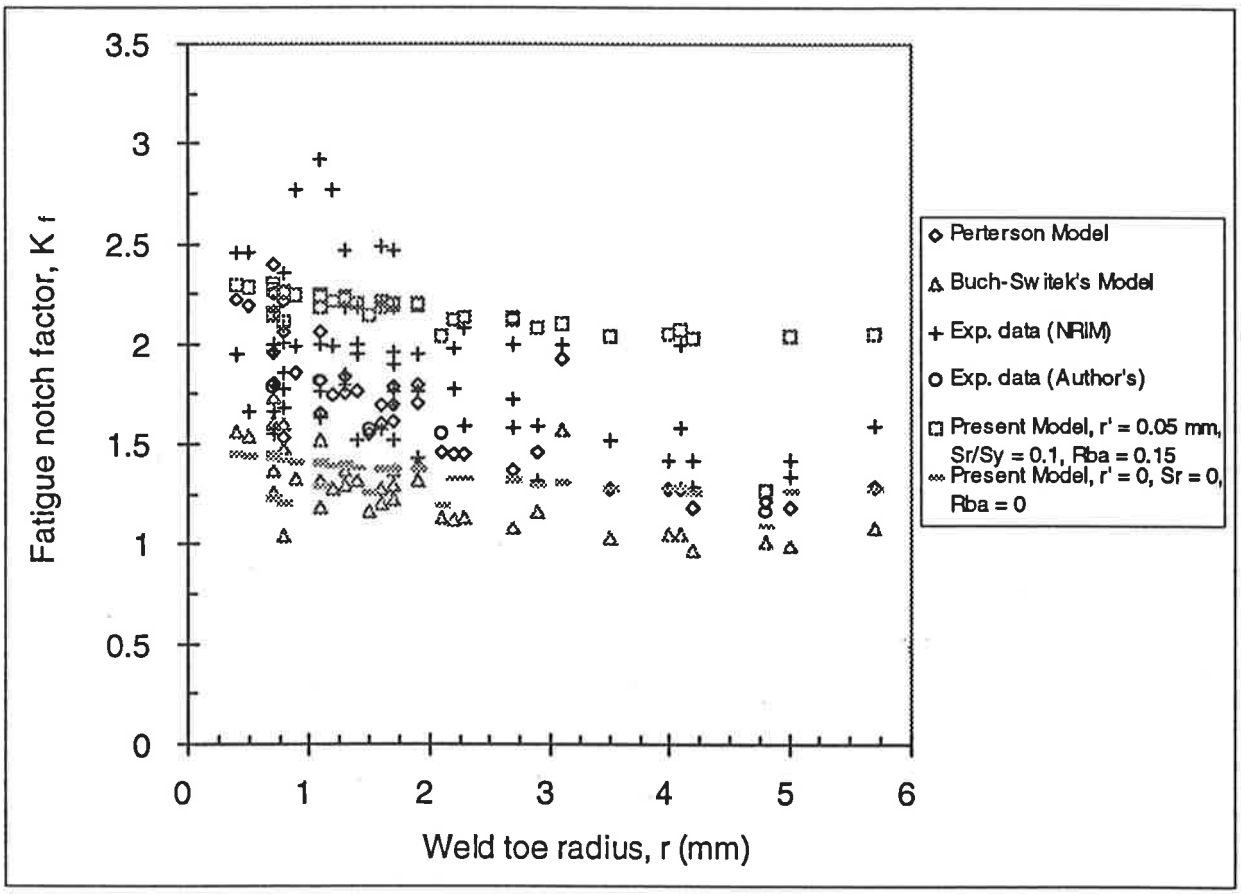

Figure 5.60 A comparison of the values of (K_f) predicted by theoretical models with the experimental data (NRIM, Fatigue Data Sheet, 1983) as the function of the weld toe radius (r).

Figure 5.60 shows that the values of (K_f) predicted by the present model covers the majority of the available experimental data except for a few data points due to a small weld toe radius ($r < 1.7$ mm). This mismatch may be due to the magnitude of the undercut at the weld toes of specimens which produced these data points, were higher than that assumed for the upper boundary of the scatter band of (K_f) ($r' > 0.05$ mm). It also shows that the predicted values of the lower boundary of (K_f) when the weld toe radius was more than 2.5 mm ($r > 2.5$ mm) were in good agreement with that predicted by Peterson's model. However, if the weld toe radius was less than 2.5 mm, the values of (K_f) predicted by Peterson's model were much higher than the lower boundary of the (K_f) predicted by the author's model. Furthermore, in this case the values of (K_f) predicted by Peterson's model fall into a large scatter values of the available experimental data. This suggests that Peterson's model failed to predict the values of (K_f) of a welded joint with a relatively small weld toe radii (e.g. $r < 2.5$ mm) as it was based only on the theoretical stress concentration factor (K_t) and the notch root radius (ρ) (Eq. (3.40)). Figure 5.60 also shows that Buch-Switek's model underestimated the values calculated from experimental data. Furthermore, the fatigue notch factor of butt-joints tended to decrease as the weld toe radius increased.

Figures 5.61 shows the values of the fatigue notch factor (K_f) predicted by the author's model, the author's fatigue test results and available fatigue data (NRIM Fatigue Data Sheet, 1983) with respect to variations in the flank angle (θ). The values of (K_f) predicted by Peterson's and Buch-Switek's equations (Eqs. (3.40) and (3.41) respectively) for variations in (θ) are also shown. It shows that the values of (K_f) predicted by the present model includes most of the available experimental data. Further, the values of (K_f) tended to increase as the value of the flank angle increased.

The values of (K_f) predicted by Peterson's model again fall into a large scatter band of the available experimental data i.e. Peterson's model fails to predict the experimental data. In contrast the values of (K_f) predicted by Buch-Switek's model again underestimate the experimental data.

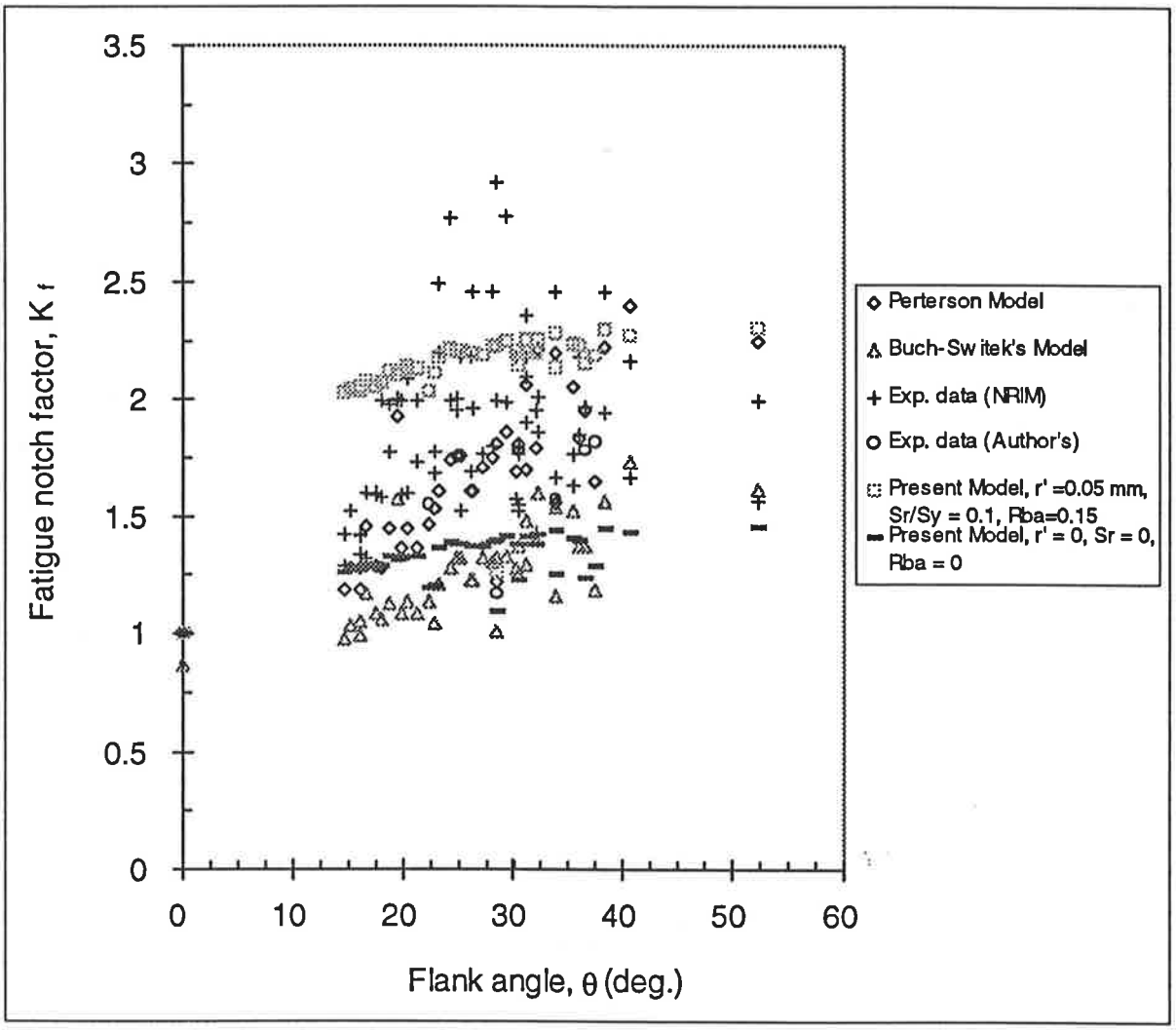

Figure 5.61 A comparison between the values of (K_f) predicted by theoretical models with the experimental data (NRIM, Fatigue Data Sheet, 1983) as a function of the flank angle (θ).

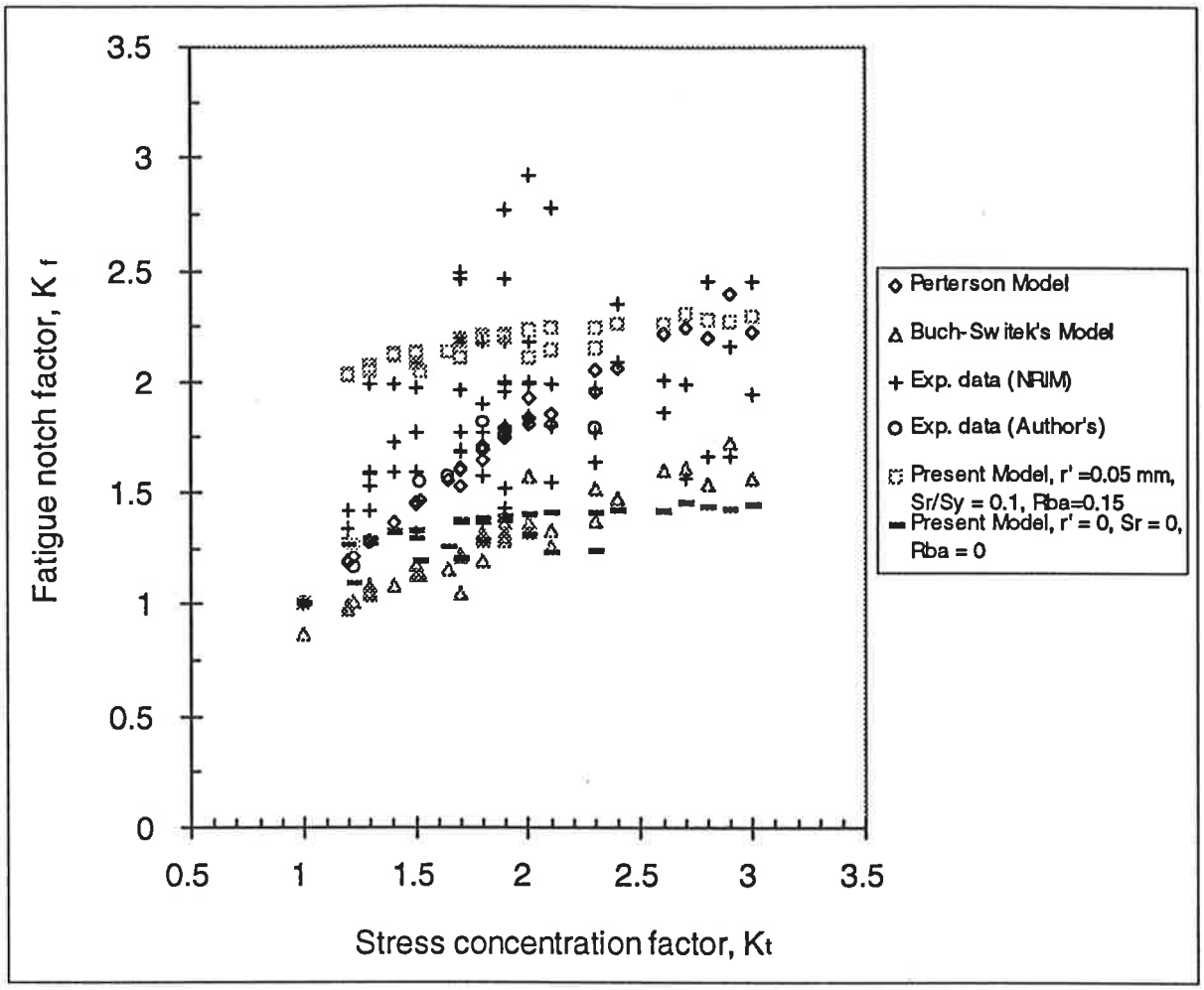

Figure 5.62 A comparison between the values of (K_f) predicted by theoretical models with the experimental data (NRIM, Fatigue Data Sheet, 1983) as a function of (K_t).

Figures 5.62 shows the values of the fatigue notch factor (K_f) predicted by the author's model, the author's fatigue test results and the available fatigue data (NRIM Fatigue Data Sheet, 1983) with respect to the variation in the stress concentration factor (K_t). The values of (K_f) predicted by Peterson's and Buch-Switek's equations (Eqs. (3.40) and (3.41)) subjected to variations in the stress concentration factor (K_t) are also shown. The variations of (K_f) predicted by the present model includes most of the available experimental data. The values of (K_f) tended to increase as the value of

(K_t) increased. Furthermore, the values of (K_f) predicted by Peterson's model again fall into a large scatter band of the experimental data and thus highlights the weakness of that model.

Figure 5.62 also shows that the values of (K_f) predicted by Buch-Switek's model again underestimate the experimental values for the stress concentration factor of less than 2.5 ($K_t < 2.5$). However, for the higher stress concentration factor ($K_t > 2.5$) there is a better agreement between the experimental values of (K_f) and the Buch-Switek's model.

5.8.2 **Verification of the effect of residual stresses**

Figure 5.63 shows the effect of residual stresses on the predicted fatigue life compared with the available experimental data (Wahab, 1984). It shows that the ratios between the experimental and predicted fatigue life are between 0.5 to 2.5. This difference between the calculated fatigue life and the experimental data is reasonable since the standard deviation (SD) of the experimental data in terms of log(N) is of the order of 0.201 (Wahab, 1984). This means that at the 95 % confidence limits of log(N) i.e (log(N) ± 2SD), the fatigue life is in the range of 0.4N to 2.52N. This indicates that the prediction of the fatigue life by the present model is acceptable as the predicted life falls within the typical scatter band of fatigue life that occurs in fatigue testing practices.

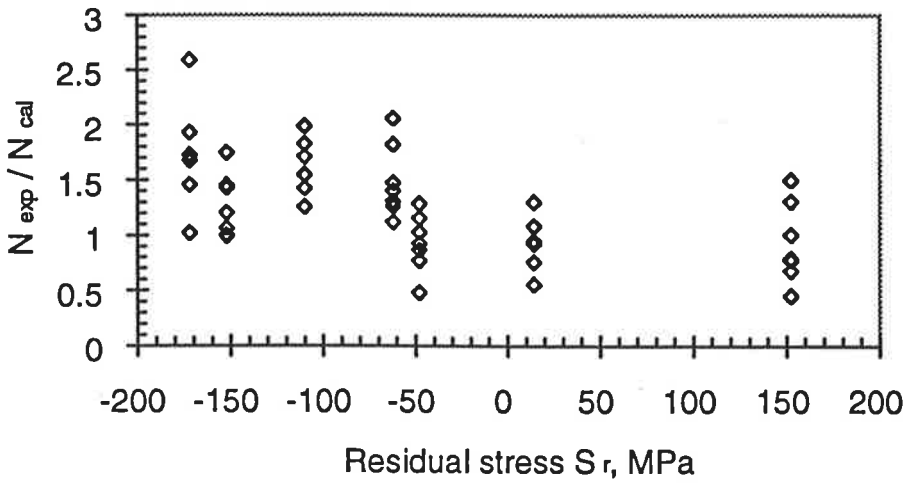

Figure 5.63 A comparison of the effect of residual stresses on the fatigue life data as predicted by the present model and the available data (Wahab, 1984).

Furthermore, Fig. 5.63 also shows that the difference between the experimental and predicted fatigue lives tended to increase as the value of the induced compressive residual stresses increases. This suggests that the higher micro-hardness of the treated surfaces (Wahab, 1984) should have an accompanying beneficial effect on the fatigue life of butt welded joints. This conclusion is consistent with the results of a study on the effect of hardness on the improvement of fatigue life (Heeschen and Wohlfahrt, 1986). However, this phenomenon needs more investigation before specific conclusions can be drawn.

5.8.3 **Verification of the effect of undercut and misalignment**

Figure 5.64 shows a comparison between the predicted S-N curves with respect to the effect of undercut and misalignment, the author's fatigue test results and some of the

experimental data available in the literature (Iida and Iino 1977, Wylde 1979). The combined effect of undercut and misalignment on the S-N curves of "perfectly stress-relieved" joint (S_r = 0) are also shown in this figure. From this figure, the effect of an undercut of 0.25 mm is found to be more significant than that of the misalignment of 5 % of the plate thickness.

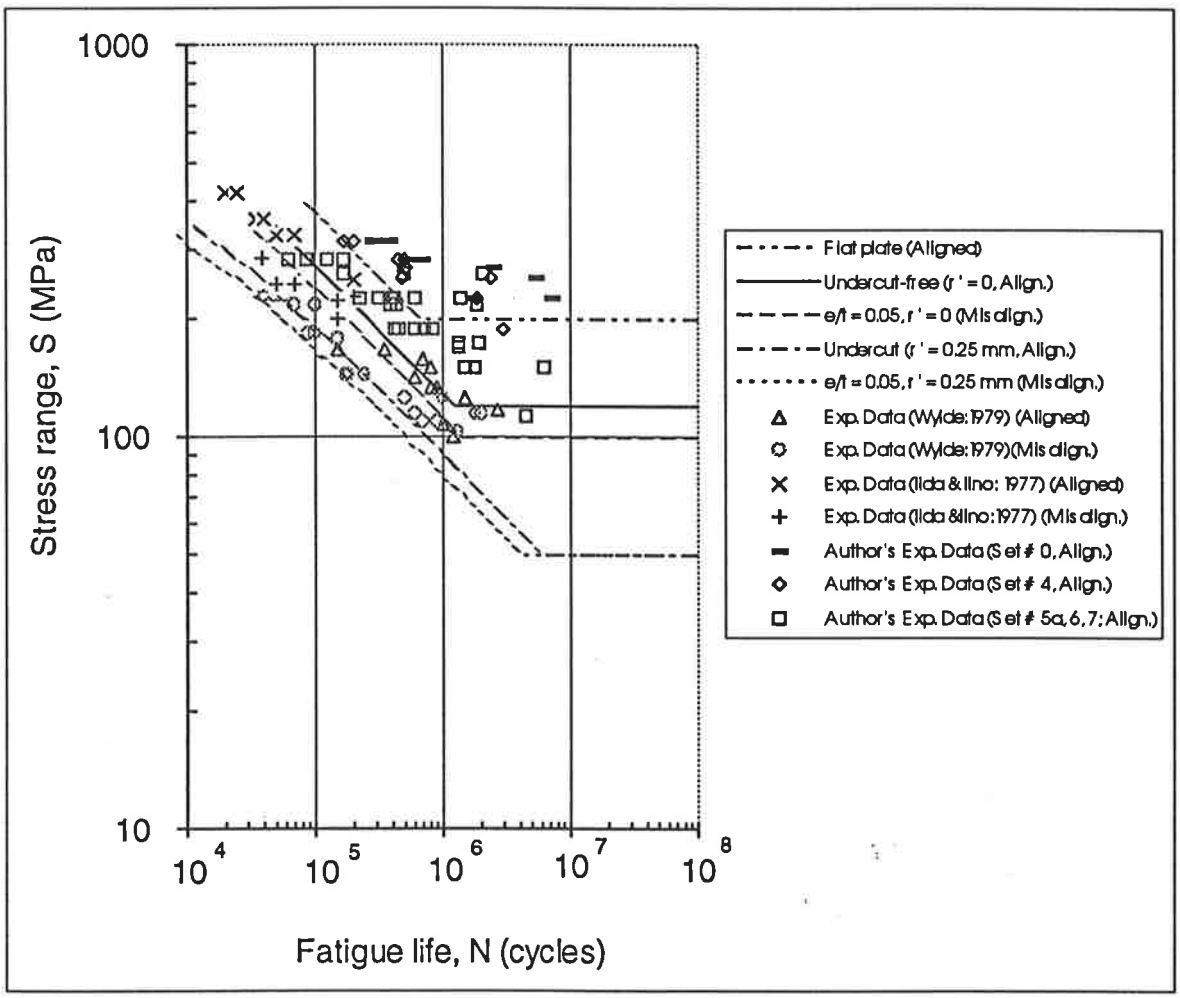

Figure 5.64 Effect of the undercut and misalignment on the S-N curves of butt-joints in perfectly stress-relieved condition (r = 1 mm, θ = 30°, ϕ = 60°, t = 12 mm, R = 0).

Figure 5.64 also shows that the author's fatigue test data is in reasonable agreement with the calculated results. The experimental data from sets #5a, 6 and 7 which represent the undercut-free aligned butt-joints with various weld geometries, have fallen within the predicted S-N curves for undercut-free aligned joints and the flat unwelded plate. However, the predicted results for the flat plate underestimated the experimental data (set # 0). Furthermore, the experimental fatigue data of butt-joints with ground weld toes (set # 4) was comparable with that of the flat unwelded specimens. This suggests that grinding of the weld toes can be used as an effective method of improving the fatigue performance of butt-welded joints.

Figure 5.64 shows that the experimental data of other researchers (Iida and Iino 1977, Wylde 1979) agrees well with the calculated results, except for the data for misaligned joints by Wylde (1979) which fall into the range of a misaligned undercut joint (e/t = 0.05, r' = 0.25 mm). It is suggested that an axial misalignment of 5 % of the plate thickness and an undercut at the weld toes of 2 % of the plate thickness can be used to represent the lower limit of the scatter band of the *S-N* curves for the actual butt-welded joints.

5.8.4 Verification of the predicted S-N curves

Figure 5.65.(a) shows a comparison between the predicted S-N curves and the author's fatigue test results. From this figure, in spite of the relatively large scatter in the test results, the fatigue data predicted by the present model is in reasonable agreement with the experimental results. However, at the lower stress levels the

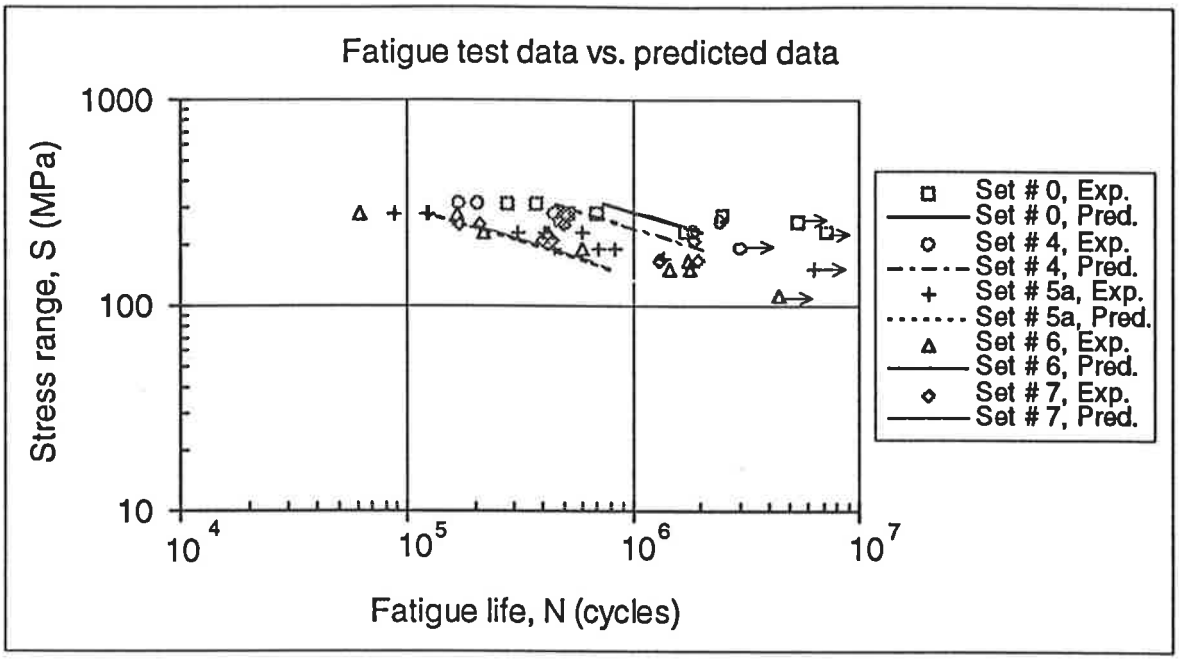

(a) A conventional representation of the S-N curves

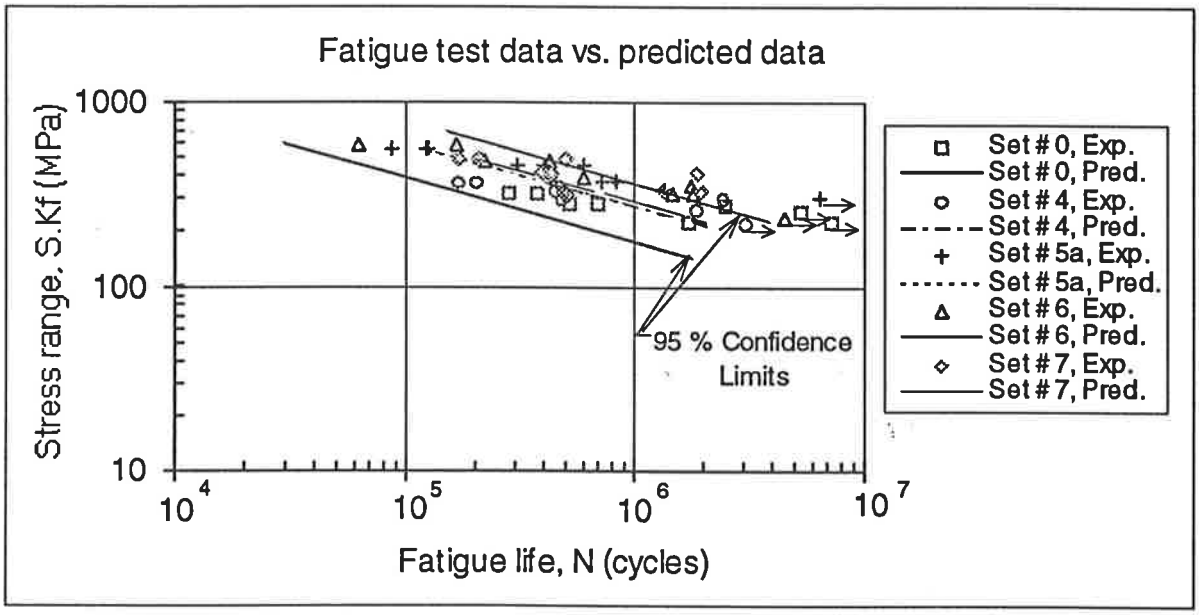

(b) A new representation of the fatigue data incorporating the values of (K_f)

Figure 5.65 A comparison of the S-N curves predicted by the present model and the author's fatigue test results.

predicted S-N curves underestimate the experimental data. This may be due to the fact that a portion of the fatigue life corresponding to crack initiation has been ignored and this portion could be quite significant at the lower stress levels.

Figure 5.65.(b) shows a proposed new representation of the fatigue S-N curves in terms of $(S.K_f)$ vs. (N) using a log-log scale. The values of (K_f) for each set of fatigue data were calculated by using Eqs. (3.35), (3.36) and (3.42). Also the 95 % confidence limits of the predicted $(S.K_f)$ vs. (N) curves are plotted in Fig. 5.65 using the value of the standard deviation specified for S-N design class B in BS 5400.

From Fig. 5.65.(b), it can be seen that the scatter band of the fatigue data is significantly reduced when the fatigue data is modified by the fatigue notch factor (K_f). Furthermore, the majority of the fatigue test results fall within the 95 % confidence limit lines. Hence, it is concluded that the present model can satisfactorily predict the fatigue behaviour of butt-joints due to the variations in weld geometry, residual stresses and combined loading conditions (axial and bending).

Figure 5.66. shows the scatter bands of S-N curves due to the variations in butt-weld geometry. The author's fatigue test results are compared with the available experimental data from the literature (NRIM 1983, Wahab 1984). Several S-N curves representing design classes D, F, F_2 and W (BS 5400) are also constructed for comparison. In this figure, the majority of the experimental fatigue data falls between the upper boundary of the predicted S-N curves ($S_{max\text{-}pred}$) and the S-N curve for design class D (BS 5400). However, the upper boundary of the predicted S-N curve which corresponds to the lower applied stress range underestimate the fatigue data. This may

be due to some portion of the fatigue crack initiation life corresponding to the lower applied stress range being ignored in the present model.

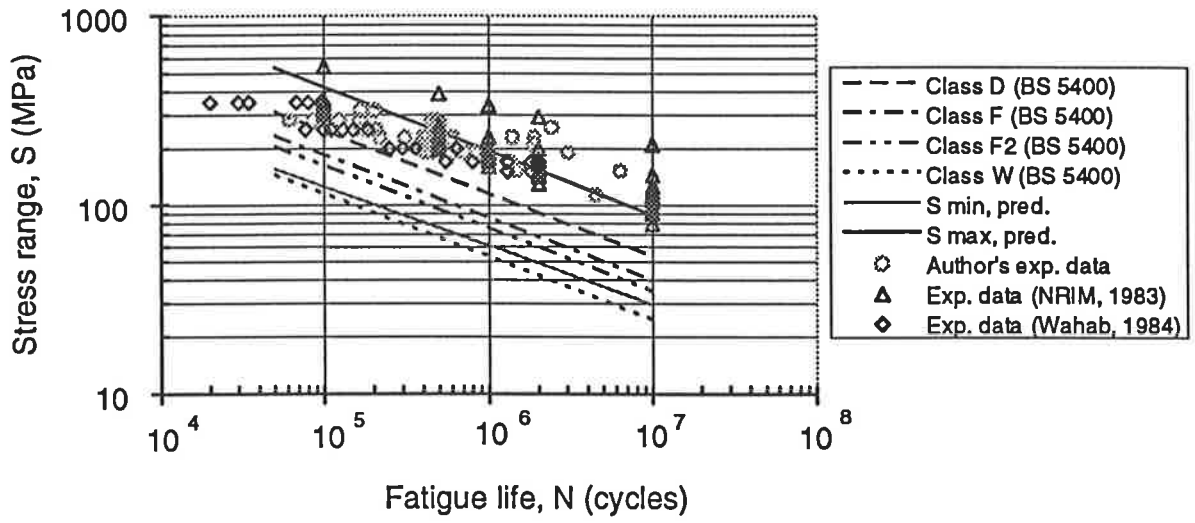

Figure 5.66 A comparison between the scatter band of the predicted S-N curves due to the variations of butt-weld geometry parameters & the available experimental data.

Figure 5.66 also shows that the predicted scatter band of S-N curves due to variations in the weld geometry parameters is in good agreement with the S-N curves covered by design classes from (D) to (W) (BS 5400). The design classes (F) and (F_2) which are commonly used for the design of butt welded joints with high stress concentrations fall in the middle of the predicted scatter band of the S-N curves. This suggests that for safe design, class (W) should be used for fatigue design of butt welded joints instead of class (F) or (F_2).

In the next Chapter, a summary of the important conclusions resulting from the present work is reported.

Chapter 6

CONCLUSIONS

The model developed in this study is capable of predicting the complex fatigue behaviour of butt-welded joints in structural steel due to variations in the weld geometry parameters, residual stresses and combined axial and bending loading conditions. From this study, the following conclusions can be drawn:

1. Butt weld geometry parameters such as the undercut tip radius (r'), the weld toe radius (r), the flank angle (θ), and the plate thickness (t) are the most significant geometrical parameters that influence the stress concentration factor at the weld toe surface. The values of the stress concentration factor (K_t) may be increased up to six (i.e. $K_t = 6$) as the values of the tip radius at the undercut or weld toe radius decrease and the values of the flank angle or the plate thickness increase. The effect of the edge preparation angle on the stress concentration factor at the weld toe surface is less significant than the other geometry parameters mentioned above.

2. The values of the stress intensity factor at the crack tip of butt-welded joints increase with decreasing values of the tip radius at the undercut (r') or the weld toe radius (r) but with the increasing values of the flank angle (θ) or the plate

thickness (t). The effect of the flank angle on the stress intensity factor is stronger than that of the weld toe radius or the plate thickness.

3. The effect of the tip radius at the undercut, weld toe radius, flank angle and the plate thickness ((r'), (r), (θ) and (t)) only influence the fatigue behaviour of the welded joint during the early stages of crack propagation as their effect on the stress concentration factor is only significant for small crack lengths up to 0.15 times the plate thickness (0.15t). Beyond this crack length, no significant effect due to weld geometry parameters was observed.

4. The flank angle influenced the stress intensity factor for crack lengths up to 0.15 times the plate thickness whilst the weld toe radius and the plate thickness influenced the stress intensity factor for the crack lengths up to 0.05 the plate thickness and 0.025 times the plate thickness, respectively. The effect of the tip radius at the undercut on the stress intensity factor was more influential than the other weld geometry parameters.

5. A mathematical model for the butt weld geometry magnification factor (M_k) has been developed and can be used for the calculation of the stress intensity factor in fatigue assessment of butt welded joints.

6. The fatigue strength of the butt-welded joint was strongly influenced by the weld geometry parameters such as the tip radius at the undercut (r'), the weld toe radius (r), the weld flank angle (θ) and the plate thickness (t) but only slightly influenced by the edge preparation angle (ϕ). The fatigue strength of butt-welded joints

increased between 9 % and 24 % as the weld toe radius increases from 0.3 mm to 2.5 mm or the flank angle decreased from 60° to 0°. The fatigue strength decreases between 11 % and 7 % as the plate thickness increases from 9 mm to 32 mm or the edge preparation angle (ϕ) increased from 45° to 90°.

7. The effect of the flank angle on the fatigue strength was found to be greater than that of either the weld toe radius or the plate thickness. The conclusion drawn by the previous researchers using only the experimental fatigue data suggested that the plate thickness was the sole geometry parameter on the fatigue strength was found to be inappropriate. It has been shown in the present work that the fatigue strength of butt-welded joints is affected by all of the geometry parameters (t, r', r, θ and ϕ).

8. The combined effect of all the weld geometry parameters (r', r, θ, ϕ and t) on the fatigue notch factor of butt welded joints is more influential than the effect of each individual geometry parameter alone.

9. Compressive residual stresses induced on the surface of welded joints by various surface treatments such as single and multiple point hammer peening, steel and glass shot peening, stress peening (loaded and peened) or tensile pre-loading improve the fatigue life and the fatigue strength of welded joints. The improvement is only due to the early stage of crack propagation and up to a crack length corresponding to the depth of the compressive residual stress field induced by surface treatments. After that crack length, the induced compressive residual stresses have a small effect on crack propagation.

10. Low levels of compressive residual stresses (e.g less than -62 MPa) induced by surface treatments, improve the fatigue life and the fatigue strength to the same degree as post-weld stress relieving by thermal treatments (e.g. post-weld annealing).

11. The theoretical model developed confirms that the fatigue life and fatigue strength of butt-welded joints can be improved by modifying the weld geometry parameters as follows:

    (i) Decreasing the tip radius at the undercut of the weld toes or eliminating the weld toe undercut completely can improve the performance of the joints.

    (ii) Increasing the weld toe radius

    (iii) Reducing the flank angle. The more significant improvement occurs when the flank angle is decreased below 20°. The best case is to flush-grind the weld bead (weld reinforcement) to the level of the base plate.

    (iv) Reducing the plate thickness

    (v) Reducing the edge preparation angle

12. An explanation has been given for the well known plate thickness effect which decreases the fatigue life and the fatigue strength of welded joints. However, for the lower range of the plate thicknesses (less than 10 mm) this effect was found to be insignificant.

13. The initial crack shape aspect-ratio plays an important role in the fatigue crack propagation life. The initial semi-circular surface crack is less harmful than the semi-elliptical or the edge crack. However, there is an insignificant effect for a large range of initial crack shape aspect ratios ranging from 0.2 to 1.0. This suggests that for the fatigue assessment of butt-welded joint using LEFM, an initial crack aspect ratio of 0.2 is appropriate.

14. The reduction of the fatigue strength of welded joints with a weld toe undercut is almost twice of that of the joints without an undercut when compared with flush-ground welded plate. The fatigue limit of the aligned butt-joints can be improved by up to 140 % by the elimination of the undercut at the weld toes alone.

15. The combined axial and bending load condition resulted from axial misalignments during fabrication can decrease the fatigue limit of butt-joints by between 17 % and 58 % due to the variations in the misalignment level from 5 % to 50 % (e/t from 0.05 to 0.5) respectively. The fatigue limits of the undercut-free misaligned joints can be improved by between 20 % and 140 % by eliminating misalignments by 5 % to 50 % respectively.

16. The presence of an undercut at the weld toes can significantly increase the detrimental effect of the tensile residual stress and combined loadings and reduces the effectiveness of the beneficial compressive residual stresses.

17. The presence of undercuts at the weld toes after surface treatments can decrease the effectiveness of the surface treatment by up to 48 %. If the undercut is

eliminated after the surface treatments, the improvement in the fatigue limits of stress-relieved misaligned and aligned joints can be expected by up to 300 % and 320 % respectively.

18. Surface Treatments which induce compressive residual stresses are more effective for the welded structures with high levels of tensile residual stresses of the magnitude of the yield stress. The fatigue limit of the treated joints can be improved by as much as 700 % and 950 % compared to the as-welded misaligned and aligned joints respectively.

19. Under the influence of a high tensile residual stress field, the slope of the *S-N* curve is not constant and the effect of the misalignment becomes more significant than that of the undercut. However, when the magnitude of the tensile residual stress is reduced or changes to a compressive field, the effect of an undercut plays a dominant role.

20. The presence of a misalignment of 5 % of the plate thickness and an undercut of 2 % of the plate thickness are fairly representative for the lower boundary of the actual *S-N* curves of butt-joints.

21. The values of the fatigue notch factor predicted by the present model are generally in good agreement with the author's fatigue test results and available fatigue data. However, the fatigue notch factors predicted by Peterson's and Buch-Switek's models do not provide as good an agreement with all the available experimental data.

22. The present model is capable of predicting fatigue curves affected by the four most important weld geometry parameters (r', r, θ and t), normalised residual stresses (S_r/S_y) and the combined loading ratio (R_{ba}).

23. The predicted S-N curves resulting from the variations in the weld geometry parameters, residual stresses and the combined loading conditions is in good agreement with S-N curves covered by the S-N design curve classes D to W (BS 5400). The S-N design curves for classes F and F_2 which are commonly used for the design of butt-welded joints with high stress concentrations fall in the middle of the predicted scatter band of S-N curves. This suggests that for safe design, class W should be used for fatigue design of butt-welded joints rather than class F.

24. An explanation for the effectiveness of the post-weld treatments (e.g grinding of weld toe and surface treatments), which are commonly used in practice to improve the fatigue performance of welded structures, has been proposed. It provides an opportunity for recommendations to be made for the more efficient use of post-weld treatments for particular cases.

General Comments:

The numerical approach developed in this study can be used satisfactorily to predict the overall effect of butt-weld geometry parameters, residual stresses and the combined loading conditions. It makes it possible to explain the combined effect of all the weld geometry parameters including an undercut at the weld toe, misalignment and residual stresses. This approach is relatively simple and practical for the "fitness-for-purpose" assessment of fatigue of welded joints and welded structures. The results

obtained from this study not only give a clear explanation for the practical methods commonly used to improve fatigue performance of welded joints and welded structures but also gives an insight into the fundamental basis of the fatigue enhancement methods that can be developed in the future. This study also suggests an initiative for the establishment of a new standard procedure for the evaluation of the fatigue test.

Chapter 7

RECOMMENDATIONS

7.1 Introduction

The present work focuses on the effect of various influential parameters on the fatigue crack propagation life of butt-welded joints. The fatigue crack propagation life dominates the total life of welded joints with high stress concentrations at the weld toes. This assumption was based on the fact that the portion of fatigue crack initiation in welded joints with high stress concentrations can be ignored due to the existence of crack-like defects already embedded in the welded joints in the form of slag or other non-metallic inclusions at the weld toes. However, this assumption is conservative because the welded joints are not always defective and even if sharp notches exist at the weld toes, a certain period of crack initiation is required before a fatigue crack starts to propagate (Jack and Price, 1970). This explains why the model developed in this study which considers only the period of crack propagation underestimates the experimental fatigue data at the lower levels of the applied stress range or in the high cycle fatigue regime (Chapter 5).

Mattos and Lawrence (1977) reported that for a certain range of stresses, the fatigue crack initiation life of butt-welded joints could be as much as 40 % and as little as 20 % of the total fatigue life. This is likely to be more significant especially for the

high cycle fatigue regime where the crack initiation portion may dominate the total fatigue life. Therefore, in order to improve the predicability and reliability of the present model, an additional component which estimates the fatigue crack initiation life of welded joints needs to be included in future work.

There is an established procedure for using low-cycle fatigue concept to estimate the fatigue crack initiation life of notched members (Lawrence, 1977). It is assumed that a smooth specimen under appropriate control can be used to simulate the stress-strain behaviour of the metal at the notch root. The fatigue crack initiation life of the smooth specimen will then be the same as that of the notched member. Topper and Morrow (1970) pointed out that the requirements for the estimation of fatigue crack initiation life of notched members are as follows:

(i) A fracture mechanics analysis to determine the stress-strain behaviour at a critical location

(ii) Knowledge of the cyclic stress-strain properties of the material at the notch root

(iii) Knowledge of the fatigue properties of the material for use in the evaluation of the cumulative damage procedure

(iv) A cumulative fatigue damage summation method to accurately predict crack initiation life of a notched member for any arbitrary stress-strain sequence on a reversal by reversal basis.

7.2 Recommendations for Future Work and for Industrial Practices

7.2.1 Recommendations for future work

In the present work, a semi-elliptical surface crack propagation model has been used to investigate the combined effect of the various weld geometry parameters (such as the tip radius at the undercut (r'), the weld toe radius (r), the flank angle (θ), the plate thickness (t) and the edge preparation angle (ϕ), residual stresses and combined axial and bending loading conditions on the fatigue behaviour of butt welded joints. The weight function method and the superposition principle have been used in this study. A good understanding of the nature of the combined effect of weld geometry, residual stresses and loading conditions on the fatigue of butt welds was established. However, an improvement in the present model is desirable and could be obtained by focusing on the methods which effectively include crack initiation into the model.

Improving the present model by including the period of fatigue crack initiation in the numerical modelling would make it possible to predict more precisely the effect of weld geometry, residual stresses and the combined loading conditions on the fatigue behaviour of the butt-joints. In particular, when the effects of the weld geometry are significant during the early stages of the crack growth (corresponded to the crack length of 15 % of the plate thickness) then adopting the semi-elliptical crack propagation model incorporating the crack initiation part of the fatigue life would be even more appropriate.

The present model could also be improved if a better crack growth law could be developed which incorporated the effect of the crack opening and closure during loading. This phenomenon was first reported by Elber (1970, 1971) and investigated by several other researchers (Lal et al., 1979,1980). However, no research has yet been carried out on the effect of crack closure in welded joints with complex geometry and high post-weld tensile residual stresses.

Another aspect for the future work is to look into the effect of the hardness on the fatigue behaviour of butt-joints. Also the heat input levels due to the welding process parameters (voltage, current and speed) and the relation between these parameters and the weld geometry should be investigated. An attempt to experimentally investigate heat input levels due to the welding process parameters was carried out in this work by using four different levels of heat input to obtain various weld bead geometries (sets # 4, # 5, # 6 and # 7, Table 4.1). The fatigue limits obtained for these sets of test specimens (sets # 4 to # 7) were plotted against the levels of the heat input. However, the results obtained were not conclusive due to the scatter of the fatigue data corresponding to small changes in the heat input levels. Furthermore, the differences in the number of weld passes used to fabricate the test specimens may have caused the fluctuation in the effect of the heat input. Therefore these results are not reported in this work.

A better result would have been obtained if a larger range of heat inputs were chosen and the number of weld passes during fabrication of each set of the test specimens was unchanged.

7.2.2 Recommendations for the industrial practices

The outcome of the present study suggests that the fatigue performance of butt welded structures can be significantly improved by using one of the following measures:

- Eliminating the undercut at the weld toes completely (e.g grinding, weld toe melting, TIG dressing)
- Modifying the weld geometry cross-section profile to get flatter welds with smaller flank angles and larger radii at the weld toes.
- Care should be taken during the welding process to minimise misalignment and angular distortion in welded joints and structures.
- Use of post-weld treatments (thermal or mechanical) to reduce the harmful effect of tensile residual stresses in welded structures wherever possible.

7.3 A Proposed New Standard for Fatigue Testing Procedures

Using the mathematical model developed in this study (Eqs. (3.35), (3.36) and (3.42)) the fatigue notch factor (K_f) for butt-welded joints subject to the variations in the weld geometry parameters (r', r, θ and t), residual stresses (S_r) and the combined loading conditions (R_{bs}) can be satisfactorily predicted. When this value of (K_f) is used in the new form of the fatigue S-N curve (i.e. by plotting ($S.K_f$) against (N) instead of (S) vs. (N)), the scatter band of the experimental fatigue data is significantly reduced (Fig. 5.65). This encouraging result suggests that a new proposal may be adopted for the standard evaluation procedures used in fatigue testing practice and described as follows:

1. Weld geometry parameters such as the tip radius at the undercut (r'), the weld toe radius (r), the flank angle (θ) and the plate thickness (t) of each fatigue test specimen needs to be measured before the test using the standard procedures described in IIW/IIS Doc. XIII-1090-90 (1990).

2. The axial and angular misalignments are measured using standard procedure mentioned above (i.e. IIW/IIS Doc. XIII-1090-90 (1990) and the corresponding combined loading ratios (R_{ba}) are calculated based on the misalignment induced bending stresses.

3. The post-weld surface residual stress at the weld toe (S_r) is measured by using micro-strain gauges bonded to the weld toes of the test specimen. The effective residual stress (welding residual stress and bending stress) at the weld toe is obtained during the first cycle by increasing the load from zero to the level of the applied stress (using a calibration program, Appendix C). A procedure to evaluate the effective residual stress using a strain gauge method is described in Appendix F.

4. The fatigue notch factor (K_f) of each test specimen is calculated using the measured values from the test specimen and the theoretical model (Eqs. (3.35), (3.36) and (3.42)).

5. The fatigue test should be carried out following the standard fatigue testing procedure described in IIW/IIS Doc. XIII-1090-90 (1990) and the values of the stress range (S) and the number of cycles to failure (N) are to be recorded.

6. The fatigue curves are to be plotted in terms of ($S.K_f$) against (N) on a log-log scale and the regression lines obtained by curve-fitting all the data points as well as the 95 % confidence limits are to be determined.

Using this new standard procedure for fatigue testing and evaluation of the butt-welded joints, the scatter band of the fatigue tests can be significantly controlled and reduced. Thus the number of test specimens required for the fatigue test can be also reduced. As a result, enormous savings in machine testing time as well as a reduction in the cost involved for materials and specimen fabrication can be expected.

REFERENCES

Ansys User's Manual, Revision 5.0, Swanson Analysis System Inc., (1992).

ASTM E647-86a, Test for Measurement of Fatigue Crack Growth Rates, *Annual Book of ASTM Standards*, (1990).

ASTM A568M-88, Standard Specification for General Requirements for Steel, Carbon and High-Strength Low-Alloyed Hot-Rolled Sheet and Cold-Rolled Sheet [Metric], *Annual Book of ASTM Standards, Volume 01.03 - Steel-Plate, Sheet, Strip, Wire, ASTM* (1990).

Australian Standard AS:4100-1990: Steel Structures, *Standards Association of Australia*, Standards House, North Sydney, NSW, Australia, (1990).

Bellow, D.G., Wahab, M.A. and Faulkner, M.G., "Prediction of Fatigue Crack Initiation and Propagation of Welded Joints", *Advance in Surface Treatments,* Pergamon Press, Volume 3., pp. 27-40, (1986).

Bellow, D.G., Wahab, M.A. and Faulkner, M.G., "Residual Stresses and Fatigue of Surface Treated Welded Specimens", *Advance in Surface Treatments,* Pergamon Press, Volume 2, pp. 85-94, (1986).

Berge, S. and Myhre, H., "Fatigue Strength of Misaligned Cruciform and Butt Joints", *Norwegian Maritime Research*, Vol. 5, No. 1, pp. 29-39, (1977).

Berge S. and Eide O. I., "Residual stress and stress interaction in fatigue testing of welded joints", *ASTM STP 776*, pp. 115-131, (1982).

Bignonnet A., "Improving fatigue strength of welded steel structures", in *Steel in Marine Structures*, Elsevier, Delft, (1987).

Bignonnet A., "Endurance des joints soudes en aciers de construction marine", *IIS/IIW Doc. 1097-83*, (1983).

Bignonnet A.; Dias A. and H.P Lieurade, "Influence of crack closure on fatigue crack propagation", *Proc. ICF6 New Dehli*, Dec. 1984, pp. 1861-1868, (1984).

Bokalrud T., "Significance of internal defects in butt welds on finite element analysis", *Colloquium on Practical Application of Fracture Mechanics*, Bratislava, July 1979, pp. 190-197, (1979).

Braid J.E.M. and Knot J.F., "Fatigue crack propagation in vicinity of weld-deposits in high strength structural steel", *IIW Doc. No. XIII-1014-81*, (1981).

Branco C.M, Radon J.C and Culver L.E, "Growth of fatigue cracks in steels", *Metal Science*, Vol. 10, pp. 149-155, (1976).

Broeck D., "*Elementary Engineering Fracture Mechanics*", Kluwer Academic Publisher, Netherland, (1986).

Buch, A., "*Fatigue strength calculation*", Technion Haiga Israel, Material Science Survey No. 6, Trans. Tech. Publication, Switzerland - Germany - UK, (1988).

Bueckner H. F., "A novel principle for the computation of stress intensity factors", *Z. Angewandte Mathemat. Mechan.*, Vol. 50, No. 9, pp. 529-546, (1970).

Castiglioni C. A. and Gianola P., "Parametric analysis of weld toe stress concentration in longitudinal attachments", *Welding International*, Vol. 6, No. 4, pp. 278-286, (1992).

Cole I., Ricci F. and Vittori O., "Effect of thickness on the fatigue life of welded joints for offshore platforms", *Welding International*, Vol. 6, No. 6., pp. 450-454, (1992).

Cooper, J. F. and Smith R. A., "Fatigue crack propagation at spot welds", *Metal Construction*, pp. 383-386, (1986).

Dattoma V., "Investigation of the fatigue behaviour of welded joints treated after welding", *Welding International*, Vol 4. No. 6, pp. 443-449, (1990).

Desvignes, M. et al., "Fatigue Processing of Shot Peened Steel", *Residual Stresses in Science and Technology*, Vol. 2., *Symposium of International Conference on Residual Stresses*, Germany, pp. 441- 448, (1986).

Dowse K.R. and Richards C.E., "Fatigue crack propagation through weld heat affected zones", *Met. Trans.* Vol. 2, pp. 599-603, (1971).

Elber W., "Fatigue Crack Closure Under Cyclic Tension", *Engng. Fracture Mechanics*, Vol. 2., pp. 230-242, (1970).

Elber W., "The Significance of Fatigue Crack Closure", in *Damage Tolerance In Aircraft Structures, STP 486, ASTM*, pp. 230-242, (1971).

Elber, W., "Effect of Shot-Peening Residual Stresses on the Fracture and Crack Growth Properties of D6AC Steel", *Fracture Toughness and Slow-Stable Cracking, ASTM STP 559*, American Society for Testing and Materials, pp. 45-58, (1974).

Elliott, S., "Electron beam welding of C/Mn steels- Toughness and fatigue properties", *Welding Journal*, Welding Res. Suppl., pp. 8-16, (1984).

Emery A.F and Walker G.E Jr., "Stress intensity factor for edge cracks in rectangular plates with arbitrary loadings", ASME Publication 68-WA/MET-18, *ASME Winter Annual Meeting and Energy System Exposition*, New York, Dec. 1-5, 1968.

Forman R. G., Kearney V. E and Engle R. M., "Numerical analysis of crack propagation in cyclic loaded structures", *J. Basic Eng., Trans. ASME*, Vol. 89, pp. 459-461, (1967).

Foth, J. et al., "Short Crack Phenomena in High Strength Aluminium Alloy and Some Analytical Tools for Their Prediction", *The behaviour of Short Fatigue Cracks*, EGF Pub. 1., Mechanical Engineering Publications, London, pp. 353-368, (1986).

Glinka G., "Effects of residual stresses on fatigue crack growth in steel weldments under constant and variable amplitude loads", *ASTM STP 677*, pp. 198-218, (1979).

Glinka G., "Residual stresses in fatigue and fracture - Theoretical analysis and experiments", in *Advances in Surface Treatments*, Vol. 4, Pergamon Press, Oxford, (1986).

Gregor V., "The effect of surface preparation by TIG remelting on fatigue life", *Zvarcske Spravy*, Vol. 3, pp. 8-11, (1989).

Guda, B; Pathak, S. D. et Radhakrishnan, V. M., "Bending fatigue of butt welded joints", *Joining and Material*, pp. 184-188, (1988).

Gurney T.R., "The effect of mean stress and material yield stress on fatigue crack propagation in steels", *Metal construction and British Welding Journal*, pp. 91-96, (1969).

Gurney T.R. and Maddox, S. J., "Determination of fatigue design stresses for welded structures from an analysis of data", *Metal construction and British Welding Journal*, pp. 418-422, (1972).

Gurney, T.R and Maddox, S. J., "A re-analysis of fatigue data for welded joints in steel", *Welding Res. Inst.*, Vol. 3, pp. 1-54, (1973).

Gurney T.R, "Finite element analysis of some joints with the welds transverse to the direction of stress", *Weld. Res. Inst.*, Vol. 6, No. 4, pp. 40-72, (1976).

Gurney T.R and Johnston G. O., "A revised analysis of the influence of toe defects on the fatigue strength of transverse non-load-carrying fillet welds", *Weld. Res. Inst.* Vol. 9, No. 3, pp. 43-80, (1979).

Gurney T.R, "An analysis of some fatigue crack propagation data for steels subjected to pulsating tension loading", *Weld. Res. Inst.*, Vol. 9, No. 4, pp. 45-59, (1979).

Gurney T. R., "*Fatigue of welded structures*", Cambridge University Press, Abington, (1979).

Gurney T.R., "Revised fatigue design rules", *Metal Construction*, pp. 37-44, (1983).

Gurney T.R, "The Fatigue Strength of Transverse Fillet Welded Joints: A study of the influence of joint geometry", *An Abington Publishing Special Report*, Abington Publishing, Abington, Cambridge, UK, (1991).

Haagensen, P. J.; Slind, T. et al., "Influence of notch severity on size effects in weld joints and notched components", *Proceeding of International Conference*, Fatigue Failures, (1988).

Haagensen, P.J., "Size effect in fatigue of non-welded components", *Proceeding of the Ninth International Conference on Offshore Mechanics and Arctic Engineering Symposium 1990*, Volume II, (1990).

Haibach E., "Fatigue strength of angular fillet welds fabricated from 50 mm plate", *European Offshore Steel Research Seminar*, Cambridge, UK, Nov. 1978, paper 7, (1978).

Harrison, J. D., "An analysis of the fatigue behaviour of cruciform joints", *Metal Construction and British Welding Journal*, p 333-335, (1969).

Harrison, J.D., "An analysis of data on non-propagating fatigue cracks on a fracture mechanics basis", *Metal construction and British Welding Journal*, pp 93-97, (1970).

Harrison, J.D., "Basis for a proposed acceptance standard for weld defects, Part 2: Slag inclusions", *Metal construction and British Welding Journal*, pp. 262-267, (1972).

Harrison, J.D. (editor), "Fatigue performance of welded high-strength steels", *The Welding Institute*, UK, (1974).

Heeschen, J. and Wohlfahrt, H., "Assessment of The Influence of Shot Peening on The Fatigue Strength of Butt Welded Joints", *Residual Stresses in Science and Technology*, Vol. 2., *Symposium of International Conference on Residual Stresses*, Germany, pp. 467-476, (1986).

Hentschel K., Berger P., Roessler K. and Schmidt M., "Weld geometry as a factor controlling the fatigue strength of butt welded joints", *Welding International*, Vol. 4, No. 6, pp. 494-499, (1990).

Hentschel K., "Determination of the fatigue life of welded components by crack propagation calculations", *Welding International*, Vol. 5, No. 11, pp. 900-907, (1991).

Hobbacher A., "International recommendations for the fatigue strength of weldments", *Welding and Cutting*, 2/1992, pp. 30-35, (1992).

Huther I., Primot L., Lieurade H.P., Janosch J.J., Colchen D. and Debiez S., "Weld quality and the cyclic fatigue strength of steel welded joints", *Welding in The World*, Vol. 35, No. 2, pp. 118-133, (1995).

IIW Commission XIII, Working Group 1, "Fatigue testing of welded components", *Welding in the World*, Vol. 29, No. 9-10, (*IIS/IIW Doc. XIII-1090-90*), (1991).

Itoh, Y., "Fatigue life prediction for GMA welded butt joints in a C-Mn-Si steel", *Welding Journal*, Welding Res. Suppl., pp 50-56, (1987).

Jandel Scientific Tablecurve Manual, version 3.03, *AISN Software*, 1991

Janosch J.J, Lipinski P. and Lebienvenu, "Investigation into the fatigue strength of a fillet welded assemblies in E-36 steel as a function of the penetration of the weld subjected to tensile and bending loads", *IIW Doc. No. XIII-1430-91*, pp. 13-43, (1991).

Jubb, J.E.M., "Undercut or Toe Groove - the Cinderella Defect", *Metal Construction*, February, pp. 94-, (1981).

Kanazawa T., Oba H. and Machida S., *Society of Naval Architects of Japan J.*, Vol. 109, pp. 359-369, (1961).

Kim, Chongmin; Diesburg, D.E. et al., "Effect of Residual Stress on Fatigue Fracture of Case-Hardened Steels - An analytical model", *Residual Stress Effects in Fatigue, ASTM STP 776*, pp. 224-234, (1982).

Kim, D. S. and Tsai, C. L. and Wylde, J. G, "Numerical Analysis of crack propagation behaviour in a welded joint", *Proceeding of the Eighth Inter. Conference on Offshore Mechanics and Arctic Engineering*, The Hague - March, pp. 153-158, (1989).

Knight J.W, "Some basic fatigue data for various types of fillet welded joints in structural steel", *Weld. Res. Inst.*, Vol. 6, No. 3, pp. 22-42, (1979).

Kobayashi H., Nakamura H. and Nakazawa H., "The elastic fracture toughness and the fatigue crack growth resistance in base metals and weldment of A 533 B-1 and 304 steels", Paper C38/80, *I. Mech. E.*, (1980).

Lal K. M et al., "An assessment of crack closure in Fatigue using the Westergaard Stress Function", *Fatigue of Engng. Mater. and Structures*, Vol. 1, pp. 203-215, (1979).

Lal K.M et al. , "On the effective stress range factor in fatigue", *J. Eng. Mater. and Technology*, Vol. 102, pp. 147-152, (1980).

Langhaar, H. L., "*Dimensional analysis and theory of model*", John Willey & Sons Inc., London, (1967).

Lawrence, F. V. et Munse, W. H., "Fatigue crack propagation in butt weld containing joint penetration defects", *Welding Journal*, Weld. Res. Suppl., pp 221-225, (1973).

Lawrence, F. V., "Estimation of fatigue crack propagation life in butt welds", *Welding Journal*, Weld. Res. Suppl., p 213-220, (1973).

Le May, I., "Fatigue damage mechanism and short crack growth", *AGARD Conf. Proc. No. 328*: Behaviour of Short Cracks in Airframe Components, Toronto, Canada, 19-24 September 1982, pp. 2-1 to 2-11, (1982).

Lieurade H.P., Maillard-Salin C., Truchon M., "Fissuration par fatigue d'assemblages soudes en aciers HLE", *IABSE Colloquium*, pp. 137-144, (1982).

Lieurade H. P., "Effect of residual stresses and stress ratio on the fatigue strength of welded components", *Welding in the World*, Vol. 26. No. 7/8, pp. 158-187, (1988).

Lieurade H. P. et al., "Efficiency of improvement techniques on the fatigue strength as a function of the type of welded joint", *Welding in the World*, Vol. 31. No. 4, pp. 20-23, (1993).

Maddox, S. J., "Calculating the fatigue strength of a welded joints using fracture mechanics", *Metal construction and British Welding Journal*, p. 327-331, (1970).

Maddox S.J., "Fatigue crack propagation in weld metal and HAZ", *Metal Const. and Br. Weld J.*, Vol. 2, pp. 285-289, (1970).

Maddox, S. J., "Fatigue crack propagation data obtained from parent plate, weld metal and HAZ in structural steels", *The Weld. Res. Inst. Report E/48/72*, (1972).

Maddox S. J., "Assessing the significance of flaws in welds subject to fatigue", *Welding Journal*, Res. Sup., Sept. 1974, pp. 401-409, (1974).

Maddox S. J., "A fracture mechanics analysis of the fatigue behaviour of a fillet welded joint", *Res. Weld. Inst.*, Vol. 6, No. 5, pp. 1-34, (1976).

Maddox S.J. , Gurney T.R., Mummery A.M and Booth G.S, " An investigation of the influence of applied stress ratio on fatigue crack propagation in structural steel", *Weld. Res. Inst. Rep. 72/1978/E*, (1978).

Maddox S. J., "Influence of tensile residual stresses on the fatigue behaviour of welded joints in steel", *ASTM 776*, 63-96, (1982).

Maddox, S.J., "The influence of tensile residual stresses on the fatigue behaviour of welded joints in steel, Residual Stress Effects in Fatigue", *ASTM STP 776, American Society for Testing and Materials*, pp. 63-96. (1982).

Maddox S. J., "Fatigue of stress-relieved fillet welds under part-compressive loading", *The Welding Institute, The IIS/IIW Doc. XIII-1143-84*, (1984).

Maddox, S. J., "Fitness-for-Purpose Assessment of Misalignment in Transverse Butt Welds Subject to Fatigue Loading", *IIW/IIS Doc. XIII-1180-85*, 1985.

Maddox, S. J., "Improving the fatigue strength of welded joints by peening", *Metal Construction*, April 1985, pp. 12-16, (1985).

Maddox S. J. and D. Webber, "The effect of tensile residual stresses on the fatigue strength of transverse fillet welded Al-Zn-Mg alloy", *Proc. Int. Conf. on Fatigue of Welded Construction*, Brighton, April 1987, The Welding Institute, UK, (1987).

Maddox, S. J., "Revision of the fatigue clause in BS PD 6493", *Proc. Int. Conf. "Weld Failures"*, London, The Welding Institute, paper 47, pp. 307-320, (1988).

Maddox, S. J., "*Fatigue strength of welded structures*", Cambridge University Press, Abington, (1991).

Maddox, S.J., "Fatigue assessment of welded structures", *Welding in the World*, Vol. 32, pp. 33-42, (1993).

Martins Ferreira, J. A. and Moura Branco, A. A., "Influence of the radius of curvature at the weld toe in the fatigue strength of fillet welded joints", *Inter. J. Fatigue*, Vol. 11, No. 1, pp. 29-36, (1989).

Masumoto I., Matsuda K., Iwata H. and Hasegawa M., "Effect of prestrain and hammer peening on fatigue strength improvement of mild steel welded joint", *Trans. of Japan Welding Society*, Vol. 15, No. 2, October 1984, pp. 14-20, (1984).

Mateffy, V. K.; Mikan, J. M. and Abel, A., "Fatigue of welded joints - The effect of stress relieving", *Proceeding of Ninth Australasian Conference on Mechanics of Structures and Materials, ASCMS 9*, Published by the University of Sydney, (1984).

Matsuoka K., Takahashi I., Yoshii T. and Fujii E., "Influence of residual stress on fatigue strength of non-load-carrying fillet welded joints", *Trans. Japan Welding Society*, Vol. 24, No. 1, pp. 70-77, (1993).

Mattos, R. J. and Lawrence, F. V., "*Estimation of the fatigue crack initiation life in welds using low-cycle concepts*", Published by Society of Automotive Engineers Inc., (1977).

Miki, C. and Nishino, F. et al., "Fatigue crack growth in corner weld of Box-section Bridge Truss Chords", *IABSE Colloquium Lausanne*, (1982).

Miki, C., Mori, T. et al, "Effect of stress ratio and tensile residual stress on near threshold fatigue crack growth", *Structural Eng. and Earthquake Eng.*, Vol. 3, No. 1, pp. 175-182, (1986).

Nakamura, H.; Ohta, A; Nishijima, S. et al, "A method for obtaining conservative S-N data for welded structures", *ASTM Publ.* (1988).

Nelson, D. V., "Effect of residual stress on fatigue crack propagation", *Residual Stress Effects in Fatigue, ASTM STP 776*, pp. 172-194, (1982).

Newman J.C., Jr. and Raju, I. S., "An Empirical Stress-Intensity Factor Equation for the Surface Crack", *Engineering Fracture Mechanics*, Vol. 15, No. 1-2, pp. 185-192, (1981).

Nihei M, Kamakura M., Sasaki E., Kanao M and Inagaki M., "Effect of specimen size and test frequency on fatigue properties of SM50B butt welded joints", *Trans. of National Research Institute for Metals*, Vol. 24., No. 1, pp. 3-9, (1982).

Niu, X. and Glinka, G., 1989, "Stress Intensity factors for semi-elliptical surface cracks in welded joints", *Inter. Journal of Fracture*, Vol. 40, pp. 255-270, (1989).

NRIM Fatigue Data Sheet, Technical Document No. 2. 1983, "Fatigue properties for welded joints of high strength steels for welded structure", *National Research Institute for Metal*, Tokyo - Japan, (1983).

Ohta, A. , Sasaki, E. , Kamakura, M. et al., "Effect of Residual Stresses on Threshold Level for Fatigue Crack Propagation in Welded Joints of SM50B Steel", *Trans. JWS*, Vol. 12, No. 1, (1981).

Ohta A., Maeda Y. and Kanao M., "Significance of residual stress on fatigue properties of welded pipes", *Int. J. Pres. Ves. & piping*, Vol. 15, pp. 229-240, (1984).

Ohta A., Sasaki E., Nikei M., Kanas M. and Inagaki M., "Fatigue crack propagation rates and threshold stress intensity factors for welded joints of HT80 steel at several stress ratios", *Int. J. Fatigue*, Vol. 4., pp. 233-237, (1982).

Ohta A., "Application of fatigue crack properties of welded joints for design or inspection of structures", *Trans. NRIM*, Vol. 28, No. 2, pp. 157-165, (1986).

Ohta A., Y. Maeda, T. Mawari, S. Nishijima, H. Nakamura, "Fatigue strength evaluation of welded joints considering high tensile residual stresses", *IIW/IIS Doc. XIII-1198-86*, (1986).

Ohta, A.; Toshio Mawari et Suzuki, N., "Evaluation of effect of plate thickness on fatigue strength of butt welded joints by a test maintaining maximum stress at yield strength", *Engineering Fracture Mechanics*, Vol. 37, No. 5, pp. 987-993, (1990).

Pang H. L. J., "A review of stress intensity factor for a semi-elliptical surface crack in a plate and fillet welded joint", *The TWI Journal*, Vol. 2, No. 4, pp. 375-385, (1993).

Paris, P. C. and Erdogan, F., "A Critical Analysis of Crack Propagation Laws", *Trans. ASME*, Vol. 85 Series D, pp. 528-534, (1963).

Parker A. P, "Stress intensity factor, crack profiles and fatigue crack growth rates in residual stress fields", *ASTM STP 776*, pp. 13-31, (1982).

Parker, A.P., "*The Mechanics of Fracture and Fatigue (An Introduction)*", London - New York E. & F.N. Spon Ltd, (1981).

Petershagen, H. and Zwick, W., "Fatigue Strength of Butt Welds Made by Different Welding Processes", *IIW/IIS Doc. XIII-1048-82*, (1982).

Petershagen, H., "Influence of Undercut on The Fatigue Strength of Submerged Arc Welded fillet Connections", *IIW/IIS Doc. XIII-955-80*, (1980).

Petershagen, H., "The Influence of Undercut on The Fatigue Strength of Welds - A Literature Survey", *Welding in the World*, Vol. 28, No. 7/8, (1990).

Petershagen H., "Valuation of the dynamic strength of welded joints with imperfections - an overview", *Welding and Cutting*, 3/1990, pp. 38-40, (1990).

Peterson R. E., "Notch Sensitivity", Published in *Metal Fatigue*, Eds. Sines and Waisman, McGraw-Hill Book Co., Inc. (1959).

Pisarski H.G., "Fatigue crack propagation in an aluminium alloy weldment", *Weld. Res. Inst.*, Vol. 6, No. 4, pp. 28-39, (1976).

Pisarski H.G., "Fatigue crack propagation in an aluminium alloy weldment", *Metal Construction*, pp. 12, (1977).

Pyle, T.; Pitrun, M. et al., "Removal of fatigue damage in weld joints", *Recent trends in welding research, ASTM* Publ. (1990).

Reynolds, A. C. and Loader, D. J., "Review paper - a summary of the 1983-85 Cohesive Fatigue Programme", *Fatigue and Crack Growth in Offshore structures, Proceeding of IMechE 1986*, Vol. 2, paper C139/86, pp. 213-220 (1985).

Robakowski T. and Czuchryj J., "The effect of overloading on the strength of St3W steel welded joints", *Welding International*, Vol. 4, No. 6, pp. 425-429, (1990).

Sandifer J.P., Bowie G.E., "Fatigue crack propagation in A537 M steel", *ASTM STP 648*, pp. 185-198, (1978).

Schmidt R.A. and Paris P.C, "Threshold for fatigue crack propagation and effect of load ratio and frequency", *ASTM STP 536*, (1973).

Scierski J., "Propagation of fatigue cracks in welded joints", *Welding International*, No. 2, pp. 143-145, (1987).

Shim et al., "Determination of Residual Stress in Thick-Section Weldments", *Weld. Res. Supp., Welding J.*, pp. 305-312, Sept. (1992).

Sih G.C., "Mixed mode fatigue crack growth prediction", *Engineering Fracture Mechanics*, Vol. 13, pp. 439-451, (1980).

Sih G.C., "*Handbook of stress intensity factor for researchers and engineers*", Institute for Fracture and Solid Mechanics, Lehigh University, Bethlehem, Pennsylvania, USA, (1973).

Skokuba S., "Fatigue life prediction of cruciform joints failing at weld toe", *Welding Journal, Weld. Res. Suppl.*, pp 269-275, (1992).

Smith I. J. and Hurworth S. J., "The effect of weld geometry changes upon the predicted fatigue strength of welded joints", *The Welding Institute Report 244/1984*, July (1984).

Smith R.A and Miller K. J., "Prediction of Fatigue Regimes in Notches Components", *Int. J. Mech. Sci.*, Vol. 20, pp. 201-206, (1978).

Solumsmoen, O. H., "Fatigue tests on specimens with holes, butt and fillet welds in mild and high tensile structural steels", *Metal construction and British Welding Journal*, pp. 138-142, (1969).

Stig Berge, "On the effect of plate thickness in fatigue of welds", *Engineering Fracture Mechanics*, Vol. 21, No. 2, pp. 423-435, (1985).

Tada H., Paris P. and Irwin G., "*The stress analysis of cracks handbook*", Del. Research Corp., Hellertown, Pennsylvania, USA, (1973).

"TestStar Material Testing WorkStation, TestWare-Sx Application Manual", Dec. 1993, *MTS System Corporation*, USA, (1993).

"TestStar Material Testing WorkStation, Installation Manual, R.2.0a", Dec. 1993, *MTS System Corporation*, USA, (1993).

"TestStar System Manual Set, R.2.0a", Dec. 1993, *MTS System Corporation*, USA, (1993).

Testin R. A. ; Yung, J. Y. and Lawrence, F. V. et al., "Predicting the fatigue resistance of steel weldments", *Welding Journal*, Welding Res. Suppl., pp. 93-98, (1987).

Thieuleux J. Y., "Shot peening: a solution for fatigue failure or stress corrosion in welded joints", *Welding International*, Vol. 8 No. 7, pp. 540-543, (1994).

Toyooka, T. and Tsunenari, T. et al., "Fatigue test of residual stress induced specimens in carbon steel", *Welding Journal*, Weld. Res. Suppl., pp. 29-36, (1985).

Tsai, C. L.; Kim, D. S. et al., "Analysis of Fatigue Crack Propagation Behaviour in Fillet-Welded T-Joints", *Welding Journal*, Welding Res. Suppl., p 150-155, (1991).

Tsai, Chon L. and Dong S. Kim, "Analysis of fatigue crack propagation behaviour in fillet welded T-joints", *Engineering Fracture Mechanics*, Vol. 36, No. 4, pp. 653-660, (1990).

Underwood J.H, Pook L.P and Sharples J.K, "Fatigue crack propagation through a measured residual stress field in low alloy steel", *ASTM STP 631*, pp. 402-415, (1977).

Vosikovsky, O., "Fatigue crack growth in HY-130 steel weldments in air and water", *Welding Journal*, Welding Res. Suppl., pp. 255-258, (1980).

Wahab, M. A., "*Model analysis of fatigue life estimation of welded structures*", *Unpublished Ph.D thesis*, The University of Alberta, Edmonton, (1984).

Wohlfahrt, H. and Heeschen, J., "Possibilities for the improvement of the fatigue strength of butt welded joints of high strength structural steels", *Proceeding of IMechE*, Vol. II, (1986-1989).

Yee, R. and Burns, D.J. et al., "Thickness effect and fatigue crack development in welded joints", *Proceeding of Seventh Inter. Conf. on Offshore Mechanics and Arctic Engineering*, Houston- Texas, pp. 447-457, (1988).

Zaczec, Z., "Improvement in the fatigue strength of butt welded joints by TAG remelting of weld reinforcements", *Metal Construction and British Welding Journal*, pp. 423-425, (1984).

Appendix A

Publications Originated from This Research:

A.1 Refereed journal publications:

1. Nguyen, T. Ninh and Wahab, M. A., "The effect of residual stresses and weld geometry on the improvement of fatigue life ", paper presented at the Second Asia Pacific Conference on Material Processing, Singapore, November 16-18, 1994, also published in special issue of the *Journal of Materials Processing Technology*, Vol 48 (1995), pp. 581-588.

2. Nguyen, T. Ninh and Wahab, M. A.," A Theoretical Study of the Effect of Weld Geometry Parameters on Fatigue Crack Propagation Life", *Engineering Fracture Mechanics*, an International Journal, Vol. 51, No. 1, May 1995, pp. 1-18.

3. Nguyen, T. Ninh and Wahab, M. A., "The effect of residual stresses on fatigue of butt joints", Research Supplement, *Welding Journal*, American Welding Society, February, 1996.

4. Nguyen, T. Ninh and Wahab, M. A., "The Effect of Undercut and Residual Stresses on Fatigue Behaviour of Misaligned Butt Joints", paper is accepted for publication in *Engineering Fracture Mechanics*, an International Journal, in January 1996.

5. Nguyen, T. Ninh and Wahab, M. A., "The effect of Undercut, Misalignment and Residual stresses on the Fatigue of Butt Welded Joints", submitted to the *Fatigue and Fracture of the Engineering Materials and Structures*, an international journal. Paper is accepted for publication in 1996.

6. Nguyen, T. Ninh and Wahab, M. A., "The Effect of Weld Geometry and Residual Stresses on Fatigue of Welded Joints under Combined Loading", *Proc. of Inter. Conf. on "Advances in Materials and Processing Technologies (AMPT'95)"*, Dublin City University, August 8-12,1995, Vol. 1, pp. 292-302. This paper is also under review for publication in the *Journal of Materials Processing Technology*.

A.2 Refereed conference publications

1. Nguyen, T. Ninh and Wahab, M. A., "An Analytical 4-Parameter Model to Predict Fatigue Strength and Fatigue Notch Factor of Butt Welded Joint", *Proc. of 13th Australasian Conf. on the Mechanics of Structures and Materials (ACMSM 13)*, Uni. of Wollongong, 5-7 July, 1993, pp. 627-634.

2. Nguyen, T. Ninh and Wahab, M. A., "The Effect of Butt-Weld Geometry Parameters on Stress Intensity Factor and Fatigue Life", *Proc. of the Second Asia-Pacific Conference in Computational Mechanics*, Sydney, August 1-3, 1993, pp. 883-888.

3. Nguyen, T. Ninh and Wahab, M. A., "Theoretical Analysis of The Effect of Residual Stresses in Welded Structures on the Improvement of Fatigue Strength", *Proc. of 5th Australian Aeronautical Conference on "Fracture and Fatigue Life Enhancement"*, Melbourne, September 13-15, 1993, pp. 463-469.

4. Nguyen, T. Ninh and Wahab, M. A., "The Combined Effect of Weld Geometry Parameters on Fatigue Strength and Fatigue Notch Factor of Butt-Welded Joint", *Proc. of WTIA/AINDT Conference on " 1993 Fabcon/Fabfair"*, University of Wollongong, 27th Sept.- 1st Oct. 1993, pp. 74-79.

5. Wahab, M. A. and Nguyen, T. Ninh, "Effect of Residual Stresses Produced by Mechanical Means on the Fatigue Life of Welded Structures", *Proc. of 2nd Inter. Conf. on Surface Engineering: Coatings and Surface Treatments in Manufacturing*, Adelaide, March 7-10, 1994, pp. 308-318.

6. Nguyen, T. Ninh and Wahab, M. A., " A mathematical model to predict geometry magnification factor for stress intensity factor of butt-welded joints", *Proc. of the American Welding Society Conference on "Advanced Joining Technologies for New Materials"*, Cocoa Beach, Florida, March 2-4,1994, pp. 142-154.

7. Nguyen, T. Ninh ; Wahab, M. A and D. J. Oehlers, "An advanced study of the geometrical parameters and residual stresses on fatigue strength of welded joints", paper 29, *Proc. of 42nd National Welding Conference*, Melbourne 24-27 October, 1994, Australia.

8. Nguyen, T. Ninh and Wahab, M. A., "The Effect of Weld Geometry and Residual Stresses on Fatigue of Welded Joints under Combined Loading", *Proc. of Inter. Conf. on "Advances in Materials and Processing Technologies (AMPT'95)"*, Dublin City University, August 8-12,1995, Vol. 1, pp. 292-302.

9. Nguyen, T. Ninh, Wahab, M. A. and Yellup, J., "The effect of Undercut and Misalignment on Fatigue of Butt-Joints", *Proc. of 14th ACMSM*, Hobart 11-13 December, Vol. 1, pp. 254-259, 1995.

Appendix B

List of Equations and Tables of Variables used in Numerical Modelling

B.1 Bueckner's and Kanazawa's Weight Functions

(a) Bueckner's weight function (Bueckner, 1970)

The expression for Bueckner's weight function is written in the following form:

$$m(x,a) = [2\pi(a-x)]^{-0.5}.[1+m_1(a-x)/a + m_2((a-x)/a)^2] \quad (B.1)$$

where a - crack length for an edge crack

W - the width of the cracked body

m_1 , m_2 - functions of the ratio of crack length to strip width (a/w) and are given for $0 \leq a/W \leq 0.5$.

where $m_1 = A_1 + B_1 (a/W)^2 + C_1 (a/W)^6$

$m_2 = A_2 + B_2 (a/W)^2 + C_2(a/W)^6$

and $A_1 = 0.6147$, $B_1 = 17.1844$, $C_1 = 8.7822$

$A_2 = 0.2502$, $B_2 = 3.2899$, $C_2 = 70.0444$

(b) *Kanazawa's weight function (Kanazawa, 1961)*

The expression for Kanazawa's weight function is written in the following form:

$$G(c,y)=\{2.\sin[\pi(c+y)/w]/\ w/\ \sin(2\pi c/w)/\sin[\pi(c-y)/w]\}^{0.5} \quad (B.2)$$

where c, w - half crack length and plate width respectively

y - distance from plate center line

B.2 The equations for residual stresses in butt welded joint in as-welded and post-weld surface treated conditions:

(a) For as-welded condition (Fig. 3.5a)

$$S_r(x) = S_r(1 - 4x / t) \quad \text{if} \quad 0 \leq x \leq 0.5t \tag{B.3}$$

$$S_r(x) = S_r(4x / t - 3) \quad \text{if} \quad 0.5t \leq x \leq t \tag{B.4}$$

$$S_r(y) = S_r\cos(2\pi y/t) \tag{B.5}$$

(b) For surface-treated condition (Fig. 3.5b)

$$S_r(x) = S_r(x / d_{eff} - 1) \quad \text{if} \quad 0 \leq x \leq 1.5\, d_{eff} \tag{B.6}$$

$$S_r(x) = S_r\{[(t - 2.25\, d_{eff})x + 0.5(t - 2.25\, d_{eff})^2]/ (t - 1.5\, d_{eff})^2 - 1\} \quad \text{if} \quad 1.5d_{eff} \leq x \leq t \tag{B.7}$$

$$S_r(y) = S_r \tag{B.8}$$

where $S_r(x)$, $S_r(y)$ - residual stress in (x) and (y) direction respectively

d_{eff} - effective depth of surface treatment (due to compressive residual stress field)

t - plate thickness of the welded joint

***Table B.1** Parameters in Various Sets of Treatments used for Numerical Modelling in the present study*

Set No.	r' mm	r mm	θ Deg	ϕ Deg	t mm	2b mm	S_r MPa	R_{ba} -
1	0.05 0.15 0.25 0.35	1	30	60	12	50	0	0
2	0	0 0.5 1.0 1.5 2.0 3.5 5.0	30	60	12	50	0	0
3	0	1	5 10 15 20 30 40 60	60	12	50	0	0
4	0	1	30	45 60 70 80 90	12	50	0	0
5	0	1	30	60	6.3 9 12 16 19 25 32 50 100	50	0	0
6	0	1	30	60	12	50	0, 30,60,90, 120,150, 300 - 62 - 110 - 152 - 172	0
7	0	1	30	60	12	50	0	0.15 0.3 0.6,0.9 1.2,1.5

***Table B.2(a)** Regression coefficients a_k of the local stress distribution due to variations of butt-weld geometry parameters in pure axial loading condition (Eq. (3.39))*

Set No.	r' mm	r mm	θ deg	t mm	ϕ deg	a_1	a_2	a_3	a_4	a_5	a_6	a_7	a_8
1	0.05 0.15 0.25 0.35	1	30	12	60	4.7087 4.7364 4.1305 3.9450	48.5558 29.4958 16.7517 11.8809	43.4740 23.6836 13.0298 8.8282	-11.6304 -10.5568 -2.4996 -0.7245	-10.6413 -8.4505 -1.6230 -0.0876	1.7232 1.0938 0.0944 -0.0857	1.5603 0.7953 0.0215 -0.1263	-0.0135 -0.0149 -0.0019 -0.0004
2	0	0 0.5 1.0 1.5 2.0 2.5 3.5 5.0	30	12	60	2.0478 1.8942 1.7376 1.6169 1.5533 1.4450 1.2486	4.8714 5.2780 4.0494 2.9543 2.5324 2.1830 1.0657	3.6828 4.1773 3.1314 2.2520 1.1974 1.7101 0.5763	0.3061 -0.0149 0.2086 0.1514 0.1378 0.0320 -0.0055	0.4362 0.1075 0.3098 0.2278 0.2045 0.0827 -0.1392	0	0	0
3	0	1	0 5 10 15 20 30 40 60	12	60	1.0000 1.1962 1.3075 1.4528 1.5805 1.7376 1.7803 1.9398	0 4.2584 3.0805 3.6876 3.8639 4.0494 3.3806 3.6143	0 4.0442 2.7588 3.1693 3.2007 3.1394 2.4677 2.5476	0 0.1027 0.1237 0.1399 0.1478 0.2086 0.1831 0.3173	0 0.1256 0.1582 0.1963 0.2199 0.3098 0.2831 0.3339	0	0	0
4	0	1	30	6.3 9 12 16 20 25 32 50 100	60	1.5521 1.6630 1.7376 1.8802 1.9471 1.9955 2.1527 2.2867 2.4863	4.8670 4.0776 4.0494 3.5524 3.3575 2.6909 2.6517 2.0568 1.3002	3.6887 3.0887 301314 2.7794 2.6441 2.1187 2.1121 1.6556 1.0586	0.4952 0.3032 0.2086 0.1124 0.0854 0.0528 0.0350 0.0153 0.0039	0.7386 0.4466 0.3098 0.1759 0.1328 0.0830 0.0573 0.0260 0.0072	0	0	0
5	0	1	30	12	45 60 70 80 90	1.7173 1.7376 1.7805 1.7959 1.7207	4.8750 4.0494 3.7016 3.0427 2.4854	3.9651 3.1314 2.8024 2.1954 1.1417	0.2732 0.2086 0.1728 0.1999 0.1714	0.3744 0.3098 0.2709 0.2918 0.2514	0	0	0

***Table B.2(b)** Regression coefficients a_k of the local stress distribution due to variations of butt-weld geometry parameters in pure bending load condition (Eq. (3.39))*

Set No.	r' mm	r mm	θ deg	t mm	ϕ deg	a_1	a_2	a_3	a_4	a_5	a_6	a_7	a_8
1	0.05 0.15 0.25 0.35	1	30	12	60	5.0475 4.8274 4.1576 3.9459	52.1354 26.5856 15.0466 11.0888	51.6857 20.9864 11.1804 7.0777	8.5174 -3.5859 -1.8398 -1.7112	-5.1846 -7.1301 -3.7337 -2.6665	-0.3655 -0.0380 -0.0210 0.0118	-0.7191 0.5759 0.2840 0.2262	0.0118 0.0009 0.0010 -0.0002
2	0	0 0.5 1.0 1.5 2.0 3.5 5.0	30	12	60	2.2102 1.8599 1.8709 1.7220 1.6488 1.3977 1.3367	5.1292 3.4204 4.0800 3.0062 2.5241 0.4774 1.0657	3.6266 2.4097 2.9242 2.0756 1.6894 -0.0179 0.5763	-0.0169 0.0063 -0.0106 -0.0078 -0.0079 -0.0093 -0.0054	-0.7053 -0.4711 -0.5669 -0.4143 -0.3448 -0.0401 -0.1392	0	0	0
3	0	1	0 5 10 15 20 30 40 60	12	60	1.0000 1.2177 1.3400 1.5189 1.6559 1.8709 1.9658 2.1596	0 4.8495 3.4194 4.0243 3.9637 4.0800 3.5069 3.4670	-0.16667 4.4959 2.9238 3.3176 3.1011 2.9242 2.2817 2.0160	0 0.0114 0.0042 0.0030 -0.0006 -0.0106 -0.0142 -0.0228	0 -0.7950 -0.5379 -0.6147 -0.5859 -0.5686 -0.4623 -0.4290	0	0	0
4	0	1	30	6.3 9 12 16 20 25 32 50 100	60	1.6349 1.7664 1.8709 2.0160 2.1162 2.1930 2.4008 2.6842 2.7430	4.8913 4.2701 4.0800 3.4674 3.3396 2.6493 2.5633 1.9654 1.0122	3.2945 2.9540 2.9242 2.5182 2.4871 1.9691 1.5552 1.5866 0.7855	-0.0406 -0.0196 -0.0106 -0.0014 0.0023 0.0037 0.0060 0.0089 0.0015	-1.2688 -0.7820 -0.5669 -0.3664 -0.2863 -0.1830 -0.1414 -0.0747 -0.0184	0	0	0
5	0	1	30	12	45 60 70 80 90	1.6230 1.8709 1.8618 1.8288 1.7178	2.2929 4.0800 3.4079 2.7979 2.3195	1.5966 2.9242 2.2238 1.6205 1.2143	-0.0079 -0.0106 -0.1447 -0.0208 -0.0208	-0.3259 -0.5686 -0.4476 -0.3426 -0.2687	0	0	0

***Table B.3** Transformation functions derived for M_k-model to calculate A_i (for i = 1 to 4) (Eq. 5.1)*

Label i	Transformation Functions	Constants K_i
1	$f_1(r/t) = 1.0167 + 0.1045\,(r/t) - 0.011/(r/t)$ $f_1(\theta) = 1.0511 - 0.0411\,\theta + 0.0103\,\theta^{1.5} - 0.00068\,\theta^2$ $f_1(t/2b) = 0.9687 + 0.2811\,(t/2b)^2 - 0.2361\,(t/2b)^{2.5}$ $f_1(\theta) = 0.9679 - 34.7435/\phi^{1.5}$	1.246
2	$f_2(r/t) = 0.2156 - 0.1911\exp(r/t) + 0.0061/(r/t)$ $f_2(\theta) = -0.0562 + 0.0347\,\theta - 0.0102\,\theta\ln(\theta) - 0.00014\,\theta^2$ $f_2(t/2b) = 1.1772 - 0.2441\,(t/2b)^2 + 0.4966\,(t/2b)^2\ln(t/2b)$ $f_2(\phi) = 0.2641 - 0.0115\,\phi + 0.0021\,\phi\ln(\phi)$	159.433
3	$f_3(r/t) = 0.0631 - 0.9825\,(r/t)^2 + 2.3246\,(r/t)^3$ $f_3(\theta) = -0.0122 + 0.0069\,\theta - 0.0014\,\theta\ln(\theta)$ $f_3(t/2b) = 1.0022 + 0.0014\,(t/2b)^{6.2903}$ $f_3(\phi) = 0.0791 - 1.3664/\phi + 5.8753/\phi^2$	329.629
4	$f_4(r/t) = -0.0241 + 0.0836\ln(r/t) + 0.0479/(r/t)^{0.5}$ $f_4(\theta) = 0.0262 - 0.0086\,\theta + 0.0017\,\theta\ln(\theta)$ $f_4(t/2b) = 2.0232 + 1.0675\,(t/2b)^2 - 0.7656\exp(t/2b)$ $f_4(\phi) = -0.0116 - 0.0142\,(\ln\phi)^2 + 0.0236\,\phi^{0.5}$	238.365

***Table B.4** Transformation functions derived for K_t-model (Eq. 5.4)*

No.	Transformation functions $f_{kt}(...)$	r^2 coeff.
1	$f_{kt}(r'/t) = 740.3966 + 2243.4654(r'/t)^{1.5} - 739.3992\exp(r'/t) + 0.3989(r'/t)^{0.5}$	0.9959
2	$f_{kt}(r/t) = 0.9599 + 1.2047\exp(-r / 0.2786t)$	0.9599
3	$f_{kt}(\theta) = (0.5310 + 0.0631\theta)/(1 + 0.0480)$	0.9910
4	$f_{kt}(t/b) = 0.9940 + 0.5537 - 0.0769\exp(t/b) + 0.0077 / (t/b)$	0.9958

Appendix C

Computer Programs

C.1 Listing of a computer program for calculation of fatigue life of butt joints subjected to weld geometries, residual stresses and the combined loading (axial and bending) conditions:

The following program uses the modified Paris's law (Eqs. (3.20) and (3.21)) to calculate the crack propagation life of butt welded joints subjected to weld geometries, residual stresses and the combined loading conditions for the constant amplitude pulsating tensile loading (R=0). The stress distributions in various welded profiles along the potential crack line are input to the program in the explicit equation form. The Bueckner's and Kanazawa's weight functions are used with the Newman-Raju's solution for the semi-elliptical surface crack model to calculate the range of the effective stress intensity factor due to weld geometry, residual stresses and the combined loading (axial and bending) conditions. Simpson's rule (1/3) is used for the calculations of the integrals. Superposition principles are used to combine the effects of various stress components.

```
' MAIN PROGRAM TO CALCULATE FATIGUE LIFE OF BUTT-WELDED JOINT
' SUBJECTED TO RESIDUAL STRESSES, SURFACE CRACK GEOMETRY
' WITH UNDERCUT AT  WELD TOES IN THE COMBINED LOADINGS BASED
' ON THE WEIGHT FUNCTION TECHNIQUE, NEWMAN-RAIJU'S
' APPROACHES AND SUPERPOSITION PRINCIPLE
N = 40: K = 20: NN = 8: NNN = 6: KIC = 1900: KTH = 63
DIM NP(NN), H0(NN), SRMAX(NN), DS(NN, 2), INTEGR(N + 1), INTEG(4)
DIM F1(4), F2(4), FX(4), KTMAX(2), D1(2), D2(2), D3(2), D4(2)
DIM D5(2),D6(2), D7(2), D8(2), G1X(2), G1Y(2)
A1 = .6147: B1 = 17.1844: C1 = 8.7822
A2 = .2502: B2 = 3.2899: C2 = 70.0444
```

```
M = 3: C = 3.1E-13: B = 50
INPUT "INPUT DATA FILE NAME ?", FLI$
OPEN FLI$ FOR INPUT AS #1
INPUT "OUTPUT FILE NAME ?", FL$
OPEN FL$ FOR OUTPUT AS #2
5 PRINT #2, "A    C    MKAE    MKBE    DELTKWAEF    DELTKWBEF"
' THE FOLLOWING LOOP CONSIDERS NUMBER OF DATA POINTS  IN EACH
' SET OF WELD GEOMETRY PARAMETERS
FOR KKK = 1 TO NNN
' INPUT COEFFICIENTS FOR STRESS DISTRIBUTION FUNCTION DUE TO
' AXIAL LOADING, DI (1) AND BENDING LOAD, DI(2), (I=1 TO 8); PLATE
' THICKNESS (T), CRACK SHAPE ASPECT RATIO (RAC), COMBINED
' LOADING RATIO (RBA), CYCLIC APPLIED STRESS RATIO (R) AND
' MAXIMUM STRESS CONCENTRATION FACTORS DUE TO AXIAL &
' BENDING LOAD: KTMAX(1) & KTMAX(2).
INPUT #1, D1(1), D2(1),D3(1),D4(1),D5(1),D6(1),D7(1), D8(1),KTMAX(1), T,
RAC
INPUT #1, D1(2), D2(2),D3(2),D4(2),D5(2),D6(2),D7(2),D8(2),KTMAX(2), RBA, R
' THE FOLLOWING LOOP CALCULATES THE FATIGUE LIFE FOR VARIOUS
' LEVELS OF THE  STRESS RANGE DUE TO WELD GEOMETRY & RESIDUAL
' STRESSES AND COMBINED LOADING CONDITIONS; INTEGRALS ARE
' CALCULATED USING SIMPSON 1/3 RULE; (AI) & (AF) ARE INITIAL &
' FINAL CRACK LENGTH
FOR KK = 1 TO NN
AF = .5 * T
' INPUT RESIDUAL STRESS DISTRIBUTION FUNCTION WHICH IS DEFINED
' BY THE EFFECTIVE DEPTH OF SURFACE TREATMENTS, H0(KK), AND
' BY MAXIMUM RESIDUAL STRESS AT WELD TOE SURFACE, SRMAX(KK);
' AND VARIOUS LEVELS OF STRESS RANGE DS (KK,1) DUE TO AXIAL
' LOADING CONDITION
INPUT #1, H0(KK), SRMAX(KK), DS(KK, 1)
10 DC = 0: AI = .125: CI = AI / RAC: CI = CI + DC
DS(KK, 1) = DS(KK, 1) / (1 - R)
IF DS(KK, 1) >= SU GOTO 500
```

```
' CALCULATE STRESS RANGE DUE TO BENDING LOAD DS(KK,2)
DS(KK, 2) = RBA * DS(KK, 1)
IF AF > 10 * AI THEN
H = (AF - AI) / N
ELSE PRINT #2, "NEW VALUE OF AF IS NOT VALID, AF = ", AF
GOTO 500
END IF
ODSUM = 0: EVENSUM = 0: NP(KK) = 0: INTEGRAL = 0
FOR III = 1 TO N + 1
A = AI + (III - 1) * H
GOSUB 50
NEXT III
FOR I = 2 TO N STEP 2
ODSUM = ODSUM + INTEGR(I)
NEXT I
FOR J = 3 TO N - 1 STEP 2
A = AI + J * H
EVENSUM = EVENSUM + INTEGR(J)
NEXT J
I1 = INTEGR(1)
I2 = INTEGR(N + 1)
NP(KK) = H * (I1 + 4 * ODSUM + 2 * EVENSUM + I2) / 3
PRINT #2, " OUTPUT CRACK PROPAGATION LIFE, NP(KK) :"
PRINT #2, " H0    SRMAX    NP     DS(KK,1)    RBA   R "
PRINT #2, H0(KK), SRMAX(KK), NP(KK), DS(KK, 1), RBA, R
500 NEXT KK
NEXT KKK
PRINT "DO YOU WANT TO RERUN THE PROGRAM ?"
INPUT A$: IF A$ = "y" OR A$ = "Y" THEN GOTO 5
CLOSE #2
PRINT " END OF PROGRAM. BYE ! BYE ! "
END
```

```
' FOLLOWING SUBPROGRAM CALCULATES THE STRESS INTENSITY
' FACTORS OF A  SEMI-ELLIPTICAL SURFACE CRACK INITIATED AT THE
' WELD TOE FOR DEEPEST CRACK TIP AND CRACK FRONT AT THE PLATE
' SURFACE  UNDER THE COMBINED AXIAL AND BENDING LOADING
50 FOR L = 1 TO 4
IF L <= 2 THEN
HH = A / K
ELSE HH = CI / K
END IF
X = HH / K: GOSUB 100
F1(L) = FX(L)
ODSUMA = 0: EVENSUMA = 0: FX(L) = 0
FOR II = 1 TO K - 1 STEP 2
X = II * HH
GOSUB 100
ODSUMA = ODSUMA + FX(L)
NEXT II
FOR JJ = 2 TO K - 2 STEP 2
X = JJ * HH
GOSUB 100
EVENSUMA = EVENSUMA + FX(L)
NEXT JJ
IF L <= 2 THEN
X = A - HH / K:
ELSE X = CI - HH / K
END IF
GOSUB 100
F2(L) = FX(L)
INTEG(L) = HH * (F1(L) + 4 * ODSUMA + 2 * EVENSUMA + F2(L)) / 3
NEXT L
' CALCULATE THE RANGES OF STRESS INTENSITY FACTOR AT CRACK TIP
' FRONTS (DELTKA & DELTKB) USING NEWMAN-RAJU'S EQUATION FOR
' SEMI-ELLIPTICAL SURFACE CRACK WITH CRACK DEPTH (A) AND CRACK
' LENGTH (CI)
```

```
Q = 1 + 1.464 * (A / CI) ^ 1.65
M11 = 1.13 - .09 * A / CI
M22 = -.54 + .89 / (.2 + A / CI)
M33 = .5 - 1 / (.65 + A / CI) + 14 * (1 - A / CI) ^ 24
GA = 1: GB = 1.1 + .35 * (A / T) ^ 2
FA = 1: FB = (A / CI) ^ .5
FW = (COS((3.14159 * CI * (A / T) ^ .5) / 2 / B)) ^ (-.5)
MM = (M11 + M22 * (A / T) ^ 2 + M33 * (A / T) ^ 4)
DELTKA = DS(KK, 1) * MM * FW * (3.14159 * A / Q) ^ .5
DELTKB = DS(KK, 1) * MM * FB * GB * FW * (3.14159 * A / Q) ^ .5
' CALCULATE THE EFFECTIVE STRESS INTENSITY MAGNIFICATION
' FACTORS MKAE AND MKBE USING "SIMILARITY APPROACH",
' SUPERPOSITION AND WEIGHT'S FUNCTION TECHNIQUES
MKAE = INTEG(1) / INTEG(2)
MKBE = INTEG(3) / INTEG(4)
DELTKWAEF = MKAE * DELTKA
DELTKWBEF = MKBE * DELTKB
' TEST CONDITION FOR CRACK PROPAGATION THRESHOLD, KTH
IF DELTKWAEF <= KTH OR DELTKWBEF <= KTH THEN
DS(KK, 1) = DS(KK, 1) + 10: GOTO 10
'TEST CONDITION FOR FRACTURE TOUGHNESS OF THE MATERIAL, KIC
ELSEIF DELTKWAEF >= KIC OR DELTKWBEF >= KIC THEN
AF = AF - .05 * T: PRINT #2, "NEW VALUE OF AF = ", AF: GOTO 10
END IF
INTEGR(III) = 1 / C / DELTKWAEF ^ M
DC = H * (.9 * DELTKWBEF / DELTKWAEF) ^ M
' OUTPUT THE EVOLUTION OF THE CRACK SHAPES: CRACK LENGTH (A) &
' CRACK DEPTH (CI) AND RANGES OF THE EFFECTIVE STRESS INTENSITY
' FACTORS OF WELDED JOINTS DUE TO AXIAL AND BENDING LOADS:
' DELTKWAEF &  DELTKWBEF
PRINT #2, A, CI, DELTKWAEF, DELTKWBEF
CI = CI + DC
' TEST WETHER CRACK LENGTH HAS REACHED THE PLATE WIDTH
IF CI >= B THEN
```

```
AF = AF - .05 * T: PRINT #2, "CI > B , NEW VALUE OF AF = ", AF
GOTO 10
ELSE GOTO 30
END IF
30 RETURN
END

' FOLLOWING SUBPROGRAM CALCULATES INTEGRAL FUNCTION FOR
' STRESS INTENSITY FACTORS USING WEIGHT FUNCTION METHOD
100 IF L <= 2 THEN
GOTO 150
ELSE GOTO 200
END IF
' CALCULATE BUECKNER'S WEIGHT FUNCTION, MX
150 M1A = A1 + B1 * (A / T) ^ 2 + C1 * (A / T) ^ 6
M2A = A2 + B2 * (A / T) ^ 2 + C2 * (A / T) ^ 6
PRINT "T, A, CI, DS(KK,1), DS(KK,2),DELTKA, DELTKB, KKK ", T, A, CI,
DS(KK, 1), DS(KK,2), DELTKA, DELTKB, KKK
PRINT "DELTKWAEF, DELTKWBEF, NP, KK", DELTKWAEF, DELTKWBEF,
NP(KK), KK
' CALCULATE STRESS DISTRIBUTION FUNCTION ALONG THE POTENTIAL
' CRACK LINE DUE TO AXIAL AND BENDING LOADING: G1X(1) & G1X(2)
G1X(1) = (D1(1) + D3(1) * X + D5(1) * X ^ 2 + D7(1) * X ^ 3) / (1 + D2(1) * X +
D4(1) * X ^ 2 + D6(1) * X ^ 3 + D8(1) * X ^ 4)
G1X(2) = (D1(2) + D3(2) * X + D5(2) * X ^ 2 + D7(2) * X ^ 3) / (1 + D2(2) * X +
D4(2) * X ^ 2 + D6(2) * X ^ 3 + D8(2) * X ^ 4)
'CALCULATE RESIDUAL STRESS DISTRIBUTION FUNCTION THROUGH
' THE PLATE THICKNESS (GX2) WHERE H0(KK) =0 FOR AS-WELDED
' CONDITION & H0(KK) ≠ 0 FOR SURFACE TREATED CONDITION
IF H0(KK) = 0 THEN
IF X <= .5 * T THEN
G2X = SRMAX(KK) * (1 - 3 * X / T)
ELSE G2X = 3 * SRMAX(KK) * X / T - 2 * SRMAX(KK)
END IF
```

```
ELSEIF X <= 1.5 * H0(KK) THEN
G2X = SRMAX(KK) * (X / H0(KK) - 1)
ELSE G2X = SRMAX(KK) * (X - T) / (3 * H0(KK) - 2 * T)
END IF
MX = (1 + M1A * (A - X) / A + M2A * ((A - X) / A) ^ 2) / (2 *3.14159*(A - X)) ^ .5
' CALCULATE INTEGRAL FUNCTION FOR THE EFFECTIVE STRESS
' INTENSITY FACTOR AT THE DEEPEST CRACK TIP DUE TO AXIAL &
' BENDING LOADS, F1X & F2X
IF DS(KK, 1) <> 0 THEN
F1X = 2 * (G1X(1) + G1X(2) * RBA + G2X * (1 - R) / DS(KK, 1)) * MX
ELSE F1X = 0
END IF
F2X = 2 * MX
GOTO 300
' CALCULATE RESIDUAL STRESS DISTRIBUTION ALONG THE PLATE
' WIDTH DIRECTION AT THE SURFACE (G2Y)  AND RETRIEVE STRESS
' CONCENTRATION AT THE WELD TOE DUE TO AXIAL AND BENDING
' LOADS: G1Y(1) & G1Y(2)
200 G1Y(1) = KTMAX(1)
G1Y(2) = KTMAX(2)
IF H0(KK) = 0 THEN
G2Y = SRMAX(KK) * (1 - 6 * X ^ 2 / T ^ 2)
ELSE G2Y = (-1) * SRMAX(KK)
END IF
' CALCULATE KANAZAWA'S WEIGHTS FUNCTION, MY
MY=(SIN(3.14159*(CI+X)/2/B)/B/SIN(3.14159*CI/B)/SIN(3.14159*(CI-
X)/2/B))^.5
PRINT " MX  MY  G1X(1) G1X(2) G1Y(1) G1Y(2) G2X", MX, MY, G1X(1),
G1X(2), G1Y(1), G1Y(2), G2X
' CALCULATE INTEGRAL FUNCTION FOR THE EFFECTIVE STRESS
' INTENSITY FACTOR AT THE WELD TOE SURFACE ALONG THE PLATE
' WIDTH DUE TO AXIAL & BENDING LOADS: F1Y & F2Y
IF DS(KK, 1) <> 0 THEN
F1Y = 2 * (G1Y(1) + G1Y(2) * RBA + G2Y * (1 - R) / DS(KK, 1)) * MY
```

```
ELSE F1Y = 0
END IF
F2Y = 2 * MY
300 FX(1) = F1X: FX(2) = F2X: FX(3) = F1Y: FX(4) = F2Y
PRINT "F1X, F2X, F1Y, F2Y: ", F1X, F2X, F1Y, F2Y
RETURN: END
```

C.2 Listing of the TestStar R.2.0a (1993) computer program used to monitor the fatigue tests in MTS-testing system.

```
Procedure name      =     NINH1_60kN
File Specification  =     D:\TS2\TWSX\NINH2.000

Data File Options
        File Format     =     Excel Text File
        Log Events      =     No
        Include Procedure Description = No

Recovery Options
        Autosave enabled.
                At least every  =  5 (sec)

startup: Step
        Step Done Trigger 1 = ramptomean

        ramptomean:  Monotonic Command
                Start Trigger  = Step Start
                End Trigger    = <none>
                Segment Shape = Ramp
                Rate    =     2 kN/Sec
                Axial
                   Control Mode      = Force A SG
                   Endlevel          = 60 kN

cycling: Begin Loop
        Counter Name        =  nocycles
        Total count         =  250

dataacq: Step
        Step Done Trigger 1  = stroke cycle 1
        Stroke mon:   Data Limit Detector
                Start Trigger  = Step Start
```

End Trigger = <none>
Data Channel = Length 1
Limit Value = 2 (mm)
Limit Value is = Absolute
Trigger Options = Either Transition

stroke cycle 1: Cyclic Command
Start Trigger = Step Start
End Trigger = <none>
Segment Shape = Haversine
Frequency = 15 Hz
Repeat = 20 000 cycles
Amplitude/Mean Control = On

Axial
Control Mode = Force A SG
Endlevel 1 = 60 kN
Endlevel 2 = 6 kN

Data Trigger: Data Acquisition
Start Trigger = Step Start
End Trigger = record stroke
Mode = Peak / Valley
Buffer Type = Trigger Only
Master Channel = Force 1
Data Header = Fatigue Test: Pmax = 60 kN, R = 0.1
Sensitivity = 0.5 kN
Buffer Size = 2000

record stroke: Data Acquisition
Start Trigger = Data Trigger
End Trigger = <none>
Mode = Timed
Buffer Type = Single
Master Channel = Force 1
Slave Channel 1 = Time
Slave Channel 2 = Length 1
Slave Channel 3 = Axial Segments
Data Header = Peak / Valley
Time Increment = 0.002 (Sec)
Buffer Size = 100

Last Dacq: Data Acquisition
Start Trigger = stroke mon
End Trigger = <none>
Mode = Timed
Buffer Type = Single
Master Channel = Time
Slave Channel 1 = Length 1
Slave Channel 2 = Force 1
Slave Channel 3 = Axial Segments

Data Header = Final Readings
Time Increment = 0.001 (Sec)
Buffer Size = 2

ProgramStop: Program Control
Start Trigger = Last Dacq
End Trigger = <none>
Action = Hydraulic Interlock
Message = No Load o Program Stopped
Send To:
Screen = Yes
LUC Display = No
Data File = Yes

cycling: End Loop

Shut down: Step
Step Done Trigger 1 = shutdown
rampdown: Monotonic Command
Start Trigger = Step Start
End Trigger = <none>
Segment Shape = Ramp
Rate = 5 kN/sec
Axial
Control Mode = Force A SG
Endlevel = 0 kN
shutdown: Program Control
Start Trigger = rampdown
End Trigger = <none>
Action = Hydraulic Interlock

C.3 Listing of the TestStar R.2.0a (1993) computer program used to calibrate the strain gauges bonded to the test specimens

Procedure name = NINHCAL Default Procedure
File Specification = D:\TS2\TWSX\NINHCAL.000

Data File Options
File Format = Excel Text File
Log Events = No
Include Procedure Description = No

Recovery Options
Autosave Disabled.

load ramp: Step
Step Done Trigger 1 = ramptozero

data acq: Data Acquisition
Start Trigger = Step Start
End Trigger = <none>
Mode = Timed
Buffer Type = Single
Master Channel = Time
Slave Channel 1 = Length 1
Slave Channel 2 = Force 1
Slave Channel 3 = Volt IP7
Slave Channel 4 = Volt IP8
Data Header = Calibration of strain gauges
Time Increment = 0.1 (Sec)
Buffer Size = 2000

ramp_up: Monotonic Command
Start Trigger = Step Start
End Trigger = <none>
Segment Shape = Ramp
Rate = 1 kN/sec
Axial
Control Mode = Force A SG
Endlevel = 50 kN

hold: Hold Command
Start Trigger = ramp_up
End Trigger = <none>
Hold Time = 2 (sec)
Axial
Control Mode = Force A SG

ramp_down: Monotonic Command
Start Trigger = hold
End Trigger = <none>
Segment Shape = Ramp
Rate = 1 kN/sec
Axial
Control Mode = Force A SG
Endlevel = 0 kN

C.4 Listing of the TestStar R.2.0a (1993) computer program used to monitor tensile test in MTS-testing system.

```
Procedure name      =     TENSILE Default Procedure
File Specification  =     D:\TS2\TWSX\ TENSILE.000

Data File Options
        File Format   =     Excel Text File
        Log Events    =     No
        Include Procedure Description = No

Recovery Options
        Autosave Disabled.

Ramp_up (< 2 %): Step
        Step Done Trigger 1   =     strainlim
        Step Done Trigger 1   =     Ramp up
        strainlim : Data Limit Detector
                Start Trigger  =     Step Start
                End Trigger    =     <none>
                Limit Value    =     0.02  ( (none) )
                Limit Value is =     Absolute
                Trigger Options  =  Greater than Limit Value

        data acq: Data Acquisition
                Start Trigger  =     Step Start
                End Trigger    =     strainlim
                Mode           =     Level Crossing
                Buffer Type    =     Single
                Master Channel       =     Force 1
                Slave Channel 1      =     Length 1
                Data Header          =     Strip Tensile Test
                Level Increment      =     0.1 (kN)
                Buffer Size          =     10 000

        Ramp up: Monotonic Command
                Start Trigger  =     Step Start
                End Trigger    =     strainlim
                Segment Shape = Ramp
                Rate    = 0.1 (mm/sec)
                Axial
                        Control Mode =  Length A SG
                        Endlevel              =  50  (mm)

Ramp_up (> 2 %) : Step
        Step Done Trigger 1 = no_load_detect
        Step Done Trigger 2 = Ramp up

        no_load_detect: Data Limit Detector
```

Start Trigger = Step Start
End Trigger = <none>
Data Channel = Force 1
Limit Value = 5 (kN)
Limit Value is = Absolute
Trigger options = Either Transition

data acq: Data Acquisition
Start Trigger = Step Start
End Trigger = <none>
Mode = Timed
Buffer Type = Single
Master Channel = Force 1
Slave Channel 1 = Length 1
Data Header = Strip Tensile Test
Level Increment = 0.2 (sec)
Buffer Size = 16 000

Ramp_up: Monotonic Command
Start Trigger = Step Start
End Trigger = <none>
Segment Shape = Ramp
Rate = 0.1 (mm/sec)
Axial
Control Mode = Length A SG
Endlevel = 50 (mm)

Appendix D

Test Results

Table D.1 *Fatigue test results presented in the regression equation for S-N curve as: log N = log A - m .log S*

Set	m_{mean}	m_{mean} *Lower* 95 %	m_{mean} *Upper* 95 %	$logA_{mean}$	$logA_{mean}$ *Lower* 95 %	$logA_{mean}$ *Upper* 95 %	r^2	S_{logN} (STDEV)	S_{logS} (STDEV)	No. of data
# 0	7.772	12.971	2.573	24.982	12.348	37.616	0.69	0.255	0.033	8
# 4	5.668	8.283	3.052	19.530	13.203	25.857	0.79	0.209	0.037	9
# 5a	5.377	6.763	3.991	18.196	14.965	21.427	0.89	0.172	0.032	11
# 6	4.174	5.140	3.208	15.249	13.040	17.457	0.94	0.144	0.034	9
# 7	4.525	7.914	1.135	16.287	8.405	24.168	0.64	0.248	0.055	8

Table D.2 *Fatigue strength and fatigue notch factor (for three levels of fatigue lives at $5x10^5$, $2x10^6$ and $1x10^7$ cycles) obtained by fatigue tests*

Set	# 0	# 4	# 5a	# 6	# 7
Fatigue strength (S) at $5x10^5$ cycles (MPa)	302.7	275.4	210.9	194.1	218.7
Fatigue strength (S) at $2x10^6$ cycles (MPa)	253.3	215.7	163.0	139.2	161.0
Fatigue strength (S) at $1x10^7$ cycles (MPa)	206.1	162.6	120.8	94.6	112.8
Fatigue notch factor (K_f) at $5x10^5$ cycles	1	1.10	1.44	1.56	1.38
Fatigue notch factor (K_f) at $2x10^6$ cycles	1	1.17	1.55	1.82	1.57
Fatigue notch factor (K_f) at $1x10^7$ cycles	1	1.27	1.71	2.18	1.83

Table D.3 *The values of weld geometry profiles for various sets of fatigue test specimens used in the present study*

Set	No. of data	Radius, r (mm) Side A	Side B	r_{min} (mm)	r_{mean} (mm)	Flank angle, θ (deg) Side A	Side B	θ_{max} (deg.)	θ_{mean} (deg.)
	1	4.8	7.2	4.8		34	20	34	
	2	4.9	6.9	4.9		35	20	35	
	3	4.7	7.4	4.7		22	18	22	
# 4	4	4.9	8.5	4.9	4.75	32	19	32	28.5
	5	4.7	7.2	4.7		33	18	33	
	6	4.6	7.3	4.6		20	23	23	
	7	4.7	8.6	4.7		25	17	25	
	8	4.8	8.0	4.8		24	14	24	
	1	1.2	1.5	1.2		37	20	37	
	2	1.3	1.4	1.3		38	22	38	
	3	1.9	1.7	1.7		28	30	30	
# 5a	4	1.8	1.8	1.8	1.4	27	28	28	33.9
	5	1.0	1.3	1.0		26	32	32	
	6	1.8	1.4	1.4		25	35	35	
	7	1.2	1.6	1.2		35	19	35	
	8	1.9	1.6	1.6		36	18	36	
	1	2.3	1.2	1.2		35	30	35	
	2	2.6	1.1	1.1		36	28	36	
	3	1.1	2.5	1.1		36	25	36	
# 6	4	1.0	1.6	1.0	1.1	40	27	40	37.4
	5	1.2	2.9	1.2		42	29	42	
	6	1.2	3.1	1.2		27	35	35	
	7	1.1	2.7	1.1		30	36	36	
	8	1.0	2.5	1.0		33	39	39	
	1	2.4	4.2	2.4		20	25	25	
	2	2.5	4.7	2.5		19	28	28	
	3	2.3	4.8	2.3		20	15	20	
# 7	4	2.5	3.1	2.5	2.1	18	14	18	22.3
	5	1.5	2.8	1.5		20	19	20	
	6	1.9	3.5	1.9		25	24	25	
	7	2.1	4.3	2.1		19	20	20	
	8	1.8	4.1	1.8		22	18	22	

Appendix E

E1. The derivation for the fatigue notch factor (K_f) :

Equation (3.30) can be rewritten for a butt-joints and for a flush-ground welded joints or flat plate as:

$$S^m . N_f = A \tag{E.1}$$

$$S_o^{m_o} . N_f = A_o \tag{E.2}$$

From Eqs. (E.1) and (E.2) :

$$\frac{S_o^{m_o} / S^{m_o}}{S^{m - m_o}} = \frac{A_o}{A} \tag{E.3}$$

Equation (E.3) can be rewritten using the definition of fatigue notch factor ($K_f = S_o / S$) as:

$$K_f^{m_o} = \frac{A_o}{A} . S^{m - m_o} \tag{E.4}$$

Substituting (E.1) to (E.4) we get:

$$K_f^{m_o} = \frac{A_o}{A} . (\frac{A}{N_f})^{\frac{1}{m}.(m - m_o)} \tag{E.5}$$

By modifying Eq. (E.5) the final form for K_f can be obtained as:

$$K_f = (\frac{A}{A_o})^{-\frac{1}{m_o}} . (\frac{A}{N_f})^{\frac{1}{m_o} - \frac{1}{m}} \tag{E.6}$$

Appendix F

F1. The strain-gauge method to measure the residual stresses at the weld toes

The concept of this method is based on the superposition principle and is described below. The effective stress range applied in a welded joint can be expressed as:

$$S_{eff} = S_A + S_B + S_r \quad (F.1)$$

or

$$S_{eff} = S_A + S_{r,eff} \quad (F.2)$$

where
- S_{eff} - effective applied stress range
- S_A - nominal applied stress range due to axial loading
- S_B - nominal applied stress range due to bending load or bending stress induced by the possible misalignments
- S_r - welding residual stress embedded at the weld toe of welded joints
- $S_{r,eff}$ - effective residual stress ($S_{r,eff} = S_B + S_r$)

After the specimen was gripped and without the application of the axial stress, the strain gauges would record the effective residual stress ($S_{r,eff}$) i.e the sum of bending stress induced by any possible axial or angular misalignments and the welding residual stress.

Since the induced bending stress (S_B) depends only on the level of misalignment and the gripping force, the effective residual stress ($S_{r,eff}$) would be independent of the nominal applied stress range (S_A) if no local yielding occurs at the toes. However, if the effective stress range reaches the level of yield stress magnitude ($S_{eff} = S_y$) local yielding occurs at the weld toes and the effective residual stress would remain at the level of the yield stress ($S_{r,\,eff} = S_y$) after the nominal axial load is released. The value of the effective residual stress can be read directly from the strain gauges bonded at the weld toes after the first loading cycle.

A computer program was written for this purpose using TestStar R.2.0a (1993) in MTS-testing system (C.3, Appendix C). The readings of the strain gauges were recorded in a computer file and the results are plotted in terms of the axial nominal stress (S_A) against micro-strain as shown in Fig. F.1.

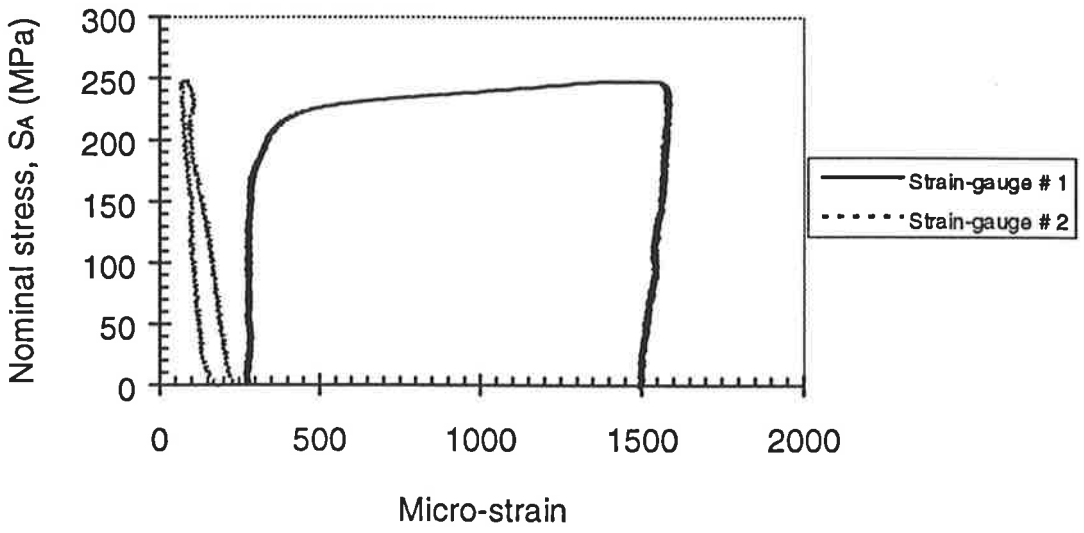

Figure F.1 The readings of the strain gauges bonded at the toes of a welded specimen after first axial loading cycle.

The values of the effective residual stresses (Eq. F.2) calculated from the readings of strain gauges # 1 and # 2 in Fig. F.1 are 310.4 MPa and 47.6 MPa respectively. It is obvious from Fig. F.1 that the yielding has occurred at the location of strain gauge # 1. The reading of the strain gauge # 2 is decreased slightly as the nominal stress (S_A) increases. This can be explained as a small amount of compressive residual stresses may be introduced on the surface of the specimen during its fabrication process.

Appendix G

G1. Tensile test stress-strain diagrams for various sets of specimens:

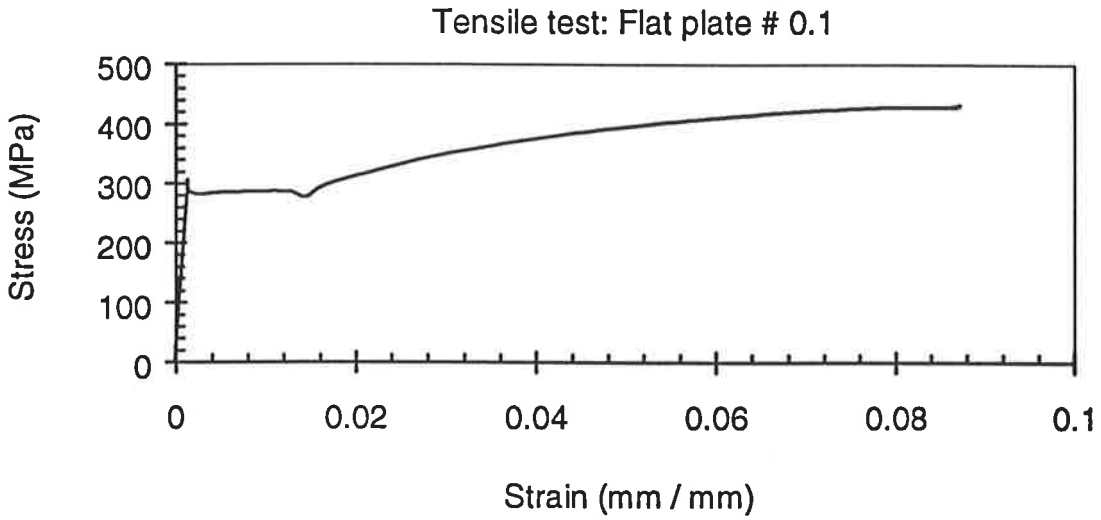

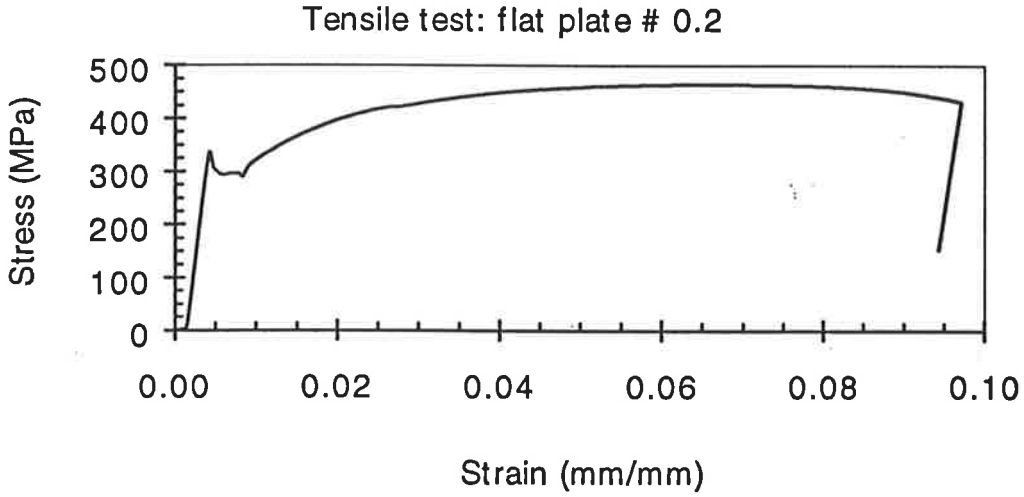

Tensile test: Spec. # 4.2

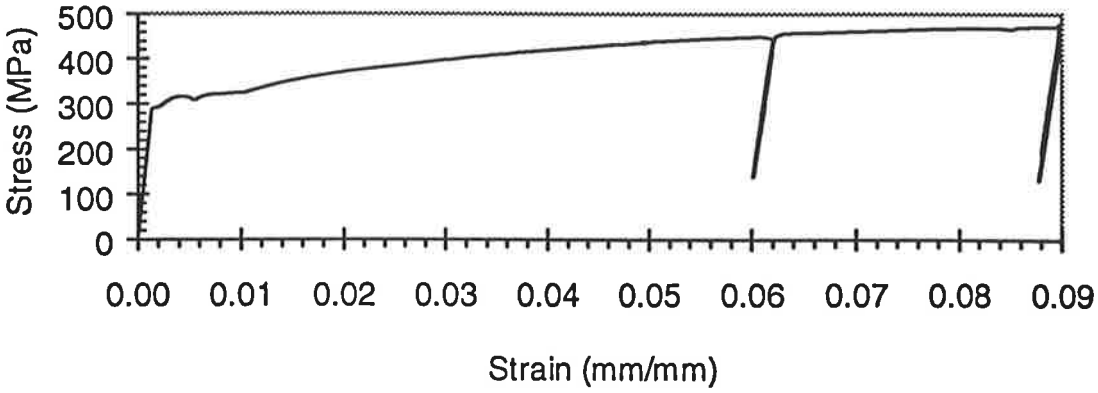

Tensile test: Spec. # 4.12

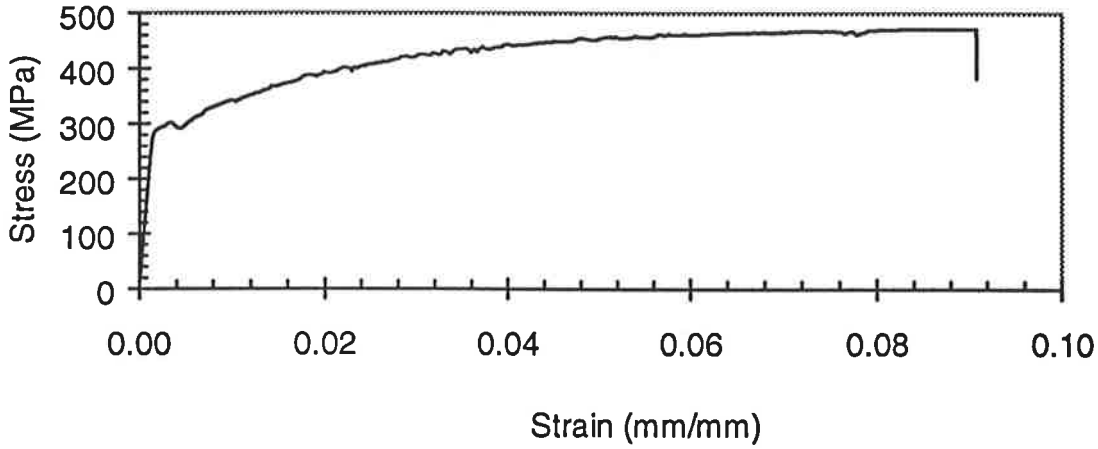

Tensile test: Spec. # 5a.4

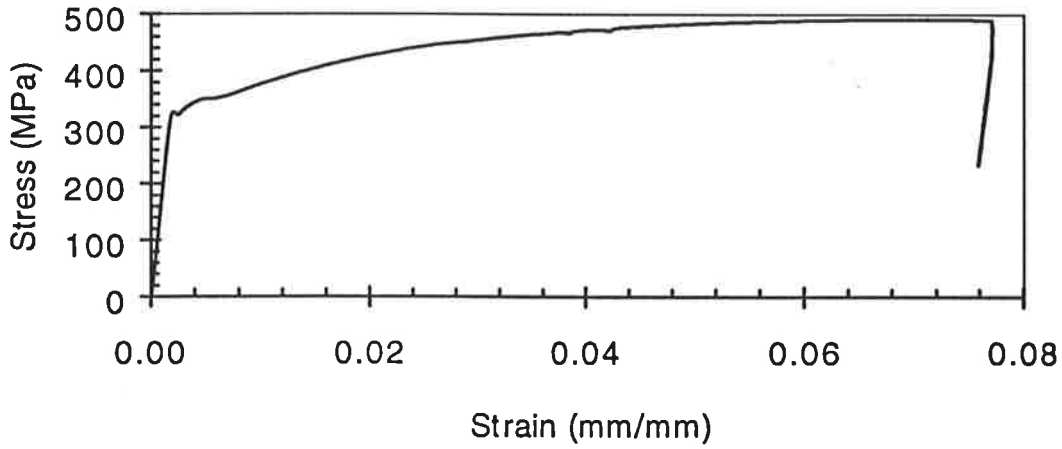

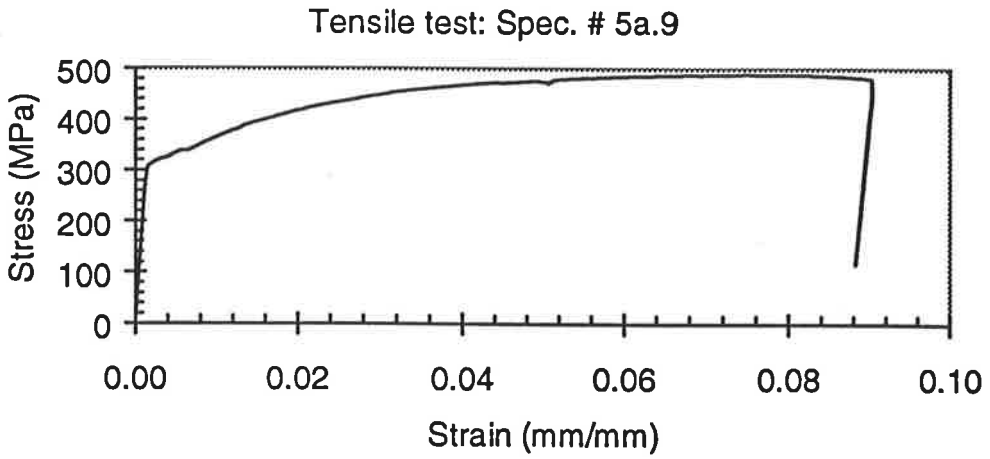
Tensile test: Spec. # 5a.9
Stress (MPa)
500
400
300
200
100
0
0.00
0.02
0.04
0.06
0.08
0.10
Strain (mm/mm)

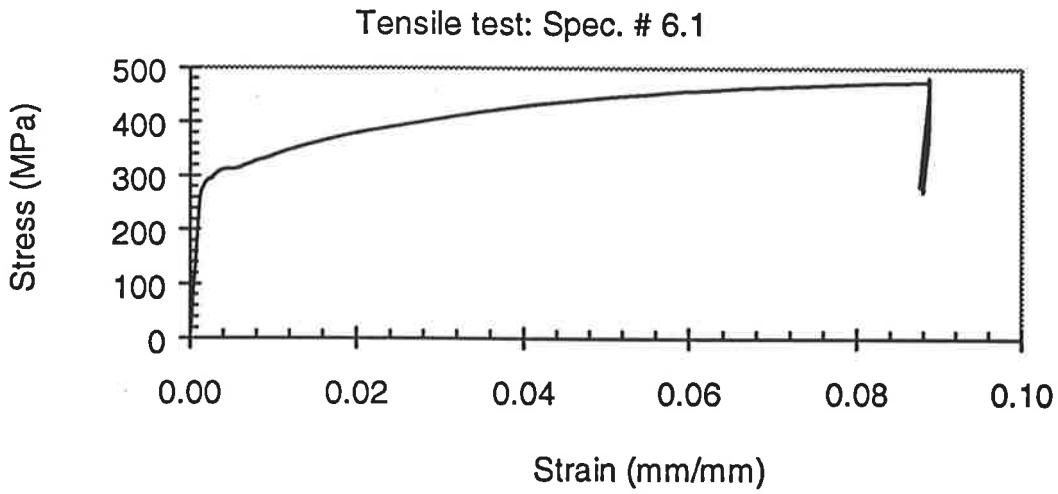
Tensile test: Spec. # 6.1
Stress (MPa)
500
400
300
200
100
0
0.00
0.02
0.04
0.06
0.08
0.10
Strain (mm/mm)

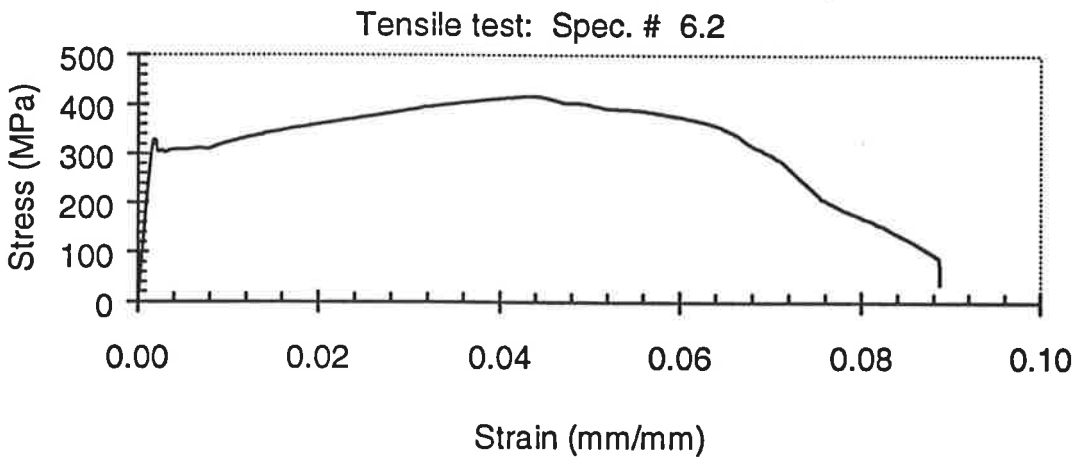
Tensile test: Spec. # 6.2
Stress (MPa)
500
400
300
200
100
0
0.00
0.02
0.04
0.06
0.08
0.10
Strain (mm/mm)

Tensile test: Spec. # 7.1

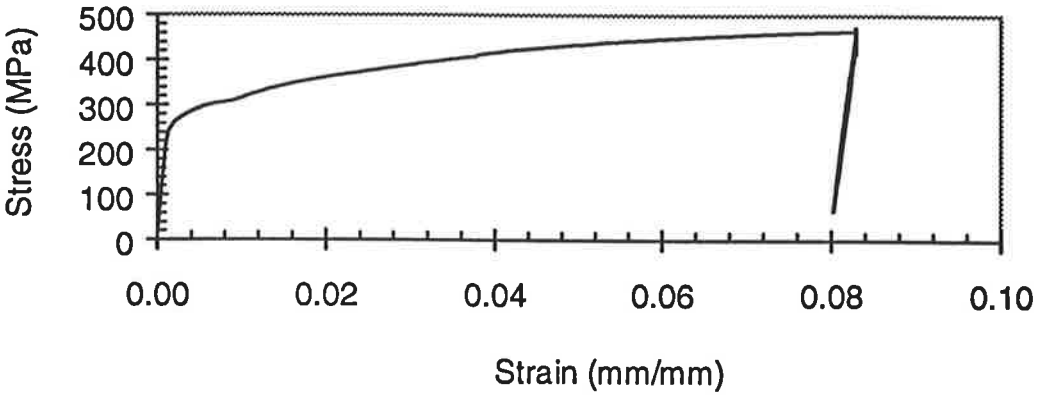

Tensile test: Spec. # 7.11

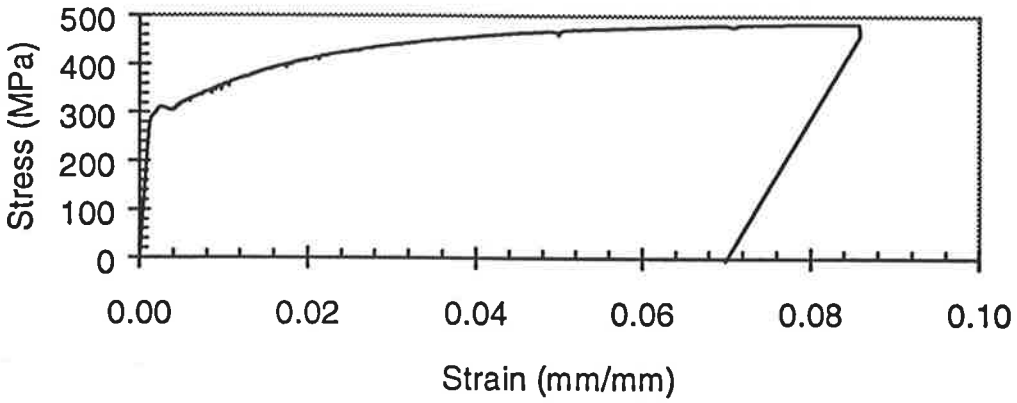

Appendix H

H.1 A copy of the published journal papers originated from this work

Nguyen, N.T., and Wahab, M.A., (1995) A theoretical study of the effect of weld geometry parameters on fatigue crack propagation life.
Engineering Fracture Mechanics, v. 51 (1), pp. 1-18.

Nguyen, N.T., and Wahab, M.A., (1995) The effect of residual stresses and weld geometry on the improvement of fatigue life.
Journal of Materials Processing Technology, v. 48 (1-4), pp. 581-588.